EXCITED STATE DESIGN OF CARBAZOLE-OXADIAZOLE COMPOUNDS FOR THERMALLY ACTIVATED DELAYED FLUORESCENCE

A Dissertation
Presented to
The Academic Faculty

by

Matthew W. Cooper

In Partial Fulfillment
of the Requirements for the Degree
Doctor of Philosophy in the
School of Chemistry and Biochemistry

Georgia Institute of Technology
May 2019

EXCITED STATE DESIGN OF CARBAZOLE-OXADIAZOLE COMPOUNDS FOR THERMALLY ACTIVATED DELAYED FLUORESCENCE

Approved by:

Dr. Seth R. Marder, Advisor
School of Chemistry and Biochemistry
Georgia Institute of Technology

Dr. Elsa Reichmanis
School of Chemical and Biomolecular Engineering
Georgia Institute of Technology

Dr. Jean-Luc Brédas
School of Chemistry and Biochemistry
Georgia Institute of Technology

Dr. Carlos Silva
School of Chemistry and Biochemistry and School of Physics
Georgia Institute of Technology

Dr. Stefan France
School of Chemistry and Biochemistry
Georgia Institute of Technology

Date Approved: November 20, 2018

To my family.

ACKNOWLEDGEMENTS

The thesis presented herein is the product of the ideas, work, and support of many people beyond my own. This includes not only my advisor, the research scientists, post-doctoral fellows, and colleagues in the Marder group, but also my friends and family who have supported me along the way.

Amongst those directly involved in the work presented in this thesis is Prof. Seth Marder, who inspires a level of scientific acumen that is rare to find in an advisor and demands a level of rigor in scientific thought and method that is uncommon in the present times. Dr. Stephen Barlow, who is always available to discuss a result or to suggest a path forward that is informed by a profound understanding of the natural world. In working alongside Dr. Yadong Zhang I have observed the most talented chemist I could have the pleasure to work with, and his expertise in organic synthesis has been the foundation of the success of our shared projects. Furthermore, the work described in this thesis is only given a proper context through collaboration with the talented Xiaoqing Zhang, who performed the device work in the laboratory of Prof. Bernard Kippelen.

Beyond those who had a hand directly in this work, the journey was made possible only by the presence of talented scientists in the Marder group and beyond. The guiding hand of research scientists in performing day-to-day activities allowed the science to be performed and reported in a safe and productive way, and credit goes to Dr. Tim Parker, Dr. Raghunath Dasari, Dr. Junxiang Zhang, and Dr. Denise Bale for this guidance. My colleagues in the trenches deserve all the credit for providing light during an oftentimes discouraging pursuit and my sincere appreciation goes to all of the talented

post-docs and fellow PhD candidates I have had the privilege of working alongside. While too numerous to list, a special thank you goes to Dr. Fadi Jradi, Dr. Karttikay Moudgil, Dr. Marcel Said, Janos Simon, Aida Demissie, Aaron McKee, Dr. Stephen Shiring, and Dr. Rylan Wolfe, as calling these people mere colleagues would undervalue the great friendship that has developed with each.

Most importantly, I wish to thank my family and friends, without which none of this would have been possible in the first place. Principle amongst them is my parents, Ron and Becky Cooper, and my siblings, Laura Nickle and Andy Cooper, for always being there no matter what I was doing or how long it took me to do it. Thank you to my extended family, for their support and belief in me and my path. To my friends back home that make me feel welcome no matter how much time has passed. To Rod and Debbie Schlieder, for welcoming me into their family. And to Kali, for her love and support and standing by me however winding the path may be. No matter how many hours are worked or how unsuccessful an experiment, having her to go home to meant that each day ended well, and I could just try again tomorrow.

TABLE OF CONTENTS

LIST OF TABLES

LIST OF FIGURES

LIST OF SYMBOLS AND ABBREVIATIONS

4CzIPN	2,4,5,6-Tetra(9*H*-carbazol-9-yl)isophthalonitrile
Ac	9,9-Dimethyl-9,10-dihydroacridine
Alq3	Tris(8-hydroxyquinoline)aluminum
CE	Current efficacy
CIE	Intentional commission on illumination
CT	Charge transfer
Cz	9*H*-Carbazole
CzDPO	Carbazole-diphenyloxadiazole
CzMPO	Carbazole-methylphenyloxadiazole
D-A	Donor-acceptor
DF	Delayed fluorescence
DPEPO	Bis(2-(diphenylphosphino)phenyl)ether oxide
DPO	2,5-Diphenyl-1,3,4-oxadiazole
E_S	Energy of singlet
E_T	Energy of triplet
EBL	Electron-blocking layer
EIL	Electron-injection layer
EML	Emissive layer
EQE	External quantum efficiency
ETL	Electron-transport layer
HBL	Hole-blocking layer
HIL	Hole-injection layer

HOMO	Highest occupied molecular orbital
HTL	Hole-transport layer
ICT	Intramolecular charge transfer
IQE	Internal quantum efficiency
ISC	Intersystem crossing
ITO	Indium tin oxide
K	Electron exchange integral
k_{fl}	Fluorescent decay rate
k_{nr}	Non-radiative decay rate
k_{RISC}	Reverse intersyctem crossing rate
LCD	Liquid crystal display
LE	Localized excitation
LUMO	Lowest unoccupied molecular orbital
MPO	2-methyl-5-phenyl-1,3,4-oxadiazole
m_s	Spin magnetic moment
OLED	Organic light-emitting diode
PE	Power efficiency
PF	Prompt fluorescence
PTCBI	3,4,9,10-Perylenetetracarboxylic bisbenzimidizole
RISC	Reverse intersystem crossing efficiency
s	Spin quantum number
S_0	Singlet ground state of a molecule
S_1	Lowest energy excited singlet state of a molecule
SOC	Spin-orbit coupling
T_1	Lowest energy excited triplet state of a molecule

TADF	Thermally activated delayed fluorescence
^{t}But*t*Cz	3,6-Bis(3,6-di-*tert*-butyl-9-carbazolyl)-carbazol-9-yl
*t*Cz	3,6-Bis(*N*-carbazolyl)-carbazol-9-yl
TD-DFT	Time-dependent density functional theory
TP3PO	1,3,5-Tri(diphenylphosphoryl-phen-3-yl) benzene
TPBi	2,2′,2"-(1,3,5-Benzinetriyl)-tris(1-phenyl-1-*H*-benzimidazole)
TTA	Triplet-triplet annihilation
γ	Fraction of injected charges that recombine to form excitons
ΔE_{ST}	Singlet-triplet energy gap
η_{out}	Outcoupling efficiency
η_{r}	Singlet-triplet branching efficiency
λ_{max}	Wavelength of maximum absorption or emission
μ	Charge-carrier mobility
μ_{HL}	HOMO-LUMO transition dipole moment
τ_{DF}	Delayed fluorescence lifetime
τ_{fl}	Fluorescence lifetime
τ_{PF}	Prompt fluorescence lifetime
Φ_{DF}	Delayed fluorescence quantum yield
Φ_{fl}	Fluorescennce quantum yield
Φ_{ISC}	Intersystem crossing efficiency
Φ_{PF}	Prompt fluorescent quantum yield
Φ_{PL}	Photoluminescent quantum yield
Φ_{RISC}	Reverse intersyctem crossing efficiency

SUMMARY

In this thesis, a study of donor-acceptor compounds comprised of 9H-carbazole and 2,5-diphenyl-1,3,4-oxadiazole moieties is presented with an emphasis on developing an understanding of how structure affects properties relevant to thermally activated delayed fluorescence (TADF). An orbital understanding of the lowest energy singlet and triplet excited states is established wherein the singlet state involves a HOMO to LUMO intramolecular charge transfer state and the triplet state is a locally excited state confined largely on the diphenyloxadiazole moiety. The orbital character of the states is confirmed through sensible structural modifications that preferentially affect the energy one of the two states, reducing the energy between them and allowing for the observation of TADF. OLEDs utilizing fluorophores that developed using the established principles the emitting species are shown to exhibit external quantum efficiencies well above what is possible if only singlet excitons are being converted to light, confirming the conversion of triplet excitons to photons in the devices. The findings show the limitations of using these materials as blue-emitters in OLEDs and provides strategies for overcoming these restrictions through rational molecular design. Further, optimized structures as well as application of the results to other donor-acceptor systems is discussed.

CHAPTER 1. INTRODUCTION

An organic light-emitting diode (OLED) is, in its simplest form, a multilayer device consisting of organic materials between two electrodes that converts electricity into light. Due to their organic nature and the fact that most active materials in them are not highly crystalline, OLEDs can be thin, lightweight, and flexible in comparison to either their inorganic counterparts or to most commercial liquid crystal display (LCD) technologies. Furthermore, OLEDs offer advantages over LCDs in power consumption, response time, and contrast ratio, but tend to be inferior in lifetime and cost metrics. Over the last three decades, OLEDs have been a subject of significant interest both in academia and in industry for application in display and solid-state lighting technologies. By 2017, the OLED market had a production capacity of over 500 million display panels with an estimated market over $20 billion,[1] including the flagship smartphones of both Apple and Samsung. Whit- light emitting OLEDs for steady-state lighting applications can be significantly more efficient than incandescent sources, and have exceeded the efficiency of fluorescent tubes.[2]

OLEDs have succeeded as a technology due to steady advancements made in both device architecture and in materials from the early, simple devices reported by Tang and Van Slyke at Eastman Kodak. While the optimization of device architectures is more of an engineering pursuit, the development of advanced materials to incorporate into the devices requires a chemical approach from the design, synthesis, and processing perspective. Insight into the fundamental physical processes governing the conversion of injected charges to photons has allowed for generational advancements in the devices,

which will be discussed in section 1.4, leading to quantum efficiency limits ca. 4 times higher than theoretically possible in early devices. Further material design must, however, address concerns relating to color purity and device stability, as well as a continuing push for efficiency, particularly at high luminance. This thesis will largely focus on these issues, with particular emphasis on the push for organic emitters with a bluer emission profile than are currently widely available.

Contained herein is a systematic study of purely organic compounds for the purpose of understanding the structure-property relationships required for thermally activated delayed fluorescence, TADF, (see CHAPTER 2), and an orbital description of the relevant ground and excited states of the compounds that give rise to these properties. The compounds are related to one another in that all incorporate common organic electronically active moieties derived from 1,3,4-oxadiazole, which is paired in this work with 9*H*-carbazole based functional groups. These building blocks offer many desirable properties including chemical and thermal stability, reasonably high charge carrier mobility, and high photoluminescent quantum yields, yet only a few examples combining these moieties have been reported in the scientific literature that exhibit TADF. The reason for this will be discussed in detail in CHAPTER 3, and physical insights gained therein will be used to develop design rules for modifying these compounds in ways that will lead to the desired photophysical properties. In the second part of the chapter, new emitters based on the compounds will be developed in accordance with the design rules established and will be incorporated into OLED devices. In CHAPTER 4, the knowledge gained will be extended with the development of an oxadiazole acceptor moiety, 2-methyl-5-phenyl-1,3,4-oxadiazole, to further fine tune and improve the compounds for

use as blue emitters in OLED devices. Finally, CHAPTER 5 will summarize the overall lessons learned, and provide a potential path forwards based on the principles established in Chapter 3 and 4 of this thesis.

1.1 OLED Structure and Function

While the first electroluminescent cells reported by Martin Pope and co-workers[3] were simple single layer devices, modern OLEDs are complex devices with multi-layer heterostructures. The structure of a conventional OLED is shown below in Figure 1, left. The physical processes that occur in an OLED cause electroluminescence after combination of an injected hole with an injected electron forms a high energy molecular species, called an exciton, which emits light upon relaxation. The electrical processes can be divided into three basic steps, shown in Figure 1, right, of charge injection from the electrodes, charge migration to the emissive layer, and charge recombination to form an exciton. In some cases, the function of several of these layers can be combined into a single layer, or omitted, and a detailed explanation of the physics behind each of these steps is beyond the scope of this thesis, but the basic function of each layer will be covered to impart a better understanding of the operating principles of an OLED.

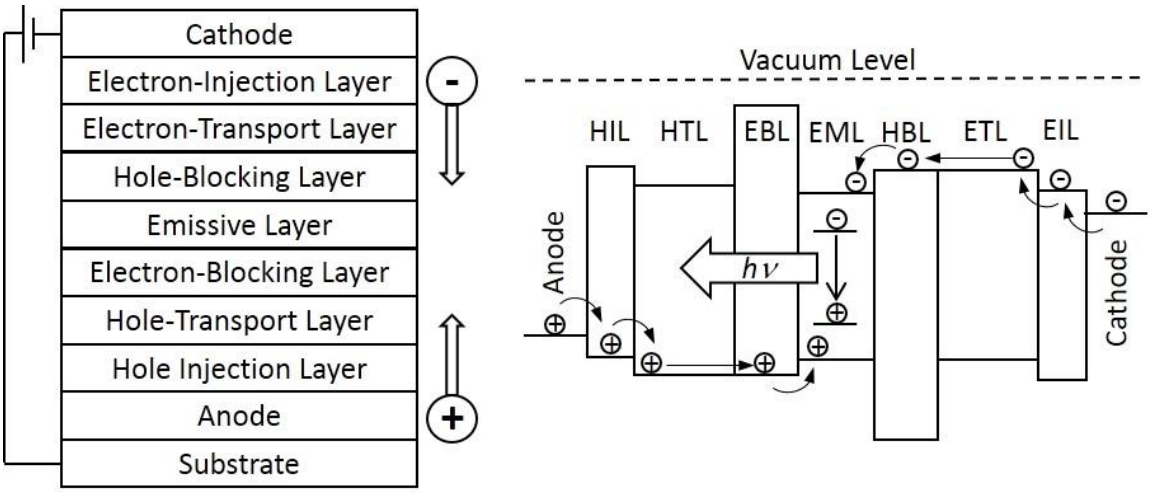

Figure 1 – (*left*) Structure of a conventional OLED. Layers in an actual OLED device may be combined or omitted. (*right*) An energy level diagram of an OLED in the absence of an applied field and neglecting any interface dipoles. Energy levels shown are the work function of the electrodes and the ionization potential and electron affinity for the organic layers, including hole-injection layer (HIL), hole-transport layer (HTL), electron-blocking layer (EBL), emissive layer (EML), hole-blocking layer (HBL), electron-transport layer (ETL) and electron-injection layer (EIL). Energy levels are estimates, often from electrochemistry.

1.1.1 Electronic Processes

Electrodes for OLED devices are chosen for their ability to provide charge injection to the organic layers, with high Fermi level (low work function) for electron injection and low Fermi level (high work function) for hole injection. The process of charge injection is generally explained as the movement of charge carriers between the electrode and the appropriate energy level in the organic injection layer, characterized by the electron affinity of the electron injection layer or the ionization energy of the hole injection layer.[4-6] The charge injection layer acts to facilitate the process of moving charge carriers from the electrode to the charge transport layer under an applied voltage by reducing the barrier for charge injection, where charge injection depends on both the properties of the interface of electrode and charge injection layer, and to the energy

difference between the Fermi level of the electrode and the appropriate energy level of the injection layer.[7-9]

Once injection has occurred, the charge transport layers allow for the charge carriers to move towards the emissive layer, EML, in the presence of an applied electric field. The rate at which the charge carriers can move in the materials is quantified by the charge mobility (μ), which describes the efficacy of a charge carrier to migrate as a function of an electric field. Charge transport in organic semiconductor materials is a process that tends to be described as occurring in a hopping regime where a charged molecule undergoes an electron-transfer reaction with a neighboring molecule, with a rate constant described by Marcus theory.[10] Early electroluminescent cells suffered from imbalanced charge transport properties due to the intrinsic disparity in charge carrier mobility, with hole mobilities typically higher than electron mobilities, in many organic semiconductors.[11] By inclusion of charge transport layers displaying high mobility for the appropriate charge carrier, along with the appropriate ionization energy or electron affinity for charge injection, charges can be moved through the device to the emissive layer at lower voltages, and charge balance can be better controlled.[12-14]

After injection and migration of the charge carriers to the emissive layer, charge recombination can occur. Recombination in organic materials is modeled using the Langevin model.[15] In this model, charge recombination occurs through Coulombic capture, and the recombination current density is a function of the mobility of both the hole and electron in the medium, as well as the charge carrier density. The rate of recombination plays a strong role in device performance, and in an ideal case, with ambipolar mobility in the EML, an increased recombination rate leads to increased

device efficiency.[16] Charge blocking layers can be included to confine the charge carriers, and therefore the charge recombination, to the emissive layer.[17-18]

1.1.2 Exciton Formation

Upon charge recombination, an exciton is formed.[19] An exciton is a high energy, electronically excited species formed by a Coulombically bound electron-hole pair. Electrons are fermions with spin quantum number $s = +1/2$ and spin magnetic moment $m_s = \pm 1/2$, denoted as "up" or as "down," with total spin operators of:

$$\langle \frac{1}{2}, +\frac{1}{2} \rangle \equiv \langle \uparrow \rangle$$
$$\langle \frac{1}{2}, -\frac{1}{2} \rangle \equiv \langle \downarrow \rangle \quad (1)$$

where the first number in the bracket for the spin quantum number s, and the second for the spin magnetic moment m_s. For a two-electron system, such as an exciton in which the hole that is Coulombically bound to the high energy electron is in a singly-occupied orbital where the spin of each electron is represented as up or down, the following combinations are possible:

$$\uparrow\uparrow, \downarrow\downarrow, \uparrow\downarrow, \downarrow\uparrow \quad (2)$$

From these four possibilities, two overall spin states are obtained from linear combinations for a two-electron system – $S = 0$ and $S = 1$, corresponding to singlet and triplet states, respectively, in which the electrons can precess in and out of phase:

$$\langle 1,+1\rangle = \langle \uparrow\uparrow \rangle$$

$$\langle 1,-1\rangle = \langle \downarrow\downarrow \rangle$$

$$\langle 0,0\rangle = \frac{1}{\sqrt{2}}[\langle \uparrow\downarrow) - (\downarrow\uparrow\rangle] \qquad (3)$$

$$\langle 1,0\rangle = \frac{1}{\sqrt{2}}[\langle \uparrow\downarrow) + (\downarrow\uparrow\rangle]$$

Given the constraint of the Pauli Exclusion Principle and the fact, noted above, that electrons are fermions, there are 4 combinations of which 3 are triplet states and 1 is a singlet state. For charge recombination that is under statistical control, the resulting ratio of triplet to singlet excitons, known as the branching ratio (η_r), would be assumed to also follow a 3:1 ratio. In fact, studies have determined 22(±3)% singlets to be obtained upon recombination of charges in an electroluminescent device, confirming the general applicability of the assumption.[20] This ratio has important implications to the efficiency of an electroluminescent device that will be discussed later.

According to Kasha's rule, an exciton undergoes vibronic and electronic relaxation to the lowest energy excited state of like spin before appreciable photophysical processes occur (eg: energy transfer or radiative decay).[21] This is due to the non-radiative decay rates from higher electronically excited states to the lowest electronically excited state being fast compared to the radiative decay rate to the electronic ground state, however it is worth noting that not all molecules obey Kasha's rule.

1.1.3 Exciton Transfer

In EMLs that contain a distinct emitter doped into the bulk organic host material, the exciton is transferred to the emitter through one of two mechanisms in a process known as sensitized emission. For singlet excitons, both Förster[22] and Dexter[23] type energy transfers to the emitter are allowed. For triplet excitons, only Dexter energy transfer is applicable. Additionally, the emitter can act as a potential well and trap charges directly, leading to the formation of excitons on the emitter. Förster transfer is a relatively long range (4-10 nm), non-radiative, dipole-dipole coupling between exciton donor and acceptor molecules that follows the selection rules of absorption and fluorescence; that is, only singlet excitons can be transferred in this way. Dexter transfer, on the other hand, occurs at short range via orbital coupling between exciton donors and acceptors and involves the intermolecular exchange of electrons. Dexter transfer only requires that spin is conserved in the system and for both singlet-singlet and triplet-triplet energy transfers are allowed. After transfer of the exciton to the emitter, the physical properties of the emitter determine the emission properties.

1.2 Basic Excited State Dynamics in Organic Molecules

An exciton localized on an emitter can undergo a number of different relaxation processes, as shown on the Jablonksi diagram in Figure 2. For typical organic emitter in an OLED, fluorescence is the only relaxation pathway that leads to light emitted from the device and any exciton in the triplet manifold will not contribute appreciably to luminescence but will decay non-radiatively. The difference in energy between the first singlet excited state (S_1) and the ground state (S_0) and the vibrational structure of them

determines the energy of the photons emitted by fluorescence, and hence the color of the OLED. In polyatomic organic compounds, a radiative transition can couple to any one of a number of energetically inequivalent vibrational levels in the ground state, which leads to broadening in the resulting emission spectrum.

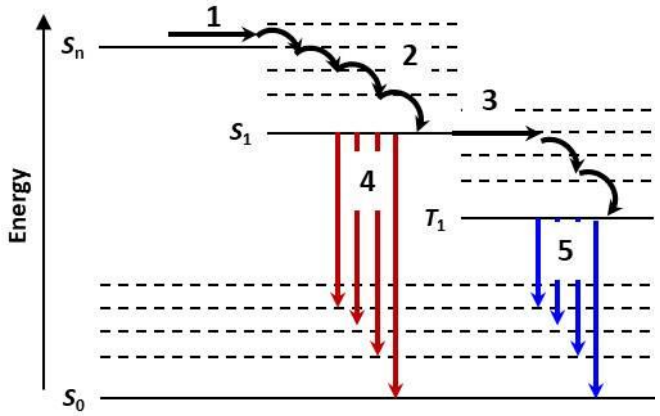

Figure 2 – Jablonski diagram showing intramolecular relaxation pathways for an exciton. Dashed lines represent vibrational states within a given electronic state. Processes include (1) internal conversion, (2) vibrational relaxation, (3) intersystem crossing, (4) fluorescence, (5) phosphorescence. Non-radiative decay to the ground state occurs via internal conversion.

Internal conversion is a radiationless transition that occurs from a higher to a lower electronic state (e.g. S_2 to S_1) with like spin through energetically degenerate vibrational modes. Vibrational relaxation occurs within an electronic state via the exchange of heat with the environment. Intersystem crossing is the spin-forbidden transition from one electronic state to a state with the different spin typically, in the context of OLEDs, from singlet to triplet. Fluorescence is the spin-allowed radiative transition from an excited electronic state to the ground state. According to Kasha's rule, emission occurs from the lowest excited level of a given multiplicity. Phosphorescence is the spin-forbidden radiative transition from an excited triplet state to the singlet ground

state, and is slow in simple organic molecules with a rate constant typically several orders of magnitude lower than that of fluorescence or internal conversion, thus phosphorescence is generally very inefficient.

1.2.1 Fluorescence

The rate at which the exciton is converted to light via the fluorescence pathway is the fluorescent decay rate, k_{fl}, and is approximated by the Strickler-Berg relationship:[24]

$$k_{fl} = 2.88 \times 10^{-9} n^2 \frac{\int F(\tilde{\nu}) d\tilde{\nu}}{\int F(\tilde{\nu})/\tilde{\nu}^3 d\tilde{\nu}} \int \frac{\varepsilon(\tilde{\nu})}{\tilde{\nu}} d\tilde{\nu} \quad (4)$$

where n is the refractive index of the medium, $F(\tilde{\nu})$ is the emission spectrum, $\tilde{\nu}$ is the wavenumber in cm^{-1}, and ε is the molar attenuation coefficient. The molar attenuation coefficient relates the concentration of a species to the attenuation of light at a given wavelength as a function of path length due to absorption. The integrals are evaluated over the $S_1 \rightarrow S_0$ emission and $S_0 \rightarrow S_1$ absorption bands, respectively. It is apparent that the fluorescent rate is dependent upon the molar attenuation coefficient. The molar attenuation coefficient is related to the experimentally determined oscillator strength of the transition, a dimensionless value that describes the probability of an electronic transition occurring between two states when interacting with light of an appropriate energy, and is determined by the area under an absorption band plotted against frequency according to the following equation:

$$f = 4.32 \times 10^{-9} \int \varepsilon(\nu)\, d\nu \quad (5)$$

The oscillator strength (*f*is proportional to the square of the transition dipole moment (μ_{ge}):

$$f \propto \mu_{ge}^2 \tag{6}$$

The transition dipole moment is a quantum mechanical quantity calculated from the wavefunctions of a molecule (see below), which allows for a connection between molecular structure and observable photophysical properties. An increased transition dipole moment for a transition leads to a concomitant increase in oscillator strength and of the integral of the molar absorptivity in a compound, which itself leads to an increased radiative decay rate through the Strickler-Berg relation. Thus, it is of interest to understand what leads to a large transition dipole moment for a given transition.

The transition dipole moment between a ground and excited state (μ_{ge}) is defined as:

$$\mu_{ge} = \int \psi_g^* \mu \psi_e \, d\tau \tag{7}$$

where ψ_g^* is the complex conjugate of the ground state wavefunction, ψ_e is wavefunction for the excited state, μ is the transition moment operator which is a product of the position and charge of the electron, and $d\tau$ represents the volume element. For this integral to be large (and thus have a high probability of a transition between the relevant states) three conditions must be met.

1. The integrand cannot be odd as the integral of an odd function, which is a function that displays symmetry with respect to the origin (taken as the center of the molecule), over all space is zero. Since the transition moment operator is itself odd, ψ_g and ψ_e cannot themselves both be even or odd, as that would lead to an odd product and a transition dipole moment of zero. In a centrosymmetric molecule, this means is that the ground and excited state of a transition cannot share the same symmetry.
2. Having a large spatial overlap, along with proper phase matching, between the ground and excited state will lead to a large value of the integral, and a large transition dipole moment, and
3. Due to the operator μ being a product of distance from the origin and charge on the electron, overlap of the orbitals at large distances from the origin will enhance the transition.

The time it takes for excitons to be converted to light through fluorescent decay rate related to the natural lifetime (τ_n), and is equivalent to the reciprocal of the fluorescent decay rate:

$$\tau_n = \frac{1}{k_{Fl}} \tag{8}$$

The natural lifetime is only directly observable in the absence of other relaxation pathways. With the inclusion of non-radiative relaxation pathways (*e.g.*, internal conversion, intersystem crossing), the related fluorescent lifetime is as follows:

$$\tau_{fl} = \frac{1}{k_{Fl} + k_{nr}} \tag{9}$$

where k_{nr} is the sum of all non-radiative decay rates that depopulate the state from which fluorescence is occurring.

Related to the fluorescent decay rate is the overall efficiency of the emitter to convert excitons to light. The photoluminescent quantum yield (PLQY) is the ratio of emitted photons to absorbed photons upon the absorption of light, and can be written as the ratio of the rates of radiative decay to the sum of the rates of all decay processes:

$$\Phi_{PL} = \frac{k_{rad}}{k_{rad} + k_{nr}} \tag{10}$$

where Φ_{PL} is the PLQY, k_{rad} is the rate of radiative decay and k_{nr} is the combined rates of all non-radiative decay pathways. For most organic compounds where phosphorescence is formally forbidden and, at least at room temperature, effectively not observed, PLQY is used interchangeably with fluorescence quantum yield (Φ_{fl}). To be more precise, for fluorescence quantum yield the rate k_{fl} replaces k_{rad}.

PLQY can be maximized by either increasing the rate of radiative decay, or by decreasing the non-radiative decay rates. The necessary conditions to increase the transition dipole moment are discussed above. The conditions to decrease non-radiative decay depend on the type of decay. For example, internal conversion to the ground state requires coupling between vibrational levels in the ground and excited states, and can be minimized with rigid molecular structures such as those found in polycyclic aromatic

hydrocarbons.[25] An oft-cited example is that of fluorescein with an intense fluorescence (Φ_{fl} = 0.92) and phenolphthalein in which fluorescence is barely measurable, but which differ structurally only in a bridging oxygen atom that rigidifies two benzene rings (Figure 3).[26] Intersystem crossing, in which the spin multiplicity of the exciton changes, is not formally allowed but can occur through the mixing of the singlet and triplet state through spin-orbit coupling.[27] The simplest way to increase spin-orbit coupling is through the heavy-atom effect.[28] Substitution of 4 iodine atoms onto fluorescein (Figure 3), for example, has little effect on the fluorescent decay rate (0.20×10^9 s^{-1} vs. 0.22×10^9 s^{-1}) but Φ_{fl} is drastically reduced to 0.14 from 0.92 (in ethanol with 1 mM NaOH) due to significant increase in the intersystem crossing rate.[29] A change in orbital type between the singlet and triplet state occurs when the angular momentum quantum number *l* is different in the orbitals containing the excited electron. The intersystem crossing rate is increased in these systems compared to those where there is no change in orbital angular momentum, which is explained by El-Sayed's rules, which state that a change in spin of a system must also be accompanied by a change in angular momentum.[30] Compounds that exhibit an n-π^* $S_1 \rightarrow S_0$ transitions tend to show increased triplet yields and low Φ_{fl}, for example benzophenone which exhibits a triplet yield approaching 100% in benzene solution upon photoexcitation.[31]

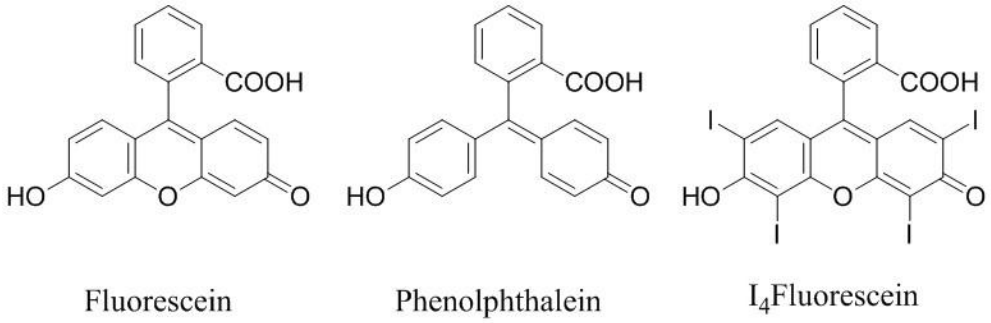

Figure 3 – Structure of fluorescein, phenolphthalein, and iodinated fluorescein

1.3 Efficiency Metrics for OLEDs

To understand the measure of efficiency in OLEDs, one must first have a basic understanding of luminance. The light output of OLEDs is designed to be viewed by the human eye. To reflect this, the light output is commonly measured in photometric instead of radiometric units. Photometric units differ from radiometric units in that they weigh the intensity or power output by the response of the human eye. The sensitivity of the human eye to incident radiation is called the photopic response, and is strongest at *ca*. 555 nm and decreases towards the blue and the red. The SI unit of luminous intensity is the candela (cd), and the related to the unit for luminous flux is the lumen (lm). Determination of luminous flux is determined from an integral of the product of the luminosity function (shown below, Figure 4**)** and the power spectral density.

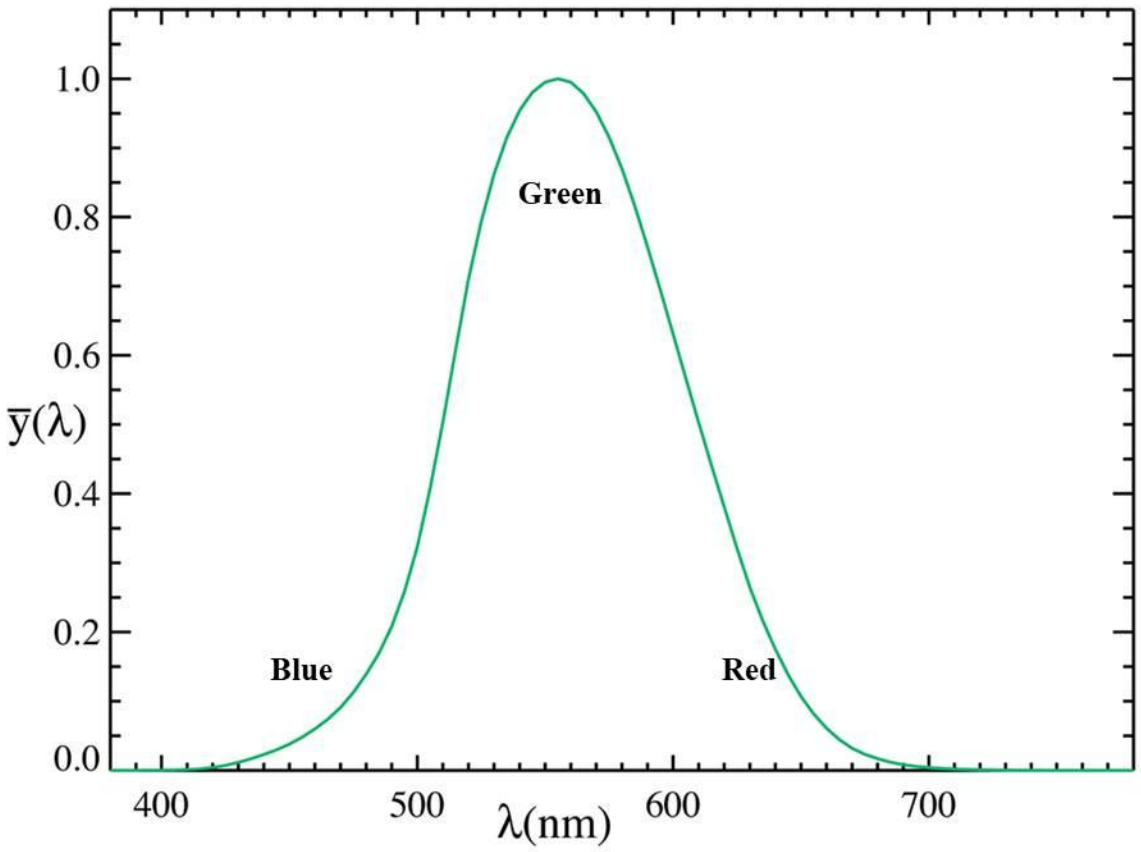

Figure 4 – International commission on illumination (CIE) photopic response curve of the "standard" human eye under high illumination. (CC BY-SA 3.0)

1.3.1 Quantum Efficiency in OLEDs

External quantum efficiency (EQE) is the metric most often quoted for quantifying the fundamental physical mechanisms of an OLED, that is the efficiency of the processes described above. Defined as the number of photons emitted in the viewing direction per electron injected into the OLED, EQE for an electroluminescent device in which the electroluminescence occurs exclusively through spin-allowed fluorescent emission is given by:[32]

$$EQE = \eta_{out} \times q \times \eta_r \times \gamma \quad (11)$$

where η_{out} is the outcoupling efficiency, or the fraction of the photons generated that that exit the device, q is the luminescent efficiency of the emitter, γ is fraction of injected charges that recombine to form excitons, and η_r is the singlet-triplet branching efficiency discussed earlier. The luminescent efficiency of an emitting species is approximated by the PLQY of the species, at least for purely fluorescent emitters, but additional relaxation pathways can be present after incorporation into an OLED[33-34] giving rise to the analogous term q.

The product of the last three terms gives the internal quantum efficiency (IQE) of the OLED:

$$IQE = q \times \eta_r \times \gamma \quad (12)$$

It follows that the EQE of an OLED is equal to the product of the IQE and the outcoupling efficiency. Outcoupling efficiency values are dependent upon the refractive indices of the materials in the specific device, but for planar devices in which the emitters have isotropically aligned transition dipole moments, they tend to around 0.20 when fabricated on glass.[35]

To maximize EQE in an OLED it is clear that the following conditions must be met: (1) device architecture and choice of materials that result in balanced charge injection and good transport to yield high γ (2) emitting species that display luminescent quantum efficiency approaching 100%, and (3) high outcoupling efficiency. If all of these

conditions are met, this places an upper limit on the EQE of a device at ca. 5% if only singlet excitons are converted to light, and ca. 20% if both triplet and singlet excitons can be converted to light, due to the 75% of excitons formed upon charge recombination that are formed in a triplet state.[20] In fact, measured EQEs in state of the art devices commonly exceed the 20% threshold, including values of up to 37% in a recently reported device that displayed high η_{out} due to emitting dipoles that were highly horizontally aligned.[36]

1.3.2 Luminous and Power Efficacies

Current efficacy, also called luminous efficacy and reported in cd/A, is comparable to the EQE in that it compares light output to charges injected. However, the current efficacy takes into account the photopic response described above and the relationship between the current efficacy and quantum efficiency of the device lies in the spectral properties of the emission. For two devices with the same EQE, the one with a more green emission will display a higher current efficacy. This quantity is most often used to quantify OLEDs for display applications.[37]

The power efficacy of an OLED is defined as the ratio of the luminous power exiting the device over the total electrical power required to drive the device at a given voltage, and is reported in lm/W. This efficacy is useful in interpreting the power dissipated by a device and is analogous to "wall-plug" efficiency (W/W) in radiometric units. Power efficacy is generally most applicable for OLEDs used as solid-state light sources.[37]

Due to the complicated structure and electrical processes in an OLED, device output is variable as function of applied voltage. Below a certain threshold, called the turn-on voltage, charges will not flow appreciably from the electrodes into the device. Above this voltage, charge carriers are injected and move towards the emissive layer under the applied potential. The Langevin charge recombination and the charge transport are some of the other electrical properties that change as a function of applied voltage. As such, the above efficacy values change as a function of applied voltage, as well. This phenomenon is termed efficiency roll-off and minimizing the decrease of device efficiency as output increases is an important consideration in device architecture,[38] and device efficiency values should be accompanied by the luminous output of the device where the efficiency metric was obtained.

1.4 A Brief History of Emitters in Electroluminescent Devices

Early attempts at generating electroluminescence in organic materials consisted of cells in which electrodes were attached directly to anthracene single crystals.[39] These cells required large driving voltages, on the order of 100 V or above, to overcome the intrinsically low charge migration and thick organic layers through which the charges had to travel in order to combine and form an exciton. Pope et al. demonstrated the ability to tune the emission properties of the cell by doping a distinct emitting species into the organic crystal of the cell.[3]

The first practical devices were reported in 1987 by Tang and Van Slyke, and were the result of advancement in the deposition of high quality thin films (thickness <100 nm) combined with the appropriate material choices and heterostructure to optimize charge

injection and transport.[40] By using a bilayer structure acting as a diode between the electrodes, electroluminescence at driving voltage as low as ca. 2.5 V and luminance over 1,000 cd/m^2 was achieved and ushered in the modern concept of the OLED. The device contained a ca. 75 nm thick layer comprised of an aromatic diamine that acted to selectively transport holes, and a ca. 60 nm thick emissive layer consisting of tris(8-hydroxyquinoline)aluminum (Alq_3) where the holes and electrons combined to form excitons before being converted to light. Device structures were further optimized as the role of the luminescent species was fully separated from charge injection and transport by incorporating a discrete electron injecting layer[41] and by doping the emitting species into a host material with appropriate electronic properties.[42] Early device architectures are shown in Figure 5**.**

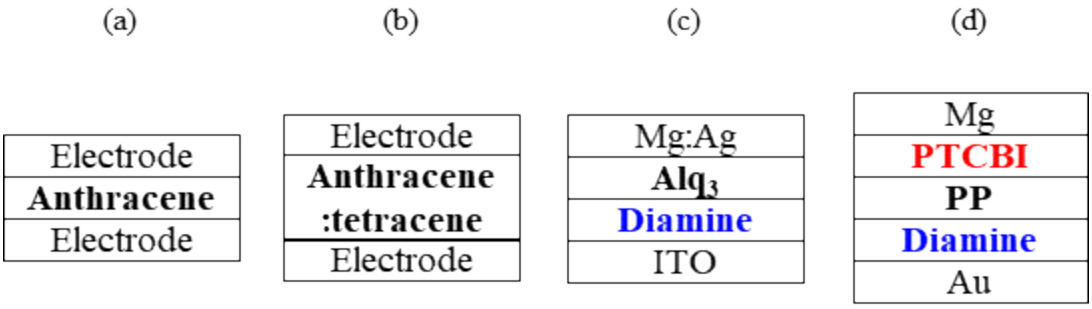

Figure 5 – Early advances in organic electroluminescent devices include (a) simple electroluminescent cells with emission from single crystals of anthracene[39] and (b) anthracene crystals doped with 0.1% (mol/mol) tetracene to trap excitons and shift the emission wavelength.[3] The first diode (c) utilized a hole-transport/electron blocking diamine layer (4,4'-cyclohexylidenebis(N,N-bis(*p*-tolyl)aniline)) alongside the emissive layer made up of tris(8-hydroxyquinoline)aluminum.[40] (c) Charges were further confined to the emissive layer, composed of a thin film of a phtaloperinone derivative (PP), by adding a distinct hole blocking, electron-transport layer comprised of 3,4,9,10-perylenetetracarboxylic bisbenzimidizole (PTCBI).[41]

1.4.1 "First-Generation" Fluorescent Emitters

By decoupling the luminescent species from the charge-blocking and charge transport necessary for an OLED to operate efficiently, focus could shift to optimizing the species where the exciton is converted to light. In this "first-generation" of OLED emitters, it was understood that increasing the fluorescence quantum yield of the emitting layer should increase the device efficiency of the OLED, as shown in Equation 11. The emissive layer in Tang and Van Slyke's diode, a neat thin film of Alq_3, was recently determined to display a photoluminescent quantum yield (PLQY), the ratio of photons emitted to photons absorbed upon photoexcitation, of 22%.[43] Assuming 20% outcoupling efficiency in a device, this places an upper limit on the external quantum efficiency at 1.1%, and in fact the measured efficiency was ca. 1.0%.[40] Doping the emissive layer with a high Φ_{fl} coumarin dye results in a thin film with PLQY ca. 4.5 times higher than the neat tris(8-hydroxyquinoline)aluminum film, and an OLED device with increased EQE of ca. 2.5%.[42] Thus, in first generation devices, emitters were optimized by increasing fluorescence quantum yields and by tuning the emission color and profile.

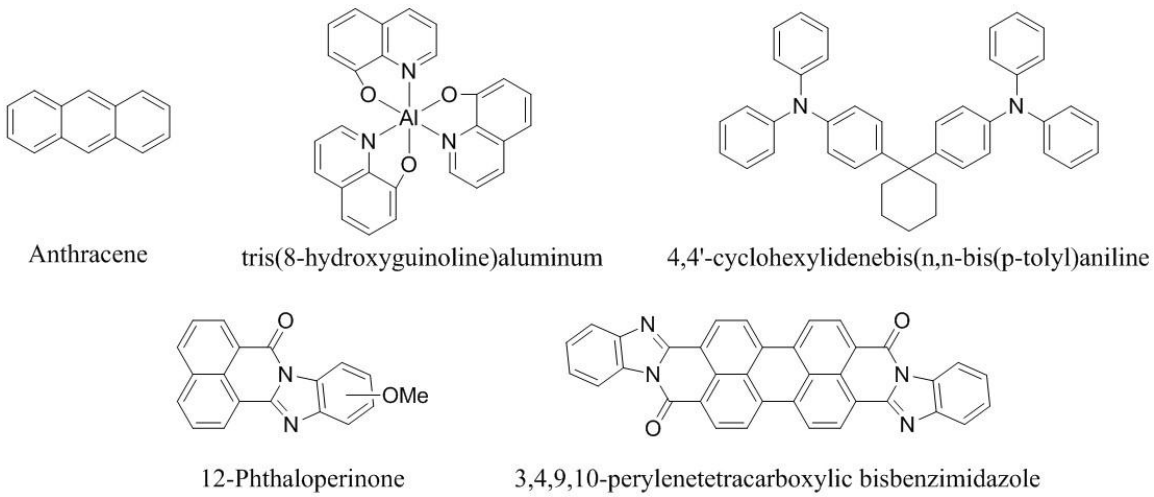

Figure 6 – Structures of the organic compounds used in early OLEDs

1.4.2 "Second-Generation" Phosphorescent Emitters

OLEDs to this point were limited to ca. 25% IQE due to the inability of the fluorescent emitters to harvest the 75% of triplet excitons formed upon charge recombination. The "second-generation" of OLEDs emerged in 1999 when Baldo et al. described a device utilizing an emitter that harvested both singlet and triplet excitons for light emission through rapid intersystem crossing from the singlet state followed by efficient phosphorescence by incorporating 2,3,7,8,12,13,17,18-octaethyl-21H,23H-porphine platinum(II) as the emitting species doped into Alq_3 as the emissive layer.[44]

The photophysics of phosphors can, in some ways, be described analogously to fluorescence. A phosphorescent quantum yield (Φ_{Ph}) describes the yield of triplet excitons that decay radiatively from the triplet state:

$$\Phi_{ph} = \frac{k_{ph}}{k_{ph} + k_{nr}} \tag{13}$$

where k_{ph} is the rate of phosphorescent decay, analogous to the rate of fluorescent decay, and k_{nr} is the sum of the non-radiative rates of decay. Like the fluorescent lifetime, a phosphorescent lifetime, τ_{ph}, can be determined and is defined as:

$$\tau_{ph} = \frac{1}{k_{ph} + k_{nr}} \tag{14}$$

It is important to remember that Φ_{PL} is not equivalent to Φ_{ph} in phosphorescent compounds in the same way as it is to Φ_{fl} in purely fluorescent compounds. The absorption of light is a process that conserves spin and produces only singlet excitons, and so the phosphorescent quantum yield must be multiplied by the yield of triplets through intersystem crossing (Φ_{ISC}) to describe the PLQY. In addition, the rate of phosphorescence cannot be understood through the Strickler-Berg relationship. For a detailed treatment of the photophysics of phosphors, see Baryshnikov et al.[45] As a result, the internal quantum efficiency of an OLED that uses a phosphorescent emitter is modified as follows:

$$IQE = q \times (0.75 + 0.25\Phi_{ISC}) \times \eta_r \tag{15}$$

where q is the phosphorescent efficiency of the emitter in the device with a branching ratio of 3:1 of triplets to singlets.

By incorporating Pt into the organic porphyrin ring of platinum-octaethyl-porphyrin (Figure 7), Baldo et al. were able to increase spin-orbit coupling through the heavy-atom effect, resulting in an increase of the intersystem crossing rate and

concomitant decrease in Φ_{fl},[46] but also a reduction of the phosphorescent lifetime and increase in phosphorescent quantum yield (91 μs and 0.50, respectively) to a level useable in light-emitting devices.[47] While the maximum EQE (EQE_{max}) obtained in these first OLEDs with phosphorescent emitters was on the order of 4%, it showed the possibility of harvesting triplet excitons and converting them to light.

The strategy of doping phosphors into the emissive layer resulted in OLEDs exceeding the ca. 25% IQE, and 5% EQE, limit imposed by purely fluorescent emitters. The first device demonstrating the ability to harvest all of the excitons formed upon charge recombination, by virtue of Φ_{ISC} and Φ_{ph} approaching unity and with IQE approaching 100%, was demonstrated by Adachi et al. in 2001. Using an iridium based emitter, bis(2-phenylpyridine)(acetylacetonate)iridium(III), that demonstrated ca. 100% phosphorescent quantum efficiency, an OLED exhibiting and IQE_{max} of 88%, and an EQE_{max} of 19% was achieved.[48] In the next ten years, highly efficient phosphors utilizing platinum, iridium, osmium, and ruthenium were developed and allowed for red-, green-, and yellow-emitting OLEDs with high efficiency.

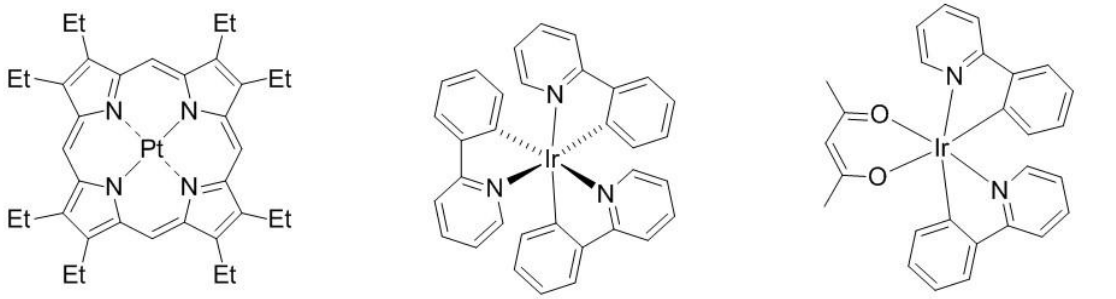

Platinum-2,3,7,8,12,13,17,18-octaethylporphyrin

fac-*tris*-(2-phenylpyridinato-C^2,*N*)iridium(III)

bis(2-phenylpyridinato-C^2, *N*)iridium(acetylacetonate)

Figure 7 – Chemical structure of some organometallic phosphors used in second-generation PhOLEDs.

Despite the generational step forward in terms of device efficiency, the requirement of heavy metals poses significant drawbacks to phosphorescent OLEDs as a technology. Osmium, ruthenium, platinum, and iridium are among the least common elements found in the earth's crust (see Figure 8), placing great financial pressures on any technological application utilizing phosphors that contain these rare elements. Furthermore, molecules exhibiting stable deep blue emission – as required for displays with high color rendering accuracy and coveted for white light applications – remain elusive.[49-51]

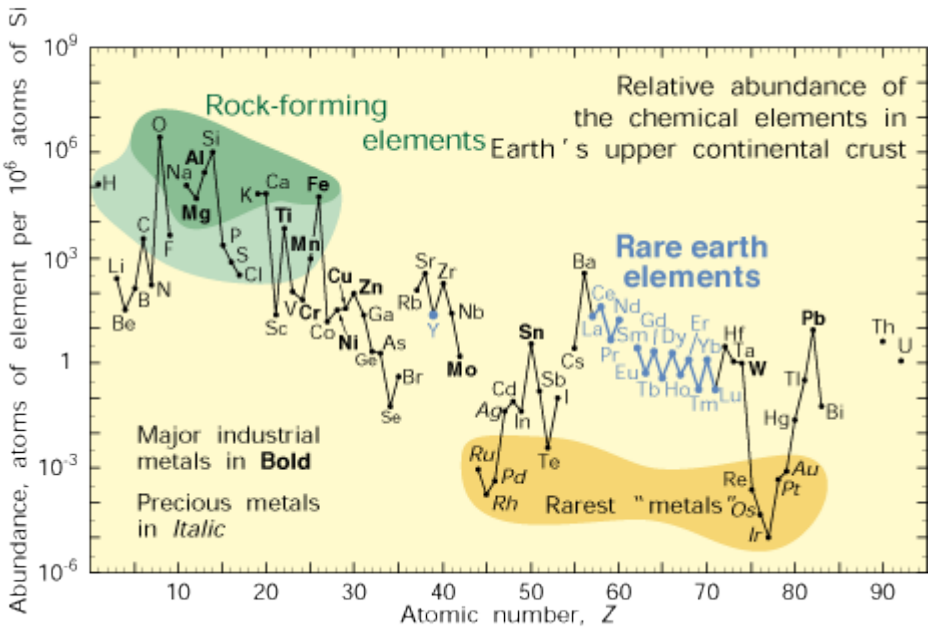

Figure 8 – Relative abundance of elements in the earth's crust. Figure courtesy of the U.S. Geological Survey.

1.4.3 "Third-Generation" Emitters Displaying TADF

One potential solution to the drawbacks of heavy-metal based phosphors while maintaining the high efficiency due to the harvesting of triplet excitons for radiative emission is TADF. In the TADF process, triplet excitons are thermally upconverted into

the singlet manifold, and then radiatively decay through the fluorescence pathway. Emission from this mechanism occurs through the spin-allowed fluorescence pathway, removing the requirement for rare earth metals, while the thermal upconversion of triplet excitons to the singlet manifold still allows for the conversion of triplet excitons to light on a time-scale and with an efficiency usable in an OLED device. Endo et al. were the first to demonstrate TADF in an electroluminescent device in 2009 using Sn-porphyrin complexes, although low efficiencies were obtained.[52]

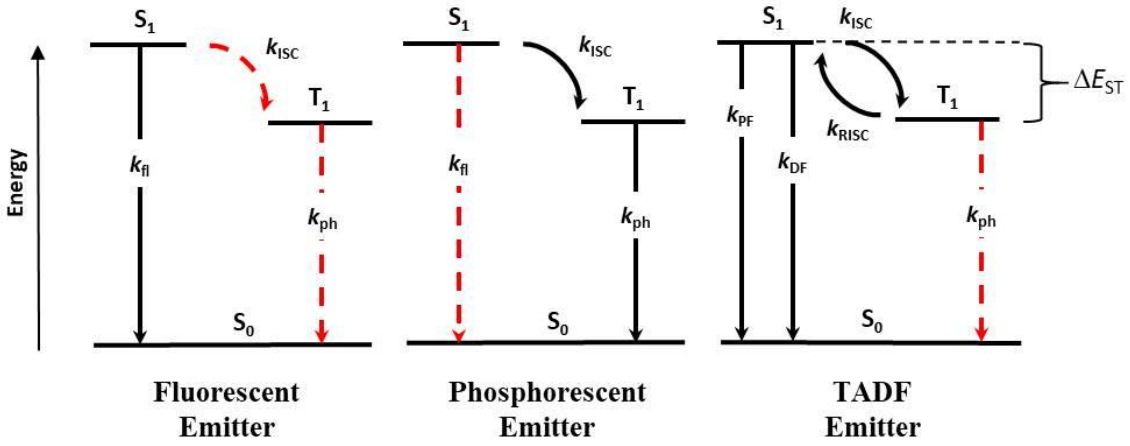

Figure 9 – Simplified Jablonski diagrams of three generations of emitters for OLED devices. Relevant pathways for light generation shown with black arrows.

In 2011, Endo et al. developed a purely organic fluorophore consisting of indolecarbazole electron-donating groups and a triazine electron-accepting group. Devices using the emitter 2-biphenyl-4,6-bis(12-phenylindolo[2,3-a] carbazole-11-yl)-1,3,5-triazine showed modest efficiency (EQE_{max} = 5.3%), but the establishment of design rules for purely organic TADF fluorophores, which will be discussed below, set the stage for further development of the field.[53] Then, in 2012, Uoyama et al. developed a series of series of organic compounds pairing carbazo-9-yl donor moieties with

phthalonitrile acceptors that demonstrated highly efficient TADF. An OLED device with the emissive layer composed of 4,4'-bis(*N*-carbazolyl)-1,1'-biphenyl doped with 1 wt% concentration of the green-blue emitter 2,4,5,6-tetra(9*H*-carbazol-9-yl)isophthalonitrile (4CzIPN) displayed an EQE_{max} of 19% and IQE > 90%, competitive with the state of the art devices using heavy metal containing phosphors, and demonstrating the ability of purely organic "third-generation," fluorescent organic compounds to harvest both singlet and triplet excitons in a highly efficient fashion.[54]

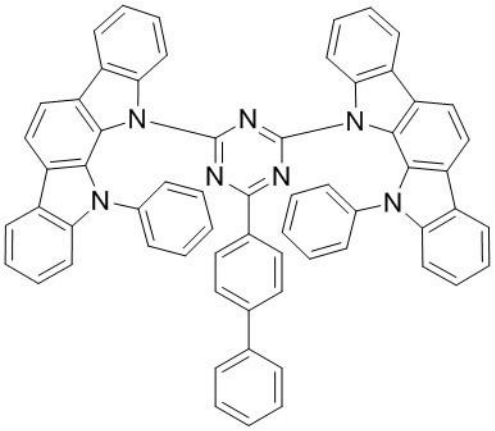

2-biphenyl-4,6-bis(12-phenylindolo [2,3-a]carbazole-11-yl)-1,3,5-triazine

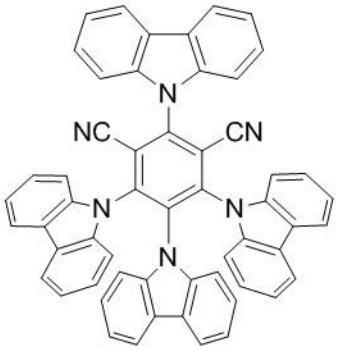

2,4,5,6-tetra(9*H*-carbazol-9-yl)isophthalonitrile

Figure 10 – Early all-organic fluorophores exhibiting thermally activated delated fluorescence.

Today, development of TADF emitters for OLED applications continues apace exploiting excimer[55] and organometallic[56] emitters in addition to purely organic fluorophores.[57] The next chapter will lay the foundation for understanding the TADF process and what physical properties of a molecule are necessary to promote efficient reverse intersystem crossing and, thus, allowing for efficient thermally activated delayed fluorescence.

CHAPTER 2. TADF THEORY AND DESIGN

2.1 Thermally Activated Delayed Fluorescence

Thermally activated delayed fluorescence, sometimes called E-type delayed fluorescence, is a radiative transition that was first observed in eosin.[58-59] Due to the long lifetime, coincident with that of the phosphorescent emission, and similar spectral line shape and energy to the fluorescent emission it was termed "delayed fluorescence." Figure 11 shows the TADF process, wherein an exciton in the triplet state is thermally upconverted to the singlet state via reverse intersystem crossing (RISC), followed by radiative emission through the fluorescent pathway. Due to the comparatively slow rate of the process relative to k_{Fl}, the time-resolved fluorescence spectrum of a compound displaying TADF shows a characteristic biexponential decay composed of a "fast" component and referred to as the prompt fluorescence (PF), and a "slow" component referred to as the delayed fluorescence (DF). Importantly, due to the role of the triplet state, TADF is quenched by molecular oxygen.[60]

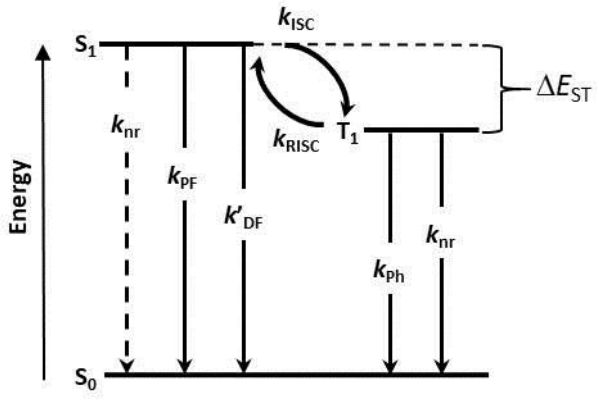

Figure 11 – Jablonksi diagram showing processes of importance in a TADF fluorophore. Prompt fluorescence decay (k_{PF}) is the same process and rate as fluorescent decay (k_{fl}). Delayed fluorescence occurs through the same pathway as prompt fluorescence but is rate limited by the reverse intersystem crossing rate (k_{RISC}), thus the apparent delayed fluorescent rate k'_{DF}. The value ΔE_{ST} is the difference in energy between the lowest energy singlet and lowest energy triplet states.

A second mechanism leading to delayed fluorescence also exists. P-type delayed fluorescence involves the interaction of two molecules in the triplet state through triplet-triplet annihilation (TTA), resulting in one molecule in the ground state and the other in a higher energy state, and if that higher energy state is a singlet state then it can go on to decay radiatively through the fluorescent pathway.

$$^3M^* + {}^3M^* \xrightarrow{TTA} {}^1M + {}^1M^* \qquad (16)$$

$$^1M^* \xrightarrow{k_{fl}} {}^1M + h\nu$$

In an ideal case in which $E(T_2) > 2E(T_1)$, TTA cannot lead to triplet excitons. In most organic compounds, however, S_n states are relatively closely spaced and TTA can occur. In a device in which every two triplet excitons annihilate to yield 1 singlet exciton, and

taking into account the branching ratio of 25% singlets to 75% triplets, a theoretical IQE_{max} is obtained:

$$IQE_{max} \leq q \times \eta_r \times \gamma = q(0.25 + \frac{0.75}{2}) \times \gamma \quad (17)$$

It is evident that with q and γ = 1, a theoretical limit of 62.5%, well below the ca. 100% IQE of devices with phosphorescent emitters, is obtained.[61]

While both E and P-type delayed fluorescent pathways give a similar emission spectrum similar to the prompt fluorescence, the fluorescence from an exciton that never left the singlet manifold, they can be differentiated based on their lifetimes and on their dependence on the concentration of species in the excited triplet state. TADF is a unimolecular process that is independent of exciton concentration, [M*] and the intensity of the emission displays a linear dependence on excitation and a lifetime that matches that of any other process that depopulates the triplet state, such as phosphorescence. TTA, on the other hand, is a bimolecular process with a rate dependent on $[M^*]^2$, thus delayed fluorescence due to TTA displays a quadratic dependence on excitation intensity, and since it removes two excitons from the triplet state and is concentration dependent, a more complicated decay rate.

2.1.1 Other Applications of Compounds Exhibiting TADF

While the large majority of recent interest in compounds exhibiting TADF has been for incorporation as the emitter in OLED devices, other applications have been demonstrated as well. Time-resolved fluorescence imaging is widely used to elucidate the

features of complex biological structures with high resolution by using probes with luminescent lifetimes longer than those of the short-lived background fluorescence and light scattering.[62] Conceptually, the long lifetimes exhibited by delayed fluorescence, which is necessary to differentiate the sensitizer from the background fluorescence in time-resolved imaging, coupled with the lack of toxic heavy metals makes such fluorophores ideal candidates for use as biological probes. Xiong et al. demonstrated this application using a fluorescein derivative in the presence of bovine serum albumin to eliminate triplet oxygen to image cancer MCF-7 cancer cells.[63]

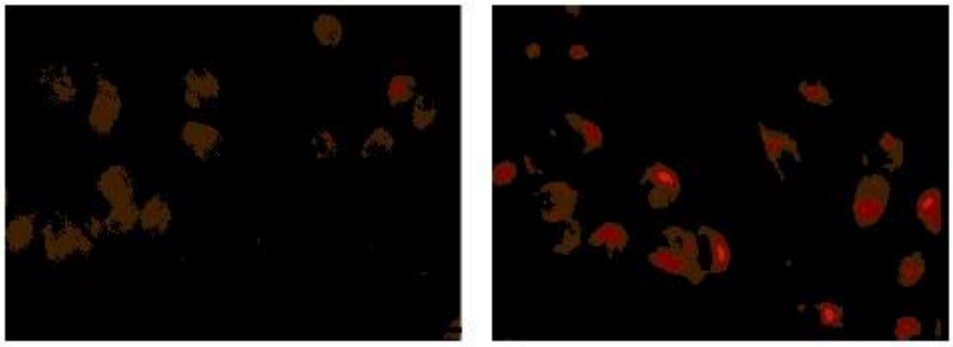

Figure 12 – Steady state luminescence (left) and time-resolved luminescence (right) images of MDF-7 cancer cells stained with a TADF fluorophore. Adapted with permission from Ref. 62. Copyright 2014 American Chemical Society.

In triplet-triplet annihilation upconversion, a low energy photon is absorbed by a "sensitizer," undergoes intersystem crossing into the triplet manifold, is transferred to an annihilator via Dexter transfer, followed by TTA and emission of a higher energy photon than those that were initially absorbed. TADF emitters have been used as the sensitizer to minimize the energy loss in the ISC process and approach the ideal case of emission photons possessing twice the energy of those absorbed.[64-66] While efficiency is still lower than in conventional materials using heavy metals to achieve high spin-orbit coupling,

some of the same factors that enhance TADF enhance the spin-orbit coupling, as will be seen below.

Other reported applications include oxygen sensing,[67] construction of fluorescent micelles,[68] and light emitting electrochemical cells.[69] Fluorophores displaying simultaneous TADF and mechanoluminesce,[70] and mechanochromism[71] have been reported (Figure 13), potentially opening additional applications as well.

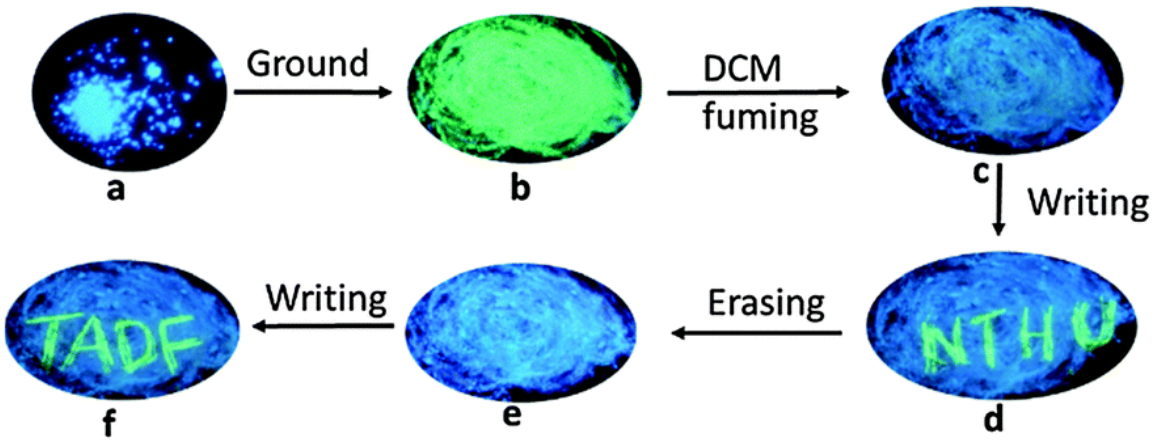

Figure 13 – Demonstration of "erasable" mechanochromism in a TADF compound highly luminescent in the solid state. Reproduced from Ref. 68 with permission from The Royal Society of Chemistry.[72]

2.2 Photophysics of Thermally Activated Delayed Fluorescence

Rationalizing the properties of fluorophores that exhibit thermally activated delayed fluorescence requires additional photophysical parameters besides those required to understand purely fluorescent or phosphorescent emitters. After excitation by absorption of light, a TADF emitter initially will undergo the same photophysical processes as a standard fluorophore. From the triplets formed through intersystem

crossing (Φ_{ISC}), some percentage will undergo RISC (Φ_{RISC}) to depopulate the triplet state back into the singlet. From there, they may emit through the fluorescent pathway, relax non-radiatively, or again undergo intersystem crossing. In this way, excitons can be recycled through the singlet and triplet state until they relax back to the ground state through radiative or non-radiative processes. Excitons that are upconverted to the singlet state through RISC and then emit radiatively via fluorescence undergo delayed fluorescence. The total fluorescent quantum yield of an emitter that displays TADF is simply a sum of the prompt and delayed fluorescence quantum yields:

$$\Phi_{fl} = \Phi_{PF} + \Phi_{DF} \tag{18}$$

where Φ_{PF} and Φ_{DF} are the fluorescence quantum yield of the prompt and delayed fluorescence, respectively. This can be expressed as a product of the prompt fluorescent quantum yield and a term that includes the ISC and RISC efficiencies:[73]

$$\Phi_{fl} = \Phi_{PF} \frac{1}{1 - \Phi_{ISC}\Phi_{RISC}} \tag{19}$$

This equation illustrates two aspects of TADF emission of import. First, the total quantum yield will always be somewhat dependent on Φ_{PF} as the ultimate decay pathway, and as the efficiency of the process approaches 0, the total quantum yield follows. Second, high intersystem crossing efficiency is not detrimental to efficiency in compounds that display TADF in the same way as it is in purely fluorescent compounds, as long as the RISC efficiency is also high.

2.2.1 The Reverse Intersystem Crossing Rate

RISC is the key process in TADF and, as a thermally activated process, it displays a temperature dependence given by the Arrhenius equation:

$$k = Ae^{-\frac{E_a}{k_B T}} \tag{20}$$

where k is the rate of the process, E_a is the activation energy, $k_B T$ is the thermal energy, and A is a pre-exponential factor. For RISC, the activation energy is estimated by the difference in energy between the lowest energy singlet and lowest energy triplet states and is denoted as the ΔE_{ST}. The exponential decrease in RISC rate as ΔE_{ST} increases places a high importance on the minimization of the barrier, a requirement that has largely dominated the early years of TADF fluorophore design.

The true theoretical framework for the reverse intersystem crossing rate was not initially well understood, and in some studies the adiabatic ΔE_{ST} was assumed to be the only physical property of the fluorophore controlling k_{RISC}, which is not the case. Ward et al. synthesized a series of phenothiazine-dibenzothiophene-*S*,*S*-dioxide fluorophores with similar ΔE_{ST} values that, when dispersed in a film, favored phosphorescence over TADF as steric hindrance around the bond between the donor and acceptor groups hindered rotation (see Figure 14).[74] This result suggested coupling to vibrational and/or rotational modes facilitated RISC. Gibson et al. explained this observation as nonadiabatic, vibronic coupling between the lowest locally excited triplet state (^{3}LE) and the lowest charge-transfer triplet state (^{3}CT) facilitating second-order coupling effects between the CT triplet and singlet states.[75-76]

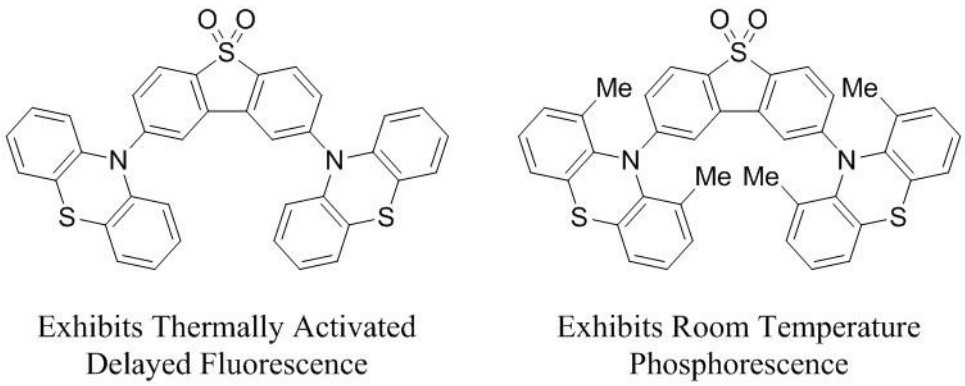

Figure 14 – Phenothiazine-dibenzothiophene-*S,S*-dioxide fluorophores favoring TADF or phosphorescence ad a function of steric hinderance to rotation about *C-N* bond.

Etherington et al. physically demonstrated the importance of the vibronic coupling between the ^{3}LE and ^{3}CT states by dispersing the fluorophore (2,8-di(10H-phenothiazin-10-yl)dibenzo[b,d]thiophene 5,5-dioxide) into a hosts with a range of polarities. Due to their relatively large excited state dipoles, intramolecular charge-transfer states are more highly stabilized in a polar medium than locally excited states. The fluorophore Etherington selected contained ^{3}LE and ^{3}CT states quite close in energy, and by modulating the dielectric constant of the material the difference between the two energies could be increased and decreases. It was shown that the k_{RISC} reached a maximum when the energy barrier of internal conversion between the ^{3}LE and ^{3}CT was at a minimum, that is to say when the vibrational levels in the respective states were equal in energy.[77] While these observations give guidelines for the design of fluorophores exhibiting TADF, a full mathematical treatment is beyond the scope of this thesis. For completeness sake, a description of k_{RISC} using Marcus theory, under the Marcus-Levich-Jortner formulation is as follows:[78]

$$k_{RISC} = \frac{2\pi}{\hbar} |\langle S_1|\hat{H}_{SO}|T_1\rangle|^2 \frac{1}{\sqrt{4\pi\lambda_M k_B T}} \sum_{n=0}^{\infty} e^{-S} \frac{S^n}{n!} exp\left[-\frac{\left(\Delta E_{ST} + \lambda_M + n\hbar\omega_{eff}\right)^2}{4\lambda_M k_B T}\right] \quad (21)$$

where $\langle S_1|\hat{H}_{SO}|T_1\rangle$ is the spin-orbit coupling matrix element between the lowest energy singlet and triplet states, λ_M is the Marcus reorganization energy, $\hbar\omega_{eff}$ is the effective energy of a mode of the relevant non-classical high-frequency intramolecular vibrations, and S is the effective Huang-Rhys factor of the mode. The importance of this equation adds is that it adds the spin-orbit coupling term.

To account for the vibronic coupling between the T_1 and T_2 states, in a framework where the ^{3}LE facilitates the RISC step through spin-orbit coupling to the S_1 state, a further second-order perturbation theory derived equation is required. The salient lesson for fluorophore design is that a one must minimize energy difference between the lowest energy ^{3}CT and ^{3}LE states to maximize vibronic coupling and increase k_{RISC}.[76] For a more detailed explanation of the theory behind reverse intersystem crossing refer to Penfold et al.[79] and Chen et al.[80] Overall, it is important to keep in mind that both minimizing the ΔE_{ST} *and* considering the energy of the localized excited states on the donor and acceptor are necessary for fast RISC and, thus, highly efficient TADF.

2.3 Designing TADF Emitters

Rational design of compounds that exhibit strong TADF for application as the emitter in OLEDs requires connecting the theoretical concepts laid out above with physical concepts under a series of design rules that will be laid out below. First, one must understand what gives rise to the energy of the relevant states in the emitter.

Quantum mechanically, for a simple two-electron two-state model corresponding to an electronic transition between the HOMO and LUMO orbitals, the energy of the lowest energy singlet (E_{S_1}) and triplet (E_{T_1}) states can be written as:[81]

$$E_{S_1} = E_H + E_L + J_{HL} + K_{HL}$$
$$E_{T_1} = E_H + E_L + J_{HL} - K_{HL} \quad (22)$$

where E_H and E_L are the one electron energies of the HOMO and LUMO orbitals, respectively, J_{HL} is the Coulomb integral and corresponds to the repulsion between the negatively charged electrons in the HOMO and LUMO, and K_{HL} is the exchange integral and corresponds to the exchange energy between the electrons in the HOMO and LUMO orbitals. The energies of the two states are the same except for the exchange integral, K, that destabilizes the singlet state and stabilizes the triplet state. Within the framework of the assumptions used in Eqn. 22 and for singlet and triplet states with a similar orbital description, the ΔE_{ST} can be described by:

$$\Delta E_{ST} = 2K_{HL} \quad (23)$$

It is evident that the ΔE_{ST} of a system can be exchanged by minimizing the electron exchange integral. The exchange integral itself is given by:

$$K_{HL} = \iint \psi_H(r_1)\psi_L(r_2)\left(\frac{e^2}{r_1 - r_2}\right)\psi_H(r_2)\psi_L(r_1)\, dr_1 dr_2 \quad (24)$$

where ψ_H and ψ_L are the electronic wavefunctions of the HOMO and LUMO, respectively, and e is the charge on the electron. The value of K can therefore be decreased, to an approximation, by decreasing the spatial overlap between the HOMO and LUMO wavefunctions, and by decreasing the integral where they do overlap by twisting orbitals out of plane of one another.[82]

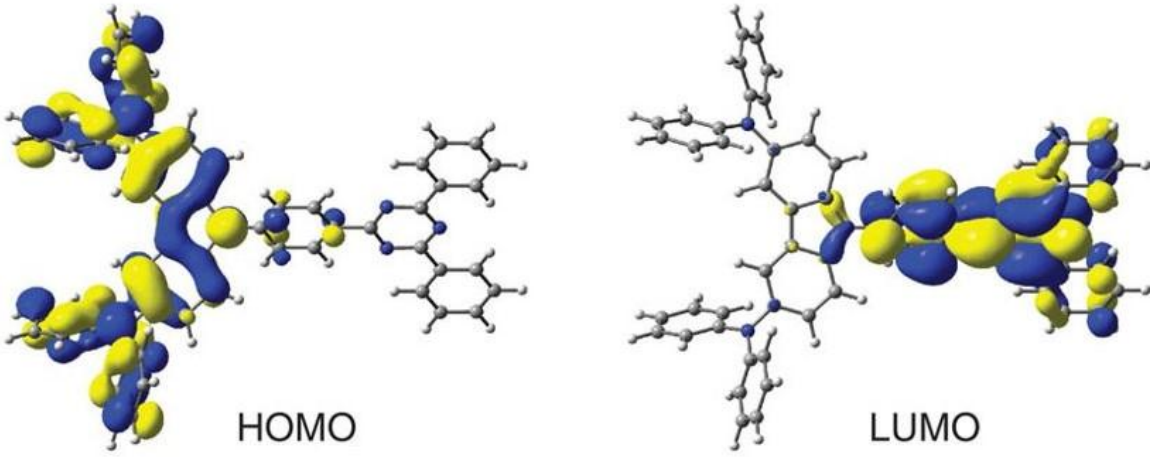

Figure 15 – Representative donor-acceptor fluorophore with TD-DFT (PBE0-6-31G(d) basis set) calculated HOMO and LUMO well confined to the donor and acceptor moieties, respectively. Copyright 2012, John Wiley and Sons, CC BY 4.0.[83]

This is the approach exploited by Adachi in the early papers showing the possibility of harvesting triplet excitons using TADF. By separating the HOMO and LUMO onto electron donor and electron acceptor moieties, respectively, the orbitals can potentially be well contained onto disparate parts of the molecule and limit the orbital overlap responsible for the exchange energy, which can be further decreased by twisting the donor and acceptor out of plane of one another. Specific applications of the idea include highly hindered donor acceptor systems,[53] π-bridged donor-acceptor compounds,[54] and donors connected to acceptors through spiro linkages.[84]

It is important to note that decreased overlap of the HOMO and LUMO also decreases the transition dipole moment between the orbitals for the HOMO-LUMO transition (μ_{HL}), as shown in Equation 7, and can be detrimental to the fluorescent decay rate of the fluorophore. A balance between these two important values must be struck. One approach was described by Hirata et al., and takes into account the differences between the exchange integral and μ_{HL}. Due to the way the exchange integral is inversely proportional to the position vector (Equation 1.24), while the transition dipole moment is linearly proportional to the position vector; if orbital overlap remains constant then as the distance of the overlap from the origin increases, ΔE_{ST} decreases and μ_{HL} increases.[85] Physically, this corresponds to increasing the delocalization of one or both of the relevant orbitals over a larger space where it does not appreciably overlap with the other orbital.

The limitation of Adachi's approach lies in the assumption that both the lowest energy singlet and triplet state are both well described as a HOMO-LUMO transition, which is only true for green, yellow, and red emitting compounds composed of donors and acceptors with high energy locally excited (LE) triplet states.[86] However, the π-π* HOMO-LUMO transition of the isolated components of a D-A compound tend to have very high spatial orbital overlap and corresponding high exchange energies. From a physical perspective, if the CT state of the D-A compound is not sufficiently low in energy then the triplet of the LE π-π* can be stabilized below that of the triplet CT state (see Figure 16). In this situation, the ΔE_{ST} is not approximated by $2K$, and Adachi's design rules fail.

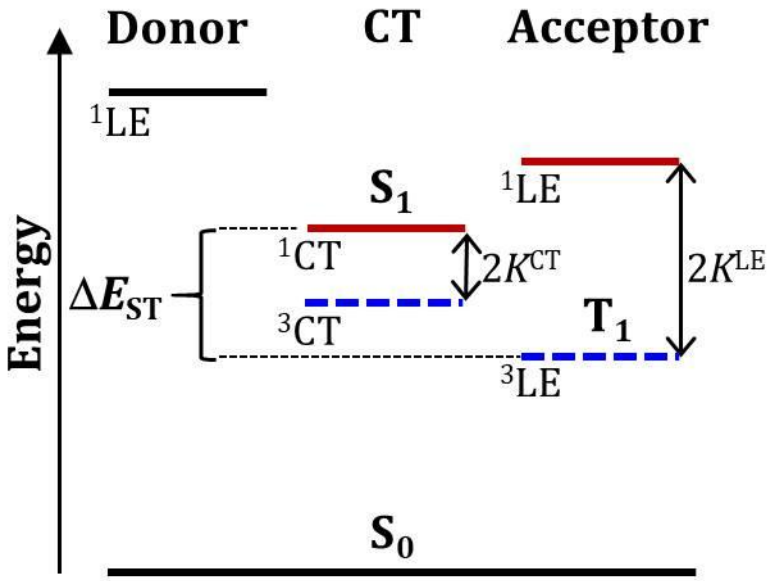

Figure 16 – Hypothetical energy level diagram of a donor-acceptor compound. The S_1 is an intramolecular CT transition from HOMO to LUMO, and the ^{3}CT is lower in energy by twice the exchange integral of the orbitals involved in the CT (K^{CT}). The increased energy of the exchange integral of the LE state (K^{LE}) on the acceptor, due to high spatial overlap, stabilizes ^{3}LE such that the transition is lower in energy than ^{3}CT and, consequently, is the T_1 state.

This idea was given a theoretical framework after Penfold noted that the ΔE_{ST} of a compound often seems to have a dependence on the energy difference between the HOMO and the LUMO, and not simply on the overlap.[87] Lee and Kim pointed out that in systems where the LE and CT states are close in energy, the associated transition displays character from both configurations, there is a mixing of CT and LE states to describe the true transition.[88] For the high energy states associated with blue emission energies in which the singlet state is well described by a HOMO to LUMO CT transition, the LE triplet states are closer in energy to the CT triplet states and substantial mixing can occur. Due to the stabilization provided by the exchange energy in triplet systems, it is energetically favorable for the hybrid CT/LE of the triplet state to show more LE character than that of the singlet state, where the exchange energy destabilizes the state.

Consequently, the configurations of the singlet and triplet state are often different, and the ΔE_{ST} is therefore higher than predicted by the simple $2K_{HL}$ approximation.

While the mixing of the LE and CT triplet states poses a limitation, it also points the way towards better design rules for TADF fluorophores. While an increase in ΔE_{ST} is problematic, differences in the orbital nature of the singlet and triplet states can actually increase the energy spin-orbit coupling matrix element and, thus, the reverse intersystem crossing rate consistent with El-Sayed's rules. Since the ΔE_{ST} of a CT transition is generally small, a careful balancing of the charge transfer singlet energy and the locally excited triplet energy should lead in a compound with a minimized ΔE_{ST} and simultaneously a high SOC, and result in fast RISC as shown in Equation 21.[78]

2.4 Characterization of TADF Emitters

The complexity of the interplay of orbitals on the RISC rates of molecules and the sensitivity of these rates to very small changes in energies means that synthesizing new compounds and measuring their properties directly is the most successful method for identifying high performing fluorophores for TADF applications. Novel compounds are characterized in the following ways to screen for their applicability as emitters.

2.4.1 Absorption and Emission Spectra

Simple absorption and emission spectra are used for determining the relative energies of the absorption and the fluorescent and phosphorescent transitions. Emitter color is, to a first approximation, determined by the energy difference between the upper and lower states of the radiative transition by:

$$\lambda_{em} = \frac{hc}{E} \tag{25}$$

where h is Planck's constant, c is the speed of light and E is the energy of the transition. Due to the requirement of blue, green, and red emitting OLEDs for displays, and the addition of yellow for white-light OLEDs, controlling the emission color is of utmost importance for emitter application.[89]

Estimating ΔE_{ST} requires estimates of the S_1 and T_1 energies, which is usually achieved by measuring the fluorescent emission and the phosphorescent emission. Figure 17 shows the photoluminescence of a hypothetical compound as a function of time. Phosphorescence is not, in general, observed in organic compounds at room temperature. This is due to the spin-disallowed transitions of intersystem crossing and phosphorescence both being slow in comparison to the spin-allowed relaxation pathways that compete, including fluorescence and vibrational relaxation. Importantly, the singlet state will be fully depopulated by these pathways before the metastable triplet state fully decays. Furthermore, by holding the sample at cryogenic temperatures, most commonly in a liquid nitrogen bath at 77 K, vibrational and collisional relaxation pathways that out-compete the phosphorescent emission can be suppressed. By taking an emission spectrum using a flash lamp and introducing a delay between the excitation pulse and the collection of emission data on the range of μs to ms, and while holding the sample at cryogenic temperatures, a phosphorescence spectrum can be collected without the strong fluorescence emission dominating the spectrum or the non-radiative decay pathways extinguishing the emission.

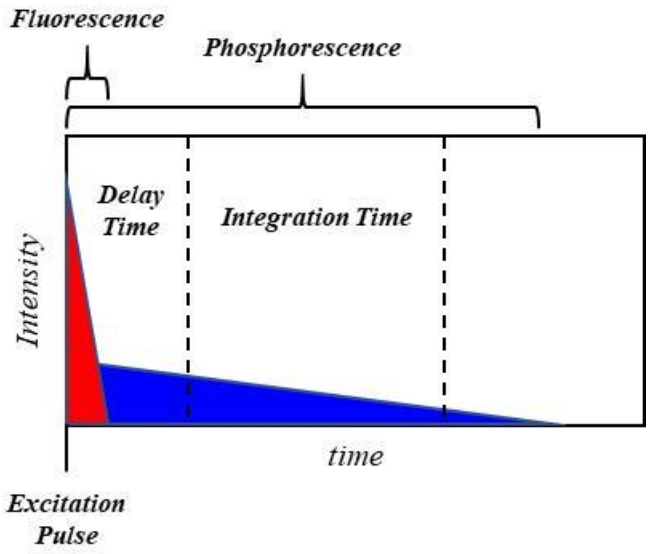

Figure 17 – Photoluminescence of a hypothetical organic compound as a function of time after excitation by a flash of light with an infinitesimally narrow pulse width. After excitation, strong prompt fluorescence (red) dominates the emission. After the S_1 state is fully depopulated, slower, weaker phosphorescent emission remains and continues to decrease as a function of time. By introducing a "delay time" after excitation, only the phosphorescent signal can be integrated, which is plotted as a function of wavelength to obtain the phosphorescence spectrum. This ignores any potential delayed fluorescent emission.

An additional note should be added for compounds with low ΔE_{ST} that display TADF. While TADF and phosphorescence both depopulate the triplet state on the same time-scale, distinguishing between the two as a practical matter is usually not an issue. The TADF spectrum occurs from the singlet manifold and is superimposable with the prompt fluorescent emission, while the phosphorescence originates in the lower energy triplet manifold and will have a red shifted emission profile and, potentially, a different line shape. As a thermally activated process, RISC (and therefore TADF) is slower at lower temperatures whereas phosphorescence, being a spontaneous emission, is not and is in fact enhanced for the reasons discussed above. Furthermore, while the luminescent lifetimes of the two processes are entwined, the intensities are not. As a practical matter,

at cryogenic temperatures the thermally activated delayed fluorescent process is largely suppressed and phosphorescence dominates. At room temperature, RISC rates in compounds that exhibit TADF tend to be faster than phosphorescent rates and TADF dominates. In compounds that display the lowest ΔE_{ST} values, the fluorescent emission and the phosphorescent emission are practically superimposed, and in these cases it may be more difficult to assign with confidence what arises from TADF and what arises from phosphorescence.

2.4.2 Determining the ΔE_{ST}

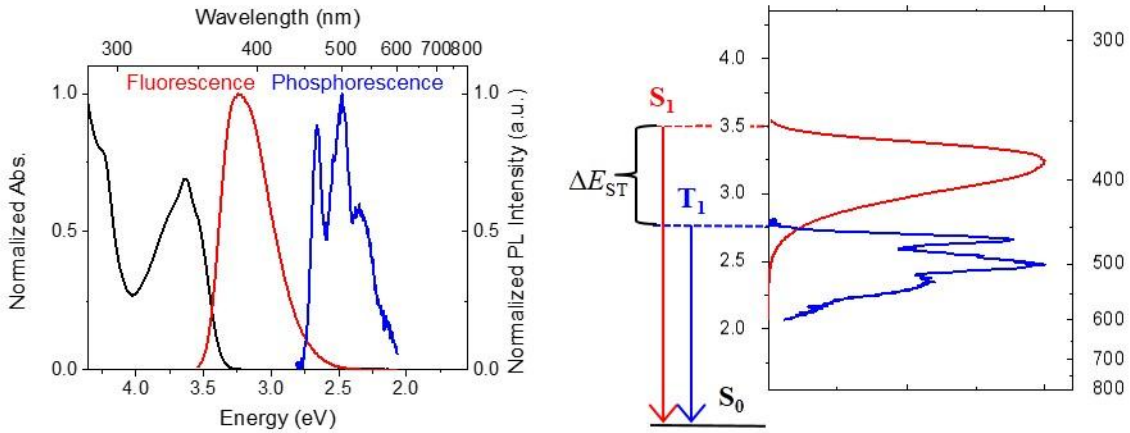

Figure 18 – (*left*) Normalized absorption, and photoluminescence spectra of an organic fluorophore plotted against energy. Room temperature photoluminescence is attributed to fluorescence (red), and photoluminescence in a frozen matrix at 77 K with a 500 µs delay of detection after excitation is attributed to phosphorescence (blue). (*right*) Using the high energy onset of the fluorescent and phosphorescent emission spectra to estimate the adiabatic singlet-triplet energy gap, the ΔE_{ST} is the difference in energy between the onset of fluorescence and the onset of phosphorescence, referenced against the ground state of the molecule as zero.

The ΔE_{ST} of a compound is generally determined in one of two ways. For the majority of new emitters, the ΔE_{ST} is estimated from the high-energy onset of the steady-state fluorescence and phosphorescent emission spectra, as shown in Figure 18. Since this value comes from the optical spectra, this is an adiabatic gap.

A more direct way to approximate the ΔE_{ST} gap is to determine the activation energy, E_a, for the reverse intersystem crossing rate (k_{RISC}) using the Arrhenius equation:

$$\ln(k_{RISC}) = \ln(A) - \frac{\Delta E_{ST}}{k_B}\left(\frac{1}{T}\right) \tag{26}$$

The determination of k_{RISC} for such a plot is not trivial, but is estimated by the following relationship:[73]

$$k_{RISC} = \frac{1}{\tau_{DF}\Phi_{ISC}}\frac{\Phi_{DF}}{\Phi_{PF}} \tag{27}$$

where τ_{DF} is lifetime of delayed fluorescence, and Φ_{ISC} is the triplet yield through intersystem crossing. Analysis of Equation 1.19 shows that when $\Phi_{DF}/\Phi_{PF} \geq 4$, Φ_{RISC} can be approximated to 1, and Φ_{ISC} can be determined by:

$$\Phi_{ISC} = \frac{\Phi_{DF}}{\Phi_{PF} + \Phi_{DF}} \tag{28}$$

If this is not the case, approximations must be made. One common approximation is assuming that internal conversion to the ground state is negligible and singlet excitons

undergo either fluorescent emission or intersystem crossing. Under this assumption, and in the absence of photochemistry, Φ_{ISC} is approximated by:

$$\Phi_{ISC} = 1 - \Phi_{PF} \tag{29}$$

As emission energy of fluorescence decreases, this approximation becomes less and less valid, according to the energy gap law, which states that non-radiative relaxation undergoes an exponential decrease in rate as the energy gap between the initial and final states increases.[90]

2.4.3 Photoluminescent Quantum Yield

The PLQY and lifetime are perhaps the two most important quantities for understanding the photophysics of a fluorophores. PLQY is a key parameter not only because of its role in many of the equations above, but also because of its relationship with q in determining the efficiency of an OLED device. As stated above, the PLQY is the ratio of photons emitted to photons absorbed after photoexcitation. There are two accepted methods for determining PLQY, relative and absolute quantum yield. All of the following discussion assumes a corrected spectrum that gives photonic output (i.e. photon flux) instead of the instrument response (generally a radiometric quantity).[91]

Relative quantum yield method for determining PLQY involves the comparison of the fluorescence of an analyte to that of a standard with known and accepted quantum yield. Relative quantum yield is performed on a standard fluorometer with 90° geometry where only a fraction of light emitted towards the detector. The determination is performed by collecting a series of steady-state fluorescence emission spectra, of both the

analyte and the standard, with absorbance at and above the excitation wavelength of 0.02-0.05 to minimize the inner filter effect and reabsorption losses. All spectra must be taken with identical instrument settings, including excitation wavelength, excitation and emission monochromator slit widths, scan speed, integration time, etc. The integrated intensity of the emission spectra are plotted vs. the absorption of the solution to yield a straight line with intercept at zero. The slopes of the lines of best fit for the analyte and standard are then used in the following equation to determine the PLQY of the analyte (Φ_A):

$$\Phi_A = \Phi_{std}\left(\frac{M_A}{M_{std}}\right)\left(\frac{\eta_A^2}{\eta_{std}^2}\right) \tag{30}$$

where Φ_{std} is the PLQY of the standard, M_A and M_{std} are the slopes obtained from the plot of integrated intensity vs. absorbance, and η_A and η_{std} are the refractive indices of the solvents in which the analyte and standard are dissolved, respectively. This technique is only valid for samples that do not exhibit fluorescence anisotropy, and as such is not applicable for thin films or powders.

Absolute quantum yield determinations are not limited by anisotropic emission and are obtained by a single measurement (plus a blank) making it in many ways preferable to a relative quantum yield determination. It does, however, require the use of an integrating sphere to collect all the light; transmitted, scattered, reflected, and emitted. Absolute PLQY is required for scattering samples such as powders and the films used to assess the performance of an emitter doped into a host.[92]

The determination itself is best performed on a sample with Abs. ≤ 0.05 and involves the collection of a spectrum that includes both the excitation wavelength and the entirety of the emission band of the analyte. Corrected spectra are divided into "absorption" and "emission" bands (see Figure 19), and the difference between the integrated intensity of these bands for the blank and analyte spectra give the PLQY as follows:

$$\Phi_{fl} = \frac{\int_{\lambda_{em}}^{\lambda_{em}} \left(F_A(\lambda) - F_B(\lambda)\right) d\lambda}{\int_{\lambda_{abs}}^{\lambda_{abs}} \left(F_B(\lambda) - F_A(\lambda)\right) d\,\lambda} \tag{31}$$

Where F_A and F_B are the spectra of the analyte and the blank, respectively, the difference of which are integrated over the emission bands and the absorption bands to directly measure the ratio of photons emitted to photons absorbed. Photon numbers determined in this way are referred to as relative photon numbers. The emergence of standalone commercial spectrometers for absolute PLQY determinations are working to make this technique more common and accessible than in the past.[93]

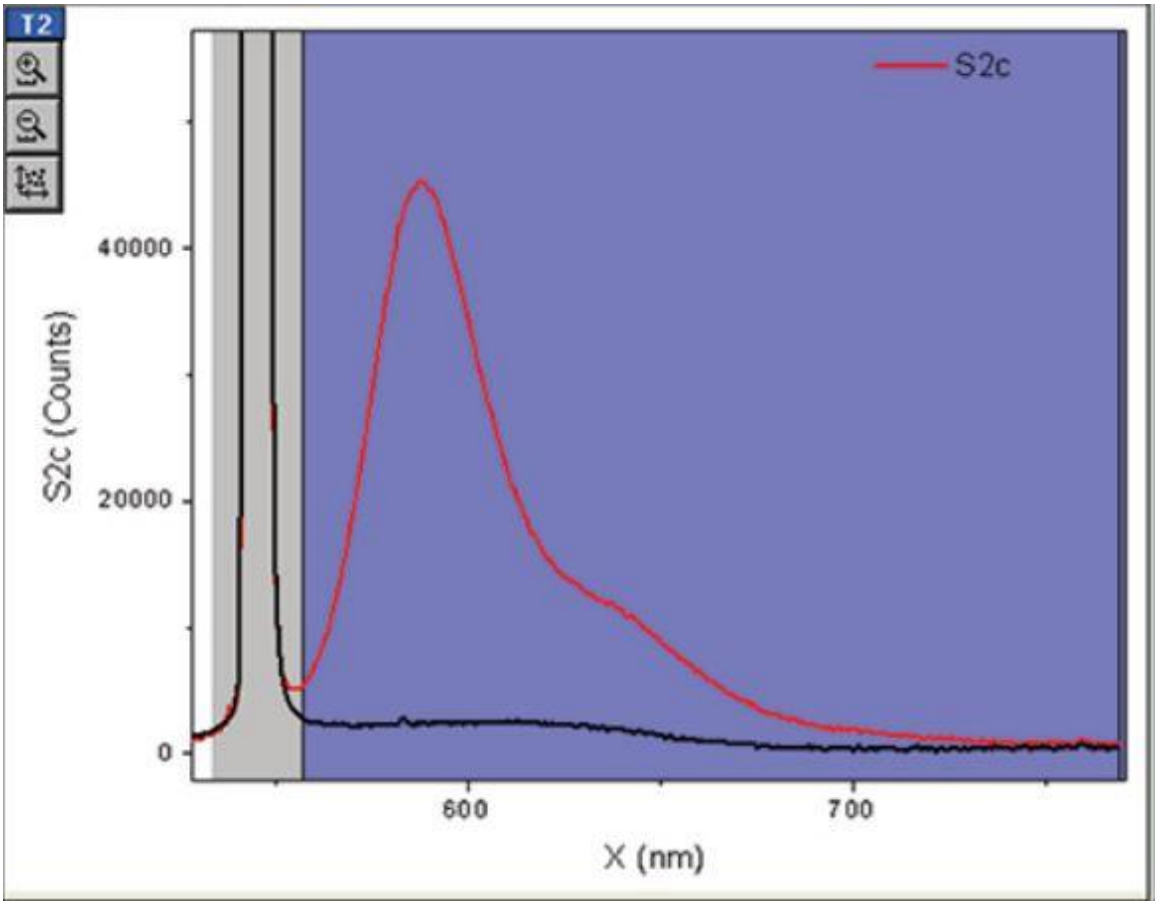

Figure 19 – Emission spectra of a blank (black) and analyte solution (red) collected in an integrating sphere. Absorption region for PLQY purposes shaded in gray, emission region shaded in purple.

2.4.4 Fluorescence Lifetime

The fluorescent lifetime (τ_{fl}) relates to the PLQY as was discussed in CHAPTER 1, and can be used in conjunction with the PLQY to determine the rate of fluorescence:

$$k_{fl} = \frac{\Phi_{fl}}{\tau_{fl}} \tag{32}$$

Practically, the fluorescence lifetime is determined in the time domain by using time-correlated single photon counting (TCSPC). The principle of TCSPC is that photons

arriving at a detector are correlated against an excitation pulse and plotted as a function of time against the excitation. By repeating the process many times, an intensity vs. time histogram showing the decay of the species of interest can be constructed. The shape of the histogram corresponds to the decay of the fluorophore as a function of time.

If a collection of fluorophores that follow a monoexponential decay is excited by an infinitesimally short pulse of light, an initial population of fluorophores in the excited state (n_0) will decay as a function of time that depends on the decay rates k_{fl} and k_{nr}:

$$\frac{dn}{dt} = \left(k_{fl} + k_{nr}\right)n(t) \tag{33}$$

where n(t) is the number of molecules excited at time t after the excitation. As was stated earlier, τ_{fl} is the inverse of the sum the rate constants for all of the decay pathways. In an experiment, the number of molecules excited is not observed, but instead fluorescent intensity (I) is, and thus the solution to Equation 33 is the exponential decay that is collected in the TCSPC experiment:

$$I(t) = I_0 exp\left(\frac{-t}{\tau_{fl}}\right) \tag{34}$$

where I_0 and I(t) is the fluorescence intensity at time 0 and at time t, respectively.[94]

For systems involving multiexponential decays, including mixtures of fluorophores or fluorophores with multiple independent decay pathways (such as in the case of TADF), the following function is fit to the data:

$$I(t) = \sum_i \alpha_i \exp\left(\frac{-t}{\tau_i}\right) \quad (35)$$

where the sum of all α is normalized to unity.[94] When the biexponential being fit is prompt fluorescence and delayed fluorescence, the resulting τ_1 and τ_2 correspond to τ_{PF} and τ_{DF}. The delayed fluorescent lifetime plays an important role in device roll-off when the fluorophore is incorporated into an emitter.[95] When characterizing TADF fluorophores, the ability of oxygen to quench triplets must be considered.

CHAPTER 3. STRUCTURE-PROPERTY RELATIONSHIPS GIVING RISE TO THERMALLY ACTIVATED DELAYED FLUORESCENCE IN DONOR-ACCEPTOR FLUOROPHORES COMPRISED OF 2,5-DIPHENYL-1,3,4-OXADIAZOLE AND 9*H*-CARBAZOLE

3.1 Introduction

In this chapter, a systematic study of the structure-property relationships of donor-acceptor compounds, comprised of 2,5-diphenyl-1,3,4-oxadiazole acceptor with carbazol-9-yl donor moieties, will be presented. Specific attention will be paid to the role of regiochemistry in simple carbazole-oxadiaozle compounds, along with strategies for modifying the donor and acceptor strengths of the constituents. The effects of these modifications on several physical properties key to the TADF process will be examined, including singlet and triplet state energies and the resulting ΔE_{ST} values, photoluminescent quantum yields, and fluorescent decay rates. Insights into the physical nature of the important excited states will be exploited to develop specific design rules for constructing DPO based fluorophores that exhibit efficient TADF. As a proof of concept, part two of this chapter will feature the design and syntheses of compounds exploiting the design rules that were established in part one, and in some cases will be incorporated into OLEDs to demonstrate the applicability as TADF emitters.

3.1.1 2,5-Diphenyl-1,3,4-oxadiazole Compounds Displaying TADF

The molecule 2,5-diphenyl-1,4,5-oxadiazole (DPO) is known for its high thermal stability and photoluminescent quantum yield and, along with its ability to be readily modified to create a diverse set of derivatives, has been widely exploited as an electron-transport materials in OLEDs.[96-101] The electron deficiency of this moiety has been utilized by incorporating DPO as the acceptor into bipolar donor-acceptor hosts for phosphorescent emitters in OLED devices,[102-104] including in combination with the ubiquitous carbazo-9-yl (Cz) donor in both molecular compounds and polymers.[102-103, 105-107] Furthermore, Cz-DPO D-A compounds have themselves been exploited as tunable emitters in conventional fluorescent OLEDs.[108-112] Hence, the use of DPO as the acceptor moiety in donor acceptor compounds might be expected to be well explored. This usage, however, has been limited to this point.

To date, DPO has been generally been paired with relatively strong electron donors resulting in devices with emission in the blue-green to yellow-green range. Zhang et al. reported the compound 2-[4-(5-phenyl-5,10-dihydrophenazine)phenyl]-5-phenyl-1,3,4-oxadiazole (Figure 20a) that the displayed an emission maximum 577 with Φ_{fl} of 0.12 in deoxygenated toluene solution (Φ_{PF} and Φ_{DF} of 0.08 and 0.04, respectively). A device incorporating the emitter displayed an EQE_{max} of ca. 10%.[113] Donor-acceptor and donor-acceptor donor compounds pairing DPO with phenoxazine were reported by Lee et al. (Figure 20b) that displayed emission maxima of 495 and 502 nm, respectively. A device incorporating 2,5-bis(4-(10*H*-phenoxazin-10-yl)phenyl)-1,3,4-oxadiazole as the emitter displayed an EQE_{max} of 14.9%.[114] Luo et al. incorporated the 10-(4-(5-phenyl-1,3,4-oxadiazol-2-yl)phenyl)-10*H*-phenoxazine (Figure 20c) donor-acceptor fluorophore

as a sidechain into a copolymer to use in the emissive layer of polymer OLEDs.[115] Depending upon the ratio of fluorophore containing monomers in the polymer, device emission maxima ranged from 478-506 nm with EQE_{max} increasing in concert with the wavelength from 1.2-4.3%.[116]

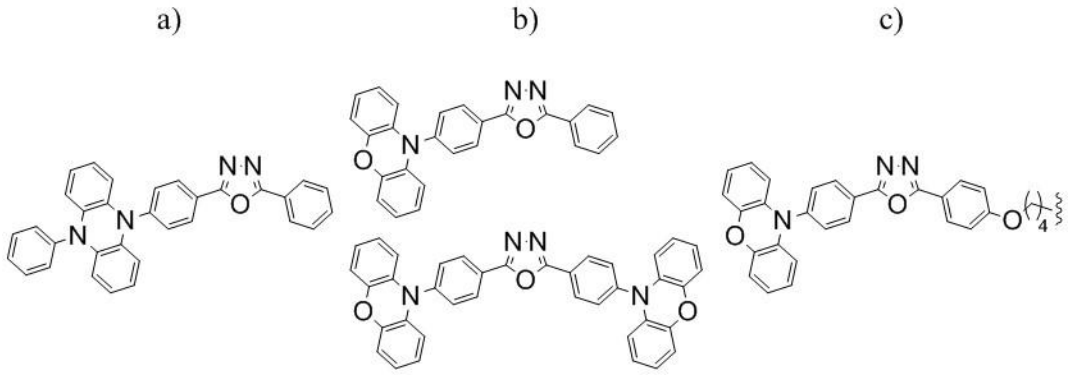

Figure 20 – Previously reported fluorophores containing 2,5-diphenyl-1,3,4-oxadiazole that display thermally activated delayed fluorescence.

Carbazole was chosen as the electron donor moiety as a ubiquitous, electron-rich component of organic optoelectronic materials.[117] Carbazole is an attractive functionality for TADF applications due to its good thermal stability and high triplet energy of ca. 3.0 eV.[118] Despite the common use of Cz as a donor in TADF applications,[119] TADF in an emitter that pairs DPO with the carbazol-9-yl donor has only recently been demonstrated. The compound 2-(2,3,4,5,6-penta(9*H*-carbazol-9-yl)phenyl)-5-phenyl-1,3,4-oxadiazole was synthesized and used as both a host and emitter in OLEDs and, as the emitting species doped into an emissive layer comprised of 1,3-bis(9*H*-carbazol-9-yl)benzene host, yielded a device with EQE_{max} up to 9.3 % and an electroluminescent emission maximum of 473 nm.[120]

3.1.2 Initial Strategies for Modifying Fluorophores

While there are myriad ways to modify organic compounds, only through series of systematic variations can structure-property relationships be deduced. To this end, three parameters will be varied from the parent compound 2-(4-(9*H*-carbazol-9-yl)phenyl)-5-phenyl-1,3,4-oxadiazole (**1**) – acceptor strength, donor strength, and connectivity. The absorption and photoluminescent properties of **1** are shown below in Figure 21. As discussed in Chapter 2, the S_1 and T_1 energy of the compound can be estimated from the onset of fluorescence and phosphorescence, 3.47 eV and 2.74 eV, respectively, for the compound. This results in an adiabatic ΔE_{ST} for the compound of 0.73, significantly too high for TADF which generally requires a ΔE_{ST} value closer to 0.1-0.2 eV or less for appreciable reverse intersystem crossing.

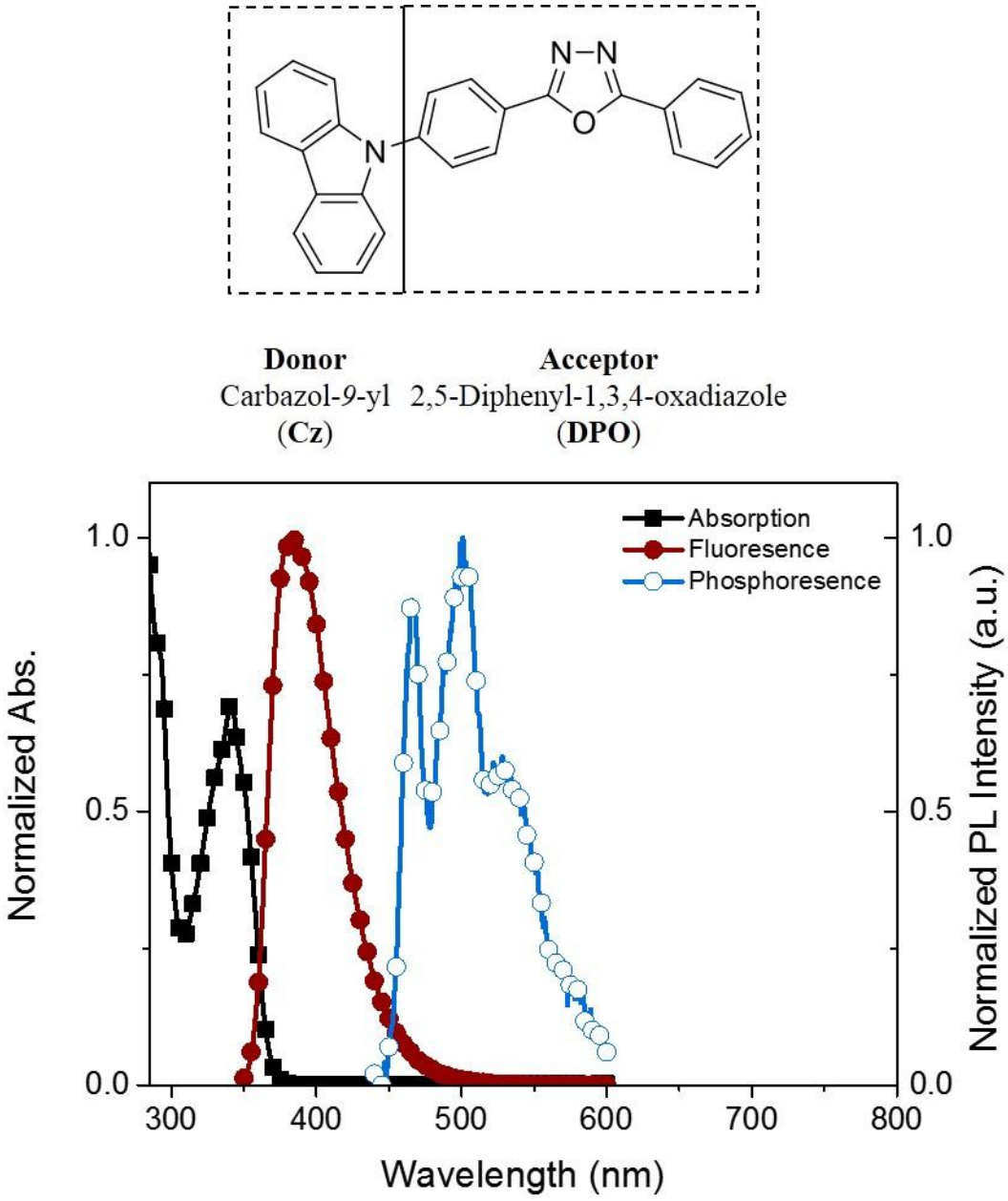

Figure 21 – (*top*) The parent carbazole-oxadiazole compound, 1. (*bottom*) Absorption and photoluminescence spectra of 1 collected in dilute toluene solution. Photoluminescence at room temperature attributed to fluorescence, and photoluminescence at 77 K with a 500 μs delay between excitation and data collection attributed to phosphorescence.

Modification of the acceptor strength correlates to a change in the electron affinity of the DPO acceptor. The approach used here is incorporation of fluorine atoms onto the

DPO structure to stabilize the LUMO. Due to the high electronegativity of fluorine (3.98 on the Pauling scale) and relatively small size, fluorine has been used to modify the energies of compounds with minimal structural perturbation. Substitution onto the aromatic backbones of organic materials has resulted in electron transport from parent compounds that display preferential hole-transport,[121-122] and substitution on emitters has also proven a successful approach to affecting the frontier orbital energies and resulting emission energy,[123-124] including emitters displaying TADF.[125] Li et al. reported a series of donor-acceptor TADF fluorophores with a number of fluorine atoms on the bridging phenylene, in much the same way as employed here, that displayed an increase in the electron affinity, inferred by the reduction potential and by DFT calculations, that increased concomitantly with fluorine substitution.[126] Using the framework that the LUMO of an intramolecular charge-transfer state is approximated by the LUMO of the acceptor, stabilization of the acceptor is expected to stabilize both the ^{1}CT and ^{3}CT state of the resulting fluorophore.

Analogously, increasing donor strength in a donor-acceptor compound should also stabilize the ^{1}CT and the ^{3}CT of the resulting fluorophore. Here we take the donor strength to correspond to the ionization energy of the carbazole donor moiety, which can be increased by substitution with electron donating substituents. For this series, 3,6-bis(*N*-carbazolyl)-carbazol-9-yl (*t*Cz) and 3,6-bis(3,6-di-*tert*-butyl-9-carbazolyl)-carbazol-9-yl (^{t}Bu*t*Cz) were included as stronger electron donors than Cz. The ionization energy of the donors can be estimated from the oxidation potential determined via cyclic voltammetry of their N-phenyl analogues. By this method, Cz,(N-phenylcarbazole) has an oxidation potential of 0.80 V (vs. Fc/Fc^+).[127] The donors *t*Cz (3,6-bis(*N*-carbazolyl)-*N*-

phenylcarbazole) and ^{t}Bu$_4$*t*Cz (3,6-bis(3,6-di-*tert*-butyl-9-carbazolyl)-*N*-phenylcarbazole) are comparably easier to oxidize, with oxidation potential of 0.56 and 0.50 V (vs. Fc/Fc^{+}) respectively.[128]

Finally, the connectivity between the donor and acceptor can easily be chemically modified, and at first will be varied only with regards to the substitution pattern on the bridging phenylene. The exact role of connectivity has not been well covered in the literature to this point, although there is evidence that it is an important parameter for controlling RISC rates due to its inequivalent effect on singlet and triplet states.[129]

3.2 Photoluminescent Properties

3.2.1 Adiabatic Singlet and Triplet Energy of CzDPO Fluorophores

Figure 22 shows the series of compounds synthesized to investigate the modification of acceptor strength on the properties of the fluorophore. The compounds 2-(4-(9*H*-carbazol-9-yl)-3,5-difluorophenyl)-5-phenyl-1,3,4-oxadiazole (**2**) and 2-(4-(9*H*-carbazol-9-yl)-2.3,5.6-tetrafluorophenyl)-5-phenyl-1,3,4-oxadiazole (**3**) were obtained under similar nucleophilic aromatic substitution reactions as the CzDPO parent compound. Synthesis was performed in collaboration with Dr. Yadong Zhang.

Figure 22 – Series of carbazole-oxadiazole donor-acceptor compounds synthesized with increasing acceptor strength

Fluorescence and phosphorescence spectra for the compounds were collected and are shown in Figure 23. The parent compound **1** displays a fluorescence λ_{max} at 382 nm with the broad, structureless line shape consistent with an intramolecular charge-transfer band, with estimated adiabatic singlet energy from the fluorescent onset at 3.47 eV. The fluorescence spectra showed a strong dependence on substitution by fluorine on the bridging phenylene. The line shape of the fluorescent emission of compound **2** was similar, but λ_{max} was red shifted to 414 nm and the estimated adiabatic singlet energy decreased to 3.32 eV. Finally, the fluorescent emission of the tetrafluoro compound **3** was further red shifted to 444 nm and the singlet energy was further stabilized to 3.24 eV. This trend in consistent with the expectation of an S_1 state well characterized by a HOMO-LUMO transition between the electronic donor and acceptor in which increased acceptor strength, due to increasing stabilization of the LUMO localized on DPO by the electronegative fluorine atoms, stabilizes the CT transition.

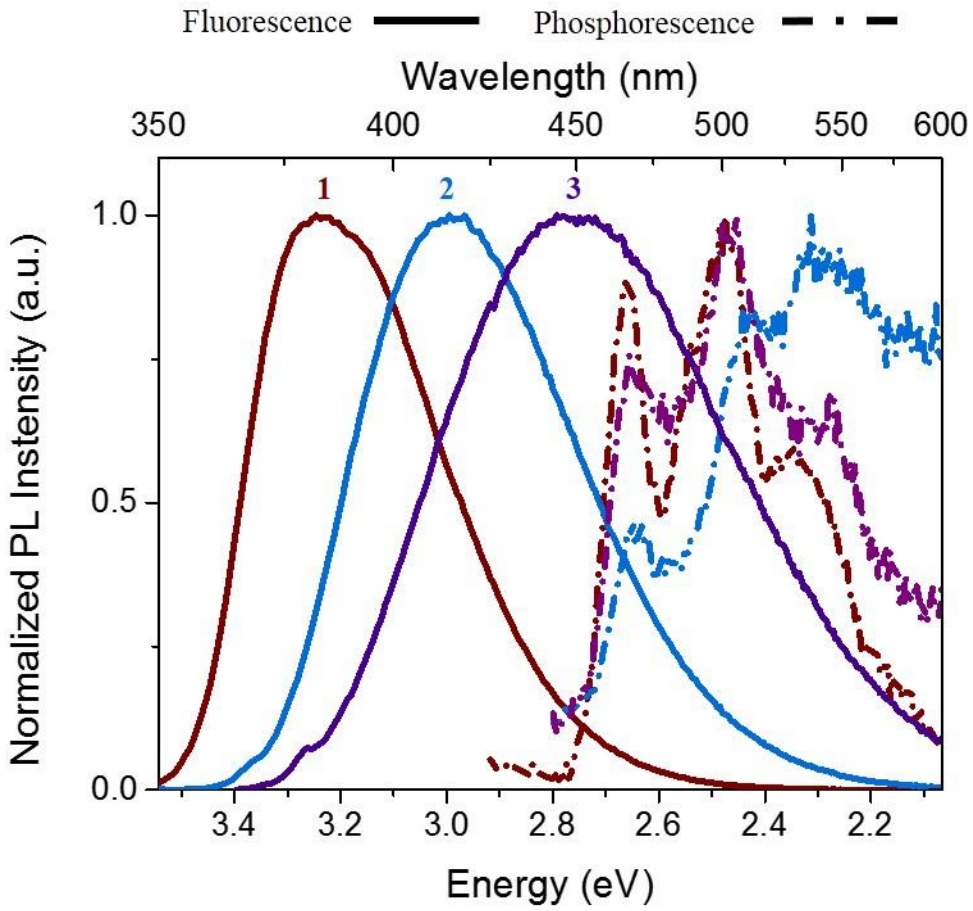

Figure 23 – Photoluminescence intensity of acceptor strength series 1, 2, and 3 plotted against energy. Fluorescence spectra collected in toluene solution (ca. 10^{-5} M) at room temperature, phosphorescence spectra collected in toluene matrix at 77 K with a 500 μs delay between excitation and detection.

The phosphorescence spectra (dashed lines, Figure 23) of the compounds in the series show the expected red shift vs. fluorescence, due to the stabilization provided by the exchange energy. Immediately apparent is that the phosphorescence spectra show, in contrast to that of the fluorescent emission, significant vibronic structure. Furthermore, the energy of the emission is virtually independent of the fluorine substitution on the DPO moiety, with the estimated triplet energy determined from the phosphorescence onset ranging from 2.74 eV in **1** to 2.75 eV in **2** and **3**. As a result, the adiabatic ΔE_{ST}

values are estimated to be 0.73, 0.57, and 0.49 eV for compounds **1**, **2**, and **3**, respectively, as a consequence of the stabilization of E_S.

The series of carbazole-derived donors with decreasing ionization potentials coupled to the DPO acceptor is shown below in Figure 24. The compounds 2-(4-(9'*H*-[9,3':6',9"-tercarbazol]-9'-yl)phenyl)-5-phenyl-1,3,4-oxadiazole (**4**) and 2-phenyl-5-(4-(3,3",6,6"-tetra-*tert*-butyl-9'*H*-[9,3':6',9"-tercarbazol]-9'-yl)phenyl)-1,3,4-oxadiazole (**5**) differ from **1** only by the donor moiety.

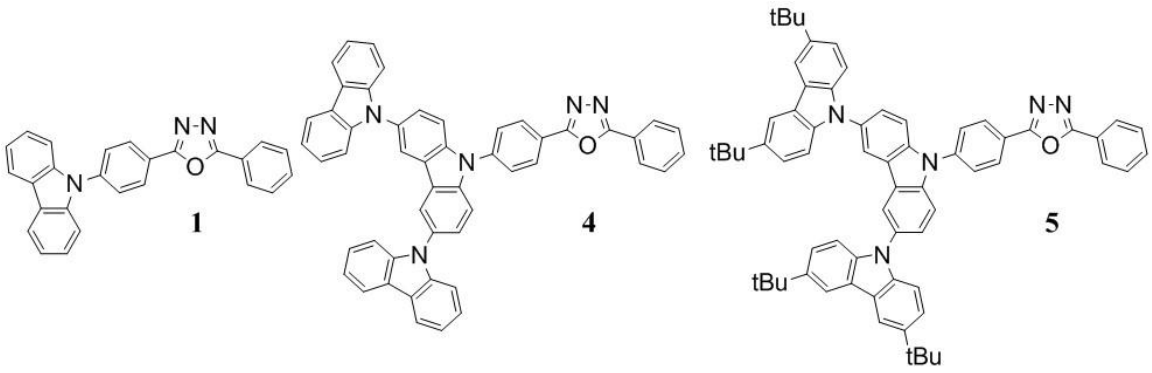

Figure 24 – A series carbazole-oxadiazole donor-acceptor compounds synthesized with increasing donor strength.

The photoluminescence spectra obtained from the compounds is shown in Figure 25. Similarly to the previous compounds, the line shapes of the fluorescent emission are all similar with a broad, unstructured emission consistent with the singlet emission being well characterized as a CT state. Relative to the fluorescence of **1** (λ_{max} = 382 nm), the λ_{max} of emission is red shifted in **4** to 407 nm, and then further to 417 nm in **5**. Furthermore, the estimated adiabatic singlet energy, as estimated from the onset of fluorescence, follows the same trend of stabilization with increased donor strength,

decreasing from 3.47 eV in **1** to 3.35 and 3.27 eV for the *tris*-carbazol-9-yl and *tert*-butyl-*tris*-carbazol-9-yl substituted oxadiazoles, respectively.

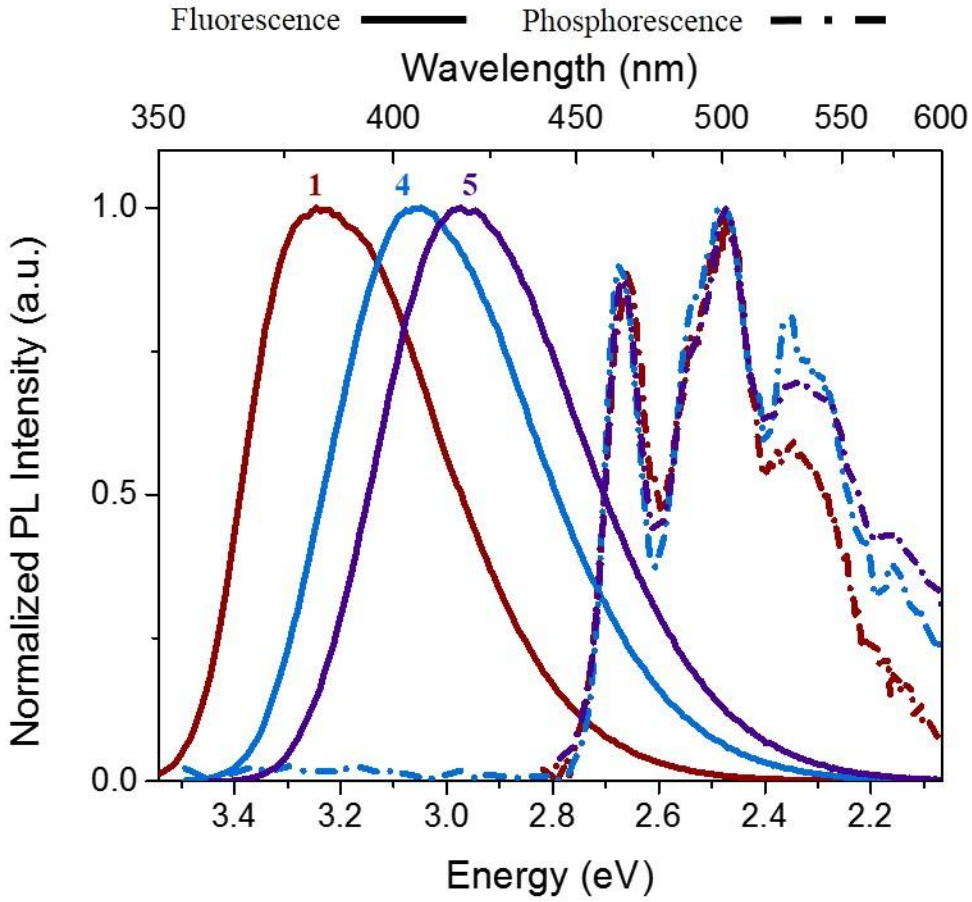

Figure 25 – Photoluminescence intensity of donor strength series 1, 4, and 5 plotted against energy. Fluorescence spectra collected in toluene solution (ca. 10^{-5} M) at room temperature, phosphorescence spectra collected in toluene matrix at 77 K with a 500 µs delay between excitation and detection.

The phosphorescence spectra are also shown in Figure 25 and confirm the observations about the triplet state from the previous series. Contrary to the fluorescent emission, the phosphorescent emission spectra show the vibronic structure consistent with an emission arising from a locally excited triplet state. Furthermore, the phosphorescence spectra of all three compounds are essentially superimposable,

indicating the adiabatic energy of the triplet state is decoupled from the strength of the donor moiety of the fluorophore, and thus from the CT state. The estimated triplet state energies for **1**, **4**, and **5** are each 2.74(±0.01) eV. Again, as a result of the sensitivity of the singlet state and the insensitivity of the triplet state to the donor strength, the resulting estimated ΔE_{ST} energies, 0.73, 0.61, and 0.52 eV, respectively, decreased as a direct consequence of the stabilization of the singlet state.

Compounds with the same donor and acceptor but different connectivity between them, that is *meta* and *ortho* connectivity between the carbazole and oxadiazole substituents in addition to the *para* connectivity of the compounds above, were also prepared and are shown in Figure 26. For example for **1**, moving the donor to the *meta* position yielded 2-(3-(9*H*-carbazol-9-yl)phenyl)-5-phenyl-1,3,4-oxadiazole (**6**), along with the *t*Cz and ^{t}But*t*Cz analogues, 2-(3-(9'*H*-[9,3':6',9''-tercarbazol]-9'-yl)phenyl)-5-phenyl-1,3,4-oxadiazole (**7**) and 2-phenyl-5-(3-(3,3'',6,6''-tetra-*tert*-butyl-9'*H*-[9,3':6',9''-tercarbazol]-9'-yl)phenyl)-1,3,4-oxadiazole (**8**). Similarly, connection of the carbazol-9-yl donor in the *ortho* position yields 2-(2-(9*H*-carbazol-9-yl)phenyl)-5-phenyl-1,3,4-oxadiazole (**9**), with *t*Cz and ^{t}But*t*Cz analogues, 2-(2-(9'*H*-[9,3':6',9''-tercarbazol]-9'-yl)phenyl)-5-phenyl-1,3,4-oxadiazole (**10**) and 2-phenyl-5-(2-(3,3'',6,6''-tetra-*tert*-butyl-9'*H*-[9,3':6',9''-tercarbazol]-9'-yl)phenyl)-1,3,4-oxadiazole (**11**). Within each connectivity group, the donor series followed the same singlet and triplet trends as were observed for the *para* connected compounds; singlet energy decreased as donor strength increased while triplet energy was largely independent of the structural change.

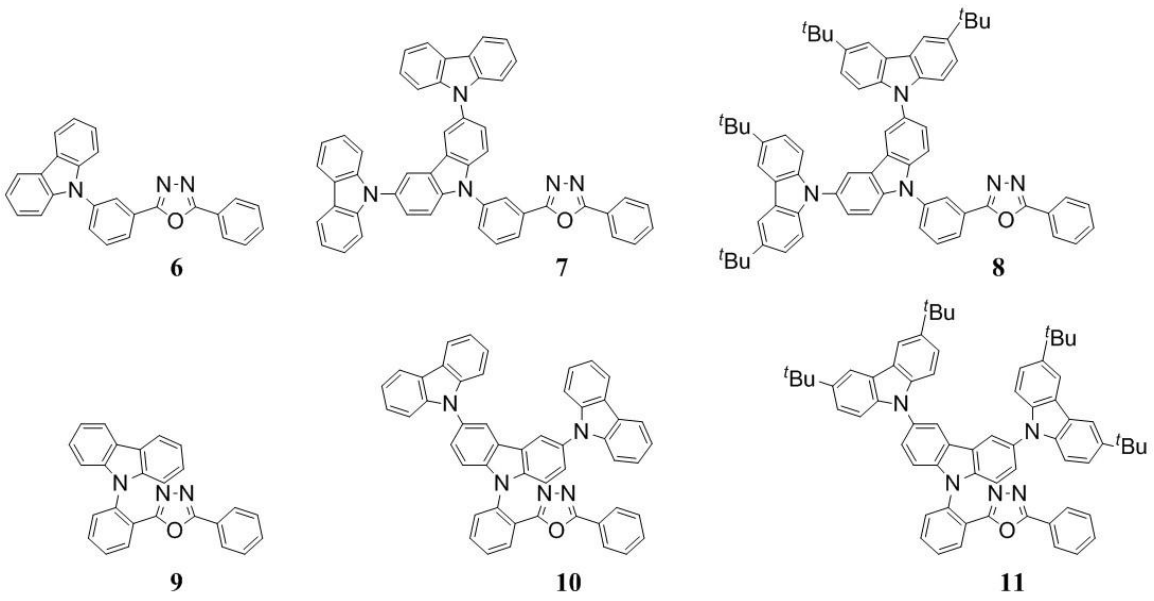

Figure 26 – Carbazole-oxadiazole compounds synthesized with varied connectivity.

When the compounds are compared on the basis of connectivity, however, a different set of observations is apparent. A representative example, the series comprised of the Cz-DPO fluorophores, is shown in Figure 27. In all compounds, placement of the donor in the 3- position relative to the oxadiazole leads to the highest energy singlet. For example, the singlet energy, estimated from the fluorescence onset, of **7** is 3.39 eV and is higher than either **4** or **10** (3.35 and 3.20 eV, respectively). This effect is not as strong as the previous observations about donor and acceptor strength. Compounds **1** and **6** show onset energies that are approximately equivalent, although the λ_{max} is higher in energy by ca. 80 meV.

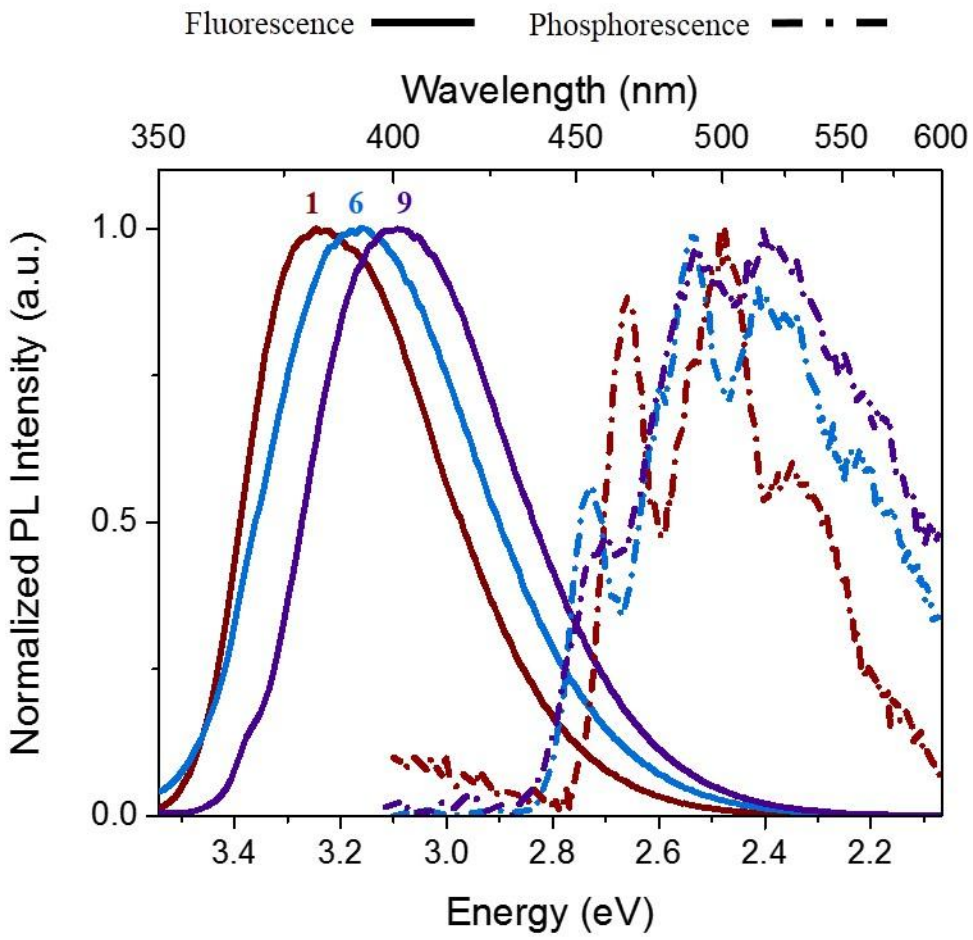

Figure 27 – Photoluminescence intensity of connectivity series 1, 6, and 9 plotted against energy. Fluorescence spectra collected in toluene solution (ca. 10^{-5} M) at room temperature, phosphorescence spectra collected in toluene matrix at 77 K with a 500 μs delay between excitation and detection.

Turning our attention to the triplet energy of the compounds, the connectivity between donor and acceptor moiety reveals the first approach for modulating the triplet energy yet observed in these compounds. In each series, the triplet energy increases as the connectivity between the donor and acceptor is changed from *para* to *meta*, and then again as it is changed to *ortho*. For example, the triplet energy of **1** increases from 2.74 to 2.80 eV in compound **6,** and then again (slightly) to 2.82 eV in compound **9**. The same progression is observed in the *t*Cz compounds (2.74, 2.80, 3.02 eV for the 4-, 3, and 2-

substituted compounds, respectively) and in the ^{t}But*t*Cz compounds (2.71, 2.80, and 2.83, respectively). All steady state photoluminescence data is tabulated below.

Table 1 – Tabulated Steady-State absorption and photoluminescence data of simple carbazole-oxadiazole compounds. Absorption and fluorescence data collected in toluene solution (ca. 10^{-5} M) at room temperature. Phosphorescence collected in toluene matrix at 77 K with 500 µs delay between excitation and data acquisition.

Compound	Absorption	Fluorescence		Phosphorescence		ΔE_{ST}
	λ_{max} /nm	λ_{max} /nm	Onset /eV	λ_{max} /nm	Onset /eV	/eV
1	341	382	3.47	466, 501	2.74	0.73
2	290, 333	414	3.32	468, 536	2.75	0.57
3	288, 344	444	3.24	508	2.75	0.49
4	294, 342	407	3.35	464, 500	2.74	0.61
5	298, 333, 350	417	3.27	465, 501	2.75	0.52
6	293, 338	392	3.47	454, 489	2.80	0.67
7	293, 342	404	3.39	454, 488	2.80	0.59
8	298, 335, 348	416	3.33	455, 490	2.80	0.53
9	293, 336	401	3.43	462, 492	2.82	0.61
10	293, 328, 341	431	3.20	497	2.83	0.37
11	298, 225, 348	439	3.13	457, 464	2.83	0.30

3.2.2 Fluorescence Decay Rates in CzDPO Fluorophores

Understanding how to control singlet and triplet energy levels to minimize the ΔE_{ST} is only one facet of optimizing a molecular system for thermally activated delayed

fluorescent applications. The photoluminescent quantum yield must also be considered, or more specifically, the fluorescent decay rate must be maximized relative to the non-radiative decay rates. To this end, the absolute quantum yields and the fluorescent lifetimes of the compounds introduced above were determined. Again, one can consider the relative fluorescent efficiency and lifetime as a property of donor/acceptor strength and as a property of substitution pattern. For these compounds, which contain relatively large ΔE_{ST} values of 0.3 eV and higher, no TADF signal is observed and so the PLQY is attributed entirely to prompt fluorescence.

Immediately apparent in the data from the compounds reported here is the strong dependence of the PLQY on the regiochemistry of the compound. With the exception of the fluorinated compounds, in which fluorescence is significantly quenched, each case of a carbazol-9-yl donor *para* to the oxadiazole moiety yields a compound with high Φ_{fl}, with Cz, *t*Cz, and ^{t}But*t*Cz yielding fluorophores that display Φ_{fl} of 0.92, 0.99, and 0.89, respectively. Meanwhile, the *meta* and the *ortho* substituted regioisomers display modest values that range from 0.05 to 0.33. It is noted that in the determination of PLQY the precision is often taken to be ±10%, nevertheless, it is clear that the *para* regioisomers display a significantly more efficient fluorescence. What is not observed is a significant difference of the PLQY between substitutions in the 2- and 3-positions. Further analysis requires an understanding of the decay rates involved. Fluorescent lifetimes were determined and are collected in Table 2, along with the calculated fluorescent decay rates (k_{fl}), calculated according to Equation 32. A representative set of fluorescent transients from **1**, **6**, and **9** are shown in Figure 28, where the compound displaying the highest PLQY, 0.92, also has a fluorescent lifetime less than half of the other isomers, 2.12 ns as

opposed to 5.29 and 5.18 ns for **6**, and **9**, respectively. As can be seen in Table 2, the *para* substituted fluorophore in each other set of regioisomers also shows a τ_{fl} half of those of the other compounds. The calculated rates of fluorescence for these compounds are in the range of 10^8 s^{-1}, which is comparable to highly efficient fluorophores such as fluorescein.[29] The other compounds have fluorescent decay rates an order of magnitude lower.

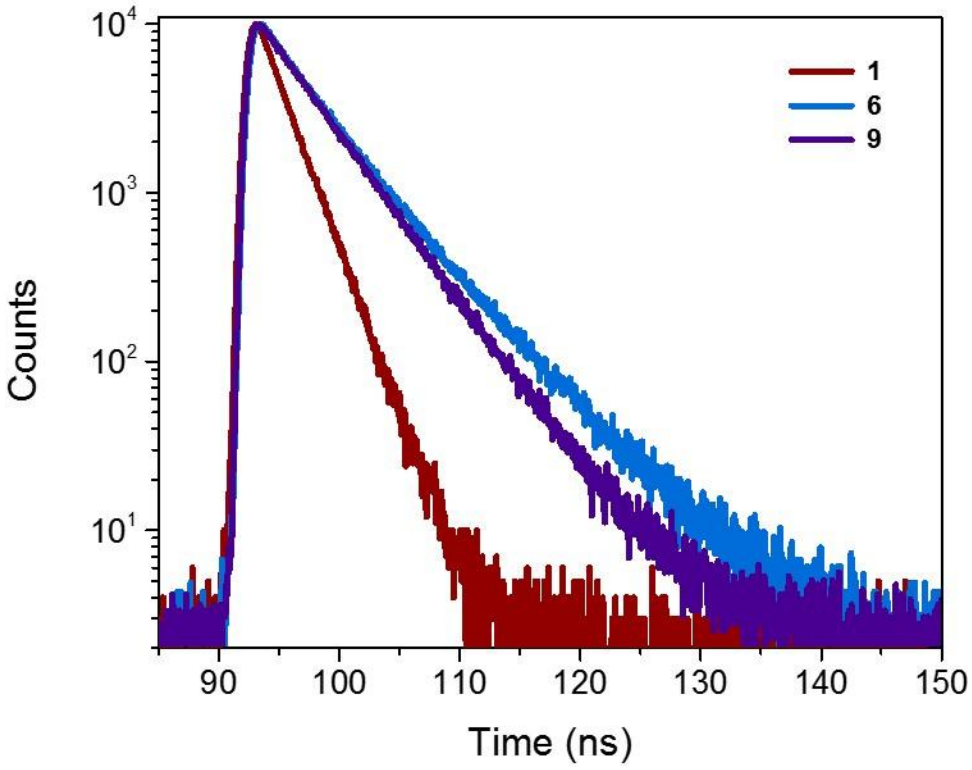

Figure 28 – Transient fluorescence of carbazole-oxadiazole regioisomers 1, 6, and 9.

The mesomeric effect can be invoked to explain the dependence of the fluorescent rate on the connectivity. Substitution of a donor in the 3- position is expected to lead to a HOMO with minimal spatial overlap with the LUMO, of which the highest coefficients

on the phenylene would be in the 2-, 4-, and 6- positions relative to the π-electron withdrawing oxadiazole. Substitution in the 2-position likely leads to a twisting of both the carbazole and the oxadiazole relative to the bridging phenylene, increasing the orthogonality of the carbazole localized HOMO and the oxadiazole localized LUMO and thus decreasing the overlap between them. In both cases, the decreases HOMO-LUMO overlap would lead to a decrease in the transition dipole moment, as shown in Equation 7, and thus the rate of fluorescence and the PLQY.

Table 2 – Fluorescence quantum yield (Φ_{fl}), fluorescent lifetime (τ_{fl}), and rate of fluorescence (k_{fl}) of simple carbazole-oxadiazole compounds. Data collected in air equilibrated toluene solution (ca. 10^{-5} M) at room temperature.

Compound	Φ_{fl}	τ_{fl} /ns	k_{fl} /10^7 s^{-1}
1	0.92	2.12	43.4
3	0.21	6.68	3.13
4	0.99	3.32	29.8
5	0.89	3.83	23.2
6	0.05	5.29	0.95
7	0.33	6.23	5.30
8	0.17	7.42	2.29
9	0.18	5.18	3.50
10	0.10	6.27	1.59
11	0.11	7.15	1.54

3.3 Strategies for Obtaining TADF in Carbazole-Oxadiazole Compounds

3.3.1 Orbital Nature of the Relevant Electronic States

Trends observed in the energies of the S_1 and T_1 states, as well as the fluorescent decay rates, with systematic alteration of the donor strength, acceptor strength, and connectivity provide insight into the physical nature of the relevant excited states that must be understood to design compounds that exhibit thermally activated delayed fluorescence. The structure property relationships observed are laid out below.

Both the donor strength and the acceptor strength of the compound show a strong correlation with the energy of the singlet state, as characterized by the fluorescent emission. Figure 29 shows the monotonic decrease of singlet energy with increasing donor or acceptor strength in each series of like compounds. This is to be expected if the transition is well characterized as an intramolecular charge-transfer transition between the LUMO and the HOMO, which are themselves well represented by the orbitals on the DPO acceptor and the Cz donor. Furthermore, with the exception of the fluorinated DPOs, fluorescent decay rates are largely independent of the structure of the donor amongst these compounds. On the other hand, the energy of the triplet emission is virtually independent of the donor or acceptor strength. Thus, the ΔE_{ST} is directly dependent on the HOMO-LUMO gap ($\Delta E_{H\text{-}L}$), which is in turn controlled by the energy of the intermolecular charge-transfer state for carbazole-oxadiazole compounds with like connectivity. In principle, as donor and/or acceptor strength is arbitrarily increased, the energy of the singlet state will approach the energy of the triplet state and this relationship will no longer hold as the T_1 state will become better described by ^{3}CT

orbitals and Adachi's design rule of minimizing the spatial overlap between the HOMO and LUMO will determine the ΔE_{ST}.

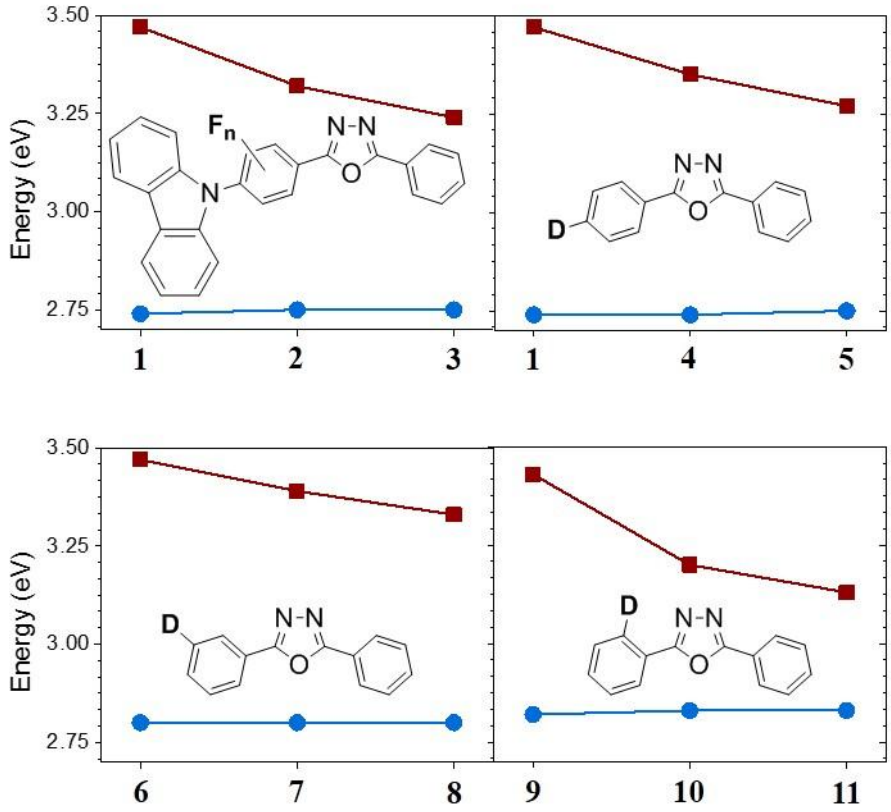

Figure 29 – Compounds grouped by connectivity to show effect of donor or acceptor strength on singlet (red squares) and triplet (blue circles) energy. Compound number is shown on x-axes, lines on the chart are drawn to guide the eye.

Turning our attention to role of connectivity, Figure 30 shows the compounds grouped by donor type, with the singlet and triplet energies as a function of the regiochemistry. As noted above, the singlet energy of the compounds containing a donor in the 3-position is slightly higher than in the 2- and 4-positions. This is likely due to the mesomeric effect. It is known from reactivity patterns that the 2-, 4-, and 6-positions of a

benzene ring substituted with a π-electron accepting group have increased orbital coefficients of the LUMO,[130] and so a donor attached at the 3-position would not benefit from the additional electronic stabilization provided on the atoms in those locations. The increase in the energy of the triplet state as the donor and acceptor move closer together around the phenylene bridge is quite apparent in Figure 30 and suggests an entirely different physical approach for controlling triplet energy than that for controlling singlet energy.

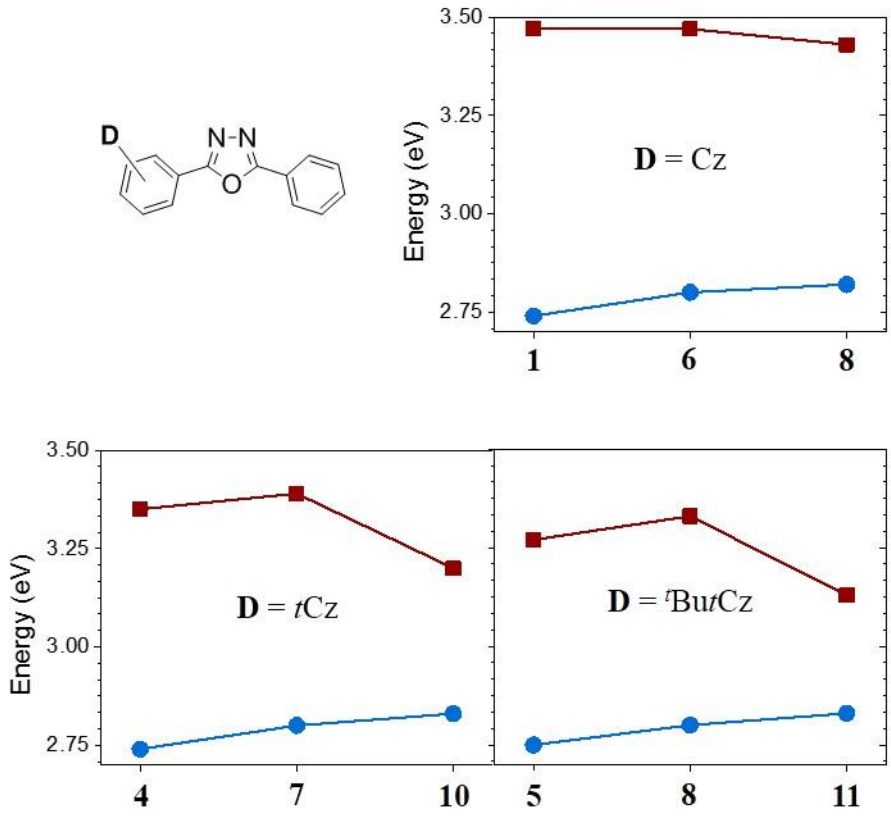

Figure 30 – Compounds grouped by donor type to show effect of connectivity on singlet (red squares) and triplet (blue circles) energy. Compound number is shown on x-axes, lines on the charts are drawn to guide the eye.

To rationalize what is physically causing this change in triplet energy with substitution pattern requires an understanding of the triplet state of the fluorophores. As was demonstrated above, the energy of the triplet state in these carbazole-oxadiazole fluorophores is decoupled from the strength of the donor or the acceptor, and from the resulting energy of the CT state that dominates the singlet emission. The vibronic structure of the spectral envelope also provided compelling evidence that the orbital character of the triplet emission differed significantly from the orbitals from which the singlet emission originated. The evidence suggests that the triplet state is characterized by a localized excitation on either the donor carbazole or the acceptor diphenyloxadiazole.

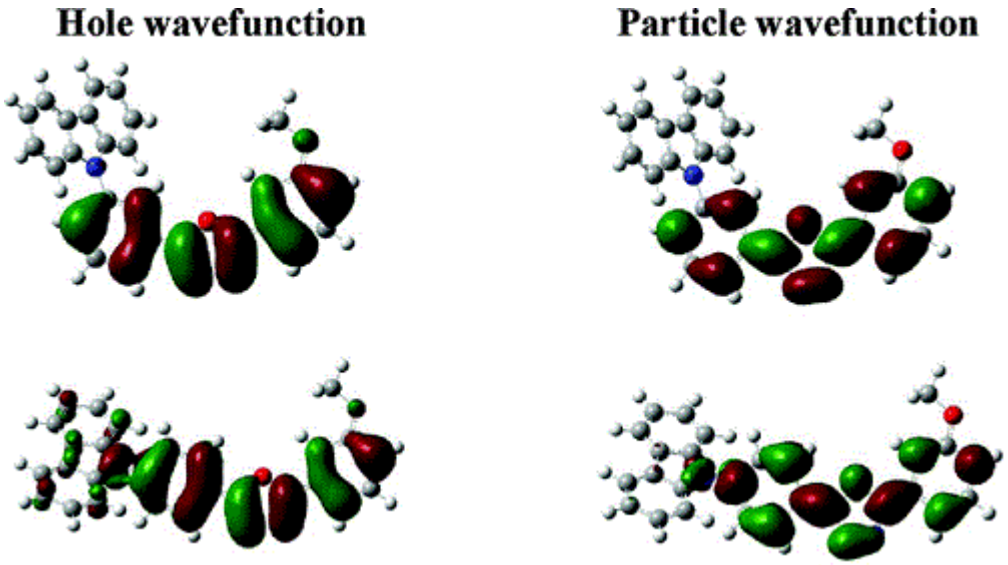

Figure 31 – Natural transition orbitals for T_1 state calculated (TD-DFT, B3LYP/6-31G(d,p)) for 2-(4-(Carbazol-9-yl)phenyl)-5-(3-methoxyphenyl)-1,3,4-oxadiazole (top) and 2-(3,5-Di(carbazol-9-yl)phenyl)-5-(3-methoxyphenyl)-1,3,4-oxadiazole (bottom). Reprinted with permission from Ref. 104 Copyright 2011 American Chemical Society.[105]

The phosphorescent spectra of the compounds above tend to contain vibronic structure that resembles that of an isolated N-phenyl-carbazole compound.[131] However, natural transition orbital analysis performed based on TD-DFT calculations on compounds very similar to **1** and **6** suggest that the T_1 state is actually localized on the DPO moiety.[105] If this is indeed the case, increasing the energy of the LE state spread over the DPO group would increase the T_1 energy of the fluorophore, although a significant increase may lead to a similar Cz localized T_1.

Steric crowding induced by placement of the donor carbazole or carbazole derivative vicinal to the oxadiazole could potentially twist the bridging phenylene out of plane of the oxadiazole. This would be expected to decrease the conjugation across the three rings of the DPO moiety and increase the energies of the relevant transitions and would, if the above calculations are correct, explain the increase in T_1 energy in the resulting fluorophore. However, it could also be argued that if the T_1 state is, instead, localized on the N-phenyl-carbazole that it is due to the necessary concomitant steric crowding on the carbazol-9-yl twisting the carbazole backbone out of plane of the phenyl group. Crowding on the non-bridging phenyl group, however, would only affect the conjugation on the DPO backbone, and so a similar increase in triplet energy due to such a modification would provide strong evidence that the triplet is a LE on the DPO. Figure 32 shows that this is precisely what is observed after substitution of isopropyl groups onto the 2',6'-positions of a published analogue to compound **1**, while substitution of a methyl group ortho to the carbazol-9-yl group of a published analogue to compound **1** has a negligible effect[132] confirming the key role of the DPO moiety in the triplet energy of these carbazole-oxadiazole fluorophores.

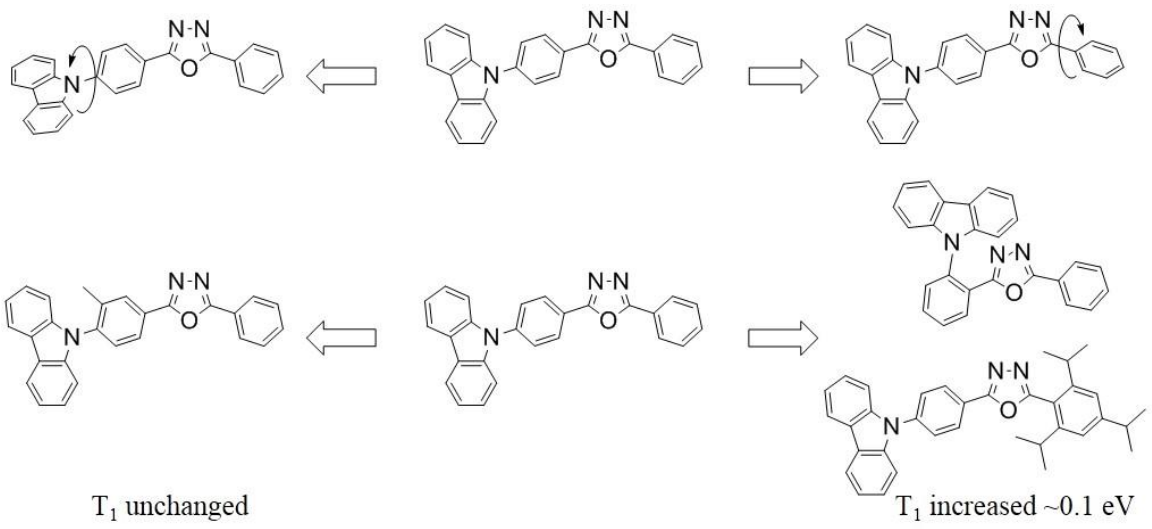

Figure 32 – Increase in T_1 energy is observed in simple carbazole-oxadiazole compounds upon steric crowding between oxadiazole and either the bridging or the non-bridging phenyl group, but not between the carbazole and the bridging phenylene.

Putting together the above information gives the following orbital and state pictures for the systems investigated. The HOMO and the LUMO are well approximated as the localized HOMO of the Cz and the LUMO of the DPO, and the fluorescent transition arises from an intramolecular charge-transfer state involving the HOMO and LUMO orbitals. In the triplet manifold, however, the increased energy of the exchange integral between orbitals involved in a locally excited state (K^{LE}) on the DPO moiety is sufficiently large relative to that of the CT transition (K^{CT}) that the ^{3}LE state has lower energy than the ^{3}CT state, and thus the T_1 is characterized by this ^{3}LE state. An energy level diagram of this is shown in Figure 33. As such, structural changes stabilize the CT state or destabilize the LE state of DPO lead to a decrease in the ΔE_{ST}. Additionally, *para* connectivity between the carbazol-9-yl donor and 1,3,4-oxadiazole acceptor results in a

fluorescent decay rate an order of magnitude higher (ca. 10^8 s^{-1}) than in the *meta* or *ortho* position.

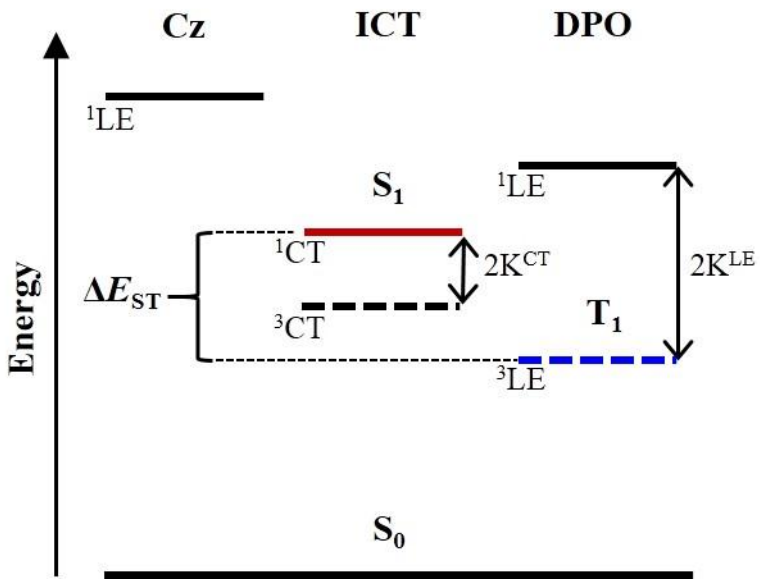

Figure 33 – Generic energy level diagram of the carbazole-oxadiazole fluorophores studied.

With an understanding of orbital nature of the relevant excited states, new compounds can be designed using the design rules laid out above with structures that minimize ΔE_{ST} values for the purpose of increasing reverse intersystem crossing rates. To wit, three approaches were explored:

1) Designing compounds with stronger donors and/or acceptors decrease the $\Delta E_{H\text{-}L}$ such that the ^{1}CT approaches the ^{3}LE in energy and ΔE_{ST} is minimized.
2) Designing compounds with large amounts of steric hindrance designed to break conjugation across the DPO acceptor moiety and push the ^{3}LE upwards towards the ^{1}CT to minimize ΔE_{ST}, although this may be expected to reduce the k_{Fl}.

3) A combined approach in which both the CT and LE states are modified, as described above.

3.3.2 Stabilizing the Intramolecular Charge-Transfer

Perhaps the most obvious approach is to keep increasing the donor and acceptor strengths until the singlet energy approaches that of the relatively invariant triplet energy. Moreover, this approach is fully compatible with utilizing the regiochemistry of compounds **1**, **4**, and **5** which displayed high fluorescent decay rates of ca. 10^8 s^{-1}. Figure 34 show the targeted compounds that combine the increased donor and acceptor strength.

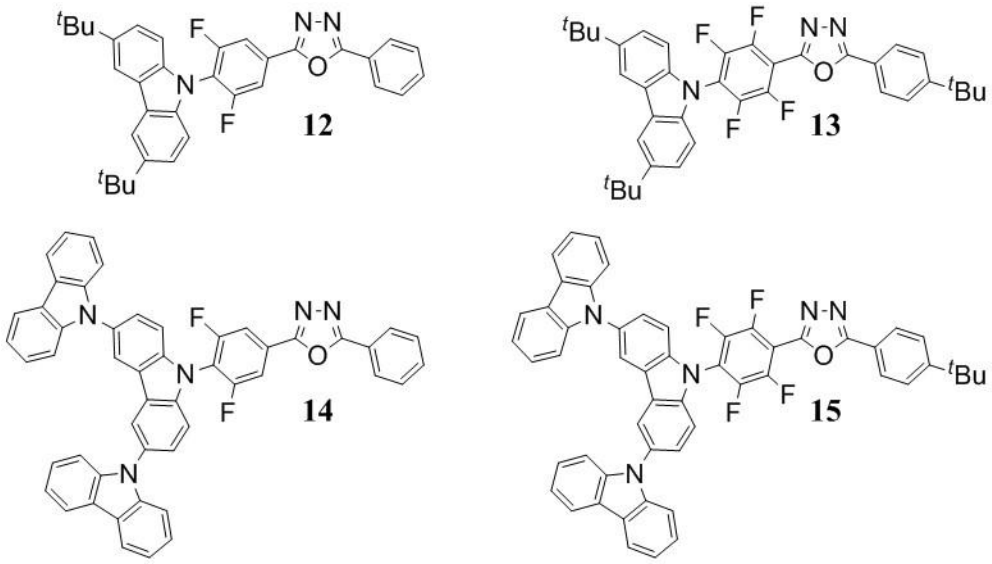

Figure 34 – Compounds with increased donor and acceptor strength

Photoluminescent characterization of the compounds showed the expected trend of the broad, structureless fluorescent CT emission that continues to red shift from compounds **1**-**5** as the CT state is further stabilized. Fluorescence and phosphorescence spectra are shown in Figure 35. Compound **12** displays a singlet energy of ca. 3.18 eV,

which, as expected, is lower than that lowest displayed by the compounds with similar regiochemistry in the previous series (**3**, S_1 of ca. 3.24 eV). The fluorescent onsets of compounds **13** and **14** are quite similar (3.11 vs. 3.08,) despite the fluorescent λ_{max} of **13** being lower in energy than that of **14** (476 and 454, respectively). Compound **15**, combining the *tris*carbazole donor with strongest tetrafluoro-DPO acceptor, demonstrated the lowest energy CT state in the series, with a sky-blue emission with λ_{max} at 493 nm and an onset of fluorescence at 2.99 eV.

As can be seen in Figure 35, despite the hypsochromatic shift in the fluorescence spectra of the series the phosphorescence emissions are (still) largely superimposable. The energy of the singlet is stabilized by almost half an electron volt from the original carbazole-oxadiazole compound **1**, while the triplet energy is consistently at ca. 2.75 eV in all the compounds from this series, as well as the compounds with similar regiochemistry in the previous series. As a result, the ΔE_{ST} was decreased to 0.27 eV in **15** from 0.73 in **1** in parallel to the singlet energy decrease. As compound **15** showed a moderate ΔE_{ST}, further efforts were made to further decrease the ΔE_{ST} to a value in the range of 0.1-0.2 eV.

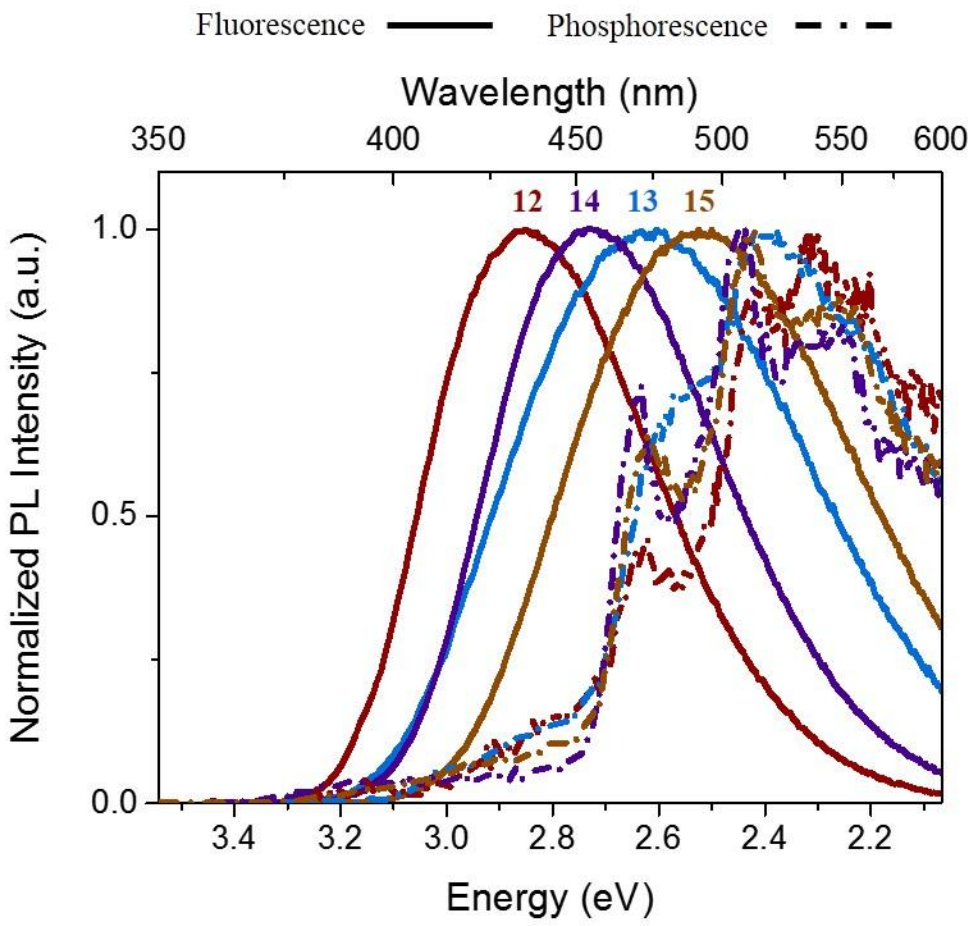

Figure 35 – Photoluminescence intensity of 12-14 against energy. Fluorescence spectra collected in toluene solution (ca. 10^{-5} M) at room temperatue, phosphorescence spectra collected in toluene matrix at 77 K with a 500 µs delay between excitation and detection.

To this end, a stronger donor was synthesized for substitution onto the DPO acceptor. The donor 9,9-dimethyl-9,10-dihydroacridine (dimethylacridane, or Ac) is structurally similar to carbazole but with a saturated carbon atom bridging the phenyl groups, which break conjugation in the structure and leads to the lone-pair of electrons on the nitrogen atom to be less conjugated into the phenylenes and therefore more available for donation. The HOMO of Ac is estimated from cyclic voltammetry to be at ca. -5.26

eV,[133] contrasted with ca. -5.30 in the strongest donor investigated above, *t*Cz. Two new fluorophores were synthesized with the stronger Ac donor and are shown below.

Figure 36 – Acridane-oxadiazole fluorophores 16 and 17.

Photophysical characterization of Ac containing compounds **16** and **17** are consistent with and extend the observations of the previous compounds in the series with increasing donor and acceptor strength. Figure 37 shows the further red shift in the fluorescence with the same triplet energy of ca. 2.75. The ΔE_{ST} in **17**, still following the singlet energy, is reduced to ca. 0.13 eV; an energy at which TADF may be expected to be possible.

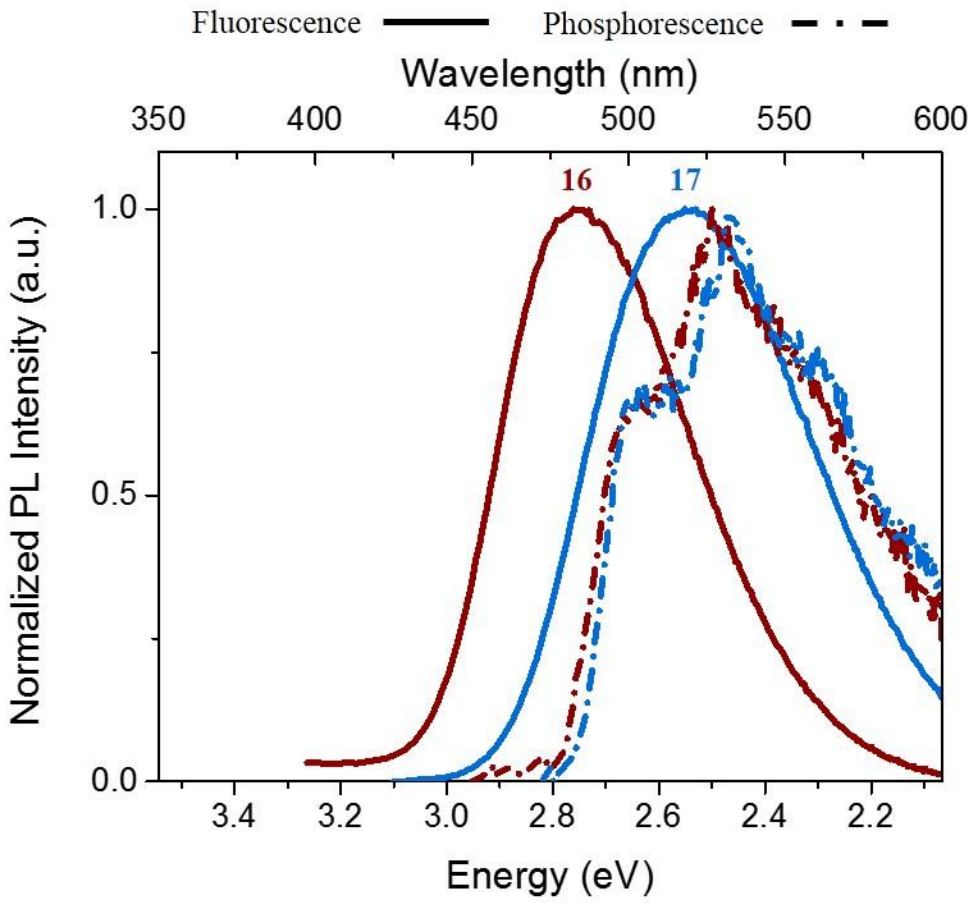

Figure 37 – Photoluminescence spectra of 16 and 17 (plotted versus energy). Fluorescence spectra collected in toluene solution (ca. 10^{-5} M) at room temperatue, phosphorescence spectra collected in toluene matrix at 77 K with a 500 µs delay between excitation and detection.

Due to the polar, charge separated nature of an intramolecular charge-transfer state, it is stabilized by a highly polarizable environment more than the ground state which displays a comparatively small dipole moment. As a result, a compound with an ICT S_1 state displays a large Stokes shift, with the photoluminescence and not the absorption red shifting with increasing solvent polarity.[94].

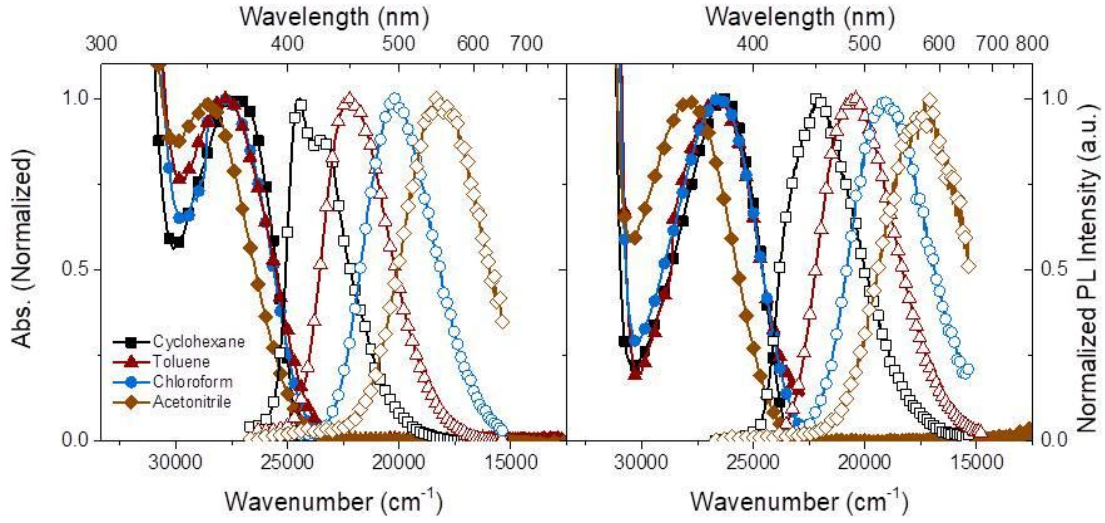

Figure 38 – Absorption (closed symbols) and photoluminescence (open symbols) of compound 16 (left) and 17 (right), plotted against energy, in a variety of solvents.

Table 3 – Tabulated steady-state absorption and photoluminescence data of simple compounds 12-17. Absorption and fluorescence data collected in toluene solution (ca. 10^{-5} M) at room temperature. Phosphorescence collected in toluene matrix at 77 K.

Compound	Absorption	Fluorescence		Phosphorescence		ΔE_{ST}
	λ_{max} /nm	λ_{max} /nm	*Onset* /eV	λ_{max} /nm	*Onset* /eV	/eV
12	296, 353	435	3.18	473, 536	2.73	0.45
13	292, 355	476	3.11	516	2.75	0.36
14	295, 342	454	3.07	471, 506	2.73	0.34
15	294, 341	493	2.99	473, 512	2.74	0.27
16	289, 360	449	3.02	496	2.78	0.24
17	290, 376	490	2.88	503	2.75	0.13

To confirm the nature of the S_1, absorption and photoluminescence spectra were collected in solvents with a range of polarities and are shown in Figure 38. It is seen that

the for both compounds the absorption is only weakly solvent dependent, while the emission is substantially red shifted, and, therefore, the Stokes shift, is significantly increased, with increasing solvent polarity, as expected for compounds in which the emissive state has a dipole moment much larger than that of the ground state.

3.3.2.1 TADF Properties of ***17***

Due to the relatively low ΔE_{ST} values displayed by **17**, further investigation into whether the compound displayed TADF was performed. Figure 39 shows the absorption and photoluminescence of the compound plotted against wavelength. The absorption spectrum shows an absorption maximum at 290 nm that is attributed to π-π* transitions localized on DPO.[102] The broad, lower intensity absorption band at 376 nm is consistent with an intramolecular CT transition between the acridane donor and diphenyloxadiazole acceptor, as is seen in the fluorescence spectrum as discussed above, and is more well resolved from the localized absorption bands that in the CzDPO compounds previously investigated.

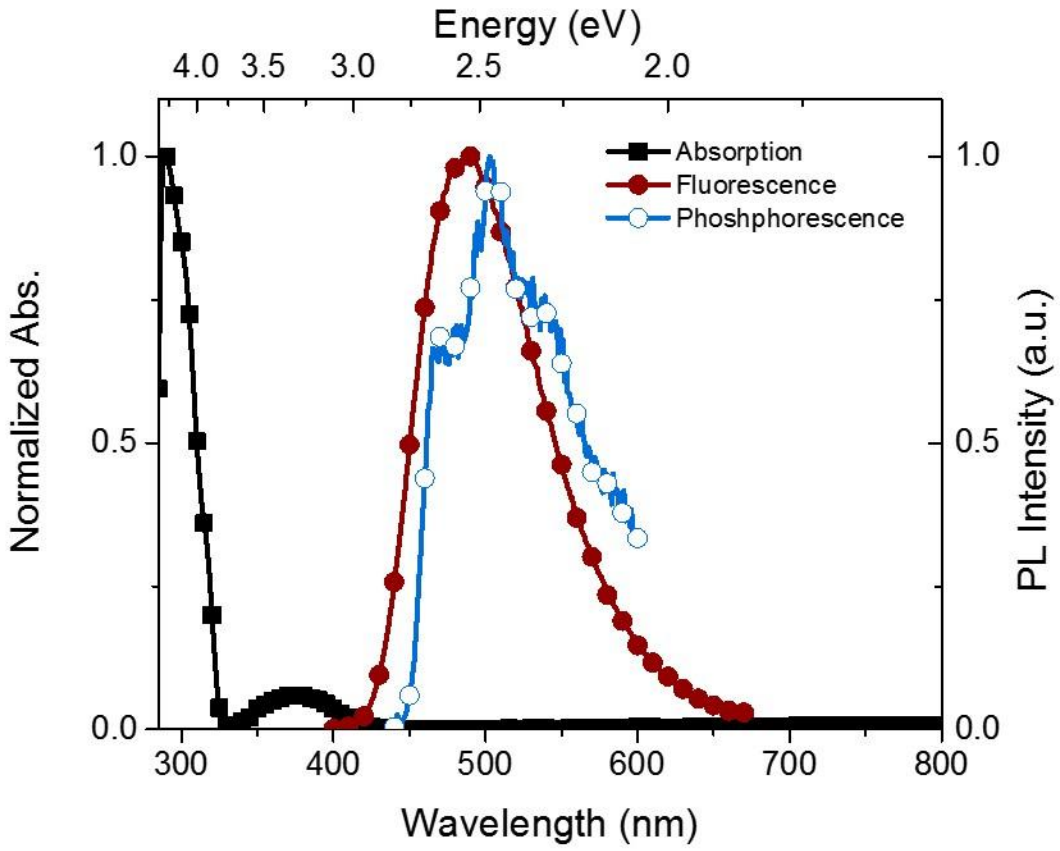

Figure 39 – Absorption and photoluminescence spectra of 17 collected in dilute toluene solution, with photoluminescence at room temperature attributed to fluorescence, and photoluminescence at 77 K with a 500 μs delay between excitation and data collection attributed to phosphorescence.

To probe whether the decreased ΔE_{ST} of **17** would lead to TADF, the transient photoluminescence in dilute toluene solution was collected, and is shown in Figure 40. After sparging the solution with nitrogen gas to reduce the concentration of triplet-quenching molecular oxygen, a two-component decay is observed. The fast component, with a lifetime of 8.8 ns, and the slow component, with a lifetime of 179 μs, are assigned to prompt fluorescence and TADF, respectively. Upon equilibrating with air, the slow component disappears, consistent with a delayed emission pathway in which the exciton spends time in the triplet manifold. Furthermore, the PLQY increases from 0.16 in air-

equilibrated solution to 0.24 upon sparging with nitrogen. Thus, the stabilization of the CT state in **17** lowers the singlet sufficiently for efficient RISC from the T_1 state, leading to TADF in the compound. In contrast, **16** showed only a single, fast component in the transient fluorescence after sparging with nitrogen, and the PLQY only slightly increases, from 0.16 to 0.18.

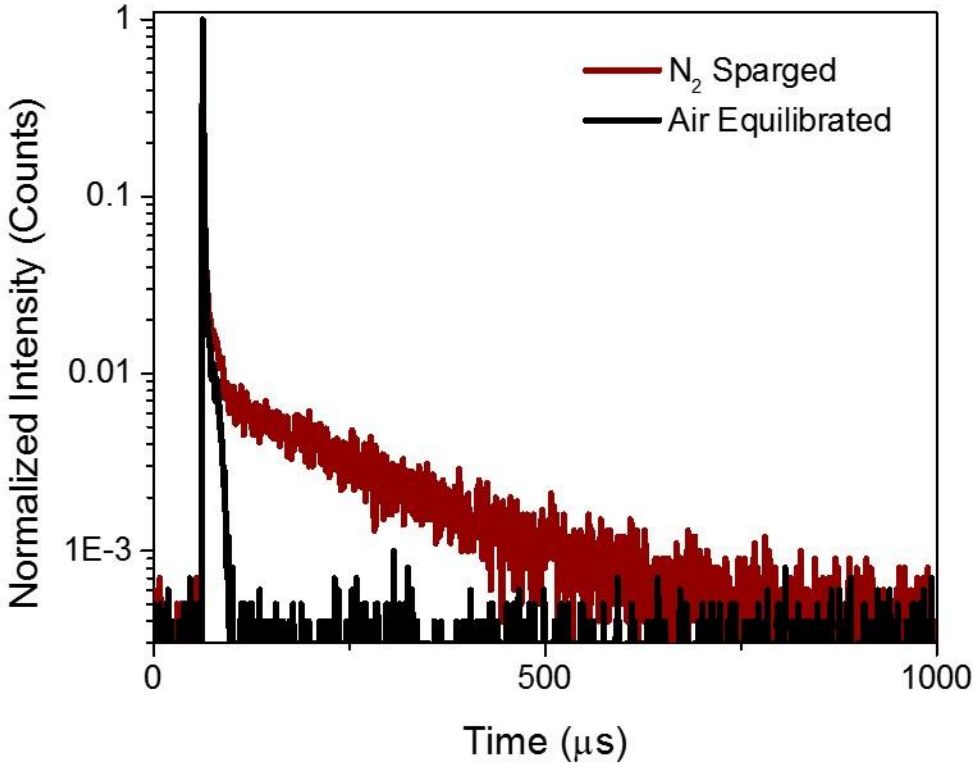

Figure 40 – Time-resolved fluorescence of 17 collected in toluene solution before and after sparging with nitrogen gas to minimize oxygen in solution.

Determining the reverse intersystem crossing rate using Equation 27 is complicated by the fact that the ratio of delayed fluorescence to prompt fluorescence quantum yield is less than 4, and thus Equation 28 will underestimate the Φ_{ISC}, while

equation 29 will overestimate it. However, they can be used to give us an upper and lower limit for Φ_{ISC}, and thus the k_{RISC}. Using these approximations gives a range of 0.5-1.0 × 10^4 $s^{-1,}$ which is low for highly efficient TADF emitters as may be expected due to the relatively high ΔE_{ST} of 0.13 eV.

Table 4 – Tabulated fluorescence and TADF quantum yields and lifetimes for compound and key rate constants for compounds 17 in toluene solution.

Compound	PLQY	Lifetime		k_{fl}	k_{RISC}	ΔE_{ST}
	Φ_{PF}; Φ_{DF}	τ_{PF} /ns	τ_{DF} /μs	/$10^7 s^{-1}$	/10^4 s^{-1}	/eV
17	0.16;0.12	8.8	179	1.8	0.5-1.0	0.13

To better understand the properties of the emitter in an environment more relevant to an OLED device, thin films containing compound **17** doped at 12.5 wt.% into a thin film comprised of bis(2-(diphenylphosphino)phenyl)ether oxide (DPEPO), obtained via spin-casting from chloroform in air followed by drying under high vacuum, were also photophysically characterized (See Figure 41, below). The ambient-temperature steady-state emission and the 77 K delayed emission are both quite similar to the corresponding spectra acquired in toluene solution, but with slight red shifts in the maxima and onsets, and a slightly larger estimated ΔE_{ST} value of 0.16 eV. The delayed fluorescence lifetime of 113 μs is somewhat shorter than that in toluene solution.

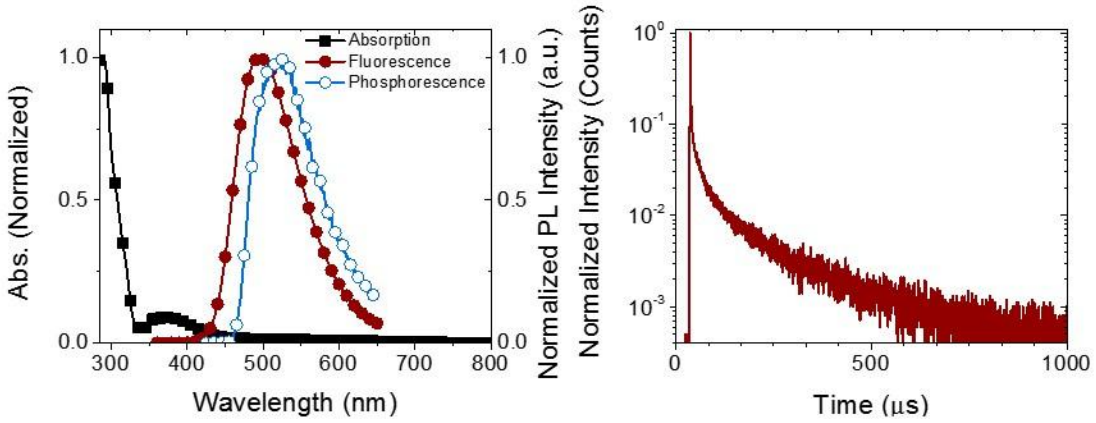

Figure 41 – Photoluminescence of 17 doped into DPEPO thin film (12.5 wt%) with absorption, fluorescence (300 K), and phosphorescence (77 K, 500 μs delay between excitation and data collection) on left, time resolved photoluminescence under

Finally, **17** was incorporated into an OLED to assess its electroluminescent properties. Device fabrication was performed by Xiaoqing Zhang, in the laboratory of Prof. Bernard Kippelen. The device structure, shown below in Figure 42 (a) along with chemical structures of organic materials used, was as follows: glass/ITO/ MoO_3 (15 nm)/Poly-TriCZ (80 nm)/DPEPO: **17** (25 nm, 25 wt.%)/TP3PO(4 nm)/ TPBi(50 nm)/LiF(1 nm)/Al(50 nm)/Ag(100 nm). The thin layer of molybdenum trioxide was evaporated as a hole-injection layer. The 80 nm-thick Poly-TriCZ hole-transporting layer was spin-coated (500 rpm for 60 s) from a chlorobenzene solution (10 mg/ml) and thermally annealed (110 °C for 2 min) in a nitrogen-filled glove box. The emissive layer (EML) was deposited via a co-evaporation of DPEPO:emitter with a dopant concentration of 25 wt.%. DPEPO was selected due to its high triplet state energy of ca. 3 eV.[134] Sequentially deposited TP3PO and TPBi layers used as electron transport layers. Lithium fluoride was deposited to improve the electron injection between a 50 nm-thick aluminum cathode and the organic layers. A silver layer was deposited atop the

aluminum to assist with the contact between the devices and the test set-up. The typical OLED active area was 3.0 × 3.0 mm. All thermal vacuum depositions were performed at pressures below 1.0×10^{-7} Torr.

The electroluminescent spectrum of the OLED under a bias of 5 V, shown in Figure 42(b), matched the photoluminescent spectrum of **17** in dilute toluene solution, displaying blue-green emission with λ_{max} at 494 nm and CIE coordinates of x = 0.22 and y = 0.46. Current-voltage-luminance characteristics and external quantum efficiency (EQE) are shown in Figure 42(c) and (d), respectively. At low luminance (ca. 10 cd/m^2) the device displayed a high EQE_{max} of 21.9%, well above the theoretical maximum EQE of a device that converts into light only the singlet excitons that form as singlets formed on charge recombination,[44] and providing further support that triplet excitons are being upconverted to singlets through the TADF process in **17**. The high EQE_{max} is attributed to the relatively high PLQY of the compound in the solid state, which was determined to be 0.72 under a stream of nitrogen when a thin film of the fluorophore doped into a DPEPO (12.5 wt.%) was prepared via spin-casting from chloroform in air and dried under high vacuum. On the other hand, the device displayed significant efficiency roll-off, to which the τ_{DF} of 179 μs is likely a major contributor,[135] as the EQE at a luminance of 1,000 cd/m^2 was reduced to 6.9%. While the different character of the S_1 and T_1 state would be expected to afford a larger spin-orbit coupling than a compound where both S_1 and T_1 have CT character,[78] the ΔE_{ST} of ca. 0.13 eV evidently prevents particularly fast reverse intersystem crossing in this compound as evidenced by the estimated RISC rate of ca.10^4 s^{-1} which is on the low-end of the value predicted for such an activation energy.

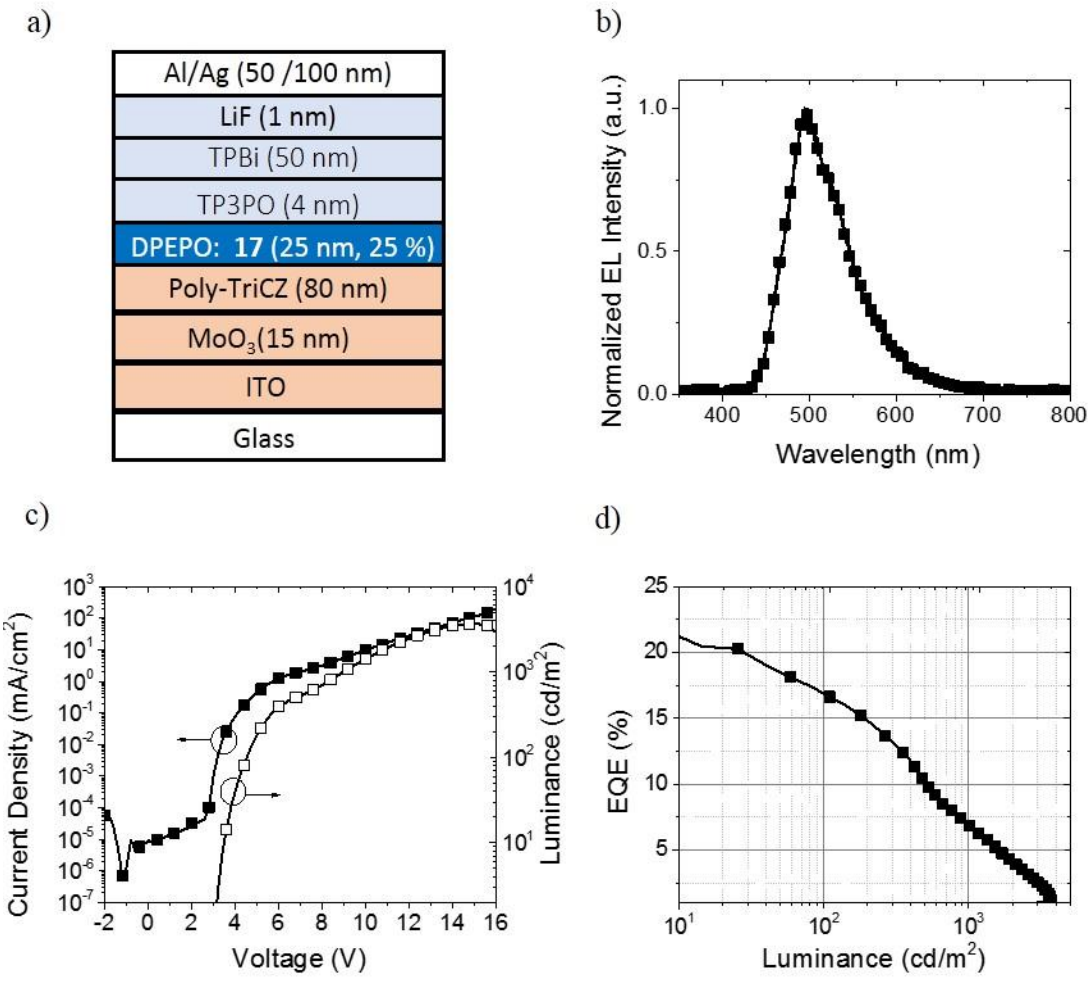

Figure 42 – (a) Device structure, (b) electroluminescence (EL) spectrum, (c) current-voltage-luminance (J-V-L) characteristics and (d) external quantum efficiency of OLED device containing 17 as the emitter.

In summary, TADF was achieved in compound **17** by stabilization of the intramolecular charge-transfer state. In going from compound **1** to compound **17**, the energy of the triplet was essentially unchanged while that of the singlet decreased by ca. 590 meV, from. 3.47 to 2.88 eV. As a result, ΔE_{ST} mirrored the change in the singlet energy as it was decreased by 590 meV from 0.72 to 0.13 eV.

3.3.3 Destabilizing the 2,5-Diphenyl-1,3,4-Oxadiazole Locally Excited State

Stabilization of the intramolecular charge-transfer state to the energy level of the unperturbed ^{3}LE state located on the DPO moiety has the inherent limitation that the color of the resulting fluorescent emission is limited by the energy of that state. In compound **17**, the S_1 energy was stabilized until TADF was observed. The resulting fluorescence λ_{max} at 490 nm in toluene solution produced an OLED when doped as the emitter into a host that, while highly efficient at low luminance, displayed a blue-green emission with *CIE* coordinates x = 0.22, y = 0.46. For reference, primary blue in the National Television System Committee color gamut is at x = 0.14, y = 0.08. To obtain blue fluorescence simultaneously with a low ΔE_{ST} from these components, it is clear that the triplet energy must be increased. As the triplet energy is dependent upon the energy of the locally excited state on the DPO moiety, this corresponds to increasing the energy of that state. Figure 32 shows how to increase this ^{3}LE state by disrupting the conjugation along the DPO system using sterically bulky substitution. This approach will be explored below.

Compounds **18** and **19**, Figure 43, were prepared in order to see how an increasing number of bulky donor substituents would effect on the relevant energy levels in the resulting fluorophore. Compound **18** adds a second donor *ortho* to the oxadiazole acceptor in the 6-position, relative to compound **9**. Compound **19** adds two more donors *ortho* to the oxadiazole acceptor, in the 2',6'-positions on the benzene ring in the 5-position of oxadiazole. These compounds are not a perfect series since the donor for **18**

and **19** differs from the Cz donor for **9**, which will affect the energy of the CT transitions in the donor-acceptor compounds. However, a comparison of the triplet state energies, which have been shown to have LE character and to be found on the DPO moiety and not on the Cz, should be broadly valid.

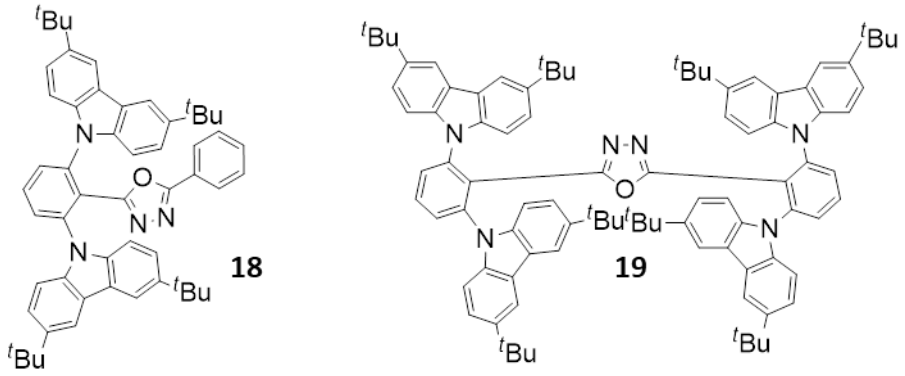

Figure 43 – Carbazole-oxadiazole compounds synthesized with increased steric crowding around the oxadiazole acceptor moiety.

Figure 44 shows the photoluminescence spectra of the compounds plotted against energy. The fluorescent emission of **18** and **19** are strikingly similar, almost superimposable upon one another, and still show the characteristic broad structureless line shape of a charge-transfer transition. Comparison to the fluorescence of **9** would not be appropriate due to the difference in the donor moiety. Turning attention to the phosphorescent emission, the triplet energy of **9** is only slightly increased by the substitution of a second donor *ortho* to the oxadiazole as in **18**, from ca. 2.82 when carbazole is in the 2-position to 2.84 eV when carbazole is substituted in the 2- and 6-positions, and displays a similar line shape. This can reasonably be interpreted as the emission coming from a similar transition well characterized by the ^{3}LE state that we have established likely lies on the DPO acceptor, with the energy of the transition

increased ca. 100 meV from that of compound **1** by twisting the phenyl bridge out of plane of the oxadiazole. The small increase in triplet energy between **9** and **18** suggests that the second donor group is largely unnecessary for increasing triplet energy and the conjugation of the bridging phenyl group to the oxadiazole was not further decreased by an appreciable amount.

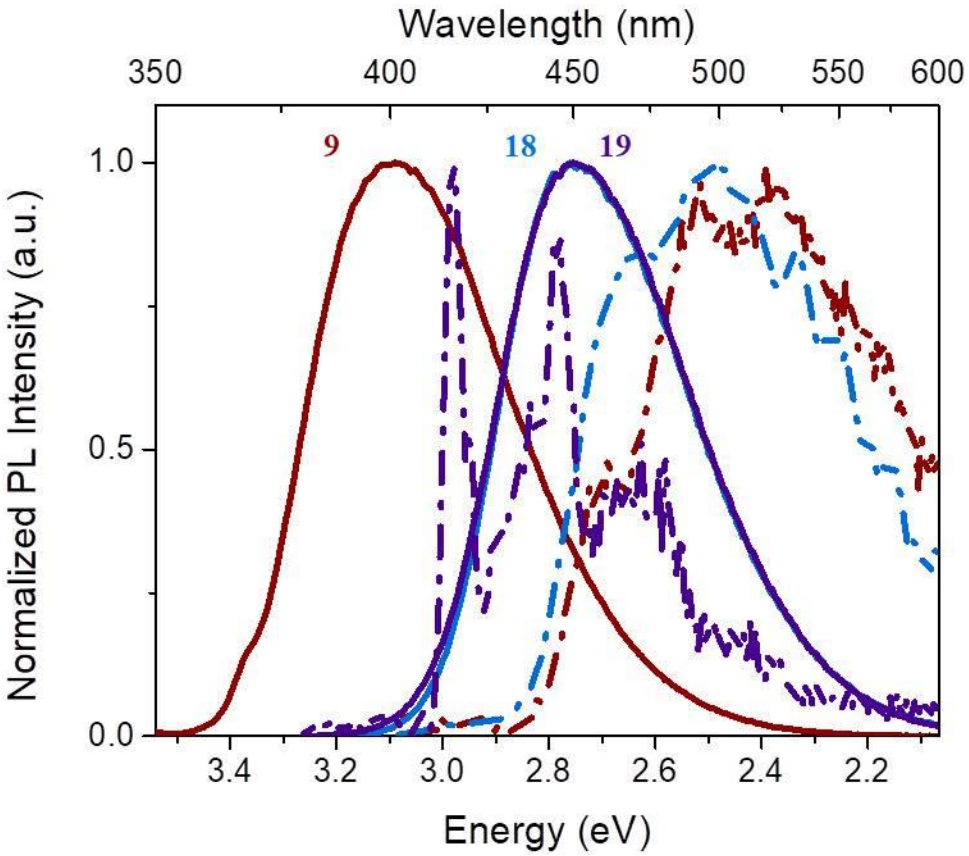

Figure 44 – Photoluminescence intensity of 9, 18, and 19 versus energy. Fluorescence spectra collected in toluene solution (ca. 10^{-5} M) at room temperatue, phosphorescence spectra collected in toluene matrix at 77 K with a 500 µs delay between excitation and detection.

With the addition of the donors to the 2' and 6' positions, the triplet energy is dramatically increased to 3.02 eV, ca. 0.30 eV higher than the starting compound **1** and

0.2 higher than the compounds with crowding only on one of the phenyl groups. Furthermore, the line shape and the energy of the phosphorescent spectrum strongly resembles that of an isolated N-phenylcarbazole molecule.[86] This can be interpreted as the conjugation across the DPO moiety being reduced to the point where the energy of the ^{3}LE state localized on DPO is higher than that of the Cz, and the T_1 is now best characterized as a ^{3}LE state localized on the Cz donor.

Table 5 – Tabulated steady-state absorption and photoluminescence data of simple compounds 18 and 19. Absorption and fluorescence data collected in toluene solution (ca. 10^{-5} M) at room temperature. Phosphorescence collected in toluene matrix at 77 K.

Compound	Absorption	Fluorescence		Phosphorescence		ΔE_{ST}
	λ_{max} /nm	λ_{max} /nm	Onset /eV	λ_{max} /nm	Onset /eV	/eV
18	289, 327, 341	449	3.02	497	2.84	0.18
19	290, 296, 326, 340	450	3.03	416, 445	3.02	0.01

The adiabatic ΔE_{ST} of these compounds follows not the singlet energy, as in all of the compounds in section 3.3.2, but instead tracks directly with the triplet energy. Compound **19**, which displays a virtually superimposable fluorescent emission with **18**, has a an estimated ΔE_{ST} of 0.01 eV, almost 0.2 eV lower than in **18**. This low ΔE_{ST}, is, again, due entirely to the increase in the triplet energy. Despite this low value, investigation into whether the compound displayed TADF revealed only a monoexponential decay in the transient photoluminescence, despite sparging with nitrogen to exclude triplet quenching oxygen. Potentially, this is due to the very low luminescence of the compound, and the slow rate of fluorescence means the compound relaxes non-radiatively before observable TADF can occur. The PLQY of **19** in toluene

was determined to be 0.02 with a fluorescent lifetime of 2.8 ns. The rate of fluorescence is 7.1×10^6 s^{-1} which is even lower than the compounds **9** and **18**, of 3.5 and 1.0×10^7 s^{-1}, respectively. This can be rationalized using the same physical explanation as for why the T_1 energy is seen to increase; as the DPO is twisted out of plane, the oscillator strength decreases as electronic overlap between the carbazole localized HOMO and the diphenyloxadiazole localized LUMO decreases.

Table 6 – Tabulated fluorescence and TADF quantum yields and lifetimes for compound and key rate constants for compounds 18 and 19 in toluene solution.

Compound	PLQY	Lifetime		k_{fl}	k_{RISC}	ΔE_{ST}
	φ_{PF}; φ_{DF}	τ_{PF} /ns	τ_{DF} /μs	/$10^7 s^{-1}$	/10^4 s^{-1}	/eV
18	0.09	8.9	-	1.0	-	0.18
19	0.02	2.8	-	0.71	-	0.01

Despite the lack of observable delayed fluorescence in compound **19** in solution, thin films in which the fluorophore was doped into a DPEPO host matrix were prepared via spin-casting from chloroform (12.5 wt. %, 1 mg/mL, 500 rpm) to examine the fluorophores in an environment more relevant to that in an OLED device. The thin film displayed a much increased PLQY of 0.30 and a clear delayed fluorescence component in the transient photoluminescent decay (Figure 45). Importantly, the *CIE* (x,y) coordinates of the photoluminescence of the film was 0.15, 0.09. This true blue emission in a compound that displays TADF is only possible through the increased triplet energy achieved by the destabilization of the ^{3}LE energy of DPO.

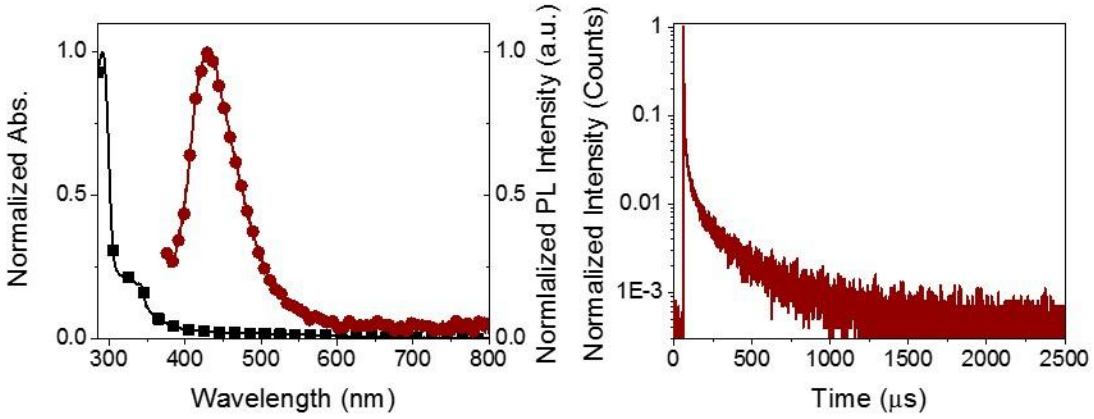

Figure 45 – Compound 19 doped (12.5 wt. %) DPEPO thin film. (*left*) Absorption (black) and photoluminescence (red) and (*right*) transient photoluminescence.

Despite the the lack of success in an OLED device, the approach of increasing the energy of the ^{3}LE on the DPO acceptor was successful in realizing a CzDPO fluorophore that displayed TADF properties while simultaneously displaying true fluorescent blue emission. This did come at the cost of a severely decreased fluorescent decay rate.

3.3.4 Combined Approach – Exploiting Regiochemistry to Decrease ΔE_{ST}

With the above compounds, limits of the approaches for decreasing the ΔE_{ST} described in Section 3.3.1 were explored. On the one hand, stabilizing the intramolecular charge transfer state towards the ^{3}LE resulted in a fluorophore (**17**) that displayed TADF with high PLQY (0.72 under a stream of nitrogen when a thin film of the fluorophore doped into a DPEPO at 12.5 wt.%), and yielded an OLED with high external quantum efficiency when doped into the emissive layer, although with significant roll-off and with blue-green emission. On the other hand, pushing the ^{3}LE state on the DPO moiety upwards towards the ^{1}CT state resulted in a fluorophore (**19**) that displayed TADF with true blue emission when doped into a thin film, but exhibited weak fluorescence and an

OLED using it as the emitter displayed low external quantum efficiency. The rest of the compounds in this chapter will fall within the boundaries set by compounds **17** and **19** in an attempt to design emitters that display high fluorescence and thermally activated delayed fluorescence while also maintaining the higher singlet energy necessary for blue emission.

Compounds **20**-**24**, shown in Figure 46, can be considered as derivatives of compound **3** with an increased level of substitution of the carbazol-9-yl donor for fluorine. The effect of an increasing number of donor substituents on the photophysics of the resulting fluorophore has been observed experimentally as a method for decreasing the HOMO-LUMO gap, the S_1 energy, and the ΔE_{ST}.[136] The effect on the S_1 energy was noted here; see compounds **9**-**11** vs. **16**. Several recent computational studies have focused on elucidating the mechanism by which the S_1 energy is reduced for the purpose of developing advanced design rules for TADF compounds. It has been calculated (ωB97X functional, 6-31G(d) basis set) that a model series of Cz-phthalonitrile-based TADF molecules show a monotonic decrease in both S_1 and T_1-state energy with increased number of Cz donors,[88] with a larger decrease for the S_1 energy leading to a parallel monotonic decrease in ΔE_{ST}. The effect on the CT-like S_1 state has been explained through stabilization of the acceptor LUMO via inductive electron withdrawal from the acceptor by the carbazol-9-yl substituents, with each additional carbazole increasing this effect.[137-139] The smaller effect on the T_1-state energy, conversely, is due to the T_1-state, at least for the less substituted compounds, being well described by a localized excitation (LE) rather than an intramolecular CT HOMO-LUMO transition.[78, 88] Additionally, and it has also been shown that increased substitution by donors can

increase spin-orbit coupling when the S_1 and T_1 states differ in character, whether they are CT vs. LE states, respectively, or whether distinct CT states that mix in to different extents in the singlet and triplet manifolds.[78, 140]

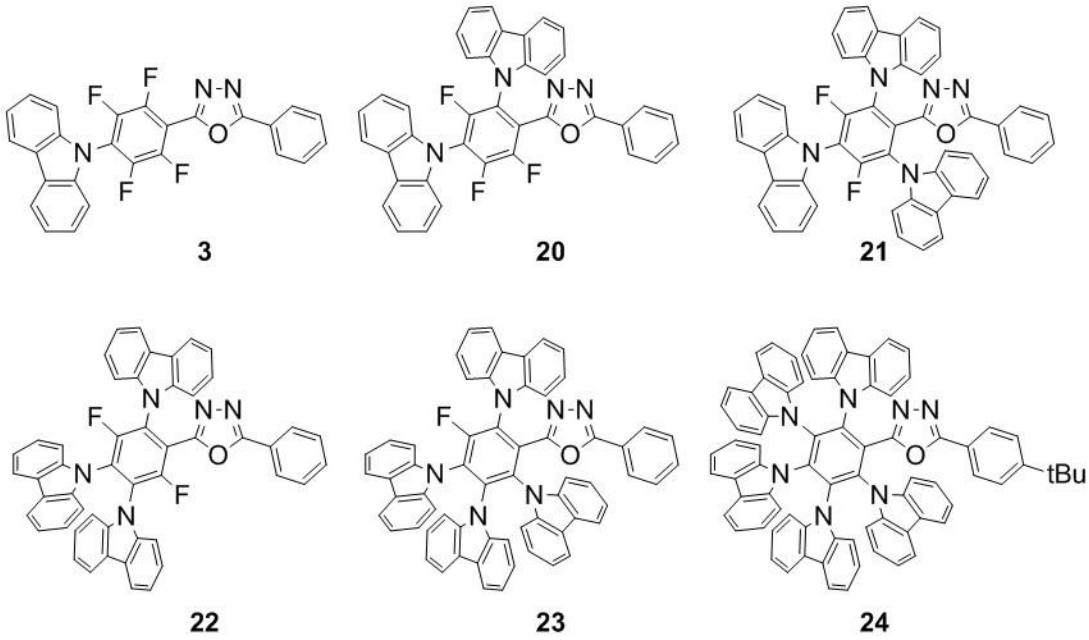

Figure 46 – Structures of $Cz_nF_{5-n}DPO$ compounds investigated.

The specific topology of the D-A TADF compound has only very recently come under systematic investigation. Kim described calculations (gt-ωB97-X functional, 6-31G(d) basis set) on Cz-phthalonitrile TADF compounds, suggesting that attachment of the donor at chemically inequivalent positions significantly affects not the LUMO of the acceptor, but the nature and energy of the donor HOMO instead.[141] The effect on the triplet state was, again, less pronounced and exhibited diminishing significance as the number of donors increased and the additive inductive effects began to dominate over mesomeric effects.[141] Geng et al. found very little change in the energy of the S_1 state by varying the connectivity in xanthone-phenylene-carbazole compounds, but were able to

raise the T_1 energy by moving from *para*- to *meta*- to *ortho*-substitution patterns,[142] similar to as seen in connectivity series above.

To help estimate the ionization potential and the electron affinity levels in the compounds relative to one another, oxidation and reduction potentials were measured using cyclic voltammetry in dichloromethane and tetrahydrofuran, respectively, and all values are referenced against a $FeCp_2^+/FeCp_2$ internal standard. The voltammograms are shown in section 3.5.3, and the data is tabulated in Table 7. In the case of nonreversible oxidation processes, potentials were estimated from the onset at a scan rate of 50 mV s^{-1}. The reduction waves were sufficiently reversible processes that $E_{1/2}$ values could be estimated. The compounds became slightly more difficult to reduce as additional carbazole groups were added, from -2.00 V for **3** to -2.19 V for **24**, suggesting fluoro has a greater stabilizing effect on the LUMO than carbazolyl, consistent with it acting as a slightly stronger electron-withdrawing group. All compounds showed irreversible oxidation behavior during the cathodic sweep, consistent with electrochemical oxidation occurring on the Cz donor.[143] The compounds are increasingly easily oxidized with additional Cz substitution, again consistent with the slightly greater electron-withdrawing effects of fluorine substituents. Values ranged from 1.17 V for **3** down to 1.00 V for **24**. Taken together, the electrochemical gap ($E_{ec}^{g} = e(E^{ox} - E^{red})$) changed minimally within the series, from 3.12 eV to 3.19 eV. This provides evidence that any significant changes in the optical properties in this series of compounds cannot be attributed purely to the relative strengths of the donor and the acceptor due to inductive effects.

Table 7 – Tabulated electrochemical potentials of compounds 3, 20-24 vs. $FeCp_2^+/FeCp_2$. Oxidative and reductive scans performed in dichloromethane and tetrahydrofuran, respectively.

Compound	Electrochemical Potential		
	E^{ox} /V	E^{red} /V	E^g /eV
3	1.17	-2.00	3.17
20	1.15	-1.99	3.14
21	1.11	-2.04	3.15
22	1.08	-2.05	3.13
23	1.02	-2.10	3.12
24	1.00	-2.19	3.19

The energy of the S_1 state, estimated using the onset of fluorescence, differs more significantly over the series (0.39 eV variation) than the electrochemical gap (0.07 eV variation). Figure 47 shows the fluorescence spectra of the compounds, collected in dilute toluene solution, plotted against energy. Compound **3** exhibits a fluorescence onset at 3.24 eV. Substituting one fluorine with carbazole yields **20** and lowers the S_1 state energy to 3.10 eV. Tri-substituted compounds **21** and **22** are at 2.85 and 3.06 eV, respectively. Addition of a fourth Cz donor on **23** resulted in onset at 2.86 eV, and pentasubstituted **24** is at 2.93 eV. Fluorescence maxima follow the same trend as the onsets.

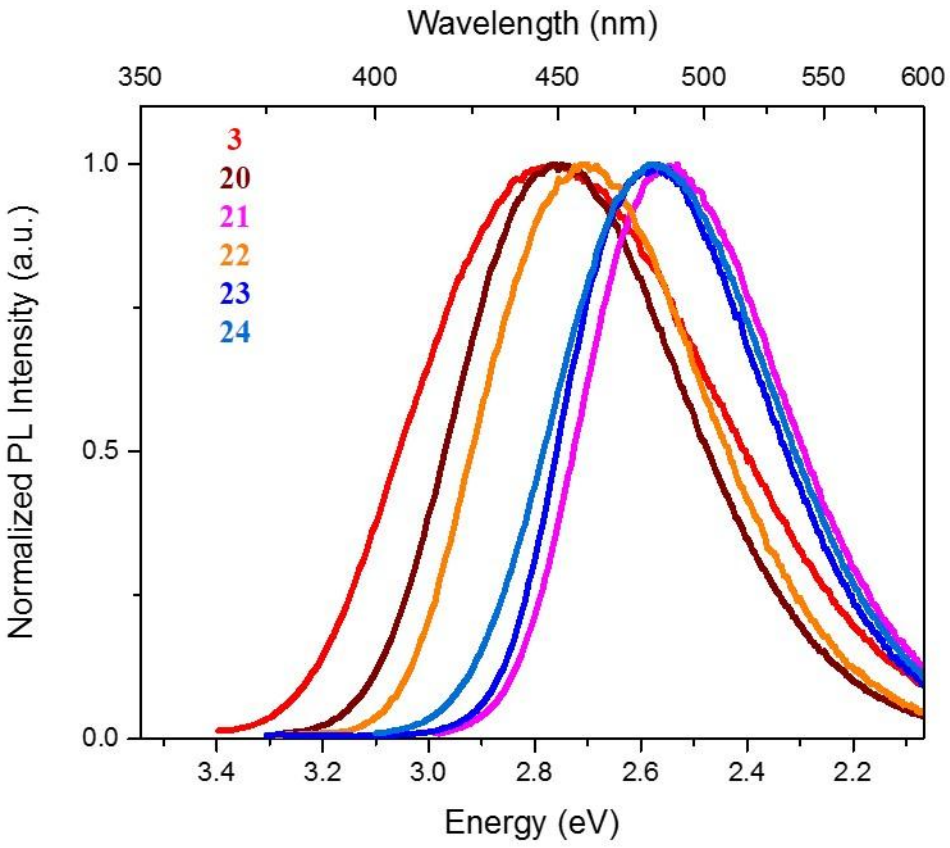

Figure 47 – Fluorescent intensity of compounds 3 and 20-24 versus energy, collected in toluene solution (ca. 10^{-5} M) at room temperature.

When interpreting the structural effects on the singlet state energies, two observations stand out. First, the range of S_1 state energies (ca. 400 meV) is significantly higher than that of the electrochemical gaps, (ca. 70 meV). Second, substitution of Cz into the 2- and 6- position provides strong stabilization of S_1, while substitution at the 3 and 5 positions has relatively little effect. The molecules can be classified into three groups based on their S_1 energies, and on how many donors are substituted in the critical 2- and 6-positions: compounds with 2,6-donors in addition to in the 4-position exhibit the most red shifted fluorescence (red shifts of 0.39, 0.38, and 0.31 eV for the onsets of **21**, **23**, and **24** vs. that of **3**); compounds substituted in only the 2-position in addition to the

4-position exhibit intermediate S_1 state energies (red shifts of 0.14 and 0.18 eV for **20** and **22** vs. CzDPO); while CzDPO has the highest S1 energy.

The T_1 energy was estimated using the onset of phosphorescence, shown in Figure 48. In contrast to the S_1 energy, which, as noted above, varied by ca. 400 meV in the series, the T_1-state energy was less sensitive to donor substitution, varying by ca. 100 meV. However, the line shapes of the phosphorescence spectra do fall into two distinct classes. The compounds that retain fluoro substituents in both 3- and 5-positions displayed a line shape resembling the phosphorescent emission of an isolated donor or acceptor; specifically a Cz-like line shape[86] is seen in **3** and a DPO-like emission[102] is seen for **20** and **21.** Previously reported quantum-chemical calculations have found the T_1-state on similar CzDPO compounds to be a LE state primarily localized on the DPO moiety.[105] The compounds that contain Cz in the 3 and/or 5 positions show an emission line shape distinct from the previous compounds, with well-resolved 0,0-peaked high-frequency (ca. 1300 cm^{-1}) vibronic structure (Figure 48). This may indicate a different T_1-state character. In particular the line shape indicates that the T_1 and S_0 geometries are primarily related through high-frequency modes; this could possibly be due to suppression of low-frequency torsional relaxations by the steric crowding of adjacent carbazole groups in the 3- and/or 5-Cz-substituted species. Noda et al. have also recently described donor substitution in the 3- and 5-positions modifying triplet states in compounds independent of the CT state.[144]

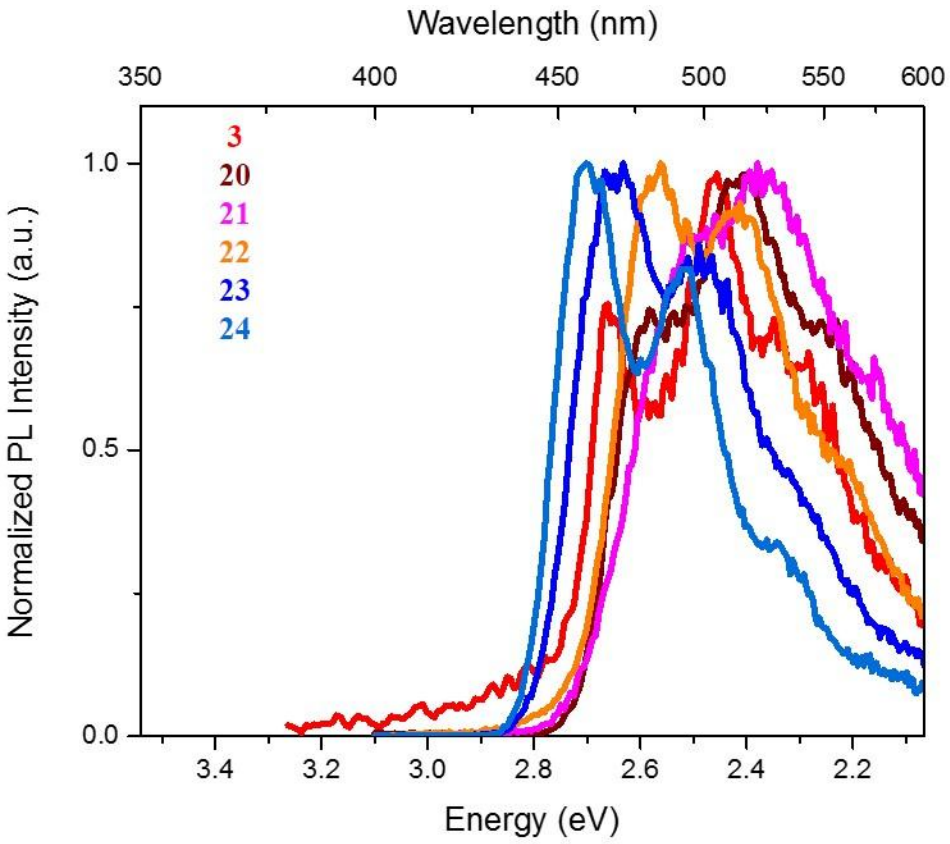

Figure 48 – Phosphorescence spectra of compounds 3 and 20-24 versus energy, collected in toluene matrix (ca. 10^{-5} M) at 77 K with a 500 µs delay after excitation.

The highest T_1 energies of the series were found for the more highly substituted **23** (2.79 eV) and **24** (2.81 eV). Due to the relatively small variation in T_1 energies, the estimated ΔE_{ST} values roughly followed the trend for the S_1 energy and are shown in Table 2. Compounds **21**, **23**, and **24** – the compounds with the lowest energy S_1-states – exhibit the smallest ΔE_{ST} values. However, it was also seen that the most highly substituted compounds, **23** and **24**, have the highest triplet energies which may be attributable to the same mechanism as shown in **Figure 32**.

Table 8 – Tabulated steady-state absorption and photoluminescence data of simple compounds 12-17. Absorption and fluorescence data collected in toluene solution (ca. 10^{-5} M) at room temperature. Phosphorescence collected in toluene matrix at 77 K.

Compound	Absorption	Fluorescence		Phosphorescence		ΔE_{ST}
	λ_{max} /nm	λ_{max} /nm	Onset /eV	λ_{max} /nm	Onset /eV	/eV
3	288, 344	444	3.24	508	2.75	0.49
20	288, 315, 329, 347	449	3.10	516	2.72	0.38
21	288, 316, 329, 345	490	2.85	521	2.73	0.12
22	289, 314, 329, 361	459	3.06	484	2.71	0.35
23	290, 319, 331	483	2.86	471	2.79	0.07
24	291, 333	482	2.93	459	2.81	0.12

To probe the potential application of these compounds as TADF emitters, fluorescence transients were collected for the more promising compounds in toluene solution that had been sparged by bubbling nitrogen for ca. 15 minutes; these are shown in Figure 49. Compound **24** displayed a biexponential fluorescent decay composed of a prompt component with a lifetime of 3.2 ns and a strong delayed luminescence component, attributed to TADF, with a lifetime of 62.8 μs. Compounds **21** and **23** also displayed biexponential fluorescent decay (prompt fluorescence τ_{fl} = 3.9 and 3.2 ns, respectively) with minor delayed fluorescence components that, while distinguishable from the instrument response function (IRF), could not be reliably fitted to determine the delayed lifetime. The long-lived luminescence components were quenched after exposure to air, consistent with TADF, where the triplet state can be quenched by oxygen before

undergoing RISC. It is worth noting that while **21** exhibited detectable TADF, regioisomer **22**, which exhibits a larger ΔE_{ST} value, does not, illustrating the importance of D-A topology in the design of TADF compounds. For compound **24**, the k_{RISC} was determined to be 5.38×10^4 s^{-1}, which is 5-10 times higher than that of compound **17**, above despite a similar ΔE_{ST}.

Thin films of the three compounds displaying TADF properties were deposited by co-evaporation of the fluorophore (25 wt.%) with a DPEPO host on a quartz substrate. The emission maxima of the films were 472, 484 and 479 nm for **21**, **23**, and **24**, respectively. Each compound displayed fluorescent decay with contribution from fast and slow components when measured under a nitrogen stream. When fit with a biexponential decay function, delayed fluorescent lifetimes of 308.7, 166.2 and 75.0 μs were determined, respectively. Absolute photoluminescent quantum yields were significantly higher than when determined in toluene solution, presumably due to decreased non-radiative relaxation rates in thin film vs. in solution.

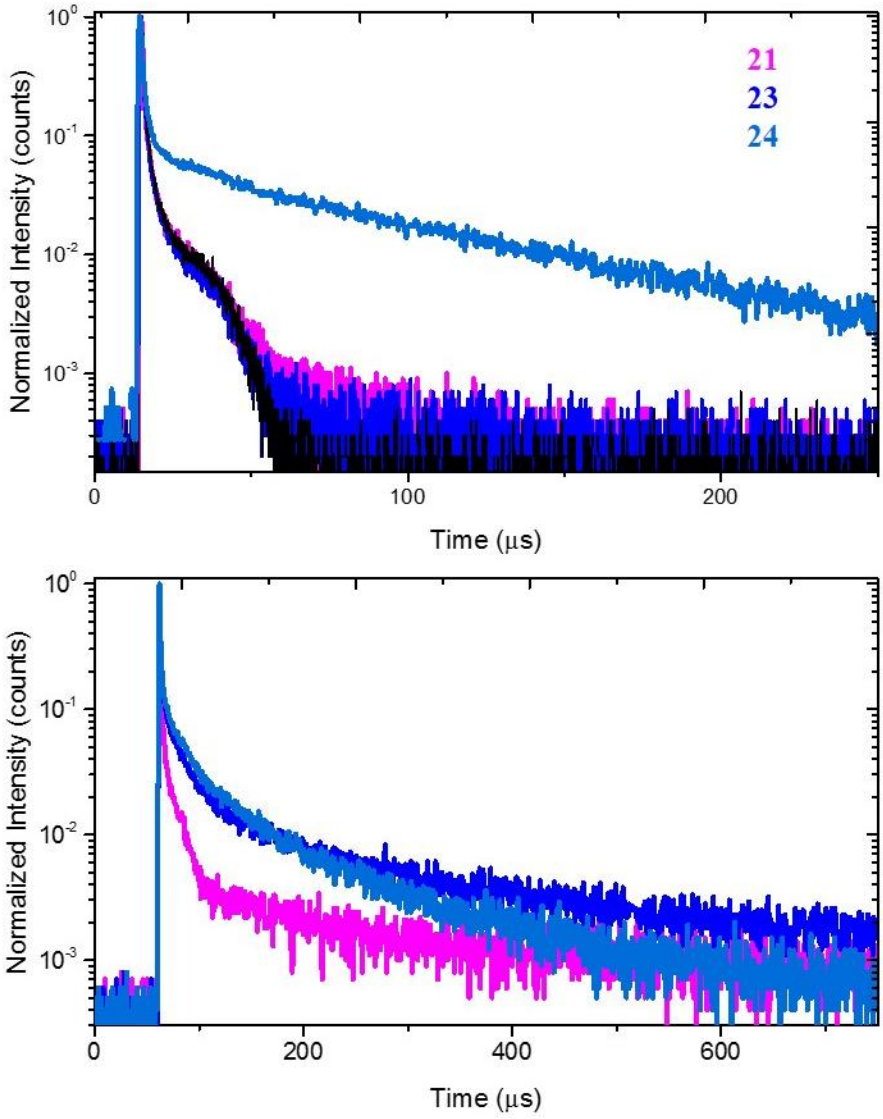

Figure 49 – Time-resolved photoluminescence of 21, 23, and 24. (*top*) Photoluminescence collected in toluene solution after sparging with nitrogen gas to minimize oxygen in solution. (*bottom*) Fluorophore (25 wt.%) doped into DPEPO thin film, transient collected under a stream of nitrogen.

Under a stream of nitrogen, the PLQYs were 0.32, 0.54 and 0.61, respectively. It is worth noting along with the change in the spectral line shape in the phosphorescent emission, the compounds with donors in the 3- and 5-positions, positions that do not

apparently play a major electronic role in the fluorescent transition, show increased TADF despite similar ΔE_{ST} values. This provides circumstantial evidence RISC mechanism relies on these substituents, likely by providing a triplet state with increased spin-orbit coupling with the ^{1}CT state.

Table 9 – Fluorescence and TADF quantum yields and lifetimes and key rate constants for compounds 3 and 20-24 in toluene solution. ΔE_{ST} estimated from spectral onsets.

Compound	PLQY	Lifetime		k_{fl}	k_{RISC}	ΔE_{ST}
	Φ_{PF}; Φ_{DF}	τ_{PF} /ns	τ_{DF} /μs	/$10^7 s^{-1}$	/10^4 s^{-1}	/eV
3	0.21	6.7	-	3.13	-	0.49
20	0.05	4.8	-	1.04	-	0.38
21	0.04;0.02	3.9	-	1.02	-	0.12
22	0.12	7.7	-	1.56	-	0.35
23	0.06;0.04	3.2	-	1.88	-	0.07
24	0.03;0.10	2.9	62.8	1.03	5.38	0.12

The performance of the three emitters exhibiting TADF discussed above was evaluated in OLEDs with the structure shown in Figure 50(a) (see 3.5.4 for chemical structures of the materials). Device fabrication was performed by Xiaoqing Zhang, in the laboratory of Prof. Bernard Kippelen. Figure 50(b) displays the normalized electroluminescence (EL) spectra of the three devices. The EL spectra of the devices exhibit more structure than the corresponding solution fluorescence spectra; in addition to

the peak at ca. 490 nm, each device also exhibits a subsidiary peak or shoulder at ca. 470 nm, and longer wavelength shoulders. However, the positions of the strongest maximum and the overall emission widths are consistent with those seen in the solution fluorescence spectra. However, in the device containing the emitter **23**, the intensity of the spectral peak at 470 nm is significantly smaller, leading to a greener light emission of the device. The existence of two peaks in these devices is due to the concentration of the emitter, and has been studied in detail by Zhang et al.[145]

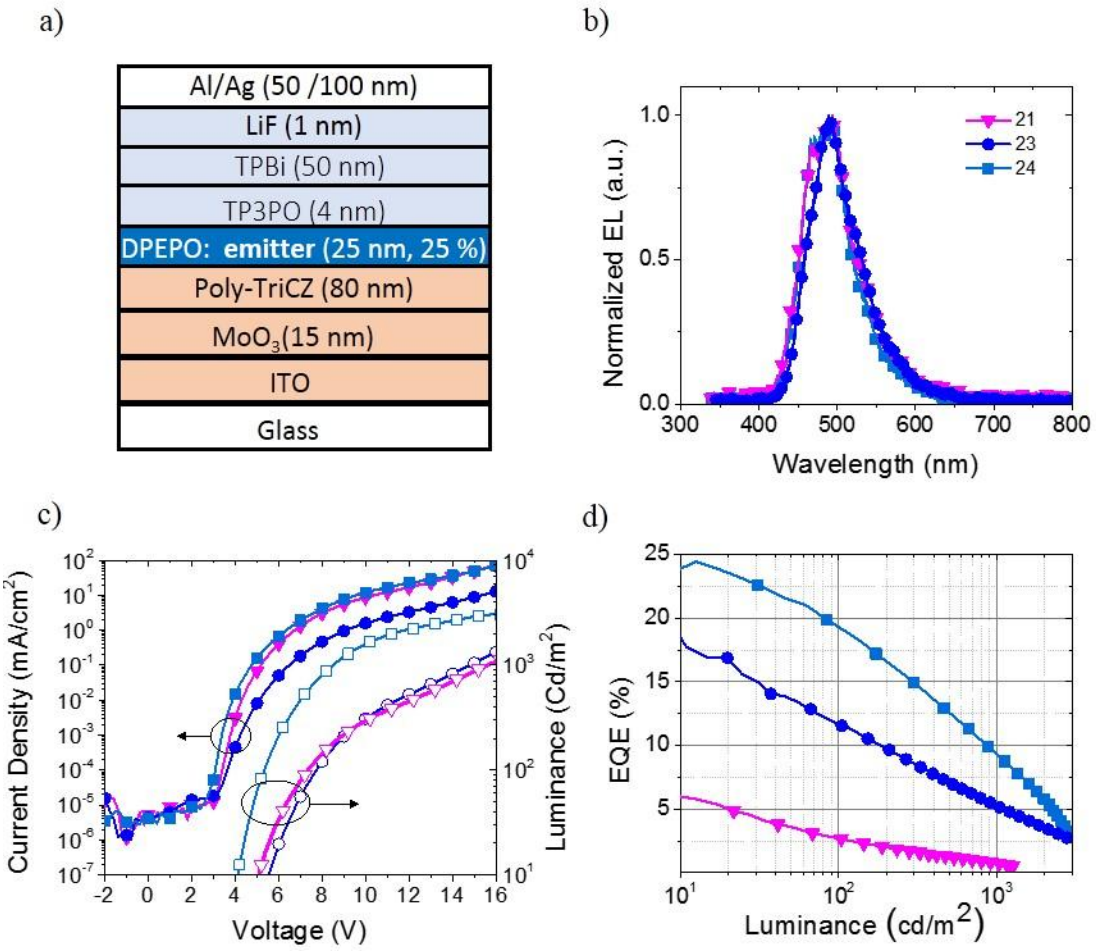

Figure 50 – (a) Device structures; (b) Electroluminescence (EL) spectra, (c) Current-voltage-luminance (J-V-L) characteristics, and (d) EQE of three devices containing 21, 23, and 24 as emitters, respectively.

Current-voltage-luminance characteristics and EQE as a function of luminance are shown in Figure 50(c) and (d), respectively. Despite having similar estimated ΔE_{ST} in solution, the compounds in which there are donors in the 3- and 5-positions displayed stronger delayed fluorescence with shorter delayed fluorescent lifetimes. This trend of spectroscopic characteristics favoring TADF was continued in the device efficiencies. EQE_{max} values in the devices ranged from 6.1% in **21**, to 17.8% in **23**, and up to 24.4% at a reference luminance of 10 cd/m^2 in **24**. Note that under higher injection conditions and at a luminance of 1,000 cd/m^2, more relevant for applications, devices with **24** yield EQE values of 9.2% in non-optimized devices. Device characteristics are summarized in Table 10. Note that *CIE* (x,y) coordinates of the devices all show a significantly more blue emission than that of compound **17**, which emitted green-blue light with chromaticity 0.22, 0.46. Despite this, the efficiency of the devices are comparable due to an increased triplet energy and increase k_{RISC} made possible by more advanced molecular design.

Table 10 – Device performance of OLEDs made using emitters 21, 23 and 24. Turn-on voltage (V_{on}) defined as that required to reach 10 cd m^{-2}. EQE, CE and PE maximum values reported at 10 cd m^{-2}.

Emitter	V_{on}	EQE_{max}	CE_{max}	PE_{max}	*CIE*
	V	*%*	*cd A^{-1}*	*lm W^{-1}*	*x,y*
21	5.1	6.1	12.3	7.7	0.17, 0.30
23	5.5	17.8	40.6	22.8	0.18, 0.36
24	4.1	24.4	46.3	34.6	0.16, 0.29

Finally, to extend the results of the best emitter thus far (**24**), the analogous compound **25** was synthesized with the expectation that the 3,6-di-*tert*-butylcarbazol-9-yl

donor would stabilize the S_1 energy relative to the T_1 in the same way as was seen in the connectivity series seen earlier. The structure and the absorption and photoluminescence are shown below in Figure 51. According to previous results, for example compound **2** vs. **12**, the energy of the singlet may be expected to decrease from that of **24** by ca. 13 meV, and in fact it decreased 9 meV to 2.84 eV. The energy of the triplet state was, notably, relatively unchanged with an energy estimated from spectral onset as 2.84 eV, approximately 0.1 eV higher than in the CzDPO model compound **1** and consistent with the twisted DPO localized triplet described in Section 3.3. The result is a decreased ΔE_{ST} of ca. 0.01 eV when estimated from spectral onsets.

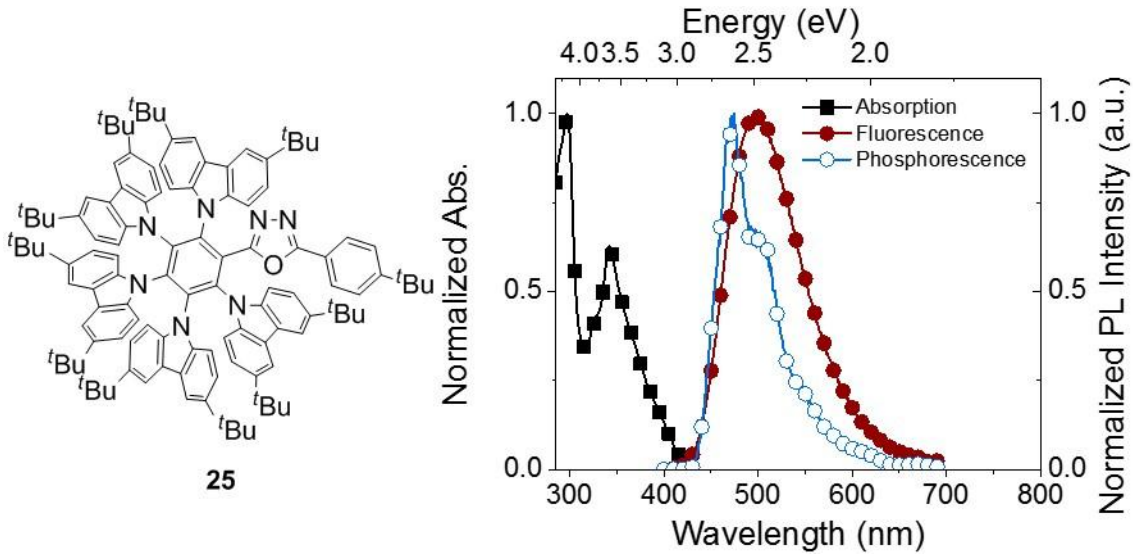

Figure 51 – Structure and absorption and photoluminescence spectra of 17 collected in toluene (ca. 10^{-5} M).

Practically, the result of this is a fluorophore that has a slightly red shifted emission from that of **24**. Transient photoluminescence reveals the strong delayed component in the biexponential decay, consistent with TADF, with a delayed fluorescent lifetime of 30.4 μs in toluene, faster than that found in **24**. Analysis of the collected data

(see Table 11) shows that the k_{RISC} is increased by a factor of 2-3 which is consistent with the lower barrier of the decreased ΔE_{ST}, while the k_{fl} is largely unchanged.

Table 11 – Steady state and time resolved photoluminescent data collected for compound 25. Data collected in dilute toluene solution (ca. 5 × 10^{-5} M), ΔE_{ST} estimated from spectral onsets.

Compound	Absorption	Fluorescence		Phosphorescence		ΔE_{ST}
	λ_{max} /nm	λ_{max} /nm	Onset /eV	λ_{max} /nm	Onset /eV	/eV
25	297, 342	496	2.84	488	2.83	0.01
	PLQY	**Lifetime**		k_{fl}	k_{RISC}	
	Φ_{PF}; Φ_{DF}	τ_{PF} /ns	τ_{DF} /μs	/10^7 s^{-1}	/10^4 s^{-1}	
	0.05;0.15	2.8	30.4	1.79	13.2	

The performance of compound **25** as an emitter was evaluated in an OLED with the structure shown in Figure 52(a), the EL spectrum is shown in (b), J-V-L characteristics in (c), and EQE as a function of luminance in (d). The chemical structures of the materials used in the fabrication of the device are shown in 3.5.4. The OLED performance confirms the strong TADF behavior of the emitter **25** as the device exhibited a very high EQE_{max} of 28.7 % at low luminance (10 cd m^{-2}), and 13.0% at 1,000 cd/m^2. The higher EQE compared to the comparable compound **24** can be attributed to the higher ϕ_{fl}, determined to be 0.81 for **25** in a thin film (12.5% in DPEPO) vs. 0.61 for **24** under similar conditions. The decreased efficiency roll-off in the device exploiting **25** as the emitter, which maintains 45% of the EQE_{max} at 1,000 cd/m^2 vs. 38% for the OLED utilizing **24**, is tentatively attributed to the decreased delayed fluorescent lifetime[146]

which is itself attributed to the decreased ΔE_{ST} due to the stronger donating strength of the *t*Cz donor of **25** as compared to the Cz donors on **24**.

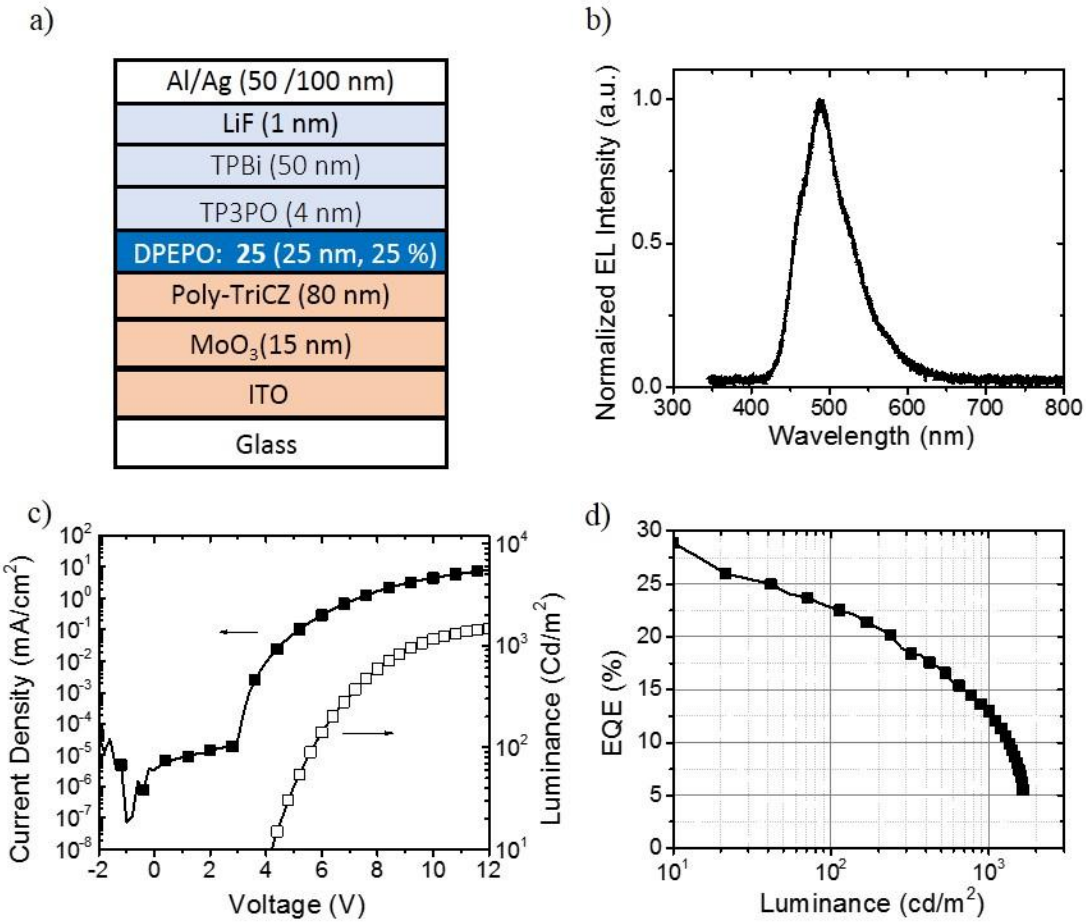

Figure 52 – (a) Device structure; (b) Electroluminescence (EL) spectrum, (c) Current-voltage-luminance (J-V-L) characteristics, and (d) EQE of device containing compound 25 as the emitter.

3.4 Conclusions

The simple donor-acceptor compound 2-(4-(carbazol-9-yl)phenyl)-5-phenyl-1,3,4 oxadiazole (**1**) is a donor-acceptor compound comprised of ubiquitous donor and acceptor moieties, but does not display detectable TADF due to a high energy (3.32 eV) singlet state well described by a an intramolecular charge-transfer from the carbazole to

the oxadiazole, and a relatively low lying ^{3}LE state located on the DPO moiety, resulting in an estimated adiabatic ΔE_{ST} of over 0.7 eV.

Multiple strategies to decrease the ΔE_{ST} were developed. Stabilization of the ^{1}CT state by increasing the strength of the donor and/or the acceptor succeeded in lowering the singlet energy independent of the triplet energy, leading to a ΔE_{ST} to ca. 0.13 eV in compound **17** while maintaining relatively high fluorescent decay rates. An OLED device incorporating this emitter displayed a high EQE_{max} of ca. 20%, implying an IQE_{max} approaching unity, but also a greenish blue emission due to the lower energy CT state. Destabilization of the ^{3}LE state by forcing the three rings of the 2,5-diphenyl-1,3,4-oxadiazole unit out of plane by using sterically bulky groups in the positions *ortho* to the oxadiazole was able to increase the triplet energy independent of the singlet state, leading to a ΔE_{ST} of ca. 0.01 eV in compound **19**, but had the concomitant effect of decreasing the fluorescent decay rate by two orders of magnitude. True blue emission, with *CIE* (x,y,) coordinates of 0.15, 0.09 while simultaneously displaying TADF was achieved, however the devices made using the compound as the emitter displayed very poor performance which we attribute to the high triplet energy of the emitter. Finally, by incorporating elements of both strategies, several compounds with sky-blue emission that displayed TADF were achieved (**21**, **23**-**25**). When incorporated into OLED devices as the emitter, the devices achieved external quantum efficiencies up to 28.7 %, validating the molecular design approaches established.

3.5 Experimental Details and Supplemental Data

All reagents were purchased from commercial sources and were used without further purification. ^{1}H, ^{13}C, and ^{19}F NMR spectra were recorded using a Bruker Avance IIIHD 500 instrument operating at 500 MHz, 125 MHz, and 470.4 MHz, respectively, or on a Varian Mercury Vx 400 operating at 400 MHz, 100 MHz, and 376.5 MHz, respectively. Chemical shifts are listed in parts per million (ppm) and were referenced using the residual nondeuterated solvent ^{1}H signal or the solvent ^{13}C resonance, or using an internal standard (trifluoroacetic acid, 76.55 ppm) for ^{19}F NMR. Column chromatography was carried out using silica gel (60 Å, 40-63 μm, Sorbent) as the stationary phase. Mass spectra were measured on an Applied Biosystems 4700 Proteomics Analyzer using MALDI or a VG Instruments 70-SE using electron impact (EI) mode. UV-Vis spectra were measured using a Cary 5000 UV-Vis-NIR Spectrophotometer. Fluorescence and phosphorescence spectra, and photoluminescent transients were collected on a Jobin Yvon Fluorolog-3 equipped with a pulsed xenon lamp, photomultiplier tube (Horiba R928), and pulsed LED excitation source (NanoLED) and were excited at 330 nm. Fluorescent lifetimes were fit using DAS6 decay analysis software. Solution and solid-state absolute photoluminescence quantum yields were deter-mined on a Quantaurus-QY C11347 spectrometer. Electrochemical data was acquired using cyclic voltammetry in 0.1 M $n\text{Bu}_4\text{N}^+\text{PF}_6^-$ in dry tetrahydrofuran (for reductive scans) or dichloromethane (oxidative scans) under nitrogen, using a CH Instruments 620D potentiostat, a glassy carbon working electrode, a platinum wire auxiliary electrode, and, as a pseudo-reference electrode, a silver wire anodized in 1 M aqueous potassium chloride solution. The scan rate was 50 mV s^{-1} and ferrocene was

added as an internal reference. Thermogravimetric analysis was performed on a Perkin Elmer Pyris-1 TGA with a scan rate of 10 °C s^{-1}.

3.5.1 Synthetic Details

2-(4-(9*H*-Carbazol-9-yl)phenyl)-5-phenyl-1,3,4-oxadiazole (**1**). To a solution of 2-(4-iodophenyl)-5-phenyl-1,3,4-oxadiazole (5.0 g, 15 mmol), carbazole (5.0 g, 30 mmol), and Cu (3.0 g, 47 mol) in DMF (30 ml) in a round-bottom flask was added potassium carbonate (10.0 g, 72.4 mmol) under nitrogen with stirring. The reaction mixture was heated in an aluminum heat block at 150 °C for 9 h. After cooling, the reaction mixture was filtered and the solid was washed with THF. The filtrate was concentrated *in vacuo* and water was added to the remaining DMF solution, and a brown solid precipitated and was collected via filtration. The crude product was purified by column chromatography using dichloromethane as the eluent. The product was recrystallized from methanol/water and the white solid product was collected by filtration (4.8 g 86%). ^{1}H NMR (400 MHz, $CDCl_3$): δ 8.39 (d, *J* = 8.8 Hz, 2H), 8.21-8.15 (m, 4H), 7.79 (d, *J* = 8.8 Hz, 2H), 7.59-7.57 (m, 3H), 7.53-7.51 (m, 2H), 7.46 (t, *J* = 6.8 Hz, 2H), 7.33 (t, *J* = 6.8 Hz, 2H). ^{13}C{^{1}H} NMR (100 MHz, $CDCl_3$): δ 164.73, 163.96, 140.85, 140.20, 131.83, 129.11, 128.52, 127.17, 126.94, 126.18, 123.79, 123.75, 122.41, 120.55, 120.44, 109.66. NMR data are consistent with those previously reported.[132]

2-(4-(9*H*-Carbazol-9-yl)-3,5-difluorophenyl)-5-phenyl-1,3,4-oxadiazole (**2**). A mixture of 2-phenyl-5-(3,4,5-trifluorophenyl)-1,3,4-oxadiazole (1.0 g, 3.6 mmol), carbazole (0.60 g, 3.6 mmol), and potassium carbonate (5.0 g, 36 mmol) in DMSO (20 ml) was stirred at room temperature for 21 h under nitrogen. Water (75 ml) was added and a white solid

precipitated, which was collected via filtration, washed with water and dried. The crude product was purified by silica gel column chromatography using dichloromethane as eluent. After removal of solvents, product was recrystallized from acetone/water and collected by filtration to yield the product as a white solid (1.4 g 93%). ^{1}H NMR (500 MHz, $CDCl_3$): δ 8.19 (d, *J* = 8.5 Hz, 2H), 8.16 (d, *J* = 8.5 Hz, 2H), 7.63-7.57 (m, 3H), 7.47 (t, *J* = 8.5 Hz, 2H), 7.36 (t, *J* = 8.5 Hz, 2H), 7.19 (d, *J* = 8.5 Hz, 2H). ^{13}C{^{1}H} NMR (125 MHz, $CDCl_3$): δ 165.42, 161.47 (d, J_{CF} = 234 Hz), 158.49, 139.98, 132.32, 129.27, 127.14, 126.34, 125.01, 123.99, 123.32, 120.95, 120.47, 117.45, 111.34 (d, J_{CF} = 26 Hz), 109.90. ^{19}F NMR (376 MHz, $CDCl_3$): δ -111.78 (d, *J* = 7.9 Hz, 2F). HRMS (EI, *m/z*): Calcd for $C_{26}H_{15}F_2N_3O$, 423.1183 [M^+]; Found 423.1181. ^{13}C{^{1}H} NMR spectrum shown in Section 3.5.5

2-(4-(9*H*-Carbazol-9-yl)-2,3,5,6-tetrafluorophenyl)-5-phenyl-1,3,4-oxadiazole (**3**). In a round-bottom flask, 2-(pentafluorophenyl)-5-phenyl-1,3,4-oxadiazole (1.03 g, 3.30 mmol), carbazole (0.570 g, 3.41 mmol), and potassium carbonate (4.42 g, 32.0 mmol) were placed under vacuum and then under nitrogen. DMSO (20 mL) was added and the reaction mixture was stirred overnight at room temperature. The reaction progress was monitored via thin-layer chromatography. Upon completion, the mixture was precipitated with water and the crude product was collected via filtration. Column chromatography (9:1 ethyl acetate/hexanes as eluent) yielded the higher R_f fluorescent product as a white powder (0.819 g, 54%). ^{1}H NMR (500 MHz, $CDCl_3$): δ 8.21 (d, *J* = 6.5 Hz, 2H), 8.16 (d, *J* = 7.5 Hz, 2H), 7.63-7.57 (m, 3H), 7.50 (t, *J* = 7.5 Hz, 2H), 7.39 (t, *J* = 8.0 Hz, 2H), 7.22 (d, *J* = 8.0 Hz, 2H). ^{13}C{^{1}H} NMR (125 MHz, $CDCl_3$): δ165.84, 155.16, 145.33 (ddt, $^{1}J_{CF}$ = 260 $^{2}J_{CF}$ = 14 Hz, $^{4}J_{CF}$ = 4 Hz), 144.14 (ddt, $^{1}J_{CF}$ = 260 $^{2}J_{CF}$ = 14 Hz, $^{4}J_{CF}$ = 4 Hz),

139.40, 132.50, 129.27, 127.30, 126.66, 124.35, 123.01, 121.65, 120.61, 119.83 (t, $^{2}J_{CF}$ = 14), 109.94, 104.51 (t, $^{2}J_{CF}$ = 14). ^{19}F NMR (470 MHz, $CDCl_3$): δ -134.94 (m, 2F), -140.38 (m, 2H). HRMS (EI, m/z): Calcd for $C_{26}H_{13}N_3OF_4$ 459.0995; Found 459.0994. Data is consistent with previously reported characterization.[147]

2-(4-(9'*H*-[9,3':6',9''-Tercarbazol]-9'-yl)phenyl)-5-phenyl-1,3,4-oxadiazole (**4**): To a solution of 2-(4-(3,6-diiodo-9*H*-carbazol-9-yl)phenyl)-5-phenyl-1,3,4-oxadiazole (0.50 g, 0.78 mmol), carbazole (1.0 g, 6.0 mmol), and Cu (1.0 g, 16 mol) in DMF (10 ml) was added potassium carbonate (3.0 g, 22 mmol) under nitrogen and stirring. The reaction mixture was heated in an aluminum heat block at 170 °C for 24 h. After cooling, the reaction mixture was filtered and the solid was washed with THF. The filtrate was concentrated *in vacuo,* then water was added to the remaining DMF solution and a brown solid precipitated which was collected via filtration. The product was purified by silica gel column chromatography using dichloromethane as the eluent. After removal of solvent, the product was recrystallized from dichloromethane/methanol. Filtration yielded the white solid product (0.30 g 53%). ^{1}H NMR (400 MHz, $CDCl_3$): δ 8.52 (d, *J* = 8.4 Hz, 2H), 8.31 (s, 2H), 8.24-8.21 (m, 2H), 8.17 (d, *J* = 8.0 Hz, 4H), 7.97 (d, *J* = 8.4 Hz, 2H), 7.76 (d, *J* = 8.0 Hz, 2H), 7.67 (d, *J* = 8.8 Hz, 2H), 7.61-7.59 (m, 3H), 7.42-7.41 (m, 8H), 7.32-7.28 (m, 4H). ^{13}C{^{1}H} NMR (100 MHz, $CDCl_3$): δ 164.96, 163.82, 141.65, 140.22, 140.07, 131.99, 130.97, 129.19, 128.90, 127.46, 127.03, 126.51, 125.92, 124.41, 123.74, 123.37, 123.19, 120.33, 119.86, 119.78, 111.25, 109.61. HRMS (MALDI, *m/z*): Calcd for $C_{50}H_{31}N_5O$ [M^+], 717.2594; Found 717.2594. Anal. Calcd for $C_{50}H_{31}N_5O$: C, 83.66; H, 4.35; N, 9.76. Found: C, 83.38; H, 4.47; N, 9.72.

2-Phenyl-5-(4-(3,3'',6,6''-tetra-tert-butyl-9'*H*-[9,3':6',9''-tercarbazol]-9'-yl)phenyl)-1,3,4-oxadiazole (**5**): To a solution of 2-(4-(3,6-diiodo-9H-carbazol-9-yl)phenyl)-5-phenyl-1,3,4-oxadiazole (0.50 g, 0.78 mmol), 3,6-di-*tert*-butyl-9*H*-carbazole (1.8 g, 6.4 mmol), and Cu (1.0 g, 16 mol) in DMF (10 ml) was added potassium carbonate (3.0 g, 22 mmol) under nitrogen with stirring. The reaction mixture was heated in an aluminum heat block at 170 °C and stirred for 22 h. After cooling, the reaction mixture was filtered and the solid was washed with THF. The filtrate was concentrated *in vacuo,* then water was added to the remaining DMF solution and a brown solid precipitated, which was collected via filtration. The product was purified by silica gel column chromatography using dichloromethane:hexanes (7:3) as the eluent. After removal of solvent, the product was recrystallized from dichloromethane/methanol. The pale-yellow product was collected by filtration (0.50 g 69%). ^{1}H NMR (500 MHz, $CDCl_3$): δ 8.52 (d, *J* = 8.4 Hz, 2H), 8.28 (s, 2H), 8.24-8.22 (m, 2H), 8.19 (s, 4H), 7.98 (d, *J* = 8.0 Hz, 2H), 7.75 (d, *J* = 8.8 Hz, 2H), 7.67 (d, *J* = 8.8 Hz, 2 H), 7.62-7.58 (m, 3H), 7.49 (dd, *J* = 8.8 Hz, 2.0 Hz, 4H), 7.37 (d, *J* = 8.8 Hz, 4H), 1.48 (s, 32 H). $^{13}C\{^{1}H\}$ NMR (125 MHz, $CDCl_3$): δ 164.94, 163.88, 142.65, 140.40, 140.02, 139.78, 131.98, 131.47, 129.20, 128.88, 127.42, 127.04, 126.18, 124.43, 123.77, 123.59, 123.20, 123.15, 119.42, 116.24, 111.08, 109.02, 34.73, 32.03. HRMS (MALDI, *m/z*): Calcd for $C_{66}H_{63}N_5O$ [M^+], 941.5033; Found, 941.5046. Anal. Calcd for $(C_{66}H_{63}N_5O)_3 \cdot H_2O$: C, 83.60; H, 6.77; N, 7.39. Found: C, 83.76; H, 6.75; N, 7.43.

2-(3-(9*H*-Carbazol-9-yl)phenyl)-5-phenyl-1,3,4-oxadiazole (**6**): To a mixture of 2-(3-iodophenyl)-5-phenyl-1,3,4-oxadiazole (0.50 g, 1.4 mmol), carbazole (1.0 g, 6.0 mmol), and Cu (1.0 g, 16 mol), and potassium carbonate (3.0 g, 22 mmol) in DMF (10 ml) under

nitrogen with stirring. The reaction mixture was heated in an aluminum heat block at 170 °C and stirred for 24 h. After cooling, the reaction mixture was filtered and the solid was washed with THF. The filtrate was concentrated *in vacuo*, then water was added to the remaining DMF solution and a brown solid precipitated, which was collected via filtration. The product was purified by silica gel column chromatography using dichloromethane:hexanes (7:3) as the eluent. After removal of solvent, the product was recrystallized from dichloromethane/methanol. The white product was collected by filtration (0.47 g, 89%). ^{1}H NMR (400 MHz, $CDCl_3$): δ 8.36 (s, 1H), 8.30-8.27 (m, 1H), 8.18 (d, *J* = 8.0 Hz, 2H), 8.16 (dd, *J* = 7.6, 2.0 Hz, 2H), 7.82-7.79 (m, 2H), 7.58-7.51 (m, 3H), 7.47-7.45 (m, 4H), 7.36-7.32 (m, 2H). ^{13}C{^{1}H} NMR (100 MHz, $CDCl_3$): δ 164.87, 163.80, 140.58, 138.71, 131.88, 130.82, 130.24, 129.08, 126.98, 126.17, 125.84, 125.77, 125.34, 123.64, 123.56, 120.43, 120.36, 109.54. ^{13}C{^{1}H} NMR spectrum shown in Section 3.5.5.

2-(3-(9'*H*-[9,3':6',9''-Tercarbazol]-9'-yl)phenyl)-5-phenyl-1,3,4-oxadiazole (**7**): To a solution of 2-(3-(3,6-diiodo-9H-carbazol-9-yl)phenyl)-5-phenyl-1,3,4-oxadiazole (0.50 g, 0.78 mmol), 3,6-di-*tert*-butyl-9*H*-carbazole (1.8 g, 6.4 mmol), and Cu (1.0 g, 16 mol) in DMF (10 ml) was added potassium carbonate (3.0 g, 22 mmol) under nitrogen with stirring. The reaction mixture was heated in an aluminum heat block at 170 °C and stirred for 22 h. After cooling, the reaction mixture was filtered and the solid was washed with THF. The filtrate was concentrated *in vacuo*, then water was added to the remaining DMF solution and a brown solid precipitated, which was collected via filtration. The product was purified by silica gel column chromatography using dichloromethane:hexanes (7:3) as the eluent. After removal of solvent, the product was

recrystallized from dichloromethane/methanol. The pale-yellow product was collected by filtration (0.35 g 62%) ^{1}H NMR (400 MHz, $CDCl_3$): δ 8.55 (s, 1H), 8.38 (d, *J* = 7.6 Hz, 1H), 8.32 (s, 2H), 8.20-8.17 (m, 6H), 7.97-7.90 (m, 2 H), 7.72-7.65 (m, 4H), 7.60-7.54 (m, 3H), 7.43 (s, 4 H), 7.42 (s, 4H), 7.32-7.26 (m, 4H). ^{13}C{^{1}H} NMR (100 MHz, $CDCl_3$): δ 165.08, 163.67, 141.69, 140.43, 138.21, 132.04, 131.25, 130.82, 130.34, 129.17, 127.06, 126.51, 126.30, 125.92, 125.54, 124.22, 123.62, 123.18, 120.31, 119.86, 119.75, 111.15, 109.64. HRMS (MALDI, *m/z*): Calcd for $C_{50}H_{31}N_5O$ [M^+], 717.2594; Found 717.2498. Anal. Calcd for $C_{50}H_{31}N_5O$: C, 83.66; H, 4.35; N, 9.76. Found: C, 83.37; H, 4.42; N, 9.75.

2-Phenyl-5-(3-(3,3'',6,6''-tetra-tert-butyl-9'*H*-[9,3':6',9''-tercarbazol]-9'-yl)phenyl)-1,3,4-oxadiazole (**8**): To a solution of 2-(3-(3,6-diiodo-9H-carbazol-9-yl)phenyl)-5-phenyl-1,3,4-oxadiazole (0.50 g, 0.78 mmol), 3,6-di-*tert*-butyl-9*H*-carbazole (1.8 g, 6.4 mmol), and Cu (1.0 g, 16 mol) in DMF (10 ml) was added potassium carbonate (3.0 g, 22 mmol) under nitrogen with stirring. The reaction mixture was heated in an aluminum heat block at 170 °C and stirred for 22 h. After cooling, the reaction mixture was filtered and the solid was washed with THF. The filtrate was concentrated *in vacuo,* then water was added to the remaining DMF solution and a brown solid precipitated, which was collected via filtration. The product was purified by silica gel column chromatography using dichloromethane:hexanes (7:3) as the eluent. After removal of solvent, the product was recrystallized from dichloromethane/methanol. The pale-yellow product was collected by filtration (0.40 g 55%) ^{1}H NMR (400 MHz, $CDCl_3$): δ 8.54 (s, 1H), 8.38 (d, *J* = 7.2 Hz, 1 H), 8.28 (s, 2H), 8.20-8.17 (m, 6H), 7.97-7.90 (m, 2H), 7.69-7.64 (m, 4H), 7.62-7.54 (m, 3H), 7.48 (dd, *J* = 8.8, 2.0 Hz, 4 H), 7.36 (d, *J* = 8.4 Hz, 4H), 1.48 (s, 32H).

$^{13}C\{^{1}H\}$ NMR (100 MHz, $CDCl_3$): δ 142.61, 140.06, 131.31, 129.18, 127.08, 124.22, 123.59, 123.13, 116.23, 110.97, 109.04, 34.73, 32.03. Calcd for $C_{66}H_{63}N_5O$ [M^+], 941.5033; Found, 941.5033. Anal. Calcd for $(C_{66}H_{63}N_5O)_2 \cdot H_2O$: C, 83.33; H, 6.78; N, 7.36. Found: C, 83.04; H, 6.79; N, 7.35.

2-(2-(9*H*-Carbazol-9-yl)phenyl)-5-phenyl-1,3,4-oxadiazole (**9**): In a round-bottom flask, 2-2(flurophenyl)-5-phenyl-1,3,4-oxadiazole (2.0 g, 8.3 mmol), carbazole (5.0 g, 12 mmol), and potassium carbonate (4.0 g, 29 mmol) was stirred in DMSO in an aluminum block at 150 °C for 24 h under nitrogen. After cooling to room temperature, water (150 mL) was added, and the precipitate was collected via filtration and washed with water. The crude product was purified by column chromatography using dichloromethane/ethyl acetate (95:5) as the eluent. The product was then recrystallized from acetone/water and filtered to yield the product as a white powder (2.8 g, 88%). ^{1}H NMR (400 MHz, $CDCl_3$): δ 8.56 (d, *J* = 8.8 Hz, 1H), 8.16 (d, *J* = 8.4 Hz, 2H), 7.83 (td, *J* = 8.8, 2.0 Hz, 1H), 7.75 (d, *J* = 8.0 Hz, 1H), 7.68 (d, *J* = 8.7 Hz, 1H), 7.35-7.7.29 (m, 3H), 7.27 (t, *J* = 8.0 Hz, 2H), 7.19 (t, *J* = 8.4 Hz, 2H), 7.08 (d, *J* = 8.7 Hz, 2H), 6.99 (d, *J* = 8 Hz, 2H). $^{13}C\{^{1}H\}$ NMR (100 MHz, $CDCl_3$): δ 164.73, 162.49, 141.69, 135.24, 133.13, 131.31, 131.21, 131.12, 129.36, 128.49, 126.48, 126.25, 123.70, 123.31, 123.00, 120.17, 120.04, 109.42. NMR data are consistent with those previously reported.[148]

2-(2-(9'*H*-[9,3':6',9''-Tercarbazol]-9'-yl)phenyl)-5-phenyl-1,3,4-oxadiazole (**10**): To a solution of 2-(2-(3,6-diiodo-9*H*-carbazol-9-yl)phenyl)-5-phenyl-1,3,4-oxadiazole (0.50 g, 0.78 mmol), carbazole (1.0 g, 6.0 mmol), and Cu (1.0 g, 16 mol) in DMF (10 ml) was added potassium carbonate (3.0 g, 22 mmol) under nitrogen with stirring. The reaction mixture was heated in an aluminum heat block at 170 °C and stirred for 18 h. After

cooling, the reaction mixture was filtered and the solid was washed with THF. The filtrate was concentrated *in vacuo*, then water was added to the remaining DMF solution and a brown solid precipitated, which was collected via filtration. The product was purified by silica gel column chromatography using dichloromethane as the eluent. After removal of solvent, the product was recrystallized from dichloromethane/methanol. The white product was collected by filtration (0.36 g 34%).^{1}H NMR (400 MHz, $CDCl_3$): δ 8.64 (d, *J* = 7.6 Hz, 1H), 8.28 (s, 2H), 8.15 (d, *J* = 8.0 Hz, 4H), 7.98-7.84 (m, 3 H), 7.56 (d, *J* = 8.8 Hz, 2H), 7.46-7.25 (m, 19H). $^{13}C\{^{1}H\}$ NMR (100 MHz, $CDCl_3$): δ 164.80, 162.29, 141.67, 141.38, 134.66, 133.45, 131.82, 131.44, 130.92, 130.62, 129.96, 128.92, 126.70, 126.51, 125.86, 124.07, 123.47, 123.09, 123.04, 120.27, 119.72, 119.69, 110.97, 109.51. HRMS (MALDI, *m/z*): Calcd for $C_{50}H_{31}N_5O$ [M^+], 717.2594; Found 717.2498. $^{13}C\{^{1}H\}$ NMR spectrum shown in Section 3.5.5.

2-phenyl-5-(2-(3,3'',6,6''-Tetra-*tert*-butyl-9'*H*-[9,3':6',9''-tercarbazol]-9'-yl)phenyl)-1,3,4-oxadiazole (**11**): To a solution of 2-(2-(3,6-diiodo-9*H*-carbazol-9-yl)phenyl)-5-phenyl-1,3,4-oxadiazole (0.50 g, 0.78 mmol), 3,6-di-*tert*-butyl-9*H*-carbazole (1.0 g, 3.58 mmol), and Cu (1.0 g, 16 mol) in DMF (10 ml) was added potassium carbonate (3.0 g, 22 mmol) under nitrogen with stirring. The reaction mixture was heated in an aluminum heat block at 170 °C and stirred for 21 h. After cooling, the reaction mixture was filtered and the solid was washed with DCM. The filtrate was concentrated *in vacuo*, then water was added to the remaining DMF solution and a brown solid precipitated, which was collected via filtration. The product was purified by silica gel column chromatography using hexanes:ethyl acetate (9:1) as the eluent. After removal of solvent, the product was recrystallized from dichloromethane/methanol. The pale-yellow product was collected by

filtration (0.55 g 75%). ^{1}H NMR (400 MHz, $CDCl_3$): δ 8.65 (d, *J* = 8.0 Hz, 1H), 8.27 (s, 2H), 8.17 (s, 4H), 7.98-7.91 (m, 2H), 7.86 (t, *J* = 7.6 Hz, 1H), 7.57 (d, *J* = 8.4 Hz, 2H), 7.47-7.33 (m, 12H), 7.18 (br. s, 3H), 1.48 (s, 32H). $^{13}C\{^{1}H\}$ NMR (100 MHz, $CDCl_3$): *δ* 164.81, 162.34, 142.54, 141.11, 140.05, 134.79, 133.40, 131.72, 131.40, 131.12, 130.94, 129.84, 128.93, 126.54, 126.37, 124.05, 123.51, 123.47, 123.05, 119.27, 116.17, 110.79, 108.94, 34.69, 32.02. HRMS (MALDI, *m/z*): Calcd for $C_{66}H_{63}N_5O$ [M^+], 941.5033; Found, 941.5074. Anal. Calcd for $C_{66}H_{63}N_5O$: C, 84.13; H, 6.74; N, 7.43. Found: C, 83.94; H, 6.81; N, 7.38.

2-(4-(3,6-Di-*tert*-butyl-9*H*-carbazol-9-yl)-3,5-difluorophenyl)-5-phenyl-1,3,4-oxadiazole (**12**): To a mixture of 2-phenyl-5-(3,4,5-trifluorophenyl)-1,3,4-oxadiazole (1.0 g, 3.6 mmol), 3,6-di-*tert*-butylcarbazole (1.0 g, 3.6 mmol), and potassium carbonate (6.0 g, 43 mmol) in DMSO (15.0 ml) was stirred at room temperature for 19 h under nitrogen. Water (80 ml) was added and the pale-yellow precipitate was collected by filtration, washed with water and dried. The crude product was purified by column chromatography using dichloromethane/ethyl acetate (99:1) as the eluent. The product was recrystallized from dichloromethane and methanol, and filtration yielded the pale-yellow product (1.6 g, 84 %). ^{1}H NMR (500 MHz, $CDCl_3$): δ 8.19 (d, *J* = 8.5 Hz, 2H), 8.14 (s, 2H), 7.98 (d, *J* = 8.5 Hz, 2H), 7.62-7.56 (m, 3H), 7.51 (d, *J* = 8.5 Hz, 2H), 7.09 (d, *J* = 8.5 Hz, 2H), 1.47 (s, 18 Hz). $^{13}C\{^{1}H\}$ NMR (100 MHz, $CDCl_3$): *δ* 165.36, 143.86, 138.38, 132.28, 129.26, 127.13, 123.97, 123.95, 123.36, 116.49, 111.39, 111.18, 109.35, 34.78, 31.97. ^{19}F NMR (376 MHz, $CDCl_3$): δ -111.84 (d, *J* = 7.9 Hz, 2F). HRMS (EI, *m/z*): Calcd for $C_{32}H_{31}F_2N_3O$, 535.2435 [M^+]; Found 535.2438. $^{13}C\{^{1}H\}$ NMR spectrum shown in Section 3.5.5.

2-(4-(*Tert*-butyl)phenyl)-5-(4-(3,6-di-tert-butyl-9*H*-carbazol-9-yl)-2,3,5,6-tetrafluorophenyl)-1,3,4-oxadiazole (**13**): A solution of 2-(4-(*tert*-butyl)phenyl)-5-(perfluorophenyl)-1,3,4-oxadiazole (0.5 g, 1.4 mmol), carbazole (0.40 g, 1.4 mmol), and potassium carbonate (2.0 g, 15 mmol) in DMSO (10 ml) was stirred at room temperature for 4 h under nitrogen. Water (80 ml) was added and the reaction mixture was filtered, and the solid obtained was washed with water. The crude product was purified by column chromatography using dichloromethane/hexanes (7:3) as the eluent. The product was recrystallized from acetone/water, and the pure product was collected by filtration (0.75 g 88 %). ^{1}H NMR (500 MHz, $CDCl_3$): δ 8.14 (s, 2H), 8.13 (d, *J* = 8.5 Hz, 2H), 7.60 (d, *J* = 8.5 Hz, 2H), 7.54 (d, *J* = 9.0 Hz, 2H), 7.12 (d, *J* = 8.0 Hz, 2H), 1.48 (s, 18H), 1.39 (s, 9H). ^{13}C{^{1}H} NMR (125 MHz, $CDCl_3$): δ 165.90, 156.25, 144.67, 137.83, 127.17, 126.28, 124.36, 124.25, 120.21, 116.65, 109.47, 35.20, 34.83, 31.92, 31.09. ^{19}F NMR (376 MHz, $CDCl_3$): δ -135.32-135.40 (m, 2F), -140.64-140.72 (m, 2F). HRMS (ESI, *m/z*): Calcd for $C_{38}H_{38}N_3OF_4$, 628.2946 $[M+H]^+$; Found 628.2946. Anal. Calcd for $C_{38}H_{37}N_3OF_4$: C, 72.71; H, 5.94; N, 6.69. Found: C, 72.73; H, 6.00; N, 6.58.

2-(4-(9'*H*-[9,3':6',9''-Terbenzo[b]indol]-9'-yl)-3,5-difluorophenyl)-5-phenyl-1,3,4-oxadiazole (**14**): A mixture of 2-phenyl-5-(3,4,5-trifluorophenyl)-1,3,4-oxadiazole (0.28 g, 1.0 mmol), 9'H-9,3':6',9''-tercarbazole (0.50 g, 1.0 mmol), and potassium carbonate (5.0 g, 36 mmol) in DMSO (20 ml) was stirred at room temperature for 22 h under nitrogen. Water (70 ml) was added and the reaction mixture was filtered, and the solid obtained was washed with water and dried. The crude product was purified by column chromatography using dichloromethane as the eluent. The pale-yellow product was recrystallized from dichloromethane and ethanol. The pale-yellow product was collected

by filtration (0.60 g, 80 %). ^{1}H NMR (500 MHz, $CDCl_3$): δ 8.31 (s, 2H) 8.22 (d, *J* = 8.0 Hz, 2H), 8.17 (d, *J* = 7.5 Hz, 4H), 8.13 (d, *J* = 7.5 Hz, 2H), 7.69 d, *J* = 8.5 Hz, 2H), 7.65-7.59 (m, 3H), 7.47 (d, *J* = 8.5 Hz, 2H), 7.44-7.39 (m, 8H), 7.32-7.28 (m, 4H). ^{13}C{^{1}H} NMR (125 MHz, $CDCl_3$): δ 165.58, 162.24, 160.51, 158.47, 141.62, 139.71, 132.43, 131.43, 129.31, 127.18, 126.66, 125.94, 125.84, 124.75, 123.24, 123.20, 120.31, 119.91, 119.81, 116.79, 116.66, 111.66, 111.62, 111.45, 109.67. ^{19}F NMR (376 MHz, $CDCl_3$): δ -111.76. HRMS (EI, *m/z*): Calcd for $C_{50}H_{29}F_2N_3O$, 753.2340 [M^+]; Found 753.2332.

2-(4-(9'*H*-[9,3':6',9''-Terbenzo[b]indol]-9'-yl)-2,3,5,6-tetrafluorophenyl)-5-(4-(tert-butyl)phenyl)-1,3,4-oxadiazole (**15**): In a round-bottom flask, 2-(4-(*tert*-butyl)phenyl)-5-(perfluorophenyl)-1,3,4-oxadiazole (0.23 g, 0.63 mmol), 9'H-9,3':6',9''-tercarbazole (0.39 g, 0.78 mmol), and potassium carbonate (2.0 g, 15 mmol) in DMSO (10 ml) was stirred at room temperature for 4 h under nitrogen. Water (80 ml) was added and the reaction mixture was filtered, and the solid obtained was washed with water. The crude product was purified by column chromatography using dichloromethane/hexanes (7:3) as the eluent. The product was recrystallized from acetone/water, and the pure product was collected by filtration (0.039 g 73 %). ^{1}H NMR (500 MHz, $CDCl_3$): δ 8.32 (d, *J* = 1.5 Hz, 2H), 8.17 (d, *J* = 7.5 Hz, 4H), 8.15 (d, *J* = 9.0 Hz, 2H), 7.73 (dd, *J* = 8.5, 2.0 Hz, 2H), 7.62 (d, J = 9.0 Hz, 2H), 7.50 (d, *J* = 8.5 Hz, 2H), 7.43-7.42 (m, 8H), 7.32-7.29 (m, 4H), 1.40 (s, 9H). ^{13}C{^{1}H} NMR (125 MHz, $CDCl_3$): δ 166.12, 156.45, 141.53, 139.14, 132.12, 127.23, 126.94, 126.34, 126.00, 125.17, 123.2, 120.36, 120.09, 120.05, 119.93, 111.51, 109.60, 35.24, 31.10. HRMS (EI, *m/z*): Calcd for $C_{26}H_{15}N_3OF_2$ [M^+], 423.1183; Found, 423.1181. ^{13}C{^{1}H} NMR spectrum shown in Section 3.5.5.

2-(4-(9,9-Dimethylacridin-10(9*H*)-yl)phenyl)-5-phenyl-1,3,4-oxadiazole (**16**): In a round-bottomed flask under nitrogen, NaH (dispersion in mineral oil, 0.55 g, 14 mmol) was added to a solution of 2-(4-fluorophenyl)-5-phenyl-1,3,4-oxadiazol (1.0 g, 4.2 mmol) and 9,9-dimethyl-9,10-dihydroacridine (0.87 g, 4.2 mmol) in anhydrous DMF (20 ml). The reaction mixture was stirred at 100 °C for 30 min. After cooling, water (50 mL) was added and the precipitate that formed was collected by filtration, washed with water and dried. Column chromatography was performed on the pale green crude product using dichloromethane:hexanes (3:1) as the eluent. The pure product was collected and concentrated in vacuo to yield a white powder (1.1 g, 63%). ^{1}H NMR (500 MHz, $CDCl_3$): δ 8.43 (d, J = 8.0 Hz, 2H), 8.20 (d, J = 5.5 Hz, 2H), 7.59-7.55 (m, 5H), 7.49 (d, J = 7.0 Hz, 2H), 7.03-6.96 (m, 4H), 6.33 (d, J = 8.0 Hz, 2H) 1.72 (s, 6H). ^{13}C{^{1}H} NMR (125 MHz, $CDCl_3$): δ 164.83, 164.03, 144.64, 140.42, 132.06, 131.88, 130.40, 129.51, 129.14, 126.98, 126.43, 125.37, 123.77, 123.61, 121.04, 114.08, 36.02, 31.16. HRMS (EI, m/z): Calcd for $C_{29}H_{23}N_3O$ $[M]^+$ 429.1841; Found 429.1833. Anal. Calcd for $C_{29}H_{23}N_3O$: C, 81.09; H, 5.40; N, 9.78. Found: C, 81.15; H, 5.28; N, 9.79.

2-(4-(9,9-Dimethylacridin-10(9*H*)-yl)-3,5-difluorophenyl)-5-phenyl-1,3,4-oxadiazole (**17**): In a round-bottomed flask under nitrogen, NaH (dispersion in mineral oil, 0.55 g, 14 mmol) was added to a solution of 2-phenyl-5-(3,4,5-trifluorophenyl)-1,3,4-oxadiazole (1.0 g, 3.6 mmol) and 9,9-dimethyl-9,10-dihydroacridine (0.75 g, 3.6 mmol) in anhydrous DMF (20 ml). The reaction mixture was stirred at room temperature for 30 min. Water (50 ml) was added and the precipitate was collected by filtration, washed with water and dried. Column chromatography was performed on the pale green crude product using dichloromethane:hexanes (3:1) as the eluent. The pure product was collected and

concentrated *in vacuo* to yield a yellow powder (1.2 g, 71%). ^{1}H NMR (500 MHz, $CDCl_3$): δ 8.21 (d, J = 6.5 Hz, 2H), 8.23 (d, J = 7.5 Hz, 2H), 7.62-7.54 (m, 5H), 7.12 (t, J = 7.0 Hz, 2H), 7.07 (t, J = 8.0 Hz, 2H), 6.43 (d, J = 8.0 Hz, 2H), 1.75 (s, 6H). ^{13}C{^{1}H} NMR (125 MHz, $CDCl_3$): δ 165.29, 161.72 (dd, $^{1}J_{CF}$ = 249 Hz, $^{3}J_{CF}$ = 5.0 Hz), 162.23 (t, J_{CF} = 3.1 Hz), 138.66, 132.20, 131.03, 129.16, 127.01, 126.75, 125.79 (t, J_{CF} = 10.6 Hz), 123.20, 121.86, 120.39 (t, J_{CF} = 16.3 Hz), 112.77, 111.59 (d, J_{CF} = 26.3 Hz), 36.03, 30.50. ^{19}F NMR (470 MHz, $CDCl_3$): δ -112.67 (d, J_{FH} = 9.4 Hz). HRMS (ESI, m/z): Calcd for $C_{29}H_{21}N_3OF_2$ $[M]^+$ 465.1653; Found 465.1642. Anal. Calcd for $C_{29}H_{21}N_3OF_2$: C, 74.83; H, 4.55; N, 9.03. Found: C, 74.56; H, 4.81; N, 8.97.

2-(2,6-Bis(3,6-di-*tert*-butyl-9*H*-carbazol-9-yl)phenyl)-5-phenyl-1,3,4-oxadiazole (**18**): In a round-bottom flask 2-(2,6-difluorophenyl)-5-phenyl-1,3,4-oxadiazole (1.0 g, 3.9 mmol), 3,6-di-*tert*-butylcarbazole (2.3 g, 8.2 mmol), and potassium carbonate were dissolved in DMSO (10 mL) under nitrogen. The reaction mixture was stirred and heated in an aluminum block at 150 °C for 24 h. After cooling to room temperature, water (50 mL) was added the resulting precipitate was collected via filtration and washed with water. The crude product was purified by column chromatography using dichloromethane/hexanes (1:1) as the eluent. The product was then recrystallized from dichloromethane/methanol, and thr product was obtained via filtration as a white powder (2.6 g, 87%). ^{1}H NMR (400 MHz, $CDCl_3$): δ 8.05 (d, J = 1.6 Hz, 4H), 8.01-7.97 (m, 1 H), 7.83 (d J = 8.0 Hz, 2H), 7.42 (dd, J = 8.4, 1.6 Hz, 4H), 7.30 (t, J = 7.6 Hz, 1 H), 7.17 (d, J = 8.8 Hz, 4H), 7.13 (t, J = 8.0 Hz, 2H), 6.91 (d J = 8.8 Hz, 2H), 1.41 (s, 36H). ^{13}C{^{1}H} NMR (100 MHz, $CDCl_3$): δ δ 163.97, 158.54, 143.02, 140.01, 139.76, 133.49, 131.05, 130.11, 128.20, 126.47, 124.29, 123.79, 123.52, 122.97, 116.33, 108.75, 34.66,

31.94. Calcd for $C_{54}H_{56}N_4O$ [M^+], 776.4454; Found, 776.4457. Anal. Calcd for $C_{54}H_{56}N_4O$: C, 83.47; H, 7.26; N, 7.21. Found: C, 83.36; H, 7.17; N, 7.19.

2,5-Bis(2,6-bis(3,6-di-*tert*-butyl-9*H*-carbazol-9-yl)phenyl)-1,3,4-oxadiazole (**19**): In a round-bottom flask, 2,5-bis(2,6-difluorophenyl)-1,3,4-oxadiazole (0.43 g, 1.5 mmol), 3,6-di-*tert*-butylcarbazole (1.8 g, 6.4 mmol), and potassium carbonate (4.0 g, 29 mmol) were stirred in DMSO for 24 h in an aluminum block at 150 °C under a nitrogen atmosphere. After cooling to room temperature, water (50 mL) was added and the precipitate was collected via filtration, and washed with water. The crude product was purified by column chromatography using dichloromethane/hexane (1:1) as the eluent. The product was then recrystallized from dichloromethane/methanol, and filtration yielded the product as a white powder (1.7 g, 90%). ^{1}H NMR (400 MHz, $CDCl_3$): δ 7.84 (d, *J* = 2.0 Hz, 8H), 7.47 (t, *J* = 7.6 Hz, 2H), 7.36 (dd, *J* = 8.4, 1.6 Hz, 8H), 7.09 (d, *J* = 8.0 Hz, 4H), 6.83 (d, *J* = 8.4 Hz, 8H), 1.46 (s, 72H). ^{13}C{^{1}H} NMR (100 MHz, $CDCl_3$): δ 159.73, 142.78, 141.46, 141.22, 133.07, 128.28, 124.88, 124.11, 123.64, 115.95, 110.28, 34.65, 32.03. MS (MALDI, *m/z*): Calcd for $C_{94}H_{102}N_6O$ [M^+], 1330.8; Found, 1330.8. Anal. Calcd for $C_{94}H_{102}N_6O$: C, 84.77; H, 7.72; N, 6.31. Found: C, 84.93; H, 7.45; N, 6.19.

2-(2,4-Di(9*H*-carbazol-9-yl)-3,5,6-trifluorophenyl)-5-phenyl-1,3,4-oxadiazole (**20**). In a round-bottomed flask, 2-(pentafluorophenyl)-5-phenyl-1,3,4-oxadiazole (0.482 g, 1.54 mmol), carbazole (0.408 g, 2.44 mmol), and potassium carbonate (3.5 g, 25 mmol) were placed under vacuum and then under nitrogen. DMSO (10 mL) was added and the reaction mixture was stirred overnight at room temperature. The mixture was precipitated with water and the crude product was separated via filtration. Column chromatography (10% ethyl acetate in hexanes as eluent) yielded the product as a white powder (0.177 g,

19%). ^{1}H NMR (500 MHz, $CDCl_3$): δ 8.16 (d, J = 8.0 Hz, 2H), 8.06 (d, J = 8.0 Hz, 2H), 7.52 (t, J = 8.0 Hz, 2H), 7.44-7.38 (m, 5H), 7.31-7.28 (m, 4H), 7.25 (t, J = 8.0 Hz, 2H), 7.20 (d, J = 8.0 Hz, 2H), 7.13 (d, J = 8.0 Hz, 2H). ^{13}C{^{1}H} NMR (125 MHz, $CDCl_3$): δ 165.09, 155.69, 152.77 (d, $^{1}J_{CF}$ = 259 Hz), 147.97 (dd, $^{1}J_{CF}$ = 262 Hz, J_{CF} =16 Hz), 146.93 (dd, $^{1}J_{CF}$ = 265 Hz, J_{CF} = 16 Hz) 140.83, 139.46, 131.99, 128.71, 126.76, 126.75, 126.69, 124.38, 123.95, 122.30, 121.64, 121.35, 121.14, 120.66, 120.58, 119.84 (t, J_{CF} = 15 Hz), 114.47 (d, J_{CF} = 11 Hz), 114.42, 109.93, 109.07. ^{19}F NMR (470 MHz, $CDCl_3$): δ -120.34 (d, J = 14 Hz, 1F), -131.78 (d, J = 24 Hz, 1F), -131.89 (dd, J = 24 Hz, 14 Hz, 1F). HRMS (ESI, m/z): Calcd for $C_{38}H_{22}N_4OF_3$ $[M]^+$, 607.1740; Found, 607.1723. Data is consistent with published characterization.[147]

2-Phenyl-5-(2,4,6-tri(9*H*-carbazol-9-yl)-3,5-difluorophenyl)-1,3,4-oxadiazole (**21**) and **2-phenyl-5-(2,4,5-tri(9*H*-carbazol-9-yl)-3,6-difluorophenyl)-1,3,4-oxadiazole** (**22**). To a round-bottomed flask was added 2-(pentafluorophenyl)-5-phenyl-1,3,4-oxadiazole (0.50 g, 1.60 mmol), carbazole (0.803 g, 4.80 mmol), and potassium carbonate (2.20 g, 16.0 mmol). The flask was evacuated and purged with nitrogen and DMSO (20 mL) was added. The reaction mixture was stirred overnight at room temperature. Upon completion, the reaction mixture was precipitated with water and the crude product was separated via filtration. Column chromatography (silica gel, 10% hexanes/dichloromethane as eluent) was performed to yield the higher R_f product 2-phenyl-5-(2,4,6-tri(9H-carbazol-9-yl)-3,5-difluorophenyl)-1,3,4-oxadiazole as a yellow powder, and the lower R_f product 2-phenyl-5-(2,4,5-tri(9H-carbazol-9-yl)-3,6-difluorophenyl)-1,3,4-oxadiazole as a white crystalline powder.

(21). Yield: 0.226 g (19%). ^{1}H NMR (500 MHz, $CDCl_3$): δ 8.19 (d, J = 2.0 Hz, 2H), 8.11 (d, J = 8.8 Hz, 4H), 7.58 (t, J = 8.8 Hz, 2H), 7.51 (t, J = 8.0 Hz, 4H), 7.46-7.37 (m, 8H), 7.33 (t, J = 8.5 Hz, 4H), 7.17 (t, J = 8.0 Hz, 2H), 6.89 (d, J = 8.4 Hz, 2H). ^{13}C{^{1}H} NMR (125 MHz, $CDCl_3$): δ 164.59, 156.65 (t, J_{CF} = 2.5 Hz), 156.41 (dd, $^{1}J_{CF}$ = 268 Hz, J_{CF} = 5 Hz), 140.90, 139.49, 131.64, 128.46, 126.67, 126.62, 126.54, 126.35, 124.39, 124.04, 123.66 (dd, J_{CF} = 14 Hz, J_{CF} = 5 Hz), 122.18, 121.60, 120.69, 119.84 (t, J_{CF} = 15 Hz), 109.89, 108.96. ^{19}F NMR (470 MHz, $CDCl_3$): δ -113.00 (s). HRMS (MALDI, m/z): Calcd for $C_{50}H_{29}N_5OF_2$ $[M]^+$, 754.2413; Found, 754.2410. Anal. Calcd for $C_{50}H_{29}N_5OF_2$: C, 79.67; H, 3.88; N, 9.29. Found: C, 79.75; H, 3.73; N, 9.45.

(22). Yield: 0.273 g (23%). ^{1}H NMR (500 MHz, $CDCl_3$): δ 8.12 (d, J = 2.0 Hz, 2H), 7.80-7.78 (m, 2H), 7.76-7.74 (m, 2H), 7.52 (t, J = 8.5 Hz, 2H), 7.44 (d, J = 8.8 Hz, 2H), 7.41 (d, J = 8.8 Hz, 1H), 7.35 (t, J = 8.5 Hz, 2H), 7.28 (t, J = 8.0 Hz, 2H), 7.24-7.21 (m, 4H), 7.15-7.08 (m 10H). ^{13}C{^{1}H} NMR (125 MHz, $CDCl_3$): δ 165. 05, 156.11 (q, J_{CF} = 2.5 Hz), 154.22 (dd, $^{1}J_{CF}$ = 263 Hz, J_{CF} = 3.8 Hz), 153.27 (dd, $^{1}J_{CF}$ = 255 Hz, J_{CF} = 3.8 Hz), 140.76, 138.58, 138.43, 131.91, 128.71, 128.12 (dd, J_{CF} = 14 Hz, J_{CF} = 3.8 Hz), 128.76, 126.75, 125.73, 125.71, 125.10 (dd, J_{CF} = 15 Hz, J_{CF} = 3.8 Hz), 124.14, 124.13, 124.05, 122.45, 121.26, 121.15, 121.03, 120.62, 120.04, 120.02, 114.01 (d, J_{CF} = 14 Hz), 109.91, 109.83, 109.35. ^{19}F NMR (470 MHz, $CDCl_3$): δ -111.64 (d, J = 14 Hz, 1F), -120.54 (d, J = 14 Hz, 1F). HRMS (MALDI, m/z): Calcd for $C_{50}H_{29}N_5OF_2$ $[M]^+$, 754.2413; Found, 753.2347. Anal. Calcd for $C_{50}H_{29}N_5OF_2$: C, 79.67; H, 3.88; N, 9.29. Found: C, 79.60; H, 4.00; N, 9.32.

2-Phenyl-5-(2,3,4,6-tetra(9*H*-carbazol-9-yl)-5-fluorophenyl)-1,3,4-oxadiazole (**23**). A solution of 2-(pentafluorophenyl)-5-phenyl-1,3,4-oxadiazole (1.0 g, 3.2 mmol), carbazole (2.13 g, 12.7 mmol), and potassium carbonate (7.0 g, 50. mmol) in DMSO (20 ml) was stirred at room temperature for 27 h under nitrogen. Water (100 mL) was added and pale yellow solid was obtained. The solid product was collected by filtration, washed with water. After drying, the crude product was purified by column chromatography using dichloromethane/hexane (8:2) as eluent. After removal of solvent, yellow solid was dissolved in dichloromethane, methanol (100 mL) was added. Dichloromethane was removed and pale-yellow solid was recrystallized from methanol solution. The solid product was collected by filtration. After drying under vacuum, the product was obtained (1.6 g, 55%). ^{1}H NMR (500 MHz, $CDCl_3$): δ 8.09 (d, J = 2.0 Hz, 2H), 7.74-7.73 (m, 2H), 7.62 (d, J = 8.4 Hz, 2H), 7.49-7.44 (m, 4H), 7.39 (d, J = 8.8 Hz, 2H), 7.32-7.27 (m, 3H), 7.23-7.20 (m, 4H), 7.15-7.06 (m, 8H), 7.03 (t, J = 8.4 Hz, 2H), 6.85-6.80 (m, 4H), 6.73 (t, J = 8.0 Hz, 2H). ^{13}C{^{1}H} NMR (125 MHz, $CDCl_3$): δ 164.30, 157.14 (d, J = 4 Hz), 156.39 (d, $^{1}J_{CF}$ = 261 Hz) , 140.95, 139.71, 138.72, 138.12, 136.64 (d, J = 2.5 Hz), 134.13 (d, J = 4 Hz), 131.47, 129.35 (d, J = 14 Hz), 128.37, 127.16 (d, J = 15 Hz), 126.95 (d, J = 1 Hz), 126.55, 126.48, 125.61, 125.55, 124.68, 124.14, 124.01, 123.72, 122.26, 121.04, 120.97, 120.70, 120.56, 120.47, 120.04, 119.54, 110.05, 109.30, 109.28. ^{19}F NMR (470 MHz, $CDCl_3$): δ -113.83 (s). HRMS (MALDI, m/z): Calcd for $C_{67}H_{37}N_6OF$ $[M]^+$ 900.3013; Found 900.3005. Anal. Calcd for $C_{67}H_{37}N_6OF$: C, 82.65; H, 4.14; N, 9.33. Found: C, 82.43; H, 4.08; N, 9.32.

2-(4-(*Tert*-Butyl)phenyl)-5-(2,3,4,5,6-penta(9*H*-carbazol-9-yl)phenyl)-1,3,4-oxadiazole (**24**). A solution of 2-(4-(*tert*-butyl)phenyl)-5-(pentafluorophenyl)-1,3,4-

oxadiazole (0.20 g, 0.54 mmol), carbazole (0.50 g, 3.0 mmol) and potassium carbonate (2.0 g, 14 mmol) in DMSO (10 ml) was stirred at 100 °C for 10 h under nitrogen. After cooling to room temperature, water (75 mL) was added and a pale-yellow solid was obtained. The solid product was collected by filtration and washed with water. After drying, the crude product was purified by column chromatography using dichloromethane/hexane (7:3) as eluent. After removal of solvents, the solid was dissolved in dichloromethane, methanol (30 ml) was added, dichloromethane was removed, and the resulting yellow solid was collected by filtration and dried under vacuum (0.55 g, 92%) was obtained. ^{1}H NMR (500 MHz, $CDCl_3$): δ 7.64-7.61 (m, 4H), 7.36 (d, J = 8.0 Hz, 4H), 7.30 (d, J = 5.6 Hz, 2H), 7.24-7.20 (m, 10H), 7.08 (d, J = 8.5 Hz, 2H), 6.97-6.95 (m, 8H), 6.79-6.73 (m, 6H), 6.68-6.65 (m, 6H), 6.61 (t, J = 7.5 Hz, 2H), 1.22 (s, 9H). ^{13}C{^{1}H} NMR (125 MHz, $CDCl_3$): δ 164.12, 157.34, 154.83, 139.73, 139.57, 138.34, 137.95, 137.04, 127.30, 126.30, 125.49, 125.24, 124.37, 124.23, 123.80, 123.60, 120.49, 120.31, 120.21, 120.02, 119.57, 119.41, 119.31, 110.75, 110.51, 109.38, 34.86, 30.98. HRMS (MALDI, m/z): Calcd for $C_{78}H_{53}N_7O$ 1103.4312 $[M]^+$; Found 1103.4295. Anal. Calcd for $C_{78}H_{53}N_7O$: C, 84.84; H, 4.84; N, 8.88. Found: C, 84.65; H, 4.72; N, 8.91.

2-(4-(*Tert*-butyl)phenyl)-5-(2,3,4,5,6-pentakis(3,6-di-tert-butyl-9*H*-carbazol-9-yl)phenyl)-1,3,4-oxadiazole) (**25**). A solution of 2-(4-(tert-butyl)phenyl)-5-(perfluorophenyl)-1,3,4-oxadiazole (0.50 g, 1.4 mmol), 3,6-di-tert-butylcarbazole (1.9 g, 6.8 mmol) and K_2CO_3 (2.0 g, 15 mmol) in DMSO (20 ml) was stirred at 50 °C for 24 h, and then at 100 °C for 26 h under nitrogen. After cooling to room temperature, water (100 ml) was added and a yellow solid was obtained. The solid product was collected by

filtration, washed with water and dried on the filter. The crude product was purified by column chromatography (silica gel) using dichloromethane/hexane (4:6) as eluent. After removal drying *in vacuo*, the product was recrystallized from dichloromethane/methanol and the yellow solid was collected by filtration. After drying under vacuum, the product was obtained as a yellow powder (1.8 g, 78 %). $^{13}C\{^{1}H\}$ NMR (125 MHz, $CDCl_3$): δ 163.74, 157.79, 154.47, 142.67, 142.58, 142.50, 139.99, 138.52, 137.85, 137.55, 137.28, 137.11, 126.67, 126.37, 124.90, 124.18, 124.11, 124.02, 122.93, 122.04, 121.97, 120.02, 115.69, 114.90, 114.88, 110.22, 110.11, 109.03, 34.81, 34.37, 34.25, 31.78, 31.76, 30.99. HRMS (MALDI, *m/z*): Calcd for $C_{118}H_{133}N_7O$ $[M]^+$ 1664.0572; Found 1664.0618. Anal. Calcd for $C_{118}H_{133}N_7O$: C, 85.10; H, 8.05; N, 5.89. Found: C, 85.08; H, 8.05; N, 5.77.

3.5.2 Thermogravimetric Analysis

a) b)

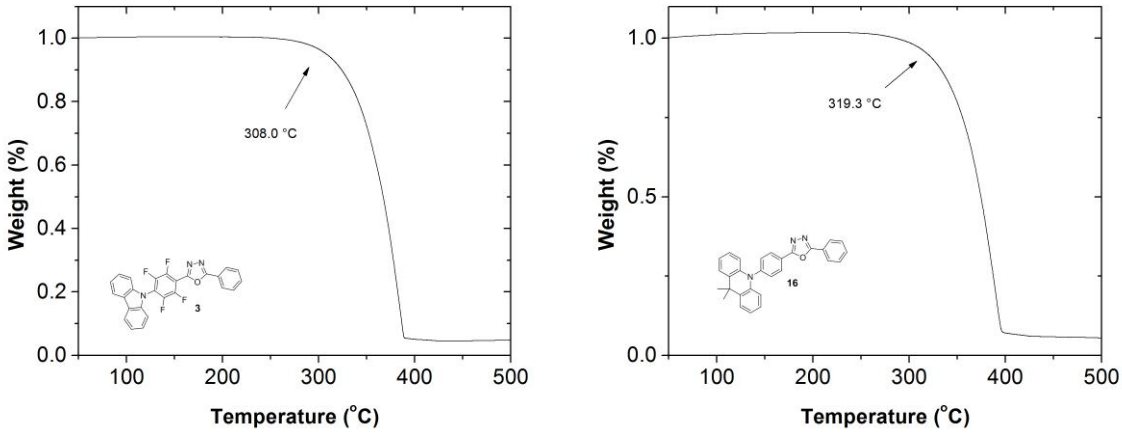

c) d)

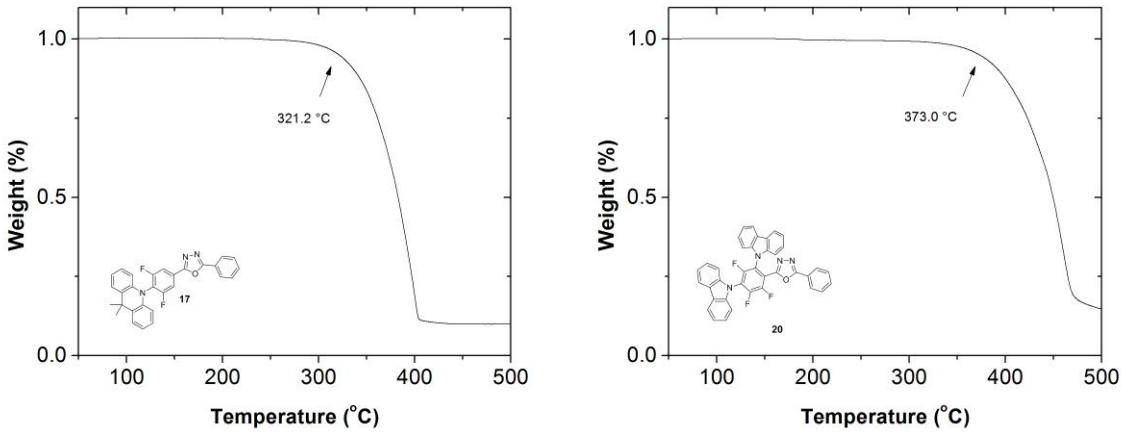

Thermogravimetric analysis of compound 3 (a), 16 (b), 17 (c), and 20 (d) with 5% weight loss temperature noted.

a)

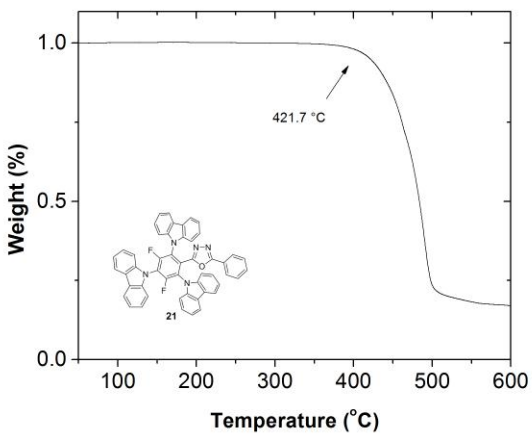

b)

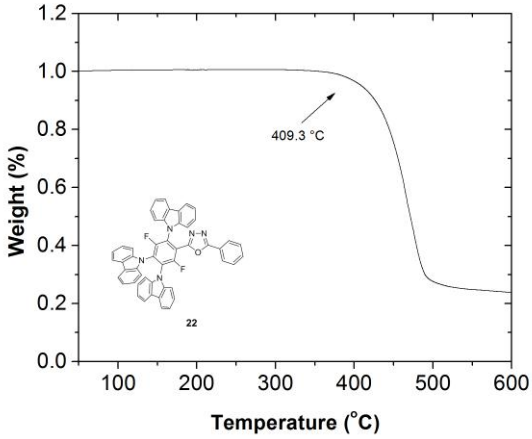

c)

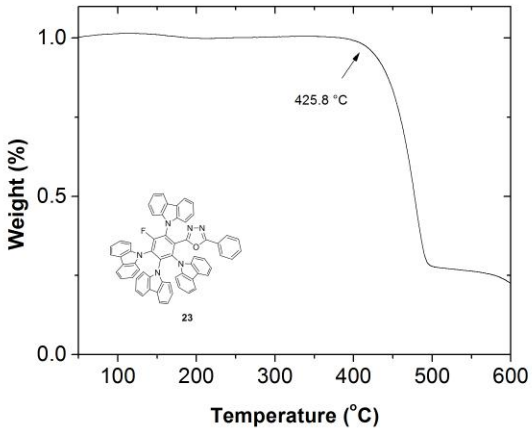

d)

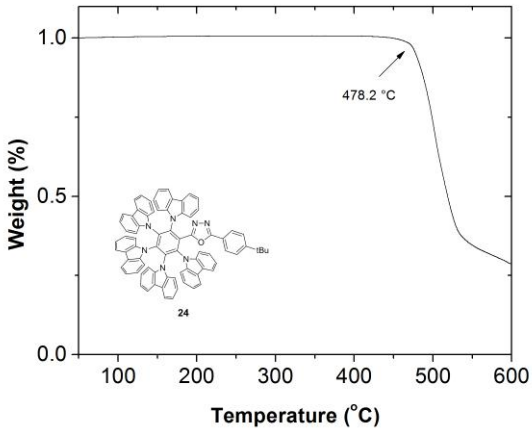

Thermogravimetric analysis of compound 21 (a), 22 (b), 23 (c), and 24 (d) with 5% weight loss temperature noted.

3.5.3 Cyclic Voltammetry

a)

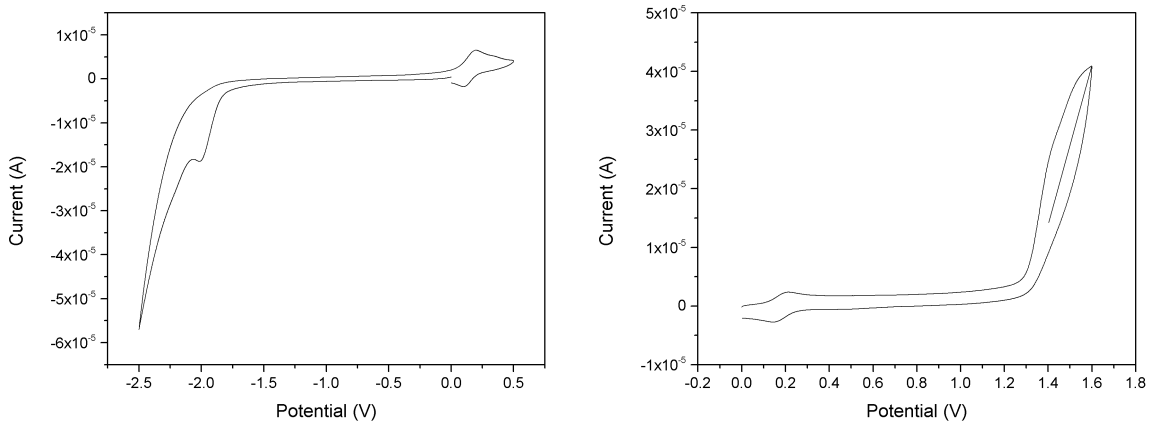

b)

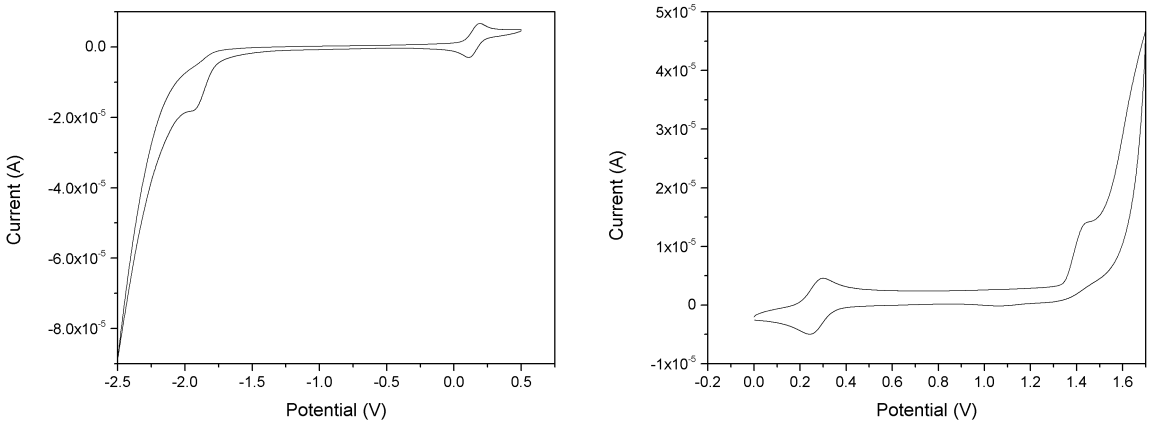

Cyclic voltammograms of 3 (a) and 20 (b) vs. ferrocene internal standard. Reductive scans on left, oxidative scans on right.

a)

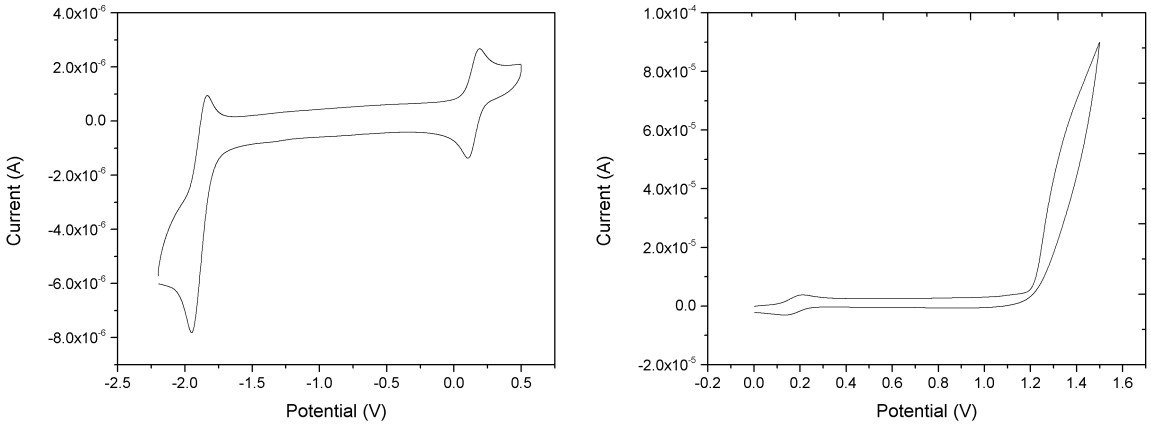

b)

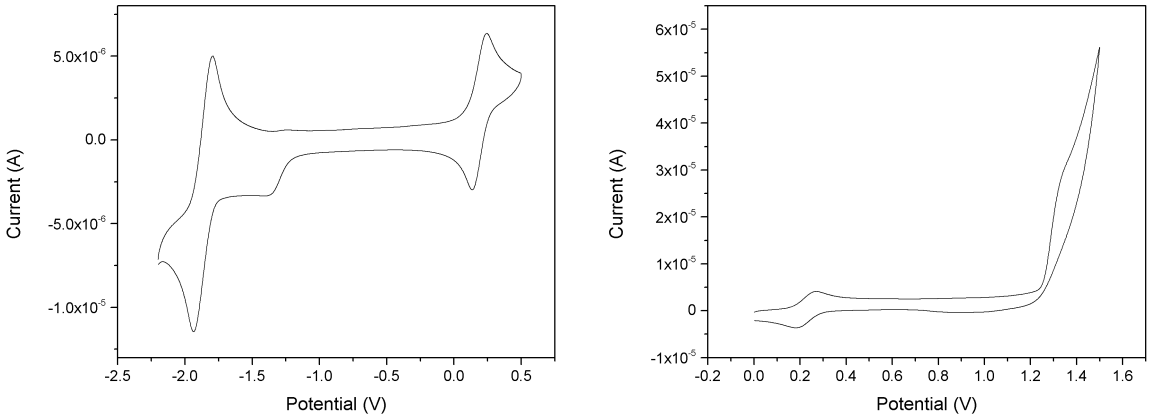

Cyclic voltammograms of 21 (a) and 22 (b) vs. ferrocene internal standard. Reductive scans on left, oxidative scans on right.

a)

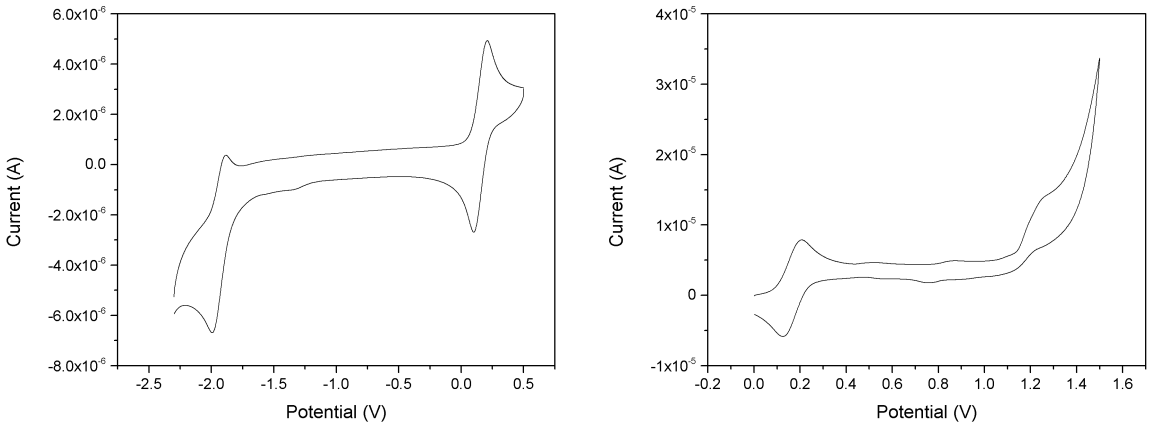

b)

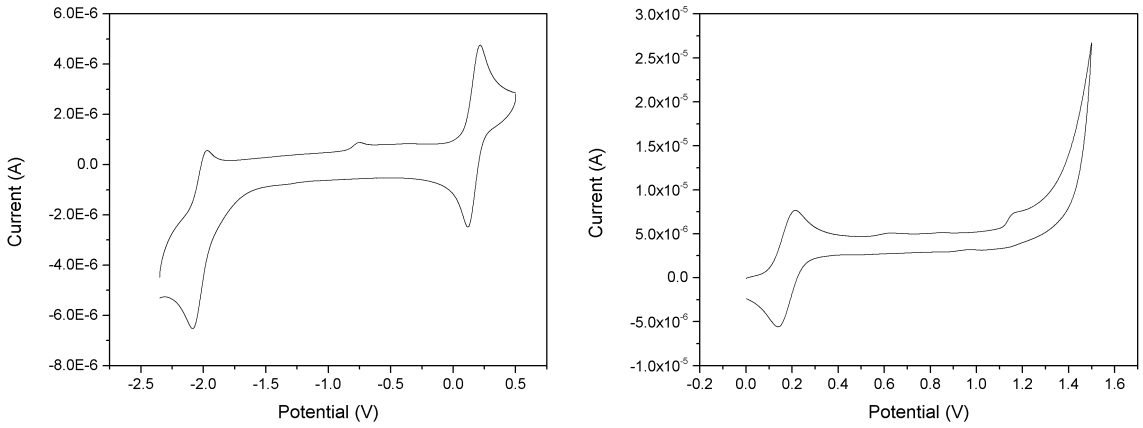

Cyclic voltammograms of 23 (a) and 24 (b) vs. ferrocene internal standard. Reductive scans on left, oxidative scans on right.

3.5.4 Chemical Structures of Compounds in OLED Devices

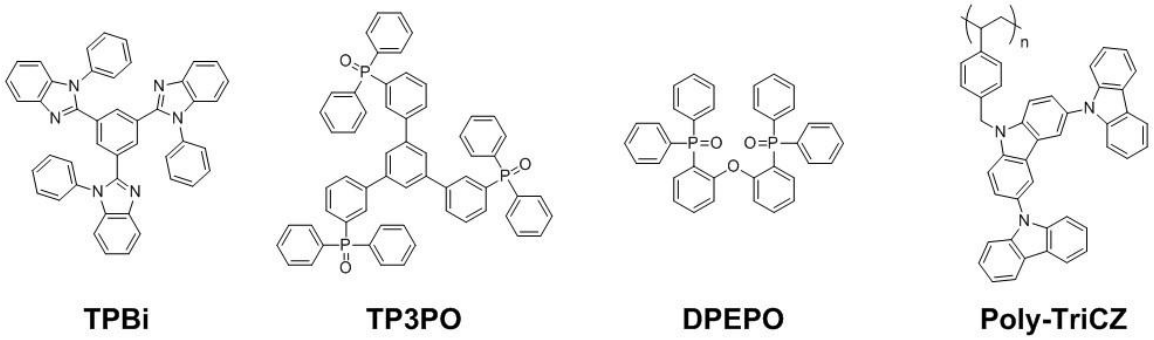

3.5.5 $^{13}C\{^{1}H\}$ NMR Spectra

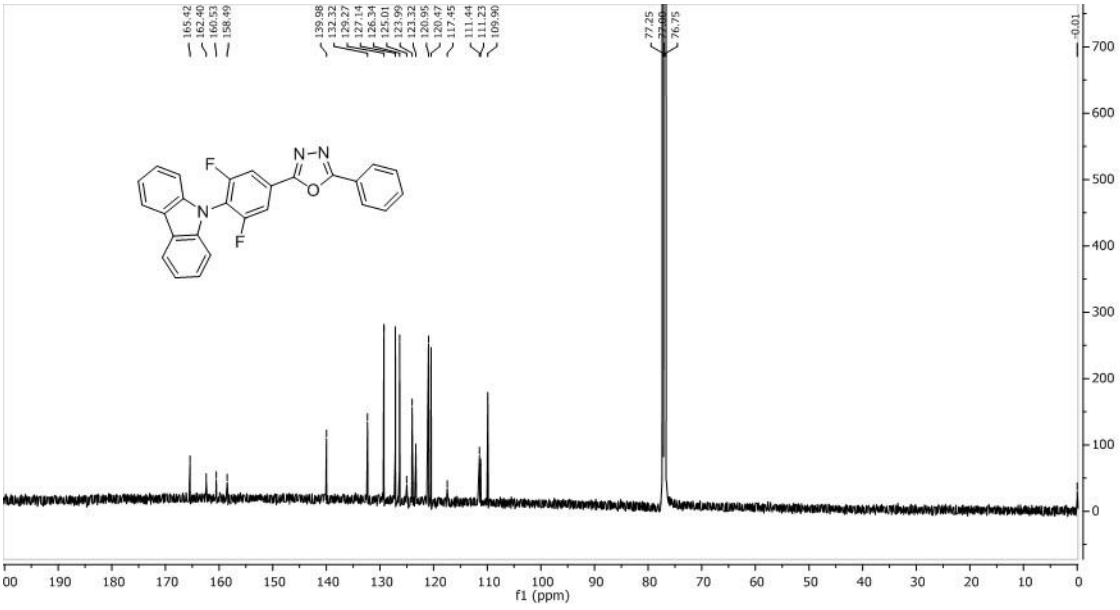

Figure 53 – $^{13}C\{^{1}H\}$ NMR spectrum (100 MHz, $CDCl_3$) of compound 2.

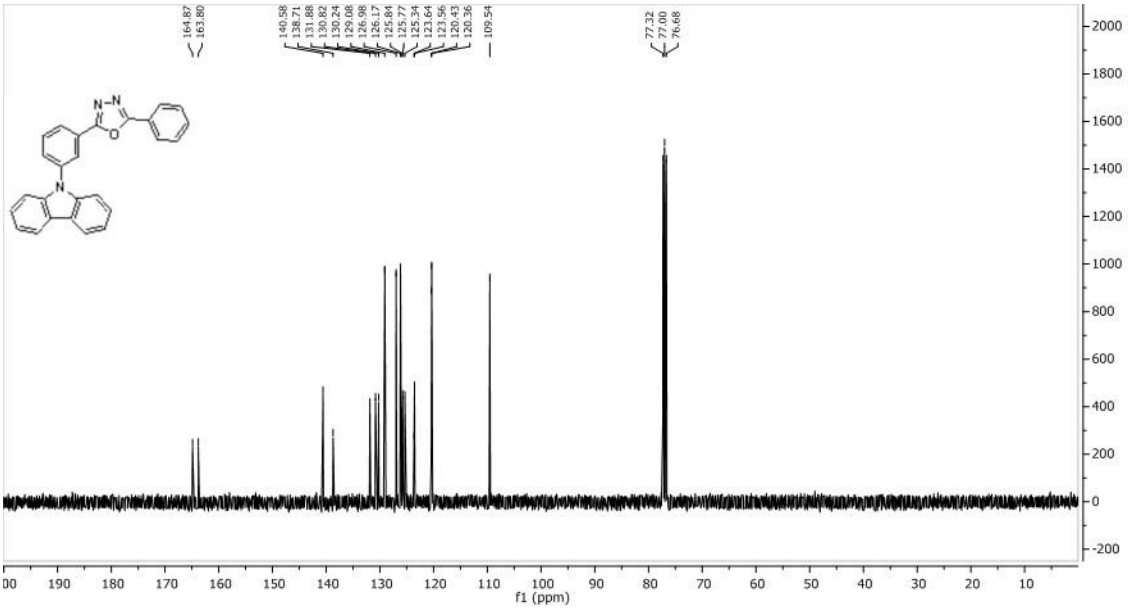

Figure 54 – $^{13}C\{^{1}H\}$ NMR spectrum (100 MHz, $CDCl_3$) of compound 6.

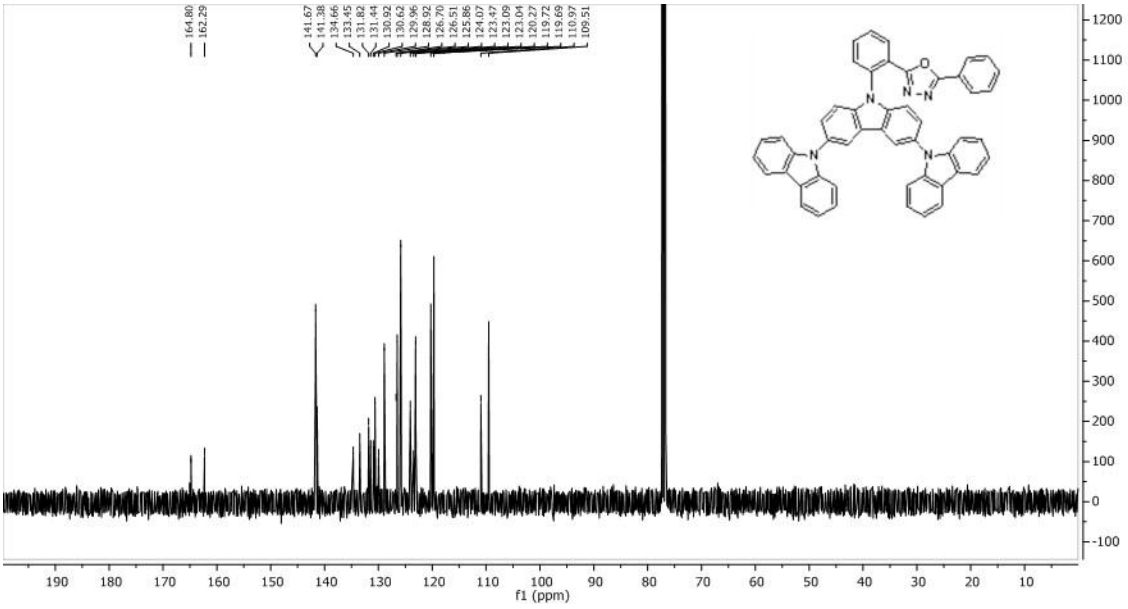

Figure 55 – $^{13}C\{^{1}H\}$ NMR spectrum (100 MHz, $CDCl_3$) of compound 10.

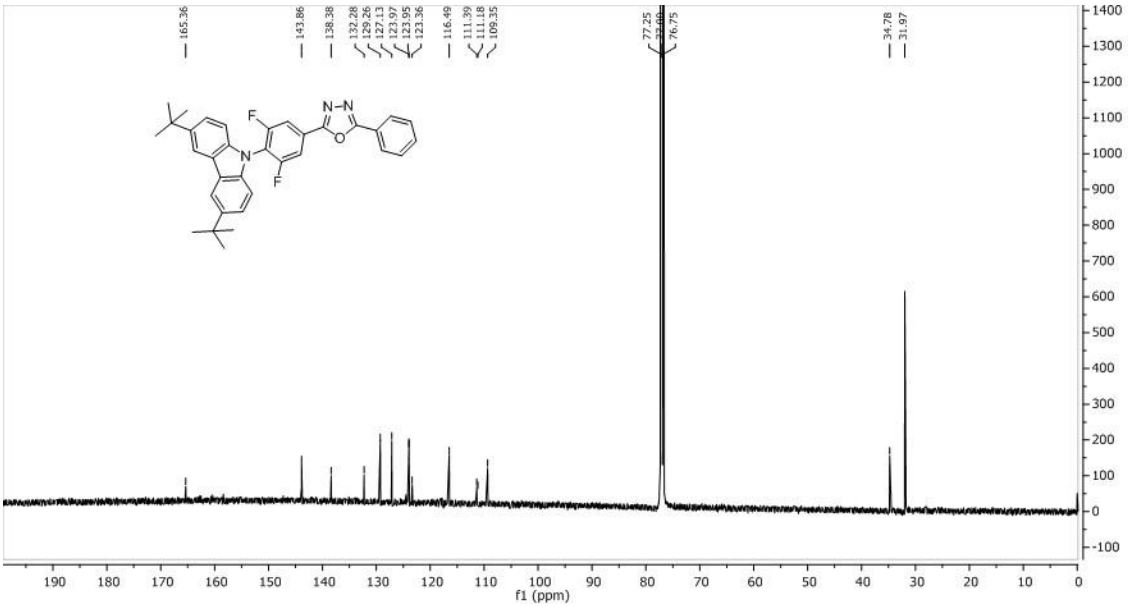

Figure 56 – $^{13}C\{^{1}H\}$ NMR spectrum (125 MHz, $CDCl_3$) of compound 12.

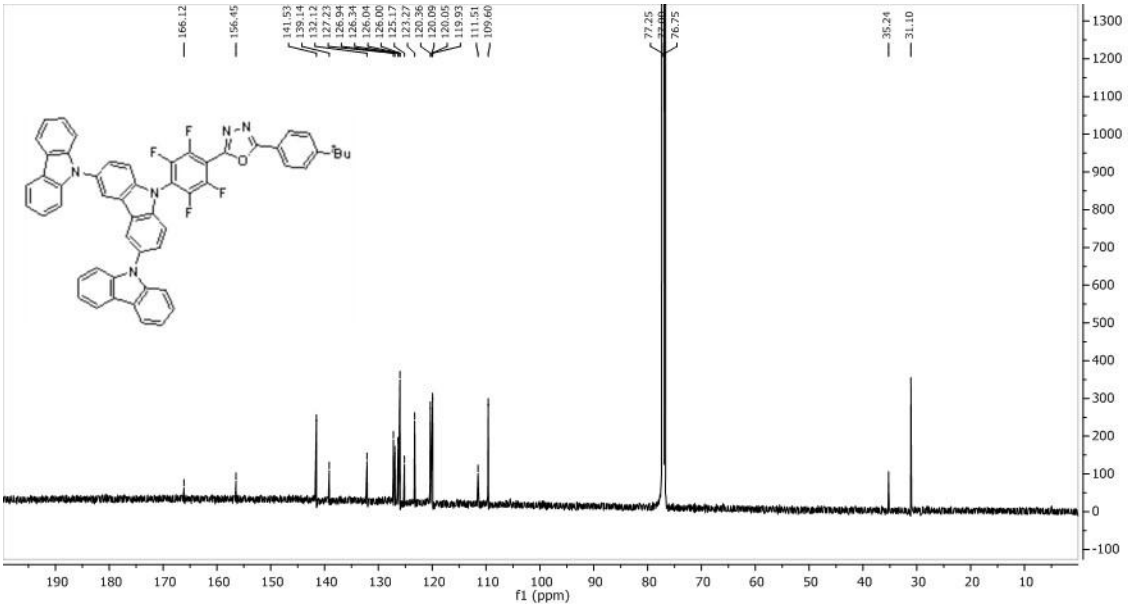

Figure 57 – $^{13}C\{^{1}H\}$ NMR spectrum (100 MHz, $CDCl_3$) of compound 15.

CHAPTER 4. THERMALLY ACTIVATED DELAYED FLUORESCENCE IN DONOR-ACCEPTOR FLUOROPHORES COMPRISED OF 2-METHYL-5-PHENYL-1,3,4-OXADIAZOLE AND 9*H*-CARBAZOLE

For a compound to display efficient thermally activated delayed fluorescence through the most commonly understood RISC mechanism (see Equation 21) the ΔE_{ST} of the compound must be small, on the order of 0.1 eV or less. This places a limitation on a D-A fluorophore that the energy of the ground state to CT transition must be approximately equivalent to, or lower than, that of the ^{3}LE of both the donor and acceptor moieties in the compound. Fluorophores that contain 2,5-diphenyl-1,3,4-oxadiazole as the acceptor are inherently limited by the ^{3}LE of the three coplanar rings, which display a dihedral angle between the 1,3,4-oxadiazole and phenyl rings of ca. 1.5°.[149] As seen in CHAPTER 3, this energy in a simple donor-acceptor compound is at approximately 2.7-2.8 eV, and it follows that the ^{1}CT energy must be approximately 2.8-2.9 eV for TADF to be realized. This limitation provides a boundary for the emission color of the resulting fluorophores that is red shifted from true blue emission, which exhibits a dominant wavelength at 445-450 nm (2.76-2.78 eV). Compound 2-(4-(9,9-dimethylacridin-10(9*H*)-yl)-3,5-difluorophenyl)-5-phenyl-1,3,4-oxadiazole (**17**) is one such compound that displays TADF. The singlet energy of ca. 2.88 eV results in a fluorescent emission with a λ_{max} of 490 nm that, when incorporated as the emitter in an OLED device, displays a green-blue emission with chromaticity (CIE *x*,*y*) of 0.22, 0.46.

While the conjugation across the three rings of DPO can be broken through appropriate substitution patterns, increasing the energy of the ^{3}LE increased as shown in Figure 32, this approach has the trade-off of reducing the rate of fluorescence, and the dependent photoluminescent quantum yield, by an order of magnitude or more, as shown in Figure 58. For example, 2-(4-(9H-carbazol-9-yl)phenyl)-5-phenyl-1,3,4-oxadiazole (**1**) has a triplet energy of 2.74 eV with a PLQY of 0.92 and a k_{fl} of 4.3×10^8 s^{-1} (in dil. toluene solution). While the triplet energy of 2-(2-(9H-carbazol-9-yl)phenyl)-5-phenyl-1,3,4-oxadiazole (**9**) is increased to 2.82 eV, the PLQY is reduced to 0.18 due to an order of magnitude decrease in the k_{fl} to 3.5×10^7 s^{-1}. Pushed to the furthest degree, the triplet energy is increased to 3.02 eV in 2,5-bis(2,6-bis(3,6-di-tert-butyl-9H-carbazol-9-yl)phenyl)-1,3,4-oxadiazole (**19**), leading to true blue emission alongside thermally activated delayed fluorescence, but with a prompt fluorescence PLQY further reduced to ca. 0.02 due to a suppressed fluorescent decay rate of k_{fl} of 7.1×10^6 s^{-1}.

An alternative approach would be to decrease the conjugation across the three rings of DPO by simply removing one of the rings. In 2-methyl-5-phenyl-1,3,4-oxadiazole, one of the phenyl groups of DPO is replaced with a methyl group. The resulting methyl-phenyl-oxadiazole still contains the electron poor 1,3,4-oxadiazole functionality but with two conjugated, coplanar rings instead of three. The decreased conjugation is anticipated to affect the energy of the HOMO and LUMO, the latter of which is of key importance to the role of the moiety as an acceptor in D-A fluorophores. Furthermore, increasing the HOMO-LUMO gap would increase the energy both the LE singlet and triplet states, and provide an increased ^{3}LE energy, possibly allowing for blue fluorescent emission with concomitant TADF.

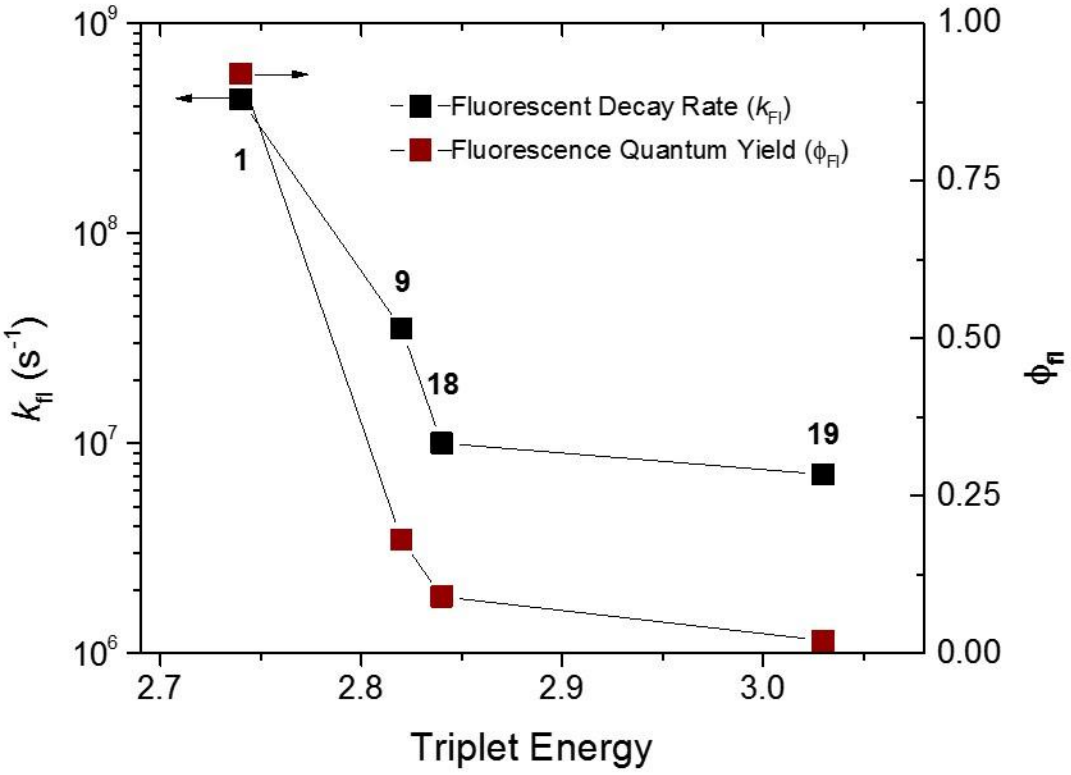

Figure 58 – Fluorescence decay rate (k_{fl}) and photoluminescent quantum yield (ϕ_{fl}) of prompt fluorescence of some CzDPO compounds versus their triplet energy as estimated from phosphorescence. Lines are included to guide the eye.

4.1 Synthesis and Characterization of 2-methyl-5-phenyl-1,3,4-oxadiazole

The unsubstituted 2-methyl-5-phenyl-1,3,4-oxadiazole (MPO) was prepared from benzhydrazide and triethyl orthoacetate to probe the properties of the acceptor before it was incorporated into donor-acceptor fluorophores. Cyclic voltammetry was performed on the compound and compared to that of 2,5-diphenyl-1,3,4-oxadiazole to gain an understanding of the acceptor strength of the compound. The reductive scan is shown in Figure 59, left, referenced against an internal standard of ferrocene. Neither MPO or DPO showed reversible reduction in the experiment, and the reduction potential were estimated

from the onset at a scan rate of 50 mV s^{-1}. DPO displayed a reduction potential of 2.49 V vs. Fc/Fc^{+}. Exclusion of the second phenyl ring makes MPO comparatively more difficult to reduce, with the reduction occurring at 2.71 V vs. Fc/Fc^{+}. The decreased reduction potential of 0.22 V of MPO shows that the moiety can be expected to act as a weaker electron acceptor when incorporated into a D-A compound than DPO.

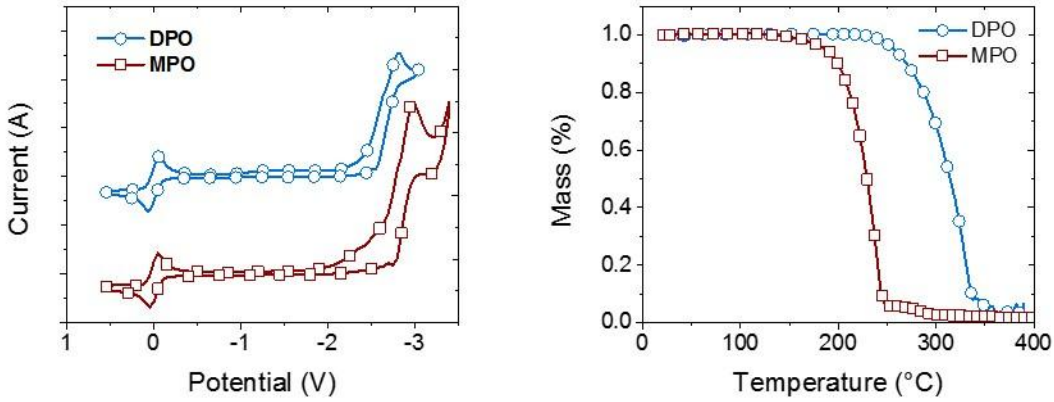

Figure 59 – (*left*) Cyclic voltammetry of 2,5-dimethyl-1,3,4-oxadiazole and 2-methyl-5-phenyl-1,3,4-oxadiazole. Reductive scan performed in THF with Fc/Fc^{+} internal standard referenced to 0 potential. (*right*) Thermogravimetric analysis of 2,5-dimethyl-1,3,4-oxadiazole and 2-methyl-5-phenyl-1,3,4-oxadiazole.

In CHAPTER 3, the energy of the ^{3}LE state of the oxadiazole was found to be of key importance to controlling the triplet energy and the ΔE_{ST} of the fluorophores. To gain an understanding of how the LE triplet energy of the MPO acceptor differed from that of DPO, phosphorescence spectra were collected and are shown in Figure 60. The λ_{max} is blue shifted from 504 nm for DPO to 434 nm for MPO, and the energy of the onset increases by ca. 0.12 eV, from 3.17 to 3.29 eV, when the phenyl group is substituted with methyl. While the energy of the ^{3}LE of MPO in a donor-acceptor compound may not be

perfectly represented by that of the isolated acceptor, the energy is certainly increased in MPO versus that in DPO.

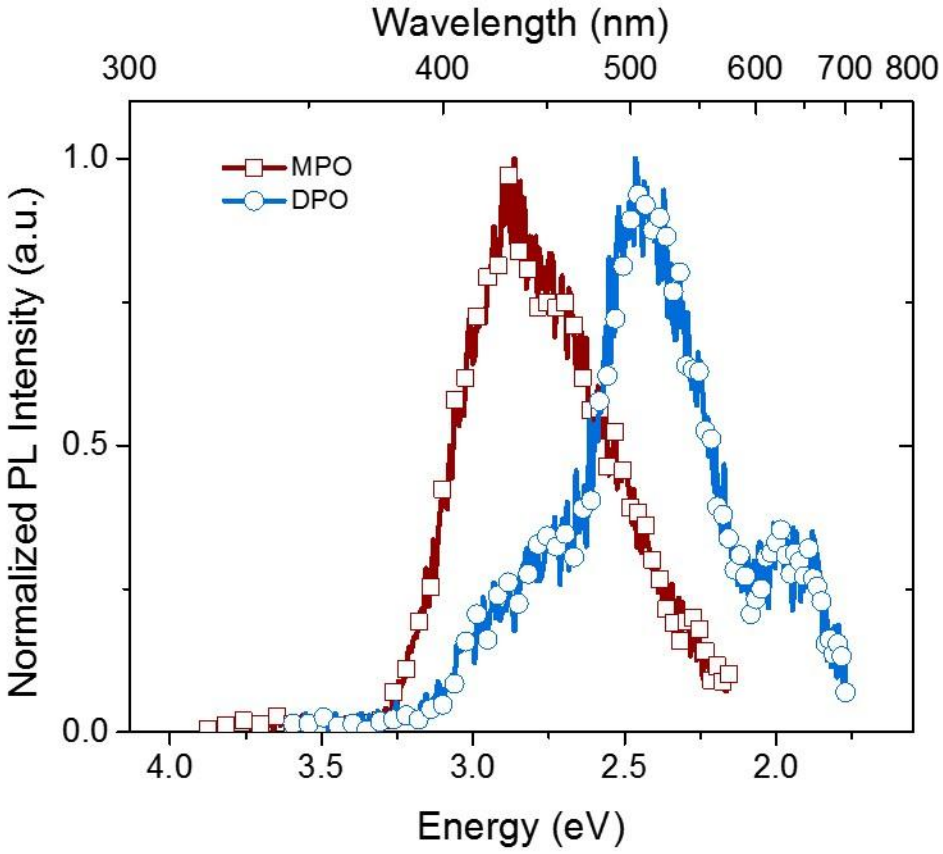

Figure 60 – Phosphorescence spectra of 2-methyl-5-phenyl-1,3,4-oxadiazole (MPO) and 2,5-diphenyl-1,3,4-oxadiazole (DPO) in 2-methyltetrahydrofuran matrix (77 K, 500 μs delay between excitation and data acquisition).

Finally, the thermal stability of acceptor was examined via thermogravimetric analysis (TGA), as shown in Figure 59, right. DPO is known to have good thermal stability, and here was seen to have a thermal decomposition temperature (T_d), defined by 5% weight loss in the TGA trace, of 257 °C. In MPO, the replacement of a phenyl group with a methyl resulted in a decreased T_d of 185 °C. Thus, D-A compounds exploiting

MPO as the acceptor may be expected to display lower thermal stability than their DPO analogues.

4.2 Fluorophores Exploiting MPO Acceptor Moieties

As in CHAPTER 3, a series of compounds containing MPO as the acceptor moiety was synthesized, and their photophysical properties were characterized in order to gain an understanding of the transitions relevant to designing MPO fluorophores that display TADF. The insights gained in the previous chapter provide us certain guidelines in this related class of compounds. A direct comparison between similar DPO and MPO based compounds will be the starting point for examining in what ways the structural differences change the properties of the resulting fluorophore and in what ways they remain similar.

In CHAPTER 3, compounds were compared to the parent CzDPO compound **1** as a reference for how structural variation affected the photophysical properties of the resulting fluorophore. The parent MPO containing fluorophore is the analogous compound **26**, 2-(4-(9H-carbazol-9-yl)phenyl)-5-methyl-1,3,4-oxadiazole. Before the MPO compounds are examined, it is worth comparing the DPO- and MPO-containing parent compounds directly. The absorption and fluorescence spectra in toluene solution and the phosphorescence spectra in toluene matrix at 77 K of the compounds were collected and are shown in Figure 61 plotted against energy.

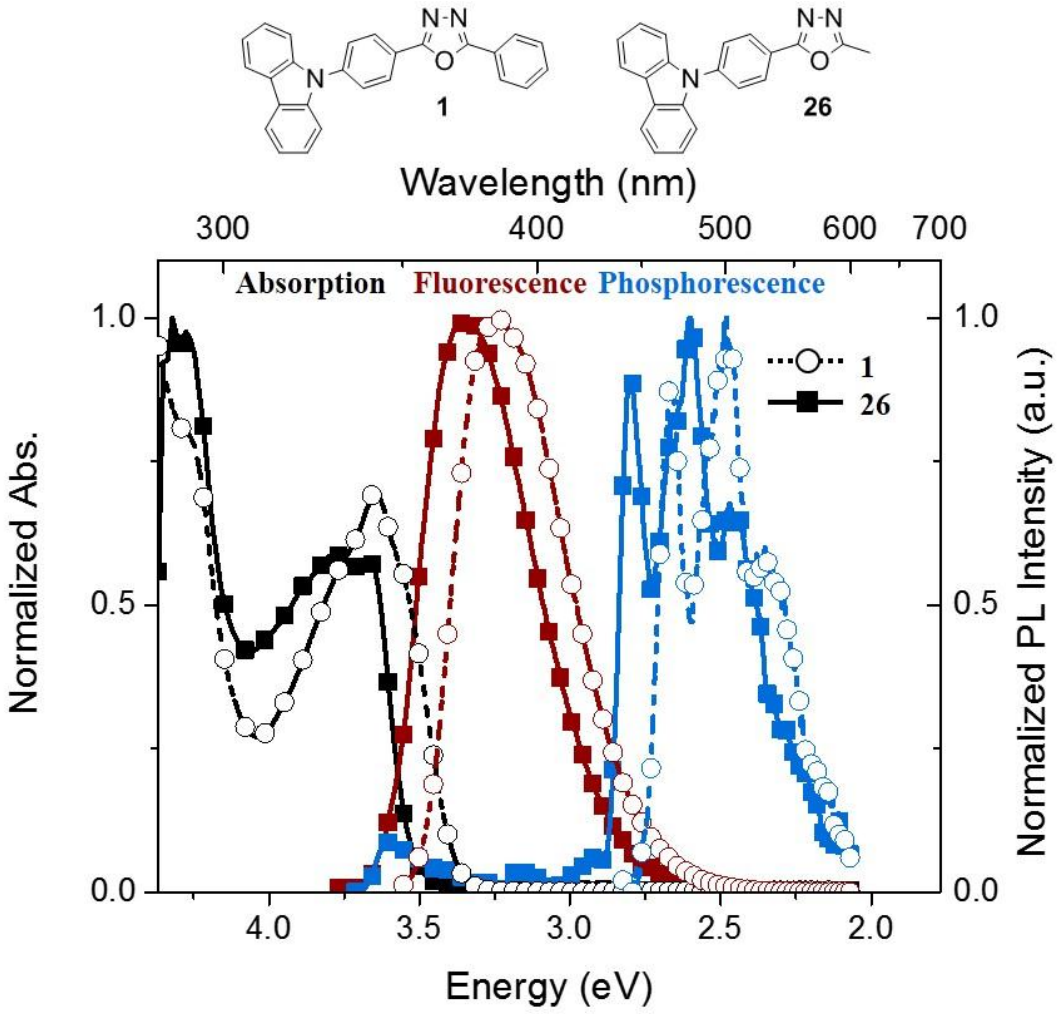

Figure 61 – (*top*) Structure of CzDPO parent compound 1, and CzMPO parent compound 26. (*bottom*) Absorption and photoluminescence spectra of compounds plotted against energy. Absorption and fluorescence spectra collected in toluene solution (ca. 10^{-5} M) at room temperature, phosphorescence spectra collected in toluene matrix at 77 K with a 500 μs delay between excitation and detection.

Immediately apparent is that the spectra of the CzMPO **26** compound look strikingly like blue shifted spectra of the CzDPO **1** (dashed lines). The absorption spectra each show a peak at ca. 3.65 eV (341 and 338 nm, respectively) corresponding to π-π* transitions on the carbazole moiety. A broad, featureless absorption peak attributed to the CT absorption is superimposed on the carbazole π-π* absorption of **1** but is blue shifted

in the absorption spectra for compound **26,** displaying a λ_{max} at 328 nm. This is mirrored in the fluorescence spectrum, which also displays the broad, structureless line shape of a CT transition, as the λ_{max} blue shifts from 382 nm in the DPO compound to 371 nm in the MPO compound. The adiabatic singlet state energy, again estimated from the high energy onset, increases from 3.47 eV in **1** to 3.59 eV in **26**. Since the donor carbazole moiety is unchanged, the increase in the CT transition energy of 0.12 eV is attributed to the increase in the LUMO energy of the compound, as seen in the cyclic voltammetry where a ca. 0.22 eV increase in the LUMO energy, as estimated from the reduction potential, was observed.

While the fluorescence spectra are attributed to donor-acceptor charge transfer states, likely between configurations well described by the HOMO and the LUMO, as was established in Section 3.2.1 the triplet state of the CzDPO compounds studied thus far have been LE states localized on the DPO moiety. The phosphorescence spectrum of the CzMPO compound **26**, like the absorption and fluorescence spectra discussed before, largely resembles that of compound **1** but is blue shifted. In compound **1**, the vibronic structure was attributed to the LE character of the transition. In compound **26**, the same vibronic structure is attributed to the same cause, a triplet state characterized as a LE on the oxadiazole donor moiety. Importantly, the triplet energy is estimated to be 2.86 eV in compound **26**, 0.12 eV higher than in compound **1**. This is the same increase in energy as is seen in an isolated MPO compound as compared to its DPO analogue, as was shown in Figure 60. Taken in whole, compound **26** displays much the same absorption and photoluminescent properties as compound **1**, but with the intramolecular CT state and the

lowest energy ^{3}LE state ca. 0.12 eV higher in energy, consistent with a higher energy LUMO orbital and triplet state in MPO than in comparison to DPO.

4.2.1 Adiabatic Singlet and Triplet Energies of CzMPO Fluorophores

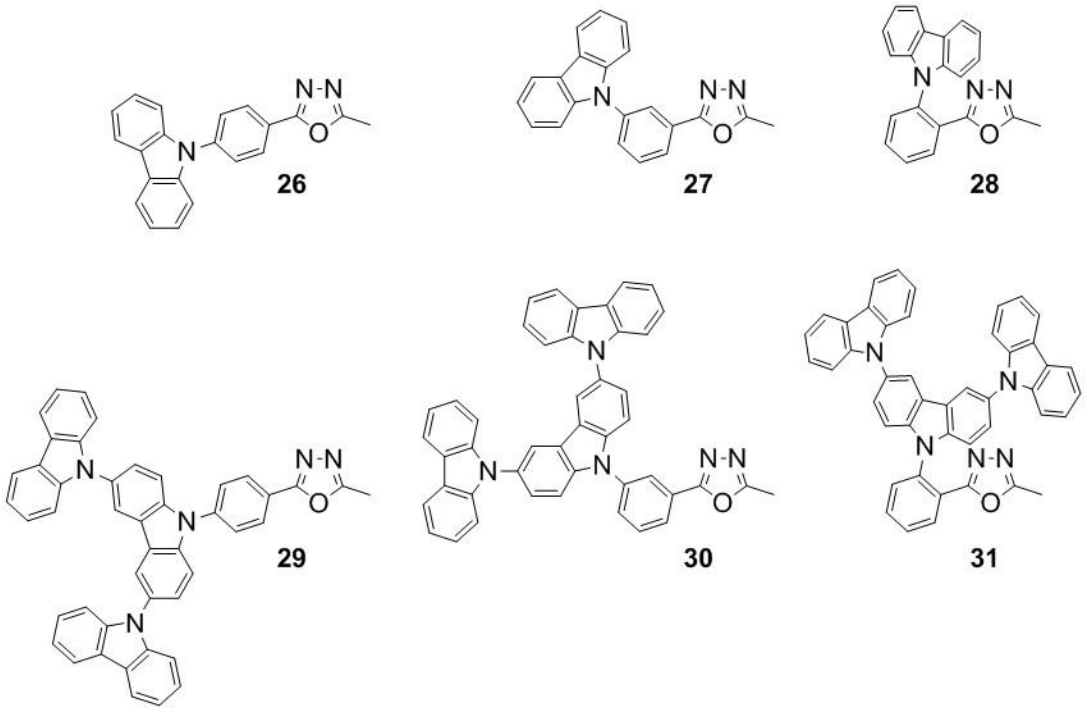

Figure 62 – CzMPO compounds synthesized and characterized with variety of connectivity between donor and acceptor and different donor strengths.

The photoluminescent properties of compounds **26**-**31**, shown in Figure 62 and synthesized in collaboration with Dr. Yadong Zhang, which are regioisomers of the simplest donor-acceptor fluorophores comprised of MPO and Cz (carbazole) or *t*Cz (*tris*carbazole), were collected in dilute toluene solution (ca. 10^{-5} M) and are summarized below in Table 12. In all cases, the fluorescence spectra displayed the expected broad, structureless line shape consistent with a CT transition. Additionally, the phosphorescence spectra retain the vibronic structure, attributed to a ^{3}LE state, seen in the

DPO compounds. While the triplet energy in the fluorophores reported here have increased ca. 0.1-0.2 eV over their DPO counterparts, they are still below that of an isolated carbazole, reported at 3.05 eV.[107] The estimated ΔE_{ST} values in these compounds range from 0.35-0.73 eV. In sum, the fluorophores exploiting MPO as the acceptor broadly mirror their DPO counterparts with regards to the energy and vibronic structure of their absorption and photoluminescence spectra.

Table 12 – Tabulated steady-state absorption and photoluminescence data of simple CzMPO compounds. Absorption and fluorescence data collected in toluene solution (ca. 10^{-5} M) at room temperature. Phosphorescence collected in toluene matrix at 77 K with 500 μs delay between excitation and data acquisition.

Compound	Absorption	Fluorescence		Phosphorescence		ΔE_{ST}
	λ_{max} /nm	λ_{max} /nm	Onset /eV	λ_{max} /nm	Onset /eV	/eV
26	288, 329, 338	371	3.59	444, 478	2.86	0.73
27	293, 326, 339	379	3.59	426, 458	2.95	0.64
28	293, 324, 337	388	3.49	468	2.97	0.53
29	288, 329, 341	383	3.40	444, 479	2.86	0.53
30	294, 327, 341	382	3.40	426, 457	2.97	0.41
31	294, 329, 343	420	3.38	457	3.05	0.35

The absorption and photoluminescence of the donor-acceptor fluorophores containing MPO as the acceptor suggest that the orbital character of the relevant singlet and triplet states can be understood analogously to those established for the fluorophore containing DPO as the acceptor, and that the same strategies for affecting the singlet and triplet energy, and their resultant effects on the ΔE_{ST} and fluorescence efficiency, would

be operative for both types of fluorophore. If this is true, then similar structural changes to the fluorophore should result in similar changes to the energy of the singlet and triplet states. Figure 63 shows the singlet and triplet energy of analogous MPO and DPO compounds, as estimated from their high energy photoluminescence onsets, as a function of connectivity (as in Figure 30). The similarity between the trends is immediate apparent, and the triplet energies show a monotonic increase as steric hindrance between the oxadiazole and the phenylene increases providing further evidence of the ^{3}LE character of the T_1 state located on the acceptor moiety. The trend in the singlet energy is less simple, but also mirrors that for the DPO analogues and is attributed to the mesomeric effect as described in Section 3.3.1.

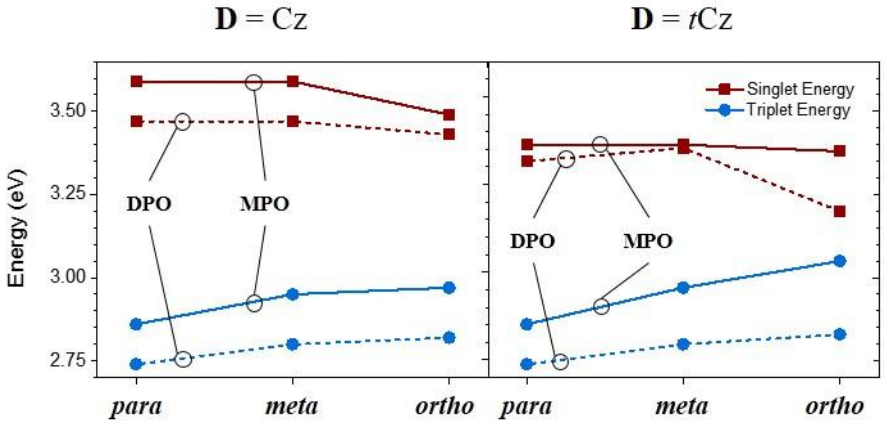

Figure 63 – Singlet and triplet energy, as estimated from the high-energy emission onset, of analogous fluorphores containing carbazole (Cz, left) and *tris*carbazole (*t*Cz, right) donors paired with diphenyloxadiazole (DPO, dashed line) and methylphenyloxadiazole (MPO, solid line) as a function of phenylene connectivity between the carbazolyl and oxadiazole groups. Lines are included as guides for the eye.

Comparing the two charts to one another allows for a comparison on donor strength, as in Figure 29. The singlet energy of the MPO fluorophores containing the Cz

acceptor are, in each case, ca. 0.10 eV higher in energy than the fluorophores containing *t*Cz. For example, the parent CzDPO compound **26** has an estimated singlet energy of 3.59 while analgous *t*CzMPO compound **29** is red shifted to 3.40 eV, due to the higher donor strength of the *t*Cz donor. The triplet energy, on the other hand, is not sensitive to the energy of the CT transition and differs by a negligible amount between the two compounds, with an estimated energy of 2.86 eV. In total, the orbital nature of the MPO containing fluorophores can be understood under the same framework established for the DPO compounds, but with a weaker acceptor leading to a blue shifted fluorescence and a higher energy triplet state consistent with a locally excited state found on the oxadiazole acceptor moiety.

4.2.2 Fluorescence Decay Rates in MPO Containing Fluorophores

In addition to minimizing the ΔE_{ST} through modulation of the singlet and triplet energy of a fluorophore, having a high fluorescence decay rate is necessary for a compound to act as an effective emitter for high efficiency OLEDs. Compound **19**, for example, displays a small ΔE_{ST} and measurable TADF, concomitant with true blue emission. However, this came at the expense of a very low fluorescent decay rate of ca. 7 $\times 10^6$ s^{-1} and a resultant PLQY of approximately 0.02 in solution.

To assess the fluorescence efficiency of the compounds, absolute photoluminescent quantum yield and fluorescent lifetime in air equilibrated toluene solution at room temperature were collected for each. This data is presented in Table 13, below. The PLQY of the *para* substituted fluorophores displayed high PLQY values of 0.93 and 0.70 for the CzMPO and the *t*CzMPO compounds **26** and **29**, respectively. This

compares well with the equivalent DPO fluorophores **1** and 4**6** (0.90 and 0.99, respectively). The high PLQY can be attributed to the high fluorescent decay rates, on the order of 10^8 s^{-1}, for the compounds. The fluorophores with *meta* and *ortho* connectivity display lower PLQYs due to their ca. 10 times lower rates of fluorescence than the *para* bridged compounds. This is attributed to the mesomeric effect, as was described in Section 3.2.2, where substitution of a donor in the 3- position is expected to lead to a HOMO with minimal spatial overlap with the LUMO, of which the highest coefficients on the phenylene would be in the 2-, 4-, and 6- positions relative to the π-electron withdrawing oxadiazole. Substitution in the 2-position likely leads to a twisting of both the carbazole and the oxadiazole relative to the bridging phenylene, increasing the orthogonality of the carbazole localized HOMO and the oxadiazole localized LUMO and thus decreasing the overlap between them. In both cases, the decreases HOMO-LUMO overlap would lead to a decrease in the transition dipole moment relative to the *para* substituted fluorophore, as shown in Equation 7, and thus the rate of fluorescence and the PLQY.

Overall, the physical properties of an isolated MPO can be understood as being similar to those of DPO but affected by the decreased conjugation due to the elimination of the second phenyl group. This raises the energy of the LUMO, as evidenced by the reduction potential (ca. 0.22 V more difficult to reduce than DPO), and increases the energy of the ^{3}LE state ca. 0.12 eV according to the phosphorescence spectra, but the compound displays lower thermal stability with a T_d ca. 72 °C lower than that of DPO. When incorporated into a donor-acceptor fluorophore with a carbazolyl donor, the MPO containing compounds display a similar intramolecular charge-transfer singlet state and

locally excited triplet state to the DPO containing compounds, but at ca. 0.10 eV higher energy, and the fluorescence decay is not appreciably quenched or enhanced in the MPO compounds versus their DPO analogues. Thus, the 2-methyl-5-phenyl-1,3,4-oxadiazole can be used to design fluorophores with higher energy luminescence but otherwise similar photophysical properties to 2,5-diphenyl-1,3,4-oxadiazole containing fluorophores.

Table 13 – Fluorescence quantum yield (Φ_{fl}), fluorescent lifetime (τ_{fl}), and rate of fluorescence (k_{fl}) of simple carbazole-oxadiazole compounds. Data collected in air equilibrated toluene solution (ca. 10^{-5} M) at room temperature.

Compound	Φ_{fl}	τ_{fl} /ns	k_{fl} /10^7 s^{-1}
26	0.93	3.00	31.0
27	0.07	4.91	1.56
28	0.21	4.50	4.28
29	0.70	3.95	17.7
30	0.10	4.85	2.22
31	0.25	4.50	5.15

4.3 Designing MPO Containing Fluorophores that Exhibit TADF

In CHAPTER 3, strategies were developed that specifically targeted methods for decreasing the ΔE_{ST} of fluorophores incorporating DPO acceptor moieties based on the orbital nature of the relevant singlet and triplet states. Namely, pushing the energy of the singlet state down or pushing the energy of the triplet state upwards, which could be done

largely independently of one another using specific approaches. These approaches were predicated on the understanding that the singlet and triplet transitions arose from distinct molecular orbitals such that structural changes designed to affect one may not have a large effect on the other. In section 4.2, it was demonstrated that similar fluorophores incorporating MPO as the acceptor behave in much the same way; that the orbital picture developed for the DPO compounds was valid for these compounds as well.

In this section, fluorophores containing the MPO acceptor that exhibit TADF will be designed using the previously gained insights from this thesis. The similarity of the photophysical properties of the MPO fluorophores to the analogous DPO fluorophores, shown above in compounds **26**-**31**, imply a similar orbital nature such that the same structural approaches should work for the same reasons.

4.3.1 2-Trifluoromethyl-5-phenyl-1,3,4-Oxadiaozle Containing Fluorophores

Decreasing the ΔE_{ST} from that displayed in the above compounds is necessary to develop MPO fluorophores exhibiting TADF. Incorporation of fluorine as an electronegative, monovalent atom in place of a phenyl hydrogen to decrease the energy of the CT state was demonstrated in Section 3.2.1, where it was shown to stabilize the S_1 by ca. 0.15 eV in the difluoro compound **2** and by ca. 0.23 eV for the tetrafluoro compound **3** relative to that of **1**. In compound **33**, fluorine atoms instead replace the non-conjugated methyl hydrogen atoms to yield the trifluoromethyl compound 2-(4-(9H-carbazol-9-yl)phenyl)-5-(trifluoromethyl)-1,3,4-oxadiazole. Trifluoromethyl groups have been included as electron withdrawing substituents in phosphorescent[150-153] and thermally activated delayed fluorescent[136, 154] emitters to stabilize LUMO energy and increase

acceptor strength. Here, the same outcome is expected. Compound **34** further incorporates two additional carbazolyl groups in the 3- and 5-poisitions. This should further stabilize the LUMO by acting as a σ-electron withdrawing group and while at the same time maintain the higher energy ^{3}CT states of MPO that may, depending on the energy and nature of the T_1, facilitate reverse intersystem crossing.[147]

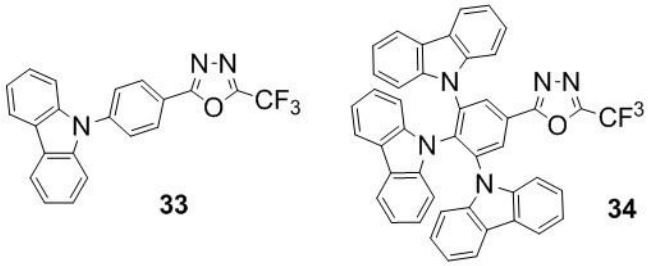

Figure 64 – Structures of trifluoromethyl containing CzMPO fluorophores studied.

Absorption and photoluminescence data were collected on the compounds in toluene solution, and the photoluminescence spectra are shown in Figure 65. The fluorescence of each compound shows the spectral line shape consistent with a charge transfer transition. The fluorescence was redshifted from λ_{max} of 371 nm in compound **26** to 405 nm in **33** by the inclusion of the trifluoromethyl group. The singlet energy was stabilized by 0.25 eV as estimated by the high energy onset of fluorescence. This stabilization is larger than was provided by four fluorine atoms attached to the bridging phenylene group (see DPO compounds **1** vs. **3**). This is attributed to fluorine, while being a strong inductively withdrawing group, acting as a weak π-electron donor on a benzene ring but acting purely as an electron acceptor when included in a aliphatic group. On the other hand, the phosphorescence spectra are effectively unchanged between the methyl and trifluoromethyl containing fluorophores, with high energy onsets found at 2.86 and

2.84 eV, respectively. This leads to a net decrease in the ΔE_{ST} from 0.73 eV in **26** to 0.50 eV in **33**, due to a stabilization of the charge-transfer state due to the electron-withdrawing trifluoromethyl group.

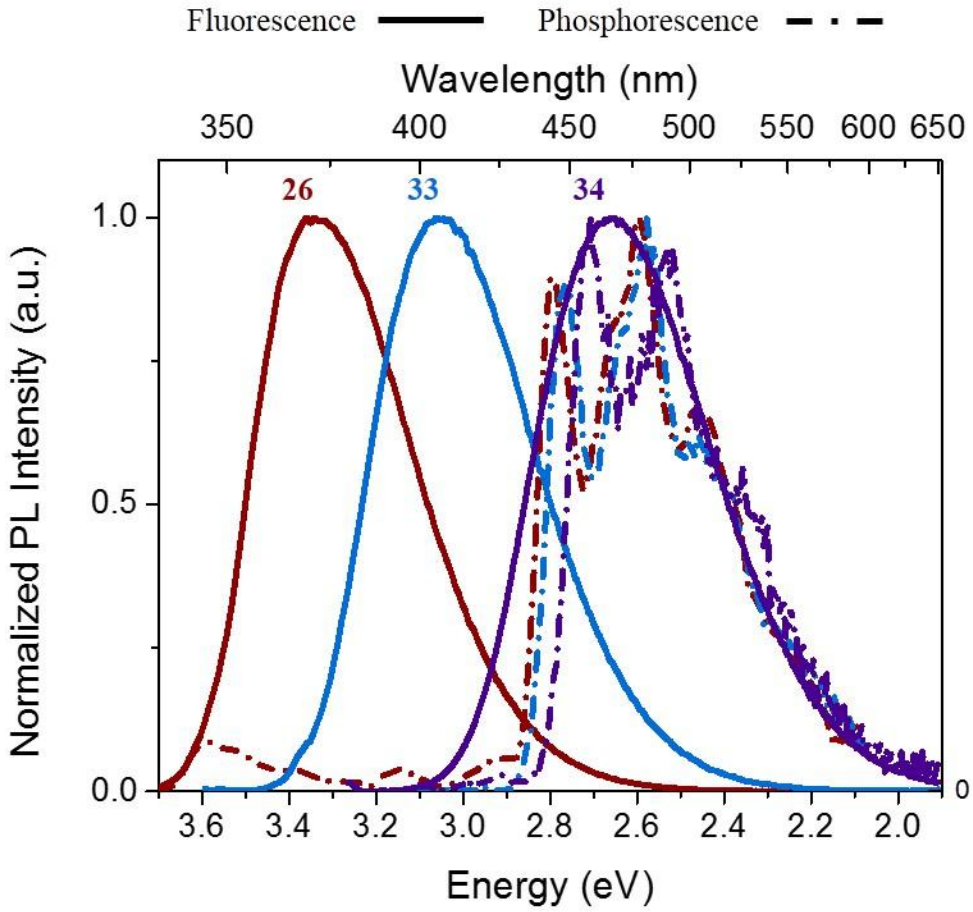

Figure 65 – Fluorescence and phosphorescence spectra of compounds 26, 33, and 34 in dilute toluene solution or toluene matric (77 K), respectively.

In compound **34**, the addition of two additional donors in the 3- and 5-positions further decreases the energy of the CT transition by stabilizing the LUMO via the σ-electron withdrawing of the electronegative nitrogen atom in addition to any increase in the HOMO energy provided by the high energy orbitals of the donor systems. As a result, the fluorescence is further red shifted from that of **33**, with a λ_{max} of 467 nm and an

estimated singlet 0.36 eV lower in energy (2.98 eV). With the phosphorescence spectrum showing that the triplet state is, again, largely unchanged, the resulting estimated ΔE_{ST} of 0.18 eV is on the high side of where thermally activated delayed fluorescence may be observed. The absorption and photoluminescence data for compounds **33** and **34** are collected in Table 14. The compounds both show significantly decreased PLQY from that of compound **26**, with the PLQY compound **33** determined to be 0.30 and 0.20 for **34**.

Table 14 – Absorption and photoluminescence properties of compounds 33 and 34 in dilute toluene solution or toluene matrix (77 K).

Compound	Absorption	Fluorescence		Phosphorescence		ΔE_{ST}
	λ_{max} /nm	λ_{max} /nm	Onset /eV	λ_{max} /nm	Onset /eV	/eV
33	286, 341	405	3.34	447, 481	2.84	0.50
34	294, 329, 343	467	2.98	458, 492	2.81	0.18

While a delayed fluorescent component was not seen in the fluorescent transient of compound **34**, the PLQY of the compound in toluene solution was seen to increase from 0.20 to 0.30 upon minimization of triplet quenching oxygen in solution. Figure 66, left, shows the increase in intensity in the steady state photoluminescence of the compound before and after sparging with nitrogen. On the right is the steady state photoluminescence and the matching photoluminescence when observed 50-100 μs after excitation with a flash lamp (data collected 100 μs after excitation but the flash lamp decay lasts ca. 45 μs). Taken together, the data suggests the fluorophore contains a triplet state that can only very slowly reverse intersystem crossing, due to the relatively the large ΔE_{ST} of 0.18 eV, but nevertheless exhibits TADF.

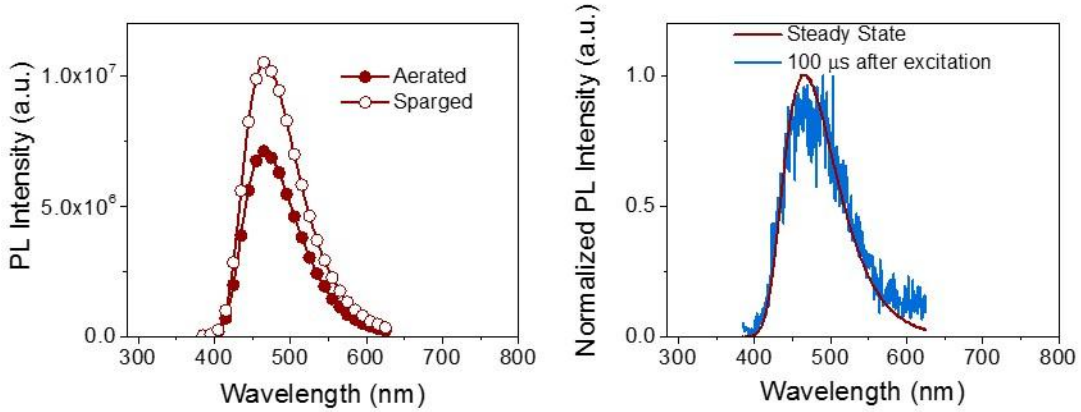

Figure 66 – Evidence of TADF in 34. (*left*) Steady-state photoluminescence before and after sparging a ca. 10^{-5} M solution in toluene with nitrogen to minimize oxygen. (*right*) Steady state photoluminescence, attributed to prompt fluorescence, and photoluminescence collected 100 µs after excitation with a flash lamp, attributed to thermally activated delayed fluorescence.

An OLED device was fabricating utilizing compound **34** as the emitter doped in a DPEPO host to evaluate the electroluminescent properties of the compound and to potentially provide additional insight into the ability of the compound to upconvert triplet excitons into emissive singlets. Device fabrication was performed by Xiaoqing Zhang, in the laboratory of Prof. Bernard Kippelen. The device structure, shown below in Figure 67(a), was as follows: glass/ITO/MoO3 (15 nm)/Poly-TriCZ (80 nm)/DPEPO: 17 (25 nm, 25 wt.%)/TP3PO(4 nm)/TPBi(50 nm)/LiF(1 nm)/Al(50 nm)/Ag(100 nm). Chemical structures of the organic materials used are shown in Section 4.5.2. The typical OLED active area was 3.0 × 3.0 mm^2. All thermal vacuum depositions were performed at pressures below 1.0×10^{-7} Torr.

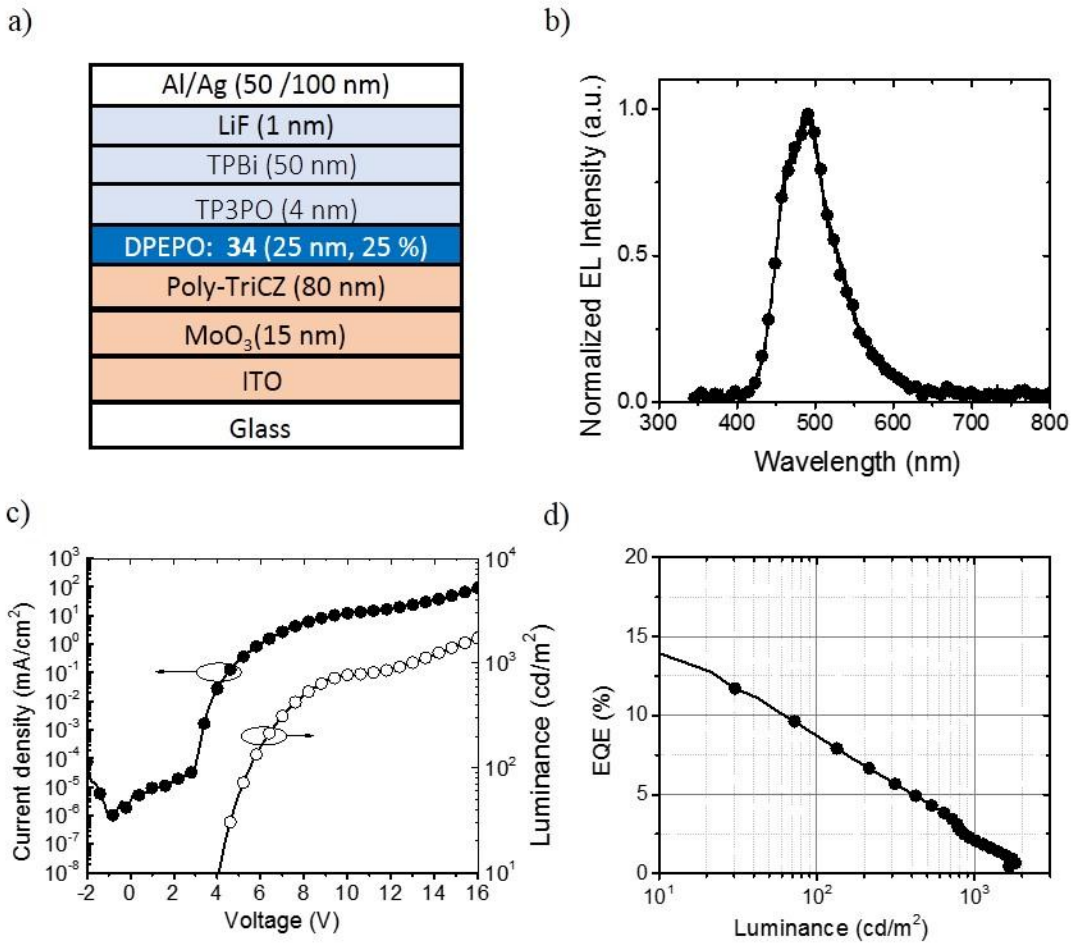

Figure 67 – (a) Device structure, (b) electroluminescence (EL) spectrum, (c) current-voltage-luminance (J-V-L) characteristics and (d) external quantum efficiency of OLED device containing 34 as the emitter.

The electroluminescence spectrum, shown in Figure 67(b), has a λ_{max} of 488 nm which is 22 nm red shifted from that of the photoluminescence and corresponds to a sky-blue emission. Current-voltage-luminance (J-V-L) characteristics are shown in Figure 67(c). The turn-on voltage for the device, defined as the voltage required at 10 cd/m^2, was 4.1 V, and displayed a power efficiency of 21.0 cd/A under a bias 5 V. The external quantum efficiency (EQE) vs. luminance is shown in Figure 67(d), and the EQE_{max} of the device was found to be 13.9%, ca. 3 times higher than the 5% theoretical limit of a purely

device employing a purely fluorescent emitter and demonstrating that triplet upconversion is occurring in the device, which is consistent to thermally activated delayed fluorescence observed for the emitter **34**. It is worth noting that the theoretical limit of a device in which triplet-triplet annihilation upconversion occurs with 100% efficiency is 12.5-18.75% (depending on outcoupling efficiency of 20-30%). The fluorescence quantum yield of compound **34** is 0.51 in a thin film (12.5 wt% in DPEPO, under a stream of nitrogen) which would preclude such efficiency values through a triplet-triplet annihilation mechanism in this device, as the EQE_{max} would be ca. 9.4% assuming no TADF. The device shows significant efficiency roll-off at increased luminance and displays an EQE of 2.1% at 1,000 cd/m_2; this is attributed to the relatively large ΔE_{ST} for the TADF emitter and resultant slow RISC.[135]

4.3.2 Pentacarbazolyl-MPO Fluorophores

The developed in CHAPTER 3 emitters that resulted in the highest efficiency OLED devices combined five carbazolyl donors with the diphenyloxadiazole acceptor. The compounds **24** and **25** exhibited sky-blue emission with estimated ΔE_{ST} of 0.12 and 0.01 eV, respectively. The low ΔE_{ST} of each compound led to fast reverse intersystem on the order of 10^4-10^5 s^{-1} and, when incorporated as the emitter in OLEDs, efficient devices with EQE_{max} values over 20%. Their MPO analogues are compounds **35** and **36**, and it was expected that they would retain the excellent TADF properties of **24** and **25** while blue shifting the emission profile of an OLED incorporating them as the emitter.

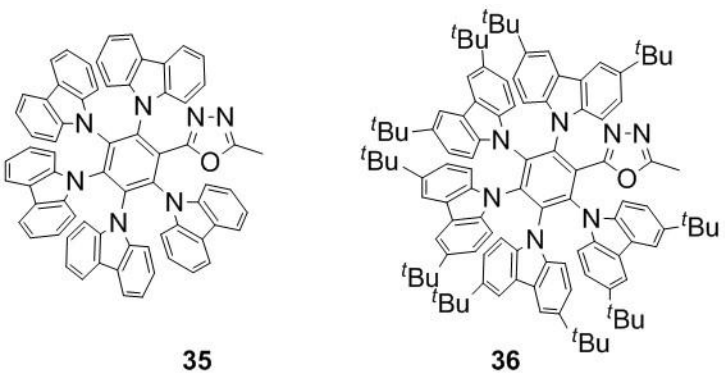

Figure 68 – Chemical structure of compounds 35 and 36.

The photoluminescent emission of the compounds is shown in Figure 69, where the structureless fluorescent emission is blue shifted from the spectra of the analogous DPO fluorophores, due to the decreased acceptor strength of the MPO moiety. The assignment of the fluorescence to an ICT state is confirmed by the sensitivity of the emission concomitant with the insensitivity of the absorption to the solvent polarity (see Section 4.5.3). Compound **35** displays a fluorescence λ_{max} of 466 nm and an onset of 2.98 eV, compared to 482 nm and 2.93 eV in the DPO compound **24**. Likewise, the *t*Cz_5MPO compound **36** displays a fluorescence λ_{max} of 485 nm and an onset of 2.90 eV, compared to 496 nm and 2.84 eV in the DPO compound **25**. The phosphorescence spectra are similar, and show onset energies of 2.86 and 2.87 eV, respectively. The spectral line shape of the phosphorescent emission, with peaks separate by 1300-1400 cm^{-1}, suggests the dominant vibronic coupling is to high-energy stretching modes, consistent with suppressed rotational relaxations due to the steric crowding around the donor and acceptor groups. Absorption and photoluminescence data are collected in Table 15.

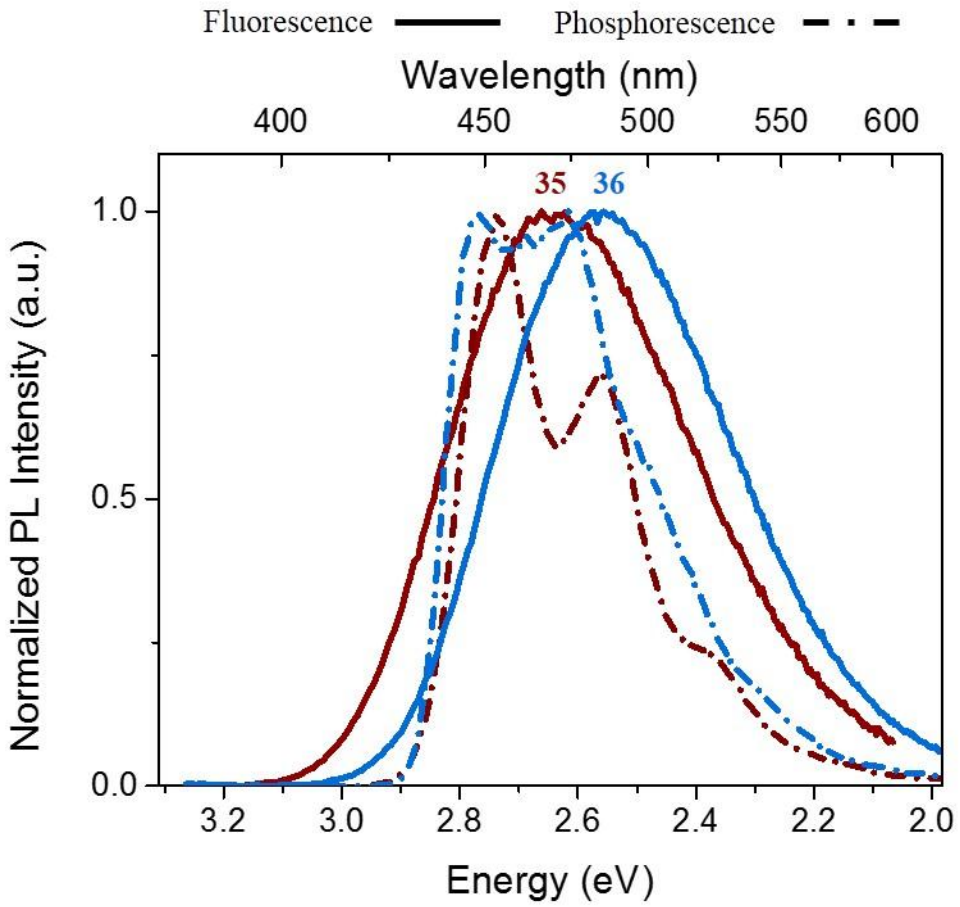

Figure 69 – Fluorescence and phosphoresce spectra of 35 and 36. Fluorescence collected in dilute toluene solution at room temperature, phosphorescence spectra collected in toluene matrix at 77 K with 500 µs delay between excitation and data collection.

Compound 35 displays an estimated ΔE_{ST} of 0.12 eV, the same as for the corresponding DPO compound despite the bluer fluorescent emission. The red shifted fluorescent emission due to the stronger *t*Cz donors of compound **36** decreases the ΔE_{ST} to ca. 0.03 eV. The transient photoluminescence (Figure 70) data in toluene solution show the biexponential decay characteristic of TADF emitters. The delayed fluorescent lifetimes of the compounds were, in fact, significantly shorter than those of the analogous

DPO compounds. The CzMPO compound **35** displayed a τ_{DF} of 11.0 μs (versus 62.8 μs for **24**), while the *t*CzMPO compound **36** had a τ_{DF} of 8.0 μs (versus 62.8 μs for **25**).

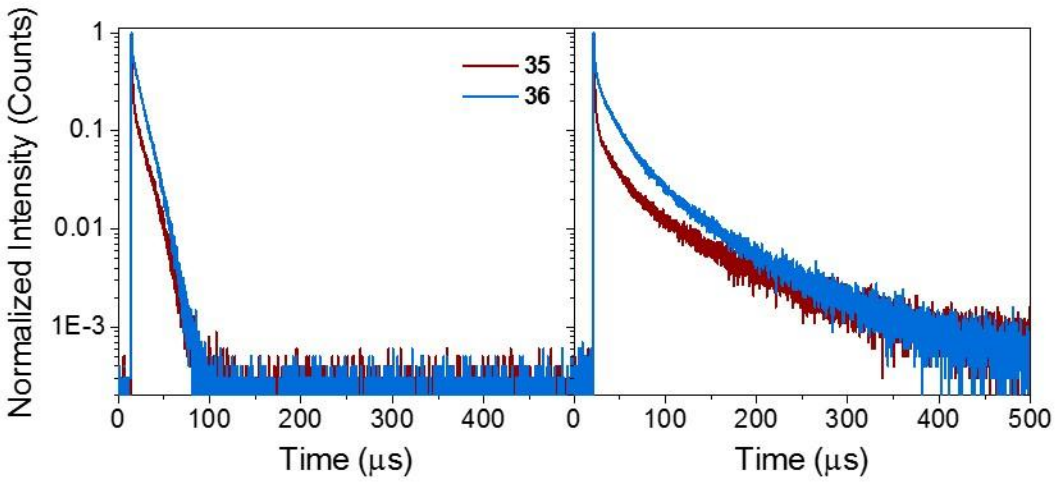

Figure 70 – Transient photoluminescence of compounds 35 and 36. (*left*) Collected in dilute toluene solution after sparging with N_2 to minimize oxygen, (*right*) Collected in thin film of fluorophore (12.5 wt.%) dispersed into DPEPO host matrix.

Absolute photoluminescent quantum yield was determined for the compounds toluene solution and is tabulated in Table 16. The prompt fluorescence in both compounds show low PLQYs of 0.08, with significantly enhanced emission upon minimization of triplet quenching oxygen by sparging with nitrogen; the total PLQY increases to 0.21 and 0.30 for **35** and **36**, respectively. The sterically crowded nature of the fluorophores prevents particularly large oscillator strengths for the CT transitions, which is reflected in the low rate of fluorescence which was calculated to be 3.5×10^6 and 3.9×10^6 s^{-1}, respectively. Overall, the prompt fluorescent properties of the compounds were very similar, with the largest difference being in the singlet energy as discussed above.

Table 15 – Tabulated absorption and photoluminescence data for compounds 35-36.

Compound	Absorption	Fluorescence		Phosphorescence		ΔE_{ST}
	λ_{max} /nm	λ_{max} /nm	Onset /eV	λ_{max} /nm	Onset /eV	/eV
35	285, 333	466	2.98	416	2.86	0.12
36	340	485	2.90	448	2.87	0.03

Turning our attention to the delayed fluorescent properties of the compounds, the effect of the decreased ΔE_{ST} in compound **36** is apparent. The Φ_{DF} is almost doubled from 0.13 to 0.22 with a concomitant decrease in the τ_{DF} of 38% from 11.0 to 8.0 μs, in comparing compound **35** to **36**. The reverse intersystem crossing rate can be calculated from Equation 27, providing the triplet yield is known. In this case, upper and lower bounds for k_{RISC} can be established by estimating the ϕ_{ISC} using Equation 28 and 29, respectively. For reference, the reverse intersystem crossing rate of a compound showing fast RISC, the archetypal TADF emitter 4CzIPN, of 2.7×10^6 s^{-1} with a ΔE_{ST} of ca 0.08 eV.[54, 155] Compound **35** shows exhibits a comparably fast reverse intersystem crossing with a k_{RISC} of ca. 2.1×10^6 s^{-1}. Compound **36**, with a ΔE_{ST} ca. 100 meV lower, undergoes reverse intersystem crossing at twice the rate, with a k_{RISC} of ca. 4.2×10^6 s^{-1}.

Finally, OLEDs fabricated using the compounds **35** and **36** as the emitter doped in a DPEPO host to were used to evaluate the electroluminescent properties of the compounds and to potentially provide additional insight into the ability of the compound to upconvert triplet excitons into emissive singlets. Device fabrication was performed by Xiaoqing Zhang, in the laboratory of Prof. Bernard Kippelen.

Table 16 – Photoluminescent quantum yields, fluorescence lifetimes, and important rates for compound 35-36 in toluene solution.

Compound	PLQY	Lifetime		k_{fl}	k_{RISC}	ΔE_{ST}
	Φ_{PF}; Φ_{DF}	τ_{PF} /ns	τ_{DF} /μs	/$10^7 s^{-1}$	/$10^4 s^{-1}$	/eV
35	0.08; 0.13	2.80	11.0	0.35	160-240	0.12
36	0.08; 0.22	3.10	8.0	0.39	370-470	0.03

The device structure, shown below in Figure 71 – (a), was as follows: glass/ITO/ MoO3 (15 nm)/Poly-TriCZ (80 nm)/DPEPO: 17 (25 nm, 25 wt.%)/TP3PO(4 nm)/ TPBi(50 nm)/LiF(1 nm)/Al(50 nm)/Ag(100 nm). Chemical structures of the organic materials used are shown in Section 4.5.2. The typical OLED active area was 3.0 × 3.0 mm^2. All thermal vacuum depositions were performed at pressures below 1.0 × 10^{-7} Torr. In contrast to the photoluminescence spectra, the EL spectra of the OLEDs fabricated using the compounds, shown in Figure 71(b), do not display emission color that is substantially blue shifted from those fabricated using the analogous DPO based emitters. The device using the emitter **35** and the device using **36** each displayed sky-blue emission with chromaticity *CIE* (*x*,*y*) values of 0.15, 0.31 and 0.15, 0.34, respectively.

The current-voltage-luminance properties of the OLEDs are shown in Figure 71 (c) and the external quantum efficiencies as a function of luminance are shown in Figure 71 (d). The OLED containing compound **35** showed an EQE_{max} of 15%, corresponding to an internal quantum efficiency of 50-75 % (based on an outcoupling efficiency of 0.20-0.30), matching well with the PLQY of a thin film of the **35** doped into a DPEPO host (12.5 wt.%, measured under a stream of nitrogen), which was determined to be 0.51, and confirming that triplet excitons are being exploited to emit light.

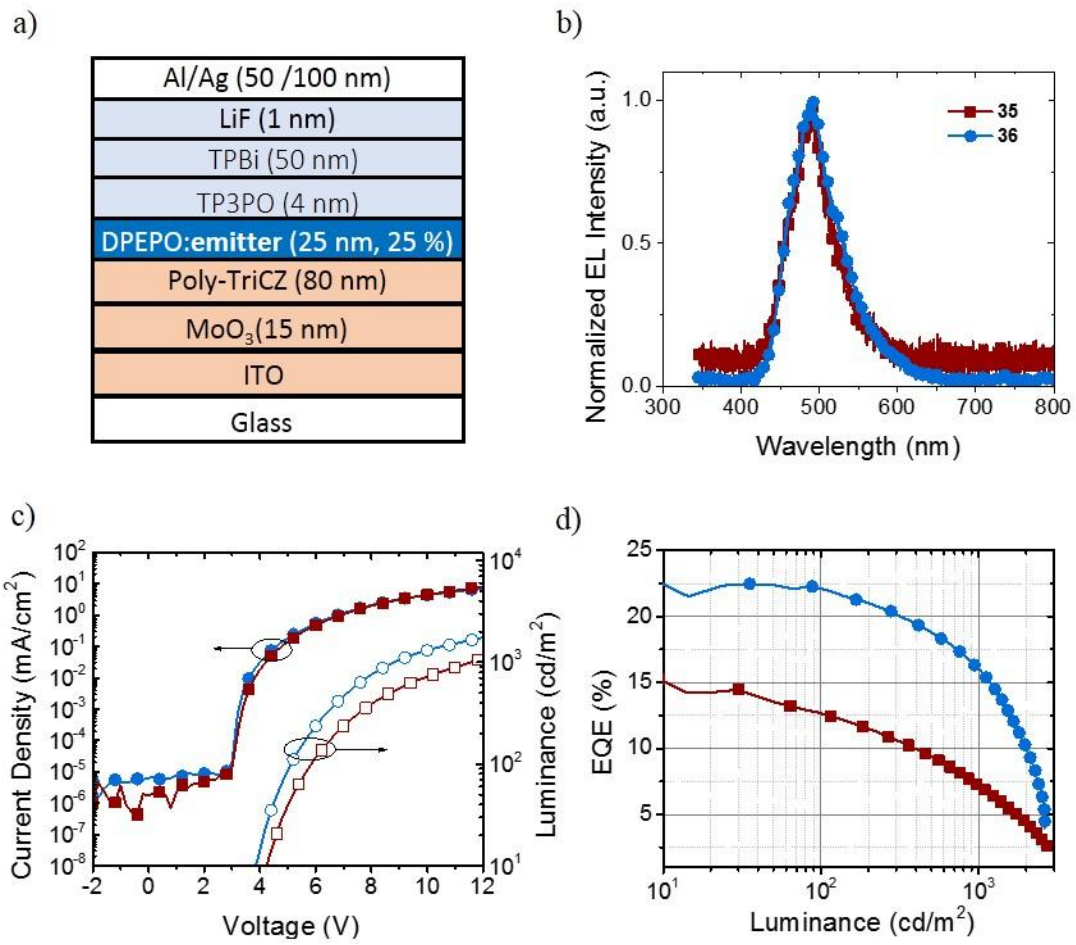

Figure 71 – (a) Device structure; (b) Electroluminescence (EL) spectra, (c) Current-voltage-luminance (J-V-L) characteristics, and (d) EQE of devices containing compounds 35 or 36 as the emitter.

Compound **36** showed a higher PLQY (0.81) when doped into a DPEPO host (12.5 wt.%) and measured under a stream of nitrogen than **35**. This is reflected in the EQE of the OLED using the device as the emitter, which displayed a maximum of 23%. This increased PLQY, and resultant increase in OLED EQE, is attributed to an increase in TADF efficiency in the compound as evidenced by the two compounds displaying an identical ϕ_{PF} but with an increased Φ_{DF} in compound **36**, as shown in Table 16, due to the high k_{RISC} in **36**. The performance of the devices is summarized in Table 17.

Table 17 – Device performance of OLEDs made using emitters 35 or 36. Turn-on voltage (V_{on}) defined as that required to reach 10 cd m^{-2}. EQE, CE and PE maximum values reported at 10, 100, and 1000 cd/m^2.

Emitter	V_{on}	*EQE at 10/100/1000 cd/m^2*	*CE at 10/100/1000 cd/m^2*	*PE at 10/100/1000 cd/m^2*	*CIE*
	V	*%*	*cd A^{-1}*	*lm W^{-1}*	*x,y*
35	4.2	15/13/7.2	30/25/14	21/13/3.7	0.15, 0.31
36	3.9	23/22/16	47/46/34	39/28/12	0.15, 0.34

Of particular note in the data obtained from the devices is the efficiency roll-off that was observed. The device in which the *t*CzMPO compound **36** was included as the emitter displayed a EQE at a luminance of 10 cd/m^{-2} of 23%, and displayed minimal efficiency roll-off at 100 cd/m^2 (EQE = 22%), and displayed a good EQE of 16% at 1,000 cd/m^2. The OLED fabricated using the analogous *t*CzDPO compound **25** displayed a higher EQE_{max}, but suffered from significantly higher efficiency roll-off as the luminance increased, and exhibited an EQE at 1,000 cd/m^2 of ca. 11%. The normalized EQE of devices made using **24**-**25** and **35**-**36** are plotted in Figure 72 in order to illustrate how the efficiency decreases as the luminance increases. In both of the MPO based emitters, the roll-off is significantly suppressed vs. the similar DPO compound. Efficiency roll-off in TADF OLEDs has been largely attributed to triplet-triplet and triplet-polaron annihilation events as the more long-lived triplet excitons build up in the device.[156] Under this assumption, the decreased τ_{DF} of the MPO compounds **35** and **36** (11.0 and 8.0 μs, respectively) when compared to the DPO based fluorophores **25** and **26** (62.8 and 30.4 μs, respectively, Section 3.3.4) results in a lower triplet concentration at similar current densities, as the triplets are more quickly converted to photons through TADF, and thus a

decreased efficiency roll-ff. This, in turn, is due to the increased k_{RISC} rates of the DPO compounds relative to their MPO analogues, of which the cause is not totally clear.

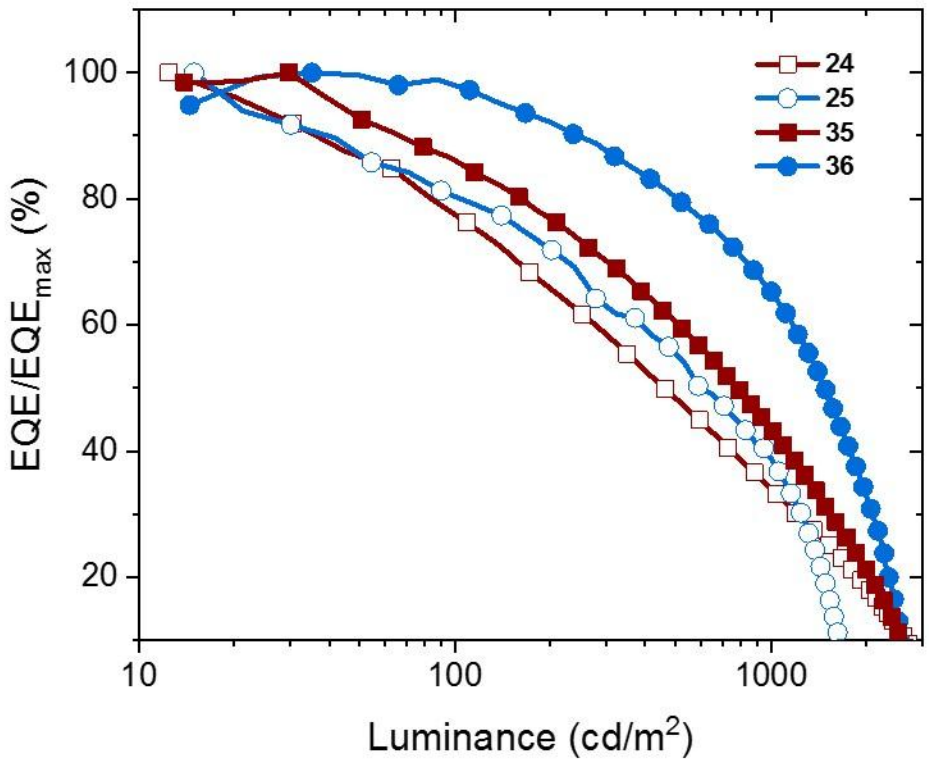

Figure 72 – External quantum efficiency, normalized to the EQE_{max} shown as a function of luminance for OLEDs fabricated using compounds 24, 25, 35, and 36 as the emitter.

4.4 Conclusions

In this chapter, fluorophores in which the electron accepting unit was 2-methyl-5-phenyl-1,3,4-oxadiazole were prepared and studied where the electron donating unit was 9-carbazole. The MPO acceptor is more difficult to reduce than the DPO moiety by ca. 0.22 eV, which is reflected in a blue shifting of the fluorescent emission of donor-acceptor compounds comprised of MPO as the acceptor when compared to similar

compounds containing DPO. Additionally, MPO contains a phosphorescent emission ca. 0.12 eV higher in energy. Simple CzMPO compounds display the same structure property relationships with regards to their singlet and triplet energies, and their fluorescent decay rates as their CzDPO analogues. Specifically, they tend to have lowest energy singlet transitions that are well characterized as an intramolecular charge-transfer while their lowest energy triplet transition instead shows characteristics of a ^{3}LE state localized on the oxadiazole moiety.

Fluorophores containing the MPO acceptor unit that exhibit TADF were designed and synthesized, including compounds **34**, **35**, and **36**. OLED devices fabricated using these compounds displayed maximum external quantum efficiencies of ca. 15% and higher, demonstrating the ability to harvest triplet excitons for luminescence, as consistent with TADF emitters. Furthermore, in similar compounds, emitters with MPO acceptor moieties displayed reverse intersystem crossing rates ca. 10 times higher than their analogous emitters that contained the DPO acceptor unit.

4.5 Experimental Details and Supplemental Data

All reagents were purchased from commercial sources and were used without further purification. ^{1}H, ^{13}C, and ^{19}F NMR spectra were recorded using a Bruker Avance IIIHD 500 instrument operating at 500 MHz, 125 MHz, and 470.4 MHz, respectively, or on a Varian Mercury Vx 400 operating at 400 MHz, 100 MHz, and 376.5 MHz, respectively. Chemical shifts are listed in parts per million (ppm) and were referenced using the residual nondeuterated solvent ^{1}H signal or the solvent ^{13}C resonance, or using an internal standard (trifluoroacetic acid, 76.55 ppm) for ^{19}F NMR. Column

chromatography was carried out using silica gel (60 Å, 40-63 µm, Sorbent) as the stationary phase. Mass spectra were measured on an Applied Biosystems 4700 Proteomics Analyzer using MALDI or a VG Instruments 70-SE using electron impact (EI) mode. UV-Vis spectra were measured using a Cary 5000 UV-Vis-NIR Spectrophotometer. Fluorescence and phosphorescence spectra, and photoluminescent transients were collected on a Jobin Yvon Fluorolog-3 equipped with a pulsed xenon lamp, photomultiplier tube (Horiba R928), and pulsed LED excitation source (NanoLED), and were excited at 330 nm. Fluorescent lifetimes were fit using DAS6 decay analysis software. Solution and solid-state absolute photoluminescence quantum yields were deter-mined on a Quantaurus-QY C11347 spectrometer. Electrochemical data was acquired using cyclic voltammetry in 0.1 M nBu$_4$N$^+$PF$_6^-$ in dry tetrahydrofuran (for reductive scans) or dichloromethane (oxidative scans) under nitrogen, using a CH Instruments 620D potentiostat, a glassy carbon working electrode, a platinum wire auxiliary electrode, and, as a pseudo-reference electrode, a silver wire anodized in 1 M aqueous potassium chloride solution. The scan rate was 50 mV s^{-1} and ferrocene was added as an internal reference. Thermogravimetric analysis was performed on a Perkin Elmer Pyris-1 TGA with a scan rate of 10 °C s^{-1}.

4.5.1 Synthetic Details

2-Methyl-5-phenyl-1,3,4-oxadiazole (**MPO**). Benzohydrazide (0.992 g, 7.29 mmol) was placed in a round bottom flask with a stir bar, which was evacuated and placed under a nitrogen atmosphere. Triethyl orthoacetate (5.0 mL, 27 mmol) was added and the reaction mixture was heated in an aluminum heat block to reflux and stirred for 24 hrs. After cooling, the excess triethyl orthoacetate was removed *in vacuo*, and the residue was

purified via column chromatography (silica gel) using dichloromethane as the eluent, followed by 5% methanol in dichloromethane. The product was obtained as a white, crystalline powder (0.471 g, 40%). ^{1}H NMR (500 MHz, $CDCl_3$): δ 8.02 (d, J = 8.5 Hz, 2H); 7.52-7.47 (m, 3H); 2.61 (s, 3H). $^{13}C\{^{1}H\}$ NMR (125 MHz, $CDCl_3$): δ 164.85; 164.58; 131.49; 128.49; 128.67; 123.94; 11.07. NMR data matches reported spectra.[157]

2,5-Diphenyl-1,3,4-oxadiazole (**DPO**): Benzohydrazide (0.992 g, 7.29 mmol) was dissolved in dry THF (25 mL) in a dry round-bottom flask under N_2 atmosphere at 0 °C in an ice bath, to which benzoyl chloride (0.85 mL, 7.34 mmol) was added dropwise. After the benzoyl chloride was added, the reaction mixture was removed from the ice bath warmed to room temperature and was stirred overnight. Then, pyridine (2 mL) was added and the reaction mixture was further stirred for 30 minutes. Water (30 mL) was added to precipitate to white a white solid, which was collected via filtration. The product (*N'*-benzoylhydrazide) was obtained as a white powder (1.39 g) and was used in the next step without further purification.

N'-Benzoylhydrazide (1.39 g, 5.79 mmol) was suspended in 10 mL phosphoryl chloride in a round-bottom flask and heated in an aluminum block at 100 °C and stirred for 6 hours. After cooling to room temperature, the reaction mixture was poured over ice and the white precipitate was collected via filtration to yield the product (1.28 g, 80%). ^{1}H NMR (500 MHz, $CDCl_3$): δ 8.16-8.14 (m, 4H), 7.56-7.54 (m, 6H). $^{13}C\{^{1}H\}$ NMR (125 MHz, $CDCl_3$): δ 164.58, 131.71, 129.07, 126.93, 123.93. HRMS (EI, *m/z*) Calcd for $C_{14}H_{10}N_2O$ $[M]^+$, 222.0793; Found 222.0801. Anal. Calcd for $(C_{14}H_{10}N_2O)_6 \cdot H_2O$: C, 74.65; H, 4.62; N, 12.44. Found: C, 74.55; H, 4.84; N, 12.28.

2-(4-(9*H*-Carbazol-9-yl)phenyl)-5-methyl-1,3,4-oxadiazole (**26**). To a solution of 2-(4-iodophenyl)-5-methyl-1,3,4-oxadiazole (5.0 g, 17.5 mmol), carbazole (3.5 g, 21 mmol), and Cu (5.0 g, 80 mol) in DMF (50 ml) was added potassium carbonate (10 g, 72 mmol) under nitrogen with stirring. The reaction mixture was heated in an aluminum heat block at 170 °C for 21 h. After cooling, the reaction mixture was filtered, and the solid residue was washed with THF. The filtrate was concentrated *in vacuo* and water was added to the remaining DMF solution. The brown precipitate was collected via filtration and washed with methanol. The solid was purified by column chromatography using dichloromethane/ethyl acetate (95:5) as the eluent. The product was recrystallized from dichloromethane/methanol and collected via filtration to yield the product as a white powder (4.9 g, 87%). ^{1}H NMR (400 MHz, $CDCl_3$): δ 8.27 (d, *J* = 8.8 Hz, 2H), 8.16 (d, *J* = 7.6 Hz, 2H), 7.74 (d, *J* = 8.8 Hz, 2H), 7.50-7.42 (m, 4H), 7.33 (t, *J* = 8.0 Hz, 2H), 2.67 (s, 3H). $^{13}C\{^{1}H\}$ NMR (100 MHz, $CDCl_3$): δ 164.26, 163.81, 140.68, 140.20, 128.31, 127.13, 126.15, 123.71, 122.49, 120.50, 120.41, 109.64, 11.16. HRMS (ESI, *m/z*): Calcd for $C_{21}H_{16}N_3O$, 326.1288 $[M]^+$; Found 326.1289. Data matches those previously reported.[132]

2-(3-(9*H*-Carbazol-9-yl)phenyl)-5-methyl-1,3,4-oxadiazole (**27**). To a solution of 2-(3-iodophenyl)-5-methyl-1,3,4-oxadiazole (5.0 g, 17.5 mmol), carbazole (3.5 g, 21 mmol), and Cu (5.0 g, 80 mol) in DMF (50 ml) was added potassium carbonate (10 g, 72 mmol) under nitrogen with stirring. The reaction mixture was heated in an aluminum heat block at 170 °C for 21 h. After cooling, the reaction mixture was filtered, and the solid residue was washed with THF. The filtrate was concentrated *in vacuo* and water was added to the remaining DMF solution. The brown precipitate was collected via filtration and washed

with methanol. The solid was purified by column chromatography using dichloromethane/ethyl acetate (95:5) as the eluent. The product was recrystallized from dichloromethane/methanol and collected via filtration to yield the product as a white powder (4.7 g, 83%). ^{1}H NMR (400 MHz, $CDCl_3$): δ 8.25 (s, 1H), 8.18-8.15 (m, 3H), 7.76-7.75 (m, 2H), 7.44 (d, *J* = 4.4 Hz, 4H), 7.36-7.29 (m, 2H), 2.63 (s, 3H). ^{13}C{^{1}H} NMR (100 MHz, $CDCl_3$): δ 164.11, 163.93, 140.49, 138.61, 130.73, 129.94, 126.11, 125.82, 125.48, 125.10, 123.53, 120.39, 120.33, 109.51, 11.10. HRMS (ESI, *m/z*): Calcd for $C_{21}H_{16}N_3O$, 326.1288 $[M]^+$; Found 326.1289. ^{13}C{^{1}H} NMR spectrum shown in Section 4.5.4.

2-(2-(9*H*-Carbazol-9-yl)phenyl)-5-methyl-1,3,4-oxadiazole (**28**). A solution of 2-(2-iodophenyl)-5-methyl-1,3,4-oxadiazole (2.5 g, 14 mmol), carbazole (2.5 g, 15 mmol), and potassium carbonate (5 g, 36 mmol) in DMSO (25 ml) was stirred under nitrogen in an aluminum heating block at 120 °C for 24 h. After cooling to room temperature, water (100 ml) was added and a white precipitate was obtained. The solid was collected by filtration, washed with water and then methanol. The crude product was purified by column chromatography using dichloromethane/hexane (1:1) as eluent. The obtained product was recrystallized from dichloromethane/methanol, and the product was obtained as a white powder by filtration (3.5 g, 77 %). ^{1}H NMR (400 MHz, $CDCl_3$): δ 8.36 (d, *J* = 8.4 Hz, 1H), 8.14 (d, *J* = 7.6 Hz, 2H), 7.78 (td, *J* = 8.0, 1.6 Hz, 1H), 7.68 (t, *J* = 7.2 Hz, 2H), 7.32 (td, *J* = 7.2, 1.6 Hz, 2H), 7.26 (td, *J* = 7.2, 1.2 Hz, 2H), 7.05 (d, *J* = 8.0 Hz, 2H), 1.84 (s, 3H). ^{13}C{^{1}H} NMR (100 MHz, $CDCl_3$): δ 163.76, 162.82, 141.30, 135.53, 132.84, 130.95, 130.45, 128.86, 126.04, 123.35, 123.19, 120.10, 119.97, 109.15, 10.14.

HRMS (ESI, *m/z*): Calcd for $C_{21}H_{16}N_3O$, 326.1288 $[M]^+$; Found 326.1289. $^{13}C\{^1H\}$ NMR spectrum shown in Section 4.5.4.

2-(4-(9'*H*-[9,3':6',9''-Terbenzo[b]indol]-9'-yl)phenyl)-5-methyl-1,3,4-oxadiazole (**29**). To a solution of 2-(4-(3,6-diiodo-9*H*-carbazol-9-yl)phenyl)-5-methyl-1,3,4-oxadiazole (0.50 g, 0.87 mmol), carbazole (1.0 g, 6.0 mmol), and Cu (1.0 g, 16 mol) in DMF (10 ml) was added potassium carbonate (3.0 g, 22 mmol) under nitrogen with stirring. The reaction mixture was heated in an aluminum heat block at 170 °C for 21 h. After cooling, the reaction mixture was filtered, and the solid residue was washed with THF. The filtrate was concentrated *in vacuo* and water was added to the remaining DMF solution. The brown precipitate was collected via filtration and washed with methanol. The solid was purified by column chromatography using dichloromethane/ethyl acetate (95:5) as the eluent. The product was recrystallized from dichloromethane/methanol and collected via filtration to yield the product as a white powder (0.46 g, 81%). ^1H NMR (400 MHz, $CDCl_3$): δ 8.40 (d, *J* = 8.8 Hz, 2H), 8.30 (d, *J* = 2.0 Hz, 2H), 8.17 (d, *J* = 7.6 Hz, 4H), 7.93 (d, *J* = 8.8 Hz, 2H), 7.74 (d, *J* = 9.2 Hz, 2H), 7.66 (dd, *J* = 8.8, 2.0 Hz, 2H), 7.43-7.39 (m, 8H), 7.31-7.27 (m, 4H), 2.71 (s, 3H). $^{13}C\{^1H\}$ NMR (100 MHz, $CDCl_3$): δ 170.74, 164.14, 164.03, 141.63, 140.04, 130.90, 128.68, 127.39, 126.47, 125.91, 124.36, 123.40, 123.16, 120.32, 119.84, 119.76, 111.23, 109.60, 11.23. HRMS (MALDI, *m/z*): Calcd for $C_{45}H_{29}N_5O$ $[M^+]$, 655.2372; Found, 655.2360. Anal. Calcd for $(C_{45}H_{29}N_5O)_2 \cdot H_2O$: C, 81.31; H, 4.55; N, 10.54. Found: C, 81.41; H, 4.56; N, 10.44.

2-(3-(9'*H*-[9,3':6',9''-Tercarbazol]-9'-yl)phenyl)-5-methyl-1,3,4-oxadiazole (**30**). To a solution of 2-(3-(3,6-diiodo-9*H*-carbazol-9-yl)phenyl)-5-methyl-1,3,4-oxadiazole (0.50 g, 0.87 mmol), carbazole (1.0 g, 6.0 mmol), and Cu (1.0 g, 16 mol) in DMF (10 ml) was

added potassium carbonate (3.0 g, 22 mmol) under nitrogen with stirring. The reaction mixture was heated in an aluminum heat block at 170 °C for 22 h. After cooling, the reaction mixture was filtered, and the solid residue was washed with THF. The filtrate was concentrated *in vacuo*, and water (75 mL) was added into the remaining DMF solution, where a brown precipitate was obtained and collected via filtration, and washed with methanol. The solid was purified by column chromatography using dichloromethane/ethyl acetate (95:5) as the eluent. The product was then recrystallized from dichloromethane/methanol and collected by filtration to yield the product as a white powder (0.40 g, 70 %). ^{1}H NMR (400 MHz, $CDCl_3$): δ 8.44 (t, *J* = 1.6 Hz, 1H), 8.31 (d, *J* = 1.6 Hz, 2H), 8.26 (dt, *J* = 7.6, 1.6 Hz, 1H), 8.17 (d, *J* = 7.6 Hz, 4H), 7.95-7.86 (m, 2H), 7.71-7.86 (m, 4H), 7.44-7.39 (m, 8H), 7.33-7.28 (m, 4H), 2.68 (s, 3H). $^{13}C\{^{1}H\}$ NMR (100 MHz, $CDCl_3$): δ 164.17, 164.02, 141.69, 140.37, 138.14, 131.18, 130.80, 130.09, 126.49, 126.31, 126.26, 125.92, 125.32, 124.22, 123.17, 120.31, 119.86, 119.75, 111.14, 109.64, 11.21. HRMS (MALDI, *m/z*): Calcd for $C_{45}H_{29}N_5O$ [M^+], 655.2372; Found, 655.2366. Anal. Calcd for $C_{45}H_{29}N_5O$: C, 82.42; H, 4.46; N, 10.68. Found: C, 82.27; H, 4.43; N, 10.77.

2-(2-(9'*H*-[9,3':6',9''-Tercarbazol]-9'-yl)phenyl)-5-methyl-1,3,4-oxadiazole (**31**). To a solution of 2-(2-(3,6-diiodo-9*H*-carbazol-9-yl)phenyl)-5-methyl-1,3,4-oxadiazole (0.50 g, 0.87 mmol), carbazole (1.0 g, 6.0 mmol), and Cu (1.0 g, 16 mol) in DMF (10 ml) was added potassium carbonate (3.0 g, 22 mmol) under nitrogen with stirring. The reaction mixture was heated in an aluminum heat block at 170 °C for 22 h. After cooling, the reaction mixture was filtered, and the solid residue was washed with THF. The filtrate was concentrated *in vacuo*, and water (75 mL) was added into the remaining DMF

solution, where a brown precipitate was obtained and collected via filtration and washed with methanol. The product was purified by silica gel column chromatography using dichloromethane as the eluent. The product was then recrystallized from dichloromethane/methanol and collected by filtration to yield the product as a white powder (0.42 g, 74 %). ^{1}H NMR (400 MHz, $CDCl_3$): δ 8.45 (dd, *J* = 8.0, 1.2 Hz, 1H), 8.28 (d, *J* = 1.6 Hz, 2H), 8.17 (d, *J* = 7.6 Hz, 4H), 7.93-7.78 (m, 3H), 7.55 (dd, *J* = 8.8, 2.0 Hz, 2H), 7.43-7.36 (m, 8H), 7.31-7.27 (m, 6H), 2.19 (s, 3H). ^{13}C{^{1}H} NMR (125 MHz, $CDCl_3$): δ 163.86, 162.56, 141.66, 141.19, 134.97, 133.20, 131.13, 130.69, 130.47, 129.69, 126.35, 125.89, 124.06, 123.49, 123.15, 120.31, 119.73, 119.62, 110.85, 109.58, 10.62. HRMS (MALDI, *m/z*): Calcd for $C_{45}H_{29}N_5O$ [M^+], 655.2372; Found, 655.2405. Anal. Calcd for $(C_{45}H_{29}N_5O)_4 \cdot H_2O$: C, 81.86; H, 4.50; N, 10.61. Found: C, 81.91; H, 4.61; N, 10.52.

2-(4-(9*H*-Carbazol-9-yl)phenyl)-5-(trifluoromethyl)-1,3,4-oxadiazole (**33**). To a flask containing 9-(4-(1H-tetrazol-5-yl)phenyl)-9*H*-carbazole) (250 mg, 0.804 mmol) suspended in dichloromethane (5 mL) was added trifluoroacetic anhydride (0.11 mL, 0.80 mmol) in dichloromethane (0.5 mL) dropwise with stirring. Upon completion of N_2 evolution, the reaction mixture was neutralized with saturated sodium bicarbonate until pH 9 was reached. The reaction mixture was extracted with diethyl ether (3 times) and the combined organic layers were dried over anhydrous magnesium sulfate, decanted, and concentrated *in vacuo*. The product was passed through a silica gel plug using diethyl ether:hexanes (1:1) as the eluent, and the was concentrated *in vacuo* to yield the product as a white powder (237 mg, 79 %). ^{1}H NMR (500 MHz, $CDCl_3$): δ 8.38 (d, *J* = 8.5 Hz, 2H), 8.16 (d, *J* = 8.0 Hz, 2H), 7.84 (d, *J* = 8.5 Hz, 2H), 7.51 (d, *J* = 8.5 Hz, 2H), 7.45 (t, *J*

= 7.0 Hz, 2H), 7.35 (t, *J* = 7.0 Hz, 2H). $^{13}C\{^{1}H\}$ NMR (125 MHz, $CDCl_3$): δ 165.93, 142.33, 140.02, 129.29, 127.29, 126.32, 123.69, 120.86, 120.56, 120.38. HRMS (EI, *m/*z): Calcd for $C_{21}H_{12}F_3N_3O$ [M^+] 379.0932; Found 379.0926. Anal. Calcd for $C_{21}H_{12}F_3N_3O$: C, 66.49; H, 3.19; N, 11.08. Found: C, 66.60; H, 3.38; N, 11.06.

2-(3,4,5-Tri(9*H*-carbazol-9-yl)phenyl)-5-(trifluoromethyl)-1,3,4-oxadiazole (**34**). To a flask containing 9,9',9''-(5(1*H*-tetrazol-5-yl)benzenetris(9*H*-carbazole) (50 mg, 0.078 mmol) suspended in dichloromethane (2 mL) was added trifluoroacetic anhydride (0.014 mL, 0.1 mmol) dropwise with stirring. Upon completion of N_2 evolution, the reaction mixture was neutralized with saturated sodium bicarbonate until pH 9 was reached. The reaction mixture was extracted with ether (3 times) and the combined organic layers were dried over anhydrous magnesium sulfate, decanted, and concentrated *in vacuo*. The product was obtained as a yellow powder (14 mg, 28%). ^{1}H NMR (500 MHz, $CDCl_3$): δ8.68 (s, 2H), 7.80 (d, *J* = 7.0 Hz, 4H), 7.38 (d, *J* = 7.5 Hz, 2H), 7.21 (d, *J* = 8.0 Hz, 4H), 7.01-7.02 (m, 8H), 6.92 (d, *J* = 8.0 Hz, 2H), 6.79 (t, *J* = 7.0 Hz, 2H), 6.65 (t, *J* = 8.0 Hz, 2H). $^{13}C\{^{1}H\}$ NMR (125 MHz, $CDCl_3$): δ164.77, 139.31, 138.64, 137.71, 135.70, 128.18, 125.64, 124.79, 123.77, 123.73, 123.07, 120.64, 120.38, 120.09, 119.47, 109.78, 109.43. HRMS (EI, *m/*z): Calcd for $C_{45}H_{26}N_5OF_3$ [M^+] 709.2089; Found 709.2078. Anal Calcd. for $C_{45}H_{26}F_3N_5O$: C, 76.15; H, 3.69; N, 9.87. Found: C, 75.97; H, 3.66; N, 9.88.

2-Methyl-5-(2,3,4,5-penta(9*H*-carbazol-9-yl)phenyl)-1,3,4-oxadiazole (**35**). In a round-bottom flask, 2-methyl-5-(perfluorophenyl)-1,3,4-oxadiazole (1.0 g, 4.0 mmol), carbazole (3.6 g, 22 mmol), and potassium carbonate were dissolved in DMSO (20 mL) in a round-bottom flask and stirred in an aluminum heating block at 70 °C for 1 h, 100 °C for 2 h, 120 °C for 14 h, and 160 °C for 4 h. After cooling to room temperature, water was added

(150 mL) and the precipitate was collected via filtration and washed with water and then methanol. The crude product was purified via column chromatography using dichloromethane as the eluent. The product was recrystallized from dichloromethane/methanol, and filtration yielded the product as a pale-yellow powder (3.8 g, 97%). ^{1}H NMR (400 MHz, $CDCl_3$): δ 7.69-7.67 (m, 4H), 7.37 (d, *J* = 7.6 Hz, 4H), 7.29 (d, *J* = 9.5 Hz, 2H), 7.21-7.17 (m, 10H), 7.00-6.94 (m, 8H), 6.77 (t, *J* = 7.2 Hz, 4H), 6.73 (d, *J* = 8.0 Hz, 2H), 6.65 (t, *J* = 7.2 Hz, 4H), 6.60 (t, *J* = 7.2 Hz, 2H), 1.53 (s, 3H). ^{13}C{^{1}H} NMR (100 MHz, $CDCl_3$): δ 163.29, 158.10, 139.60, 139.42, 138.23, 137.89, 137.84, 136.73, 127.33, 125.38, 124.37, 124.24, 123.70, 123.58, 120.55, 120.31, 120.23, 119.89, 119.42, 119.33, 110.68, 110.46, 109.52, 9.79. HRMS (MALDI, *m/z*): Calcd for $C_{69}H_{43}N_7O$, 985.3529 [M^+]; Found 985.3541. Anal. Calcd for $C_{69}H_{43}N_7O$: C, 84.04; H, 4.40; N, 9.94. Found: C, 84.05; H, 4.36; N, 9.93.

2-Methyl-5-(2,3,4,5-pentakis(3,6-di-tert-butyl-9*H*-carbazol-9-yl)phenyl)-1,3,4-oxadiazole (**36**). A solution of 2-methyl-5-(perfluorophenyl)-1,3,4-oxadiazole (0.70 g, 2.8 mmol), 3,6-di-*tert*-butylcarbazole (4.5 g, 16 mmol), and potassium carbonate (10 g, 72 mmol) in DMSO (20 ml) in a round-bottom flask and stirred under nitrogen in an aluminum heating block at 120 °C for 15 h and then at 160 °C for 9 h. After cooling to room temperature, water (100 ml) was added and a pale-yellow precipitate was obtained. The solid was collected by filtration, washed with water and then methanol. The crude product was purified by column chromatography using dichloromethane/hexane (1:1) as eluent. The obtained product was recrystallized from dichloromethane/methanol, and the product was obtained as a pale-yellow powder by filtration (3.5 g, 81 %). ^{1}H NMR (400 MHz, $CDCl_3$): δ 7.56 (s, 4H), 7.23 (s, 6H), 7.00 (d, *J* = 8.8 Hz, 2H), 6.92 (s, 8H), 6.86 (d,

J = 8.4 Hz, 4H), 6.59 (td, *J* = 8.0, 2.0 Hz, 6H), 1.60 (s, 3H), 1.29 (s, 36H), 1.22 (s, 36H), 1.18 (s, 18H). $^{13}C\{^{1}H\}$ NMR (100 MHz, $CDCl_3$): δ 163.11, 158.80, 142.75, 142.67, 142.45, 140.41, 138.15, 137.63, 137.33, 137.27, 136.70, 127.12, 124.25, 124.06, 123.87, 122.73, 122.10, 121.90, 115.44, 114.95, 114.81, 110.32, 110.03, 109.17, 34.43, 34.25, 31.85, 31.78, 31.73, 9.99. HRMS (MALDI, *m/z*): Calcd for $C_{109}H_{123}N_7O$, 1545.9789 $[M]^+$; Found: 1545.9797. Anal. Calcd for $C_{109}H_{123}N_7O$: C, 84.62; H, 8.01; N, 6.34. Found: C, 84.35; H, 7.90; N, 6.25.

4.5.2 Chemical Structures of Organic Materials Used in OLED Devices

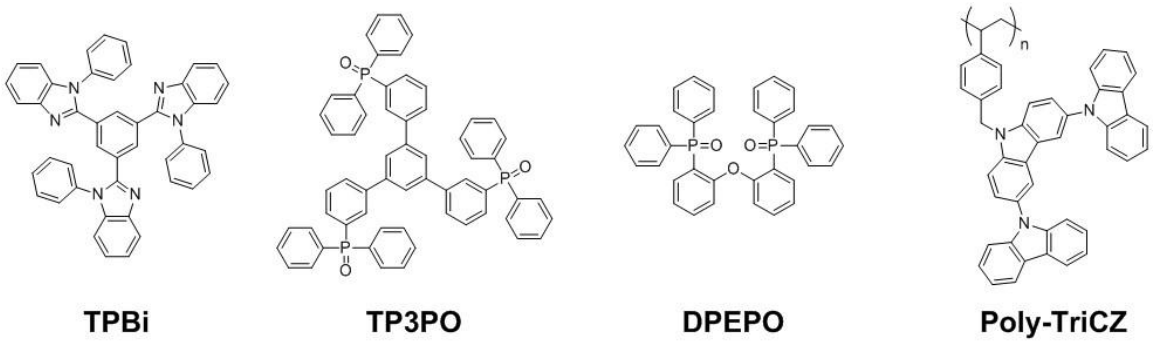

4.5.3 Solvent Dependence of Absorption and Emission Spectra

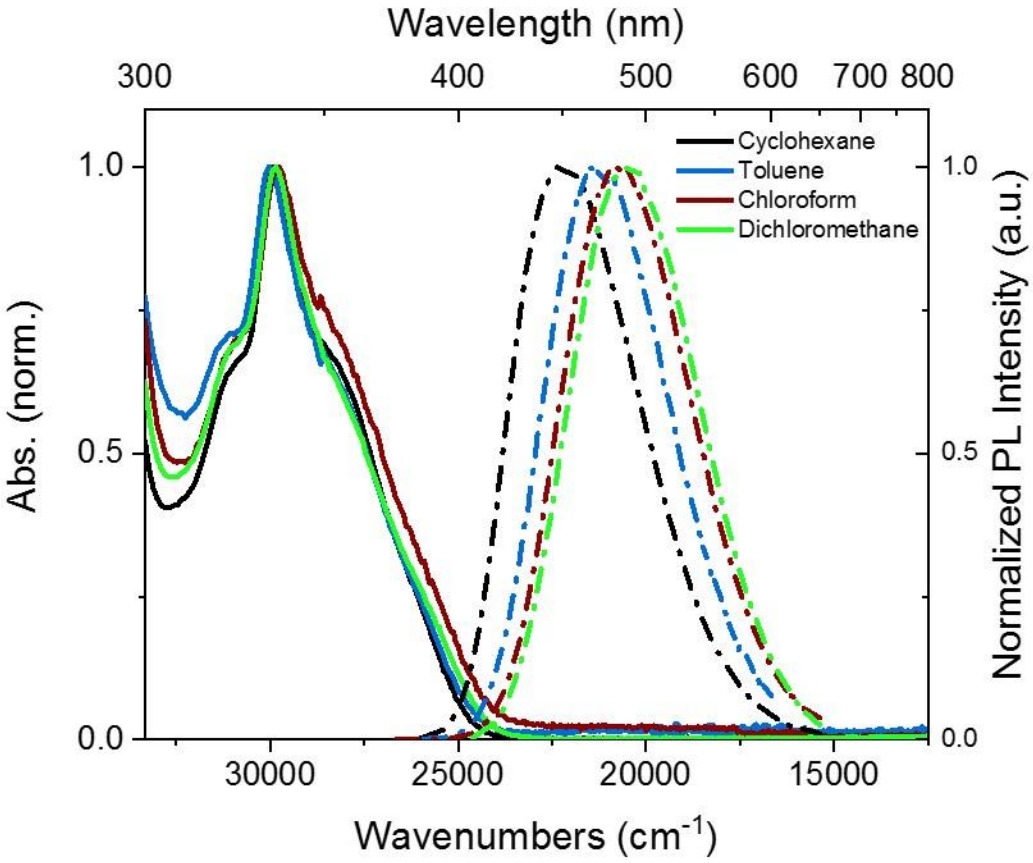

Figure 73 – Solvent dependence of absorption (solid line) and fluorescence (dashed line) of compound 35 in a variety of solvents.

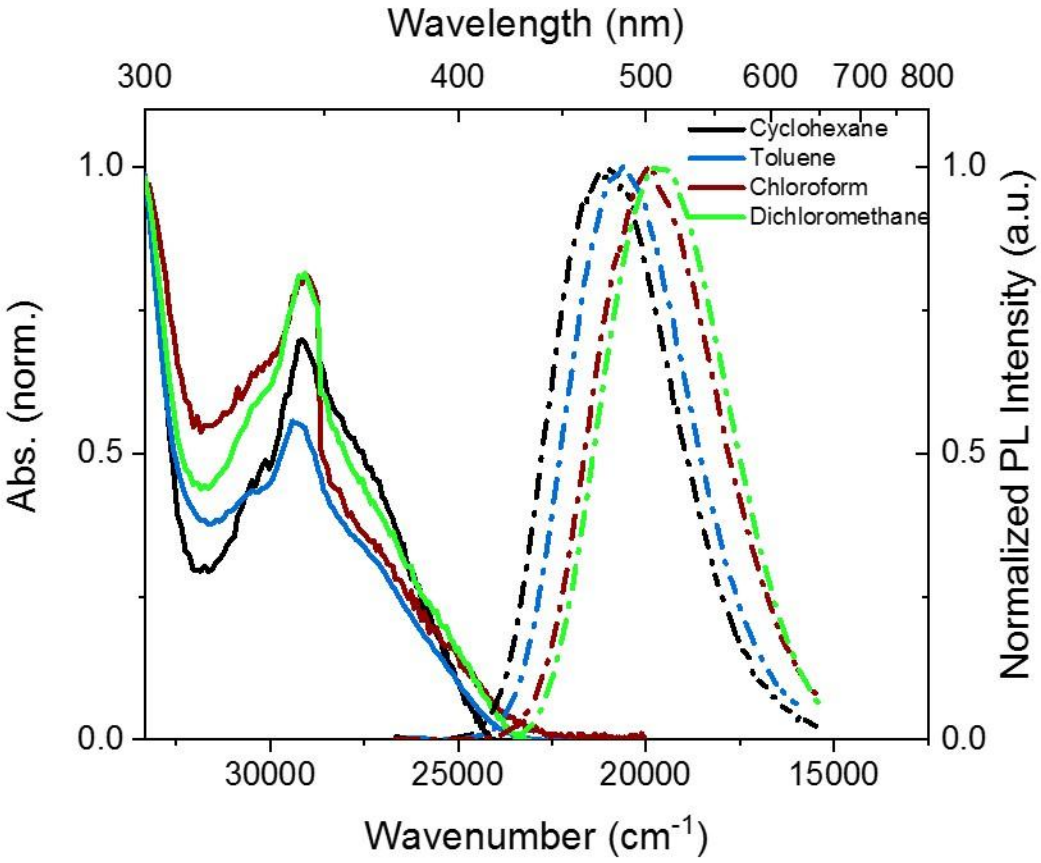

Figure 74 – Solvent dependence of absorption (solid line) and fluorescence (dashed line) of compound 36 in a variety of solvents.

4.5.4 $^{13}C\{^{1}H\}$ NMR Spectra

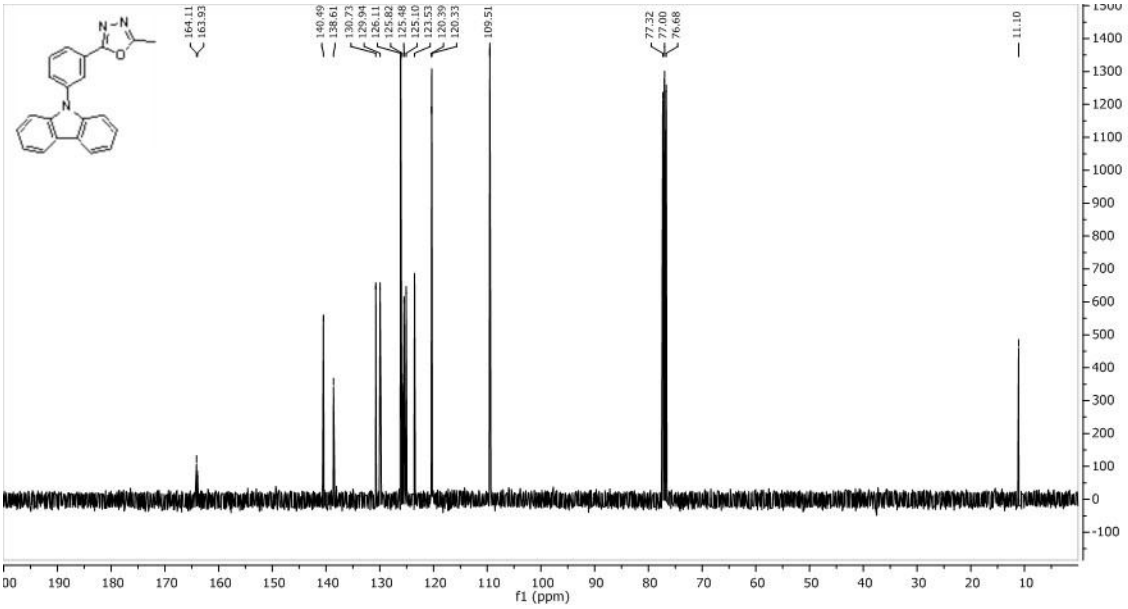

Figure 75 – $^{13}C\{^{1}H\}$ NMR spectrum (100 MHz, $CDCl_3$) of compound 27.

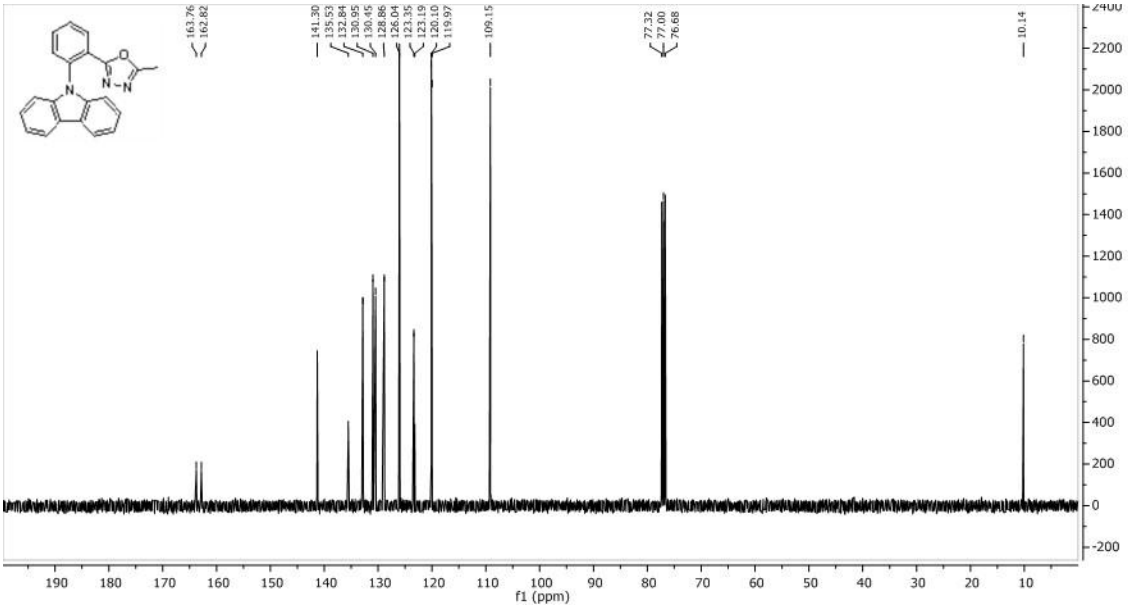

Figure 76 – $^{13}C\{^{1}H\}$ NMR spectrum (100 MHz, $CDCl_3$) of compound 28.

CHAPTER 5. CONCLUSIONS AND OUTLOOK

In this thesis, donor-acceptor compounds comprised of 9*H*-carbazole and 1,3,4-oxadiazole were systematically designed and synthesized in order to investigate the effects of donor strength, acceptor strength, and chemical connectivity and regioisomerism on photophysical properties relevant to the design of TADF emitters for third-generation organic light-emitting diodes. The compounds were synthesized, and their absorption, fluorescent and phosphorescent properties, including transient photoluminescence and photoluminescent quantum yields, were collected. The data were used to determine the energy of the singlet and triplet states to estimate the vital singlet-triplet gap for TADF fluorophores, the ΔE_{ST}, and fluorescent decay rates that must be high enough to compete with the nonradiative decay pathways that reduce OLED efficiency. The structure-property relationships between the molecules and the photophysical properties were used to draw conclusions about the nature and energy of the relevant orbitals involved in the singlet and triplet transitions. Insight from these conclusions were exploited to develop strategies for designing new fluorophores with small ΔE_{ST} values that display TADF.

5.1 Summary of Results

The singlet state of all D-A compounds studied were found to be a HOMO-LUMO, intramolecular charge-transfer transition, where, in the excited state, the hole resides on the carbazole donor moiety and the electron on the oxadiazole acceptor. By simply increasing the electron-pushing ability of the donor or the electron pulling ability of the acceptor, the ICT state was stabilized, and the energy of the singlet was decreased. The

significant, monotonic decrease in the energy of the singlet is shown in Figure 77 with a series of the synthesized fluorophores with increasing donor/acceptor strengths. The triplet state of the compounds did not show the same sensitivity to donor or acceptor strength, however, which is inconsistent with the transition arising from the same set of orbitals.

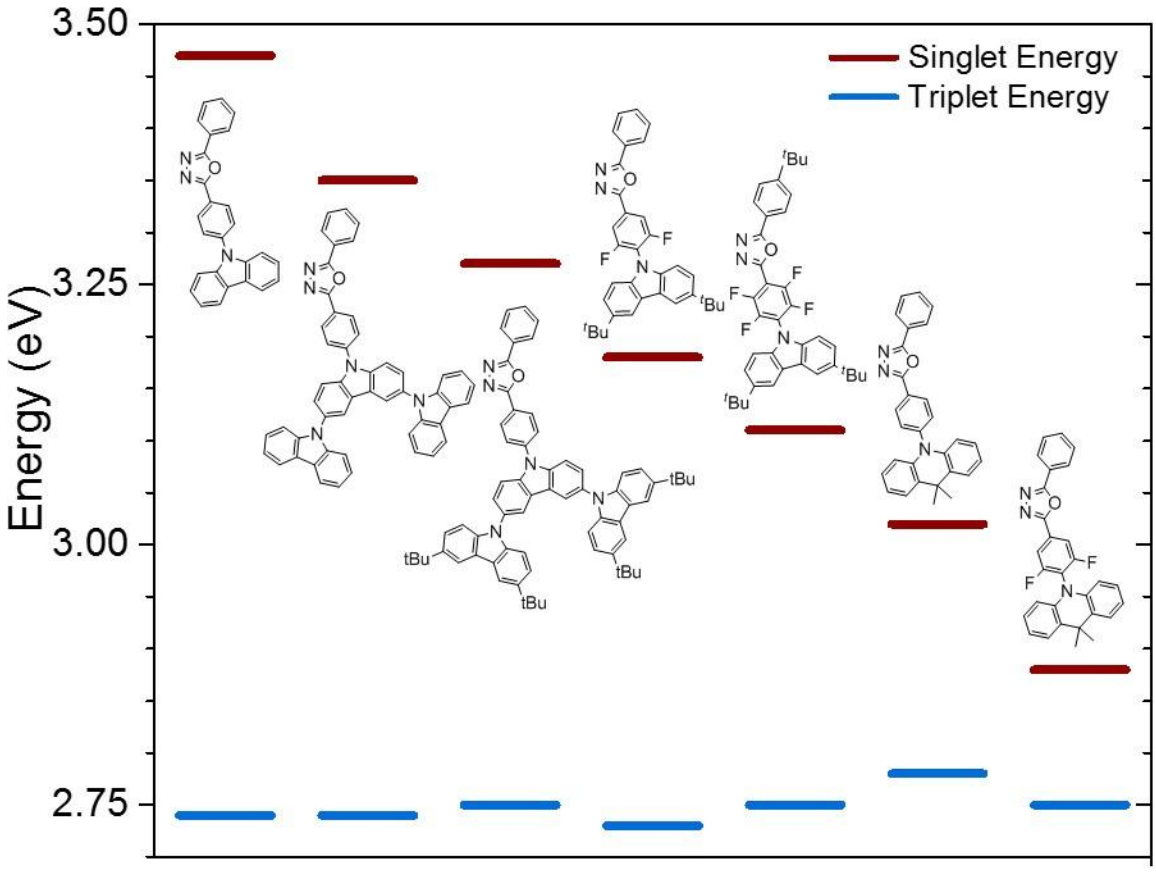

Figure 77 – Energy of the singlet (red) and triplet (blue) in compounds with increasing donor and/or acceptor strength, estimated from spectral onsets in dilute toluene solution.

Unlike the singlet exciton, the triplet state of the compounds was shown to be consistent with a localized excitation in which the hole and the electron both reside largely on the 2,5-diphenyl-1,3,4-oxadiazole moiety. This explains the insensitivity of the

emission to the energy of the ICT transition energy, and moreover explains the observations made with regards to the phosphorescence as a function of connectivity between the donor and the acceptor – as the bulky heteroaromatic groups crowded one another out of plane of the bridging phenylene, the conjugation across the DPO group is decreased and the energy of the transition was increased.

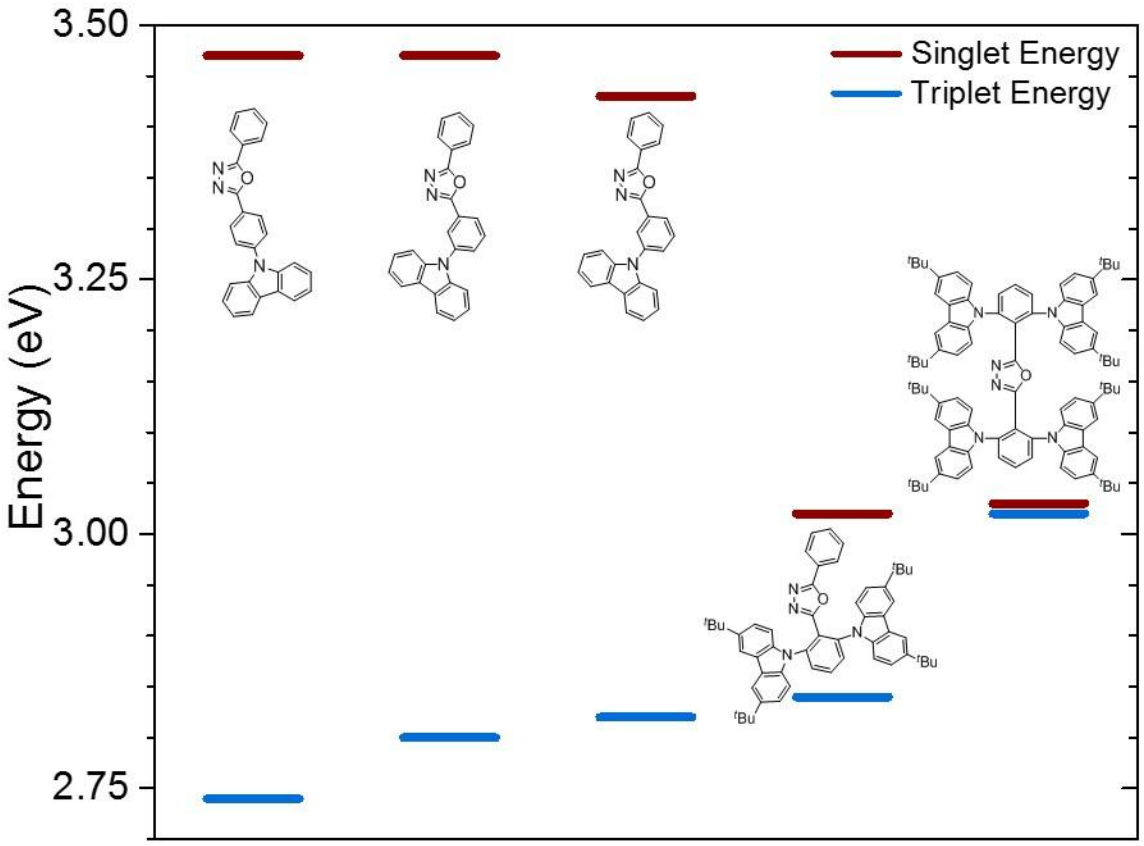

Figure 78 – Energy of the singlet (red) and triplet (blue) of compounds with increasing crowding between the donor and acceptor moieties, estimated from spectral onsets in dilute toluene solution.

By understanding the distinct orbital nature of the singlet and triplet states, compounds were designed with minimized ΔE_{ST} values, leading to TADF. One strategy involved selectively pushing the ICT down in energy until it approached that of the ^{3}LE,

and led to highly efficient OLED devices when incorporated as the emitter into the EML.[158] Another strategy, which allowed for true-blue emission color from the emitter concomitant with TADF, was pushing the ^{3}LE up in energy as far as possible with crowding around the oxadiazole functionality, although this showed little success when incorporated into an OLED device due to low fluorescent efficiency. By combining the two approaches, highly efficient devices with emission more blue than possible when only pushing the ICT state were achieved.[147] Furthermore, this work showed the importance of substitution pattern in controlling the energy of the singlet – where substitution of a donor through the electronegative N atom of carbazole in the 2-, 4- and 6-positions have an outsized affect versus substitution in the 3-, and 5-positions. Substitution in the 3- and 5-positions were, instead, shown to have more of an effect on the triplet emission and RISC.

With an understanding of the relevant orbitals involved in the S_1 and T_1 states, the acceptor moiety was modified by replacement of one of the conjugated phenyl groups with a methyl group. The energy of the ^{3}LE localized on the oxadiazole was increased as a result, allowing for lower values of ΔE_{ST} in compounds that emitted at shorter wavelengths, leading to TADF fluorophores with a more blue emission than was obtained in the comparable DPO fluorophores. Fabrication of OLEDs with lower *x* values in their *CIE* (x,y) color space while maintaining high EQE were the result. Analogous compounds displaying TADF but incorporating the MPO acceptor in place of the DPO acceptor had the unexpected side effect of showing significantly increased RISC rates ca. 10× times higher (see for example compound **24** vs. **35**). In total, a range of emission

colors from blue-green to true-blue were obtained in the OLEDs utilizing the emitters reported here.

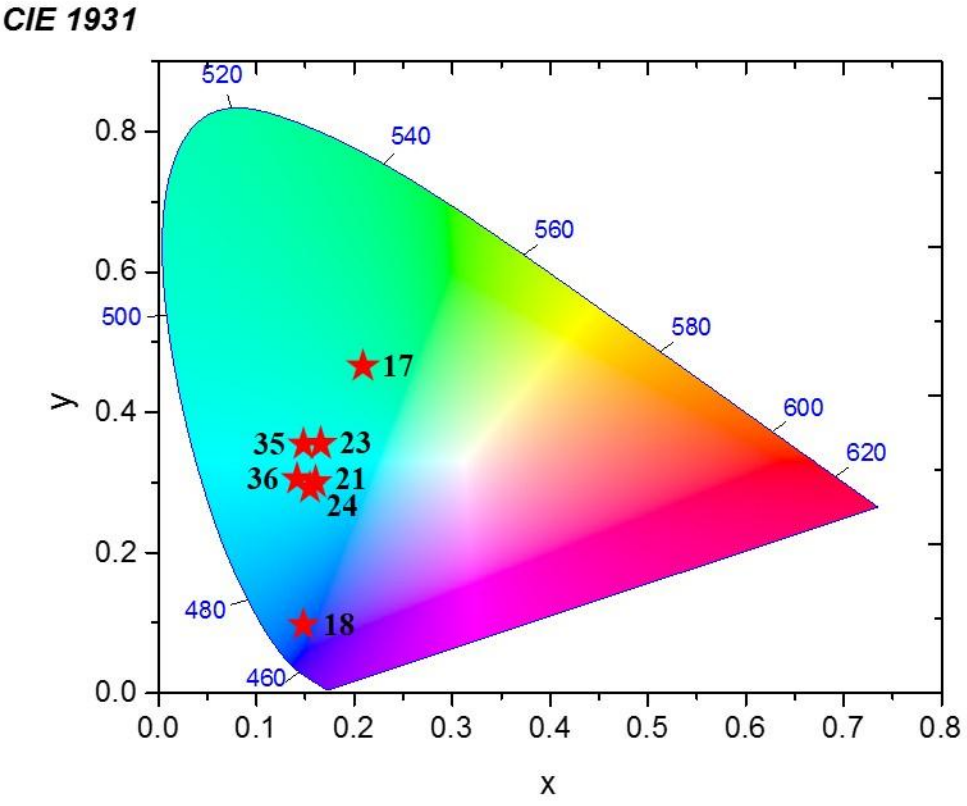

Figure 79 – Chromaticity of some OLED devices reported in this work, using the noted compound as the emitter.

5.2 Outlook

The results obtained in this work present promising strategies for modifying fluorophores to improve and fine tune their properties for use as emitters in OLEDs. To increase efficiency and decrease efficiency roll-off, RISC rates must be maximized by decreasing ΔE_{ST}, while also increasing the SOC between the triplet and singlet manifold.

While the design of increasingly blue emitters requires an increase in the energy of the fluorescent emission while maintaining a small ΔE_{ST}.

5.2.1 Increasing RISC Rates

As was seen in Section 3.3.4, the electronic interactions of substituents in different positions leads to donors in certain positions affecting distinct properties of the molecule by differing amounts. Specifically, donor substitution in the 2-, 4-, and 6-positions relative to the electron acceptor contribute electronically to the intramolecular charge transfer over those in the 3- and 5-positions. As was shown in Sections 3.3.1 and 4.2.1, singlet CT states involving charge transitions from the 3-or 5-positions are found at higher energies than the charge transitions from the 2-, 4-, or 6- positions, and it follows that their triplet counterparts are, too. This may be taken advantage of to design systems with increased SOC between the singlet and triplet state.[79]

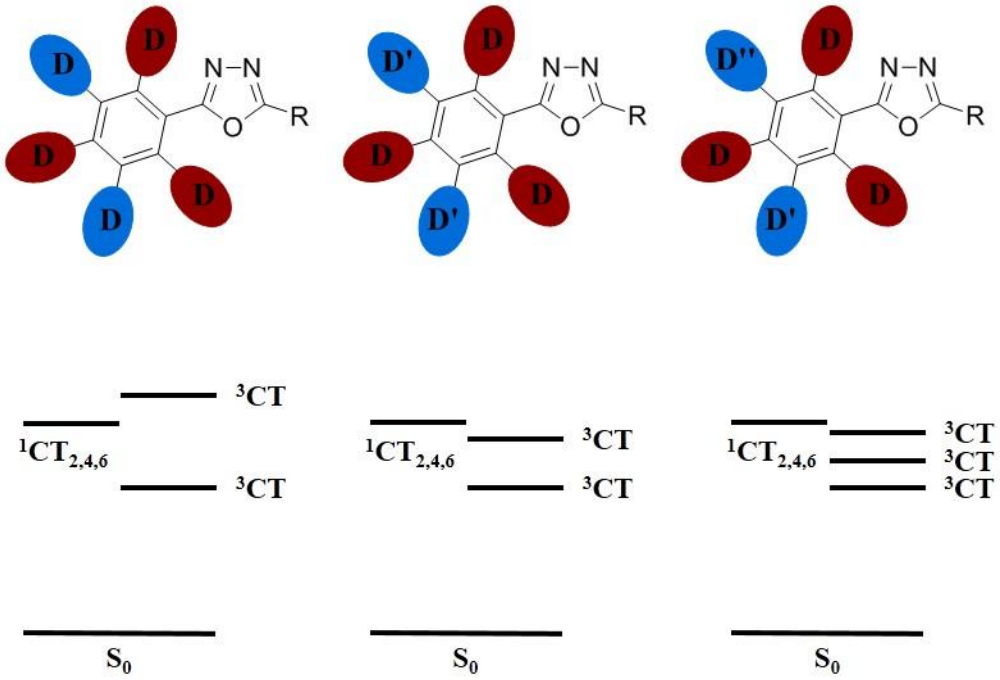

Figure 80 – Hypothetical D-A compounds (*top*) and energy level diagrams of the singlet and triplet CT sates (*bottom)* in which the donors in the 3- and 5-positions are replaced with one (*middle*) or two (*right*) different donor substituents, stronger than the donors in the 2-, 4-, and 6-positions. S_n and ^{3}LE states omitted.

By adding stronger donors to the 3- and 5-positions of the fluorophore, an additional, distinct ^{3}CT state with different symmetry but similar energy to the T_1 state may be obtained that, with proper donor selection, may be very similar in energy with the T_1 state, leading to vibronic coupling between the two states and resulting in enhanced SOC between the singlet and triplet state. Furthermore, using mixed donors in the 3- and 5-positions may lead to additional ^{3}CT states that are vibronically accessible by the T_1 state (Figure 80), and by packing more triplet states into a small energetic range SOC may be further increased through the second order coupling.[80] This strategy, using secondary donors[144] or acceptors[159] to control the energy of higher energy triplet states has very recently come under investigation. A systematic study including systems composed of

mixed donors, mixed acceptors, or both mixed donors and acceptors remains to be explored.

A further, in depth study of what is leading to the increased RISC rates in the MPO based fluorophores reported here compared to their DPO analogues remains to be performed. As the estimated ΔE_{ST} of similar compounds containing DPO and MPO acceptors are unchanged, an increase in the SOC is very likely where the increased RISC rate arise from. Naively, the increased singlet and triplet energies will decrease the energy gap between the ^{3}LE localized on the carbazole donors and the relevant, T_1 state to which it can vibronically couple. However, triplet energy of isolated *N*-phenylcarbazole molecule is approximately 3.05 eV,[106] which is high enough that the triplet of, for example, the MPO fluorophores **35** and **36** (2.86, 2.87 eV, respectively, determined in toluene matrix) may not be expected to couple significantly to the state. However, the assumption is that the energy of the ^{3}LE in an isolated fluorophore is representative of the energy of the same group incorporated into a D-A compound, where the rest of the molecule is electronically coupled and may be expected to preferentially stabilize the HOMO or LUMO of the group. Indeed, the phosphorescence spectrum of the isolated DPO and MPO compounds displayed estimated triplet energies ca. 0.40 eV higher than those of the MPO and DPO compounds where the triplet state was assigned to the ^{3}LE of the acceptor, suggesting this is not an effective way to estimate the energy of the ^{3}LE state. A further study as to precisely what is leading to this increased RISC rate is required to say more.

5.2.2 Blue Emission with High Rates of Fluorescence and RISC

The other primary challenge remaining unsolved is a blue shifting of the fluorescent emission while maintaining sufficiently high fluorescence and RISC rates to allow for efficient OLED devices. The simplest approach is to use acceptor groups with higher ^{3}LE energy than displayed in DPO or MPO. Such an approach, however, is well known and understood by the community. The lessons learned in this work, specifically the ^{3}LE energy tuning, should prove applicable to a range of other acceptor moieties with comparable structures (eg: diphenyl sulfone, 2,4,6-triphenyl-1,3,5-triazine, etc.) for obtaining higher energy triplets than otherwise might be expected in such D-A structures. In this work, fluorophores were developed that displayed true-blue emission, with *CIE* (x,y) of 0.15, 0.09 but with very low k_{fl}. Other fluorophores were developed with very high k_{RISC} on the order of 10^6 s^{-1}, but with sky blue to blue-green emission. Development of a compound or set of compounds that display both qualities remains to be done.

The problem with designing high triplet energy, blue TADF emitters lies in the stabilization of the orbitals involved in the triplet configuration to spread out on the D-A compound in such a way as to maximize the overlap and stabilize the state through the exchange integral.[78] This makes it more and more difficult to contain the hole and electron wavefunction of the triplet state to the donor and acceptor moieties, respectively, as the HOMO-LUMO gap increases. Compound **19** demonstrated a method for breaking the conjugation between the donor and acceptor sufficiently to prevent the triplet energy from dropping below the energy of the ICT state despite the blue fluorescent emission, and a high triplet energy of 3.02 was achieved in the compound. However, to use such an

approach in an efficient OLED requires an increased fluorescent decay rate that was not obtained in **19**.

Substitution of donors in the *para* position were shown to result in compounds with high fluorescent decay rates in Sections 3.2.2 and 4.2.2, and compounds combining the 2,2',6,6' donor substitution of compound **19** with donor substitution in the 4 and/or 4' positions might be expected to behave the same way. The LUMO of the DPO compounds spread over the oxadiazole and the two benzene rings, which is disrupted by the twisting in compound **19**. The HOMO of the D-A compounds should be well confined to the donor moieties, and when the donor groups are as twisted out of the plane of the bridging phenylene the oscillator strength can be expected to be suppressed, and the rate of fluorescence along with it (according to the Strickler-Berg relationship). By inclusion of less sterically constrained donors on the 4 and/or 4' positions, the LUMO that leaks out onto the phenylene should have an increased overlap with the orbitals well described by the HOMO of the donor, and an enhanced fluorescence decay may be observed.

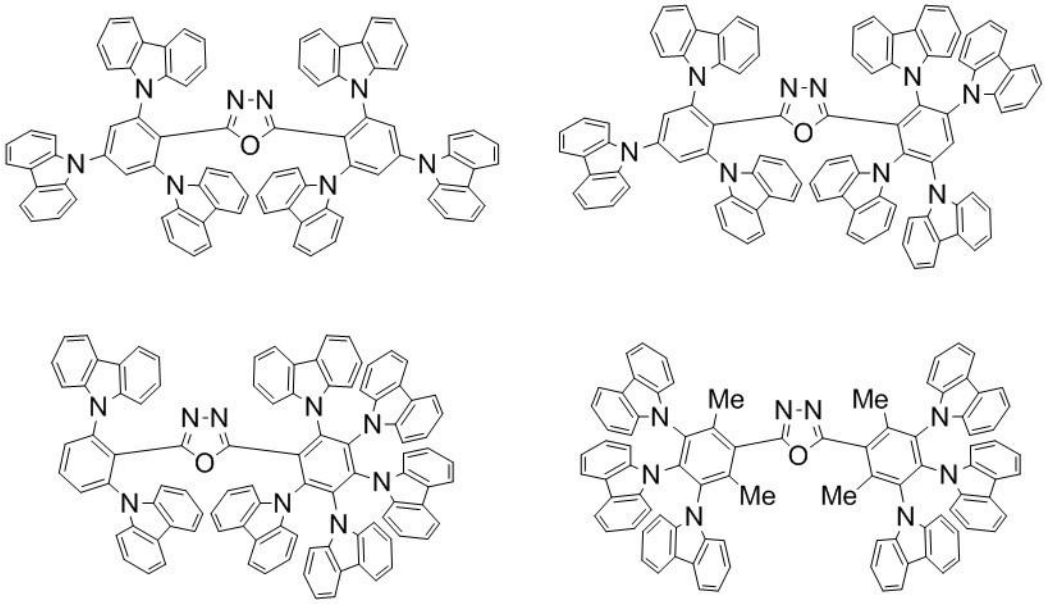

Figure 81 – Proposed structures to combine high triplet energy with increased fluorescent decay rate.

Specific structures that may result in enhanced fluorescent decay rates while maintaining high triplet energy are proposed in Figure 81. One may simply consider substituting Cz donors into the 4 and 4' positions for the reasons just discussed. However, the increased RISC rates observed with substitution of donors in the 3- and 5-positions in Section 3.3.4 suggest that inclusion of donors in those positions is also important for maximizing RISC rates. From a purely practical perspective, a compound in which every position available for substitution, such that ten carbazoles are attached to the DPO (molecular weight of 1873.7 g mol^{-1}), would very likely be too massive for the sublimation performed to ensure highly pure fluorophores prior to incorporation into an OLED. Instead, the donors could be split up such that there is substitution in each of the 3-, 4-, and 5-positions of one ring, but not both, to obtain a lighter molecule.

Finally, the groups in the 2,2’ and 4,4’ positions might not have to be donor moieties at all. Substitution of any bulky group, including a simple methyl as shown in Figure 81, may very well provide the same disruption across the DPO moiety responsible for increasing the ^{3}LE energy while allowing donor substitution in each 3,3’,4,4’, and 5,5’ position. Potentially, this could allow for dihedral angle tuning between the bridging phenyl groups and the central oxadiazole by inclusion of more or less bulky R groups, providing one more way to fine tune the photophysical properties of the compound.

REFERENCES

1. Mertens, R., *The OLED Handbook: A Guide to OLED Technology, Industry & Market*. 2018 ed.; Ron Mertens: 2018.

2. Reineke, S.; Lindner, F.; Schwartz, G.; Seidler, N.; Walzer, K.; Lüssem, B.; Leo, K., White organic light-emitting diodes with fluorescent tube efficiency. *Nature* **2009,** *459*, 234.

3. Pope, M.; Kallmann, H. P.; Magnante, P., Electroluminescence in Organic Crystals. *J. Chem. Phys.* **1963,** *38* (8), 2042-2043.

4. Scott, J. C.; Malliaras, G. G., Charge injection and recombination at the metal–organic interface. *Chem. Phys. Lett.* **1999,** *299* (2), 115-119.

5. Crowell, C. R.; Sze, S. M., Current transport in metal-semiconductor barriers. *Solid-State Electron.* **1966,** *9* (11), 1035-1048.

6. Emtage, P. R.; O'Dwyer, J. J., Richardson-Schottky Effect in Insulators. *Phys. Rev. Lett.* **1966,** *16* (9), 356-358.

7. Yang, Y.; Westerweele, E.; Zhang, C.; Smith, P.; Heeger, A. J., Enhanced performance of polymer light-emitting diodes using high-surface area polyaniline network electrodes. *J. Appl. Phys.* **1995,** *77* (2), 694-698.

8. Silveira, W. R.; Marohn, J. A., Microscopic View of Charge Injection in an Organic Semiconductor. *Phys. Rev. Lett.* **2004,** *93* (11), 116104.

9. Slyke, S. A. V.; Chen, C. H.; Tang, C. W., Organic electroluminescent devices with improved stability. *Appl. Phys. Lett.* **1996,** *69* (15), 2160-2162.

10. Marcus, R. A., On the Theory of Oxidation-Reduction Reactions Involving Electron Transfer. I. *J. Chem. Phys.* **1956,** *24* (5), 966-978.

11. C.D., D.; P.R.L., M., Organic Thin Film Transistors for Large Area Electronics. *Adv. Mater.* **2002,** *14* (2), 99-117.

12. Ma, D.; Wang, G.; Hu, Y.; Zhang, Y.; Wang, L.; Jing, X.; Wang, F.; Lee, C. S.; Lee, S. T., A dinuclear aluminum 8-hydroxyquinoline complex with high electron mobility for organic light-emitting diodes. *Appl. Phys. Lett.* **2003,** *82* (8), 1296-1298.

13. Aziz, H.; Popovic, Z. D., Study of organic light emitting devices with a 5,6,11,12-tetraphenylnaphthacene (rubrene)-doped hole transport layer. *Appl. Phys. Lett.* **2002,** *80* (12), 2180-2182.

14. Hosokawa, C.; Tokailin, H.; Higashi, H.; Kusumoto, T., Transient behavior of organic thin film electroluminescence. *Appl. Phys. Lett.* **1992,** *60* (10), 1220-1222.

15. Pope, M.; Swenberg, C. E., *Electronic Processes in Organic Crystals and Polymers*. Oxford Press: Oxford, U.K., 1999.

16. Crone, B. K.; Campbell, I. H.; Davids, P. S.; Smith, D. L.; Neef, C. J.; Ferraris, J. P., Device physics of single layer organic light-emitting diodes. *J. Appl. Phys.* **1999,** *86* (10), 5767-5774.

17. Adamovich, V.; Brooks, J.; Tamayo, A.; Alexander, A. M.; Djurovich, P. I.; D'Andrade, B. W.; Adachi, C.; Forrest, S. R.; Thompson, M. E., High efficiency single dopant white electrophosphorescent light emitting diodes. *New J. Chem.* **2002,** *26* (9), 1171-1178.

18. Adamovich, V. I.; Cordero, S. R.; Djurovich, P. I.; Tamayo, A.; Thompson, M. E.; D'Andrade, B. W.; Forrest, S. R., New charge-carrier blocking materials for high efficiency OLEDs. *Org. Electron.* **2003,** *4* (2), 77-87.

19. Frenkel, J., On the Transformation of Light into Heat in Solids. II. *Phys. Rev.* **1931,** *37* (10), 1276-1294.

20. Baldo, M. A.; O'Brien, D. F.; Thompson, M. E.; Forrest, S. R., Excitonic singlet-triplet ratio in a semiconducting organic thin film. *Physical Review B* **1999,** *60* (20), 14422-14428.

21. Kasha, M., Characterization of Electronic Transitions in Complex Molecules. *Discuss Faraday Soc.* **1950**, 14-19.

22. Forster, T., 10th Spiers Memorial Lecture. Transfer mechanisms of electronic excitation. *Faraday Discuss* **1959,** *27* (0), 7-17.

23. Dexter, D. L., A Theory of Sensitized Luminescence in Solids. *J. Chem. Phys.* **1953,** *21* (5), 836-850.

24. Strickler, S. J.; Berg, R. A., Relationship between Absorption Intensity and Fluorescence Lifetime of Molecules. *J. Chem. Phys.* **1962,** *37* (4), 814-822.

25. Vogel, M.; Rettig, W.; Sens, R.; Drexhage, K. H., Structural relaxation of rhodamine dyes with different N-substitution patterns: A study of fluorescence decay times and quantum yields. *Chem. Phys. Lett.* **1988,** *147* (5), 452-460.

26. Boguta, A.; Wróbel, D., Fluorescein and Phenolphthalein—Correlation of Fluorescence and Photoelectric Properties. *J. Fluoresc.* **2001,** *11* (2), 129-137.

27. Beljonne, D.; Shuai, Z.; Pourtois, G.; Bredas, J. L., Spin−Orbit Coupling and Intersystem Crossing in Conjugated Polymers: A Configuration Interaction Description. *J. Phys. Chem. A* **2001,** *105* (15), 3899-3907.

28. McClure, D. S., Triplet-Singlet Transitions in Organic Molecules. Lifetime Measurements of the Triplet State. *J. Chem. Phys.* **1949,** *17* (10), 905-913.

29. Zhang, X.-F.; Zhang, J.; Liu, L., Fluorescence Properties of Twenty Fluorescein Derivatives: Lifetime, Quantum Yield, Absorption and Emission Spectra. *J. Fluoresc.* **2014,** *24* (3), 819-826.

30. El-Sayed, M. A., Spin—Orbit Coupling and the Radiationless Processes in Nitrogen Heterocyclics. *J. Chem. Phys.* **1963,** *38* (12), 2834-2838.

31. Lamola, A. A.; Hammond, G. S., Mechanisms of Photochemical Reactions in Solution. XXXIII. Intersystem Crossing Efficiencies. *J. Chem. Phys.* **1965,** *43* (6), 2129-2135.

32. Rothberg, L. J.; Lovinger, A. J., Status of and prospects for organic electroluminescence. *J. Mater. Res.* **2011,** *11* (12), 3174-3187.

33. Salaneck, W.; R.; Brédas, J.-L., The metal-on-polymer interface in polymer light emitting diodes. *Adv. Mater.* **1996,** *8* (1), 48-52.

34. Chance, R. R.; Prock, A.; Silbey, R., Comments on the classical theory of energy transfer. *J. Chem. Phys.* **1975,** *62* (6), 2245-2253.

35. Kim, J.-S.; Ho, P. K. H.; Greenham, N. C.; Friend, R. H., Electroluminescence emission pattern of organic light-emitting diodes: Implications for device efficiency calculations. *J. Appl. Phys.* **2000,** *88* (2), 1073-1081.

36. Lin, T.-A.; Chatterjee, T.; Tsai, W.-L.; Lee, W.-K.; Wu, M.-J.; Jiao, M.; Pan, K.-C.; Yi, C.-L.; Chung, C.-L.; Wong, K.-T.; Wu, C.-C., Sky-Blue Organic Light Emitting Diode with 37% External Quantum Efficiency Using Thermally Activated Delayed Fluorescence from Spiroacridine-Triazine Hybrid. *Adv. Mater.* **2016,** *28* (32), 6976-6983.

37. S.R., F.; D.D.C., B.; M.E., T., Measuring the Efficiency of Organic Light-Emitting Devices. *Adv. Mater.* **2003,** *15* (13), 1043-1048.

38. Shi-Jian, S.; Eisuke, G.; Hisahiro, S.; Junji, K., Highly Efficient Organic Blue-and White-Light-Emitting Devices Having a Carrier- and Exciton-Confining Structure for Reduced Efficiency Roll-Off. *Adv. Mater.* **2008,** *20* (21), 4189-4194.

39. Helfrich, W.; Schneider, W. G., Recombination Radiation in Anthracene Crystals. *Phys. Rev. Lett.* **1965,** *14* (7), 229-231.

40. Tang, C. W.; VanSlyke, S. A., Organic electroluminescent diodes. *Appl. Phys. Lett.* **1987,** *51* (12), 913-915.

41. Adachi, C.; Tokito, S.; Tsutsui, T.; Saito, S., Organic Electroluminescent Device with a Three-Layer Structure. *Jpn. J. Appl. Phys.* **1988,** *27*, L713-L715.

42. Tang, C. W.; VanSlyke, S. A.; Chen, C. H., Electroluminescence of doped organic thin films. *J. Appl. Phys.* **1989,** *65* (9), 3610-3616.

43. César, P.-B.; Shin-ya, T.; Go, N.; A., M. V.; Pavel, A., High-Efficiency Tris(8-hydroxyquinoline)aluminum (Alq3) Complexes for Organic White-Light-Emitting Diodes and Solid-State Lighting. *Chem. Eur. J.* **2011,** *17* (33), 9076-9082.

44. Baldo, M. A.; O'Brien, D. F.; You, Y.; Shoustikov, A.; Sibley, S.; Thompson, M. E.; Forrest, S. R., Highly efficient phosphorescent emission from organic electroluminescent devices. *Nature* **1998,** *395* (6698), 151-154.

45. Baryshnikov, G.; Minaev, B.; Ågren, H., Theory and Calculation of the Phosphorescence Phenomenon. *Chem. Rev.* **2017,** *117* (9), 6500-6537.

46. Ponterini, G.; Serpone, N.; Bergkamp, M. A.; Netzel, T. L., Comparison of Radiationless Decay Processes in Osmium and Platinum Porphyrins. *J. Am. Chem. Soc.* **1983,** *105* (14), 4639-4645.

47. Papkovsky, D. B., New oxygen sensors and their application to biosensing. *Sens. Actuators, B* **1995,** *29* (1), 213-218.

48. Adachi, C.; Baldo, M. A.; Thompson, M. E.; Forrest, S. R., Nearly 100% internal phosphorescence efficiency in an organic light-emitting device. *J. Appl. Phys.* **2001,** *90* (10), 5048-5051.

49. Giebink, N. C.; D'Andrade, B. W.; Weaver, M. S.; Mackenzie, P. B.; Brown, J. J.; Thompson, M. E.; Forrest, S. R., Intrinsic luminance loss in phosphorescent small-molecule organic light emitting devices due to bimolecular annihilation reactions. *J. Appl. Phys.* **2008,** *103* (4), 044509.

50. Sivasubramaniam, V.; Brodkorb, F.; Hanning, S.; Loebl, H. P.; van Elsbergen, V.; Boerner, H.; Scherf, U.; Kreyenschmidt, M., Fluorine cleavage of the light blue heteroleptic triplet emitter FIrpic. *J. Fluorine Chem.* **2009,** *130* (7), 640-649.

51. Chi, Y.; Chou, P.-T., Transition-metal phosphors with cyclometalating ligands: fundamentals and applications. *Chem. Soc. Rev.* **2010,** *39* (2), 638-655.

52. Endo, A.; Ogasawara, M.; Takahashi, A.; Yokoyama, D.; Kato, Y.; Adachi, C., Thermally Activated Delayed Fluorescence from Sn4+–Porphyrin Complexes and Their Application to Organic Light Emitting Diodes — A Novel Mechanism for Electroluminescence. *Adv. Mater.* **2009,** *21* (47), 4802-4806.

53. Endo, A.; Sato, K.; Yoshimura, K.; Kai, T.; Kawada, A.; Miyazaki, H.; Adachi, C., Efficient up-conversion of triplet excitons into a singlet state and its application for organic light emitting diodes. *Appl. Phys. Lett.* **2011,** *98* (8), 083302.

54. Uoyama, H.; Goushi, K.; Shizu, K.; Nomura, H.; Adachi, C., Highly efficient organic light-emitting diodes from delayed fluorescence. *Nature* **2012,** *492*, 234.

55. Goushi, K.; Yoshida, K.; Sato, K.; Adachi, C., Organic light-emitting diodes employing efficient reverse intersystem crossing for triplet-to-singlet state conversion. *Nat. Photonics* **2012,** *6*, 253.

56. Yersin, H.; Leitl, M. J.; Czerwieniec, R. In *TADF for singlet harvesting: next generation OLED materials based on brightly green and blue emitting Cu(I) and Ag(I) compounds*, SPIE Organic Photonics + Electronics, SPIE: 2014; p 11.

57. Yang, Z.; Mao, Z.; Xie, Z.; Zhang, Y.; Liu, S.; Zhao, J.; Xu, J.; Chi, Z.; Aldred, M. P., Recent advances in organic thermally activated delayed fluorescence materials. *Chem. Soc. Rev.* **2017,** *46* (3), 915-1016.

58. Perrin, F., La Fluorescence Des Solutions: Induction Moleculaire. - Polarisation et durée d'émission. – Photochimie. *Ann. Phys.* **1929,** *10* (12), 169-275.

59. Parker, C. A.; Hatchard, C. G., Triplet-singlet emission in fluid solutions. Phosphorescence of eosin. *Trans. Faraday Soc.* **1961,** *57* (0), 1894-1904.

60. Grewer, C.; Brauer, H.-D., Mechanism of the Triplet-State Quenching by Molecular Oxygen in Solution. *J. Phys. Chem.* **1994,** *98* (16), 4230-4235.

61. Monkman, A. P., Singlet Generation from Triplet Excitons in Fluorescent Organic Light-Emitting Diodes. *ISRN Mater. Sci.* **2013,** *2013*, 19.

62. Hanaoka, K.; Kikuchi, K.; Kobayashi, S.; Nagano, T., Time-Resolved Long-Lived Luminescence Imaging Method Employing Luminescent Lanthanide Probes with a New Microscopy System. *J. Am. Chem. Soc.* **2007,** *129* (44), 13502-13509.

63. Xiong, X.; Song, F.; Wang, J.; Zhang, Y.; Xue, Y.; Sun, L.; Jiang, N.; Gao, P.; Tian, L.; Peng, X., Thermally Activated Delayed Fluorescence of Fluorescein Derivative for Time-Resolved and Confocal Fluorescence Imaging. *J. Am. Chem. Soc.* **2014,** *136* (27), 9590-9597.

64. Wu, T. C.; Congreve, D. N.; Baldo, M. A., Solid state photon upconversion utilizing thermally activated delayed fluorescence molecules as triplet sensitizer. *Appl. Phys. Lett.* **2015,** *107* (3), 031103.

65. Peng, J.; Guo, X.; Jiang, X.; Zhao, D.; Ma, Y., Developing efficient heavy-atom-free photosensitizers applicable to TTA upconversion in polymer films. *Chem. Sci.* **2016,** *7* (2), 1233-1237.

66. Yanai, N.; Kozue, M.; Amemori, S.; Kabe, R.; Adachi, C.; Kimizuka, N., Increased vis-to-UV upconversion performance by energy level matching between a TADF donor and high triplet energy acceptors. *J. Mater. Chem. C* **2016,** *4* (27), 6447-6451.

67. DeRosa, C. A.; Samonina-Kosicka, J.; Fan, Z.; Hendargo, H. C.; Weitzel, D. H.; Palmer, G. M.; Fraser, C. L., Oxygen Sensing Difluoroboron Dinaphthoylmethane Polylactide. *Macromolecules* **2015,** *48* (9), 2967-2977.

68. Zhu, L.; Trinh, M. T.; Yin, L.; Zhang, Z., Sequential oligodiacetylene formation for progressive luminescent color conversion via co-micellar strategy. *Chem. Sci.* **2016,** *7* (3), 2058-2065.

69. Wong, M. Y.; Hedley, G. J.; Xie, G.; Kölln, L. S.; Samuel, I. D. W.; Pertegás, A.; Bolink, H. J.; Zysman-Colman, E., Light-Emitting Electrochemical Cells and Solution-Processed Organic Light-Emitting Diodes Using Small Molecule Organic Thermally Activated Delayed Fluorescence Emitters. *Chem. Mater.* **2015,** *27* (19), 6535-6542.

70. Shidang, X.; Tingting, L.; Yingxiao, M.; Yi-Fan, W.; Zhenguo, C.; Chang-Cheng, L.; Siwei, L.; Yi, Z.; Alan, L.; Jiarui, X., An Organic Molecule with Asymmetric Structure Exhibiting Aggregation-Induced Emission, Delayed Fluorescence, and Mechanoluminescence. *Angew. Chem. Int. Ed.* **2015,** *54* (3), 874-878.

71. Xu, B.; Mu, Y.; Mao, Z.; Xie, Z.; Wu, H.; Zhang, Y.; Jin, C.; Chi, Z.; Liu, S.; Xu, J.; Wu, Y.-C.; Lu, P.-Y.; Lien, A.; Bryce, M. R., Achieving remarkable mechanochromism and white-light emission with thermally activated delayed fluorescence through the molecular heredity principle. *Chem. Sci.* **2016,** *7* (3), 2201-2206.

72. Rajamalli, P.; Senthilkumar, N.; Gandeepan, P.; Ren-Wu, C.-Z.; Lin, H.-W.; Cheng, C.-H., A thermally activated delayed blue fluorescent emitter with reversible externally tunable emission. *J. Mater. Chem. C* **2016,** *4* (5), 900-904.

73. Dias, F. B.; Penfold, T. J.; Monkman, A. P., Photophysics of thermally activated delayed fluorescence molecules. *Methods Appl. in Fluoresc.* **2017,** *5* (1), 012001.

74. Ward, J. S.; Nobuyasu, R. S.; Batsanov, A. S.; Data, P.; Monkman, A. P.; Dias, F. B.; Bryce, M. R., The interplay of thermally activated delayed fluorescence (TADF) and room temperature organic phosphorescence in sterically-constrained donor–acceptor charge-transfer molecules. *ChemComm* **2016,** *52* (12), 2612-2615.

75. Gibson, J.; Monkman, A. P.; Penfold, T. J., The Importance of Vibronic Coupling for Efficient Reverse Intersystem Crossing in Thermally Activated Delayed Fluorescence Molecules. *ChemPhysChem* **2016,** *17* (19), 2956-2961.

76. Gibson, J.; Monkman, A. P.; Penfold, T. J., The Importance of Vibronic Coupling for Efficient Reverse Intersystem Crossing in Thermally Activated Delayed Fluorescence Molecules. *ChemPhysChem* **2016,** *17* (19), 2956-2961.

77. Etherington, M. K.; Gibson, J.; Higginbotham, H. F.; Penfold, T. J.; Monkman, A. P., Revealing the spin–vibronic coupling mechanism of thermally activated delayed fluorescence. *Nat. Commun.* **2016,** *7*, 13680.

78. Samanta, P. K.; Kim, D.; Coropceanu, V.; Brédas, J.-L., Up-Conversion Intersystem Crossing Rates in Organic Emitters for Thermally Activated Delayed Fluorescence: Impact of the Nature of Singlet vs Triplet Excited States. *J. Am. Chem. Soc.* **2017,** *139* (11), 4042-4051.

79. Penfold, T. J.; Gindensperger, E.; Daniel, C.; Marian, C. M., Spin-Vibronic Mechanism for Intersystem Crossing. *Chem. Rev.* **2018**. *118* (15), 6975-7025.

80. Chen, X.-K.; Kim, D.; Brédas, J.-L., Thermally Activated Delayed Fluorescence (TADF) Path toward Efficient Electroluminescence in Purely Organic Materials: Molecular Level Insight. *Acc. Chem. Res.* **2018,** *51* (9), 2215-2224.

81. Turro, N. J.; Scaiano, J. C.; Ramamurthy, V., *Principles of Molecular Photochemistry: An Introduction*. University Sceience Books: Mill Valley, CA, 2010.

82. Milián-Medina, B.; Gierschner, J., Computational Design of Low Singlet–Triplet Gap All-Organic Molecules for OLED Application. *Org. Electron.* **2012,** *13* (6), 985-991.

83. Kaji, H.; Suzuki, H.; Fukushima, T.; Shizu, K.; Suzuki, K.; Kubo, S.; Komino, T.; Oiwa, H.; Suzuki, F.; Wakamiya, A.; Murata, Y.; Adachi, C., Purely Organic Electroluminescent Material Realizing 100% Conversion From Electricity To Light. *Nat. Commun.* **2015,** *6*, 8476.

84. Gábor, M.; Hiroko, N.; Qisheng, Z.; Tetsuya, N.; Chihaya, A., Enhanced Electroluminescence Efficiency in a Spiro-Acridine Derivative through Thermally Activated Delayed Fluorescence. *Angew. Chem. Int. Ed.* **2012,** *51* (45), 11311-11315.

85. Hirata, S.; Sakai, Y.; Masui, K.; Tanaka, H.; Lee, S. Y.; Nomura, H.; Nakamura, N.; Yasumatsu, M.; Nakanotani, H.; Zhang, Q.; Shizu, K.; Miyazaki, H.; Adachi, C., Highly Efficient Blue Electroluminescence Based On Thermally Activated Delayed Fluorescence. *Nat. Mater.* **2014,** *14*, 330.

86. Zhang, Q.; Li, J.; Shizu, K.; Huang, S.; Hirata, S.; Miyazaki, H.; Adachi, C., Design of Efficient Thermally Activated Delayed Fluorescence Materials for Pure Blue Organic Light Emitting Diodes. *J. Am. Chem. Soc.* **2012,** *134* (36), 14706-14709.

87. Penfold, T. J., On Predicting the Excited-State Properties of Thermally Activated Delayed Fluorescence Emitters. *J. Phys. Chem C.* **2015,** *119* (24), 13535-13544.

88. Lee, K.; Kim, D., Local-Excitation versus Charge-Transfer Characters in the Triplet State: Theoretical Insight into the Singlet–Triplet Energy Differences of Carbazolyl-Phthalonitrile-Based Thermally Activated Delayed Fluorescence Materials. *J. Chem. Phys. C.* **2016,** *120* (49), 28330-28336.

89. Wu, H.; Ying, L.; Yang, W.; Cao, Y., Progress and Perspective of Polymer White Light-Emitting Devices and Materials. *Chem. Soc. Rev.* **2009,** *38* (12), 3391-3400.

90. Englman, R.; Jortner, J., The Energy Gap Law for Non-Radiative Decay in Large Molecules. *J. Lumin.* **1970,** *1-2*, 134-142.

91. Würth, C.; Grabolle, M.; Pauli, J.; Spieles, M.; Resch-Genger, U., Relative and Absolute Determination of Fluorescence Quantum Yields of Transparent Samples. *Nat. Protoc.* **2013,** *8*, 1535.

92. Greenham, N. C.; Samuel, I. D. W.; Hayes, G. R.; Phillips, R. T.; Kessener, Y. A. R. R.; Moratti, S. C.; Holmes, A. B.; Friend, R. H., Measurement of Absolute Photoluminescence Quantum Efficiencies in Conjugated Polymers. *Chem. Phys. Lett.* **1995,** *241* (1), 89-96.

93. Würth, C.; Lochmann, C.; Spieles, M.; Pauli, J.; Hoffmann, K.; Schüttrigkeit, T.; Franzl, T.; Resch-Genger, U., Evaluation of a Commercial Integrating Sphere Setup for the Determination of Absolute Photoluminescence Quantum Yields of Dilute Dye Solutions. *Appl. Spectrosc.* **2010,** *64* (7), 733-741.

94. Lakowicv, J. R., *Principles of Fluorescence Spectroscopy*. Third ed.; Springer: New York, 2006.

95. Cai, X.; Li, X.; Xie, G.; He, Z.; Gao, K.; Liu, K.; Chen, D.; Cao, Y.; Su, S.-J., "Rate-limited effect" of Reverse Intersystem Crossing Process: the Key for Tuning Thermally Activated Delayed Fluorescence Lifetime and Efficiency Roll-Off of Organic Light Emitting Diodes. *Chem. Sci.* **2016,** *7* (7), 4264-4275.

96. Adachi, C.; Tsutsui, T.; Saito, S., Confinement of Charge Carriers and Molecular Excitons Within 5-nm-Thick Emitter Layer in Organic Electroluminescent Devices with a Double Heterostructure. *Appl. Phys. Lett.* **1990,** *57* (6), 531-533.

97. Adachi, C.; Tsutsui, T.; Saito, S., Blue Light-Emitting Organic Electroluminescent devices. *Appl. Phys. Lett.* **1990,** *56* (9), 799-801.

98. Kulkarni, A. P.; Tonzola, C. J.; Babel, A.; Jenekhe, S. A., Electron Transport Materials for Organic Light-Emitting Diodes. *Chem. Mater.* **2004,** *16* (23), 4556-4573.

99. Hughes, G.; Bryce, M. R., Electron-transporting Materials for Organic Electroluminescent and Electrophosphorescent Devices. *J. Mater. Chem.* **2005,** *15* (1), 94-107.

100. Hamada, Y.; Adachi, C.; Tsutsui, T.; Saito, S., Blue-Light-Emitting Organic Electroluminescent Devices with Oxadiazole Dimer Dyes as an Emitter. *Jpn. J. Appl. Phys.* **1992,** *31* (6R), 1812-1816.

101. Shirota, Y.; Kageyama, H., Charge Carrier Transporting Molecular Materials and Their Applications in Devices. *Chem. Rev.* **2007,** *107* (4), 953-1010.

102. Leung, M.-k.; Yang, C.-C.; Lee, J.-H.; Tsai, H.-H.; Lin, C.-F.; Huang, C.-Y.; Su, Y. O.; Chiu, C.-F., The Unusual Electrochemical and Photophysical Behavior of 2,2'-

Bis(1,3,4-oxadiazol-2-yl)biphenyls, Effective Electron Transport Hosts for Phosphorescent Organic Light Emitting Diodes. *Org. Lett.* **2007,** *9* (2), 235-238.

103. Tao, Y.; Wang, Q.; Yang, C.; Wang, Q.; Zhang, Z.; Zou, T.; Qin, J.; Ma, D., A Simple Carbazole/Oxadiazole Hybrid Molecule: An Excellent Bipolar Host for Green and Red Phosphorescent OLEDs. *Angew. Chem.* **2008,** *120* (42), 8224-8227.

104. Chaskar, A.; Chen, H.-F.; Wong, K.-T., Bipolar Host Materials: A Chemical Approach for Highly Efficient Electrophosphorescent Devices. *Adv. Mater.* **2011,** *23* (34), 3876-3895.

105. Zhang, Y.; Zuniga, C.; Kim, S.-J.; Cai, D.; Barlow, S.; Salman, S.; Coropceanu, V.; Brédas, J.-L.; Kippelen, B.; Marder, S., Polymers with Carbazole-Oxadiazole Side Chains as Ambipolar Hosts for Phosphorescent Light-Emitting Diodes. *Chem. Mater.* **2011,** *23* (17), 4002-4015.

106. Guan, M.; Chen, Z.; Bian, Z.; Liu, Z.; Gong, Z.; Baik, W.; Lee, H.; Huang, C., The Host Materials Containing Carbazole and Oxadiazole Fragment for Red Triplet Emitter in Organic Light-Emitting Diodes. *Org. Electron.* **2006,** *7* (5), 330-336.

107. Brunner, K.; van Dijken, A.; Börner, H.; Bastiaansen, J. J. A. M.; Kiggen, N. M. M.; Langeveld, B. M. W., Carbazole Compounds as Host Materials for Triplet Emitters in Organic Light-Emitting Diodes: Tuning the HOMO Level without Influencing the Triplet Energy in Small Molecules. *J. Am. Chem. Soc.* **2004,** *126* (19), 6035-6042.

108. Guan, M.; Qiang Bian, Z.; Feng Zhou, Y.; You Li, F.; Jun Li, Z.; Hui Huang, C., High-Performance Blue Electroluminescent Devices Based on 2-(4-Biphenylyl)-5-(4-carbazole-9-yl)phenyl-1,3,4-oxadiazole. *ChemComm* **2003,** (21), 2708-2709.

109. Justin Thomas, K. R.; Lin, J. T.; Tao, Y.-T.; Chuen, C.-H., New Carbazole−Oxadiazole Dyads for Electroluminescent Devices: Influence of Acceptor Substituents on Luminescent and Thermal Properties. *Chem. Mater.* **2004,** *16* (25), 5437-5444.

110. Linton, K. E.; Fisher, A. L.; Pearson, C.; Fox, M. A.; Palsson, L.-O.; Bryce, M. R.; Petty, M. C., Colour Tuning of Blue Electroluminescence Using Bipolar Carbazole-Oxadiazole Molecules in Single-Active-Layer Organic Light Emitting Devices (OLEDs). *J. Mater. Chem.* **2012,** *22* (23), 11816-11825.

111. Tao, Y.; Wang, Q.; Yang, C.; Zhong, C.; Zhang, K.; Qin, J.; Ma, D., Tuning the Optoelectronic Properties of Carbazole/Oxadiazole Hybrids through Linkage Modes: Hosts for Highly Efficient Green Electrophosphorescence. *Adv. Funct. Mater.* **2010,** *20* (2), 304-311.

112. Wu, X.; Wang, L.; Hua, Y.; Wang, C.; Batsanov, A. S.; Bryce, M. R., A Carbazole–Oxadiazole Diad Molecule for Single-Emitting-Component White Organic Light-Emitting Devices (WOLEDs). *Tetrahedron* **2014,** *70* (11), 2015-2019.

113. Zhang, Q.; Li, B.; Huang, S.; Nomura, H.; Tanaka, H.; Adachi, C., Efficient Blue Organic Light-Emitting Diodes Employing Thermally Activated Delayed Fluorescence. *Nat. Photon.* **2014,** *8* (4), 326-332.

114. Lee, J.; Shizu, K.; Tanaka, H.; Nomura, H.; Yasuda, T.; Adachi, C., Oxadiazole- and Triazole-Based Highly-Efficient Thermally Activated Delayed Fluorescence Emitters for Organic Light-Emitting Diodes. *J. Mater. Chem. C* **2013,** *1* (30), 4599-4604.

115. Burroughes, J. H.; Bradley, D. D. C.; Brown, A. R.; Marks, R. N.; Mackay, K.; Friend, R. H.; Burns, P. L.; Holmes, A. B., Light-Emitting Diodes Based on Conjugated Polymers. *Nature* **1990,** *347*, 539.

116. Luo, J.; Xie, G.; Gong, S.; Chen, T.; Yang, C., Creating a Thermally Activated Delayed Fluorescence Channel in a Single Polymer System to Enhance Exciton Utilization Efficiency for Bluish-Green Electroluminescence. *ChemComm* **2016,** *52* (11), 2292-2295.

117. Boudreault, P.-L. T.; Beaupré, S.; Leclerc, M., Polycarbazoles for Plastic Electronics. *Polym. Chem.* **2010,** *1* (2), 127-136.

118. Abia, A. A.; Burkhart, R. D., Triplet Excimer Emission From Carbazoyl Chromophores in Polystyrene Matrices. *Macromolecules* **1984,** *17* (12), 2739-2744.

119. Wex, B.; Kaafarani, B. R., Perspective on Carbazole-Based Organic Compounds as Emitters and Hosts in TADF Applications. *J. Mater. Chem. C.* **2017,** *5* (34), 8622-8653.

120. Zhang, D.; Cao, X.; Wu, Q.; Zhang, M.; Sun, N.; Zhang, X.; Tao, Y., Purely Organic Materials for Extremely Simple All-TADF White OLEDs: A New Carbazole/Oxadiazole Hybrid Material as a Dual-Role Non-Doped Light Blue Emitter and Highly Efficient Orange Host. *J. Mater. Chem. C.* **2018,** *6* (14), 3675-3682.

121. Sakamoto, Y.; Suzuki, T.; Kobayashi, M.; Gao, Y.; Fukai, Y.; Inoue, Y.; Sato, F.; Tokito, S., Perfluoropentacene: High-Performance p−n Junctions and Complementary Circuits with Pentacene. *J. Am. Chem. Soc.* **2004,** *126* (26), 8138-8140.

122. Babudri, F.; Farinola, G. M.; Naso, F.; Ragni, R., Fluorinated Organic Materials for Electronic and Optoelectronic Applications: The Role of the Fluorine Atom. *ChemComm* **2007,** (10), 1003-1022.

123. Kessler, F.; Watanabe, Y.; Sasabe, H.; Katagiri, H.; Nazeeruddin, M. K.; Grätzel, M.; Kido, J., High-Performance Pure Blue Phosphorescent OLED Using a Novel Bis-heteroleptic Iridium(iii) Complex with Fluorinated Bipyridyl Ligands. *J. Mater. Chem. C* **2013,** *1* (6), 1070-1075.

124. Yang, X.; Zhou, G.; Wong, W.-Y., Functionalization of Phosphorescent Emitters and Their Host Materials by Main-Group Elements for Phosphorescent Organic Light-Emitting Devices. *Chem. Soc. Rev.* **2015,** *44* (23), 8484-8575.

125. Yu, L.; Wu, Z.; Xie, G.; Zhong, C.; Zhu, Z.; Cong, H.; Ma, D.; Yang, C., Achieving a Balance Between Small Singlet–Triplet Energy Splitting and High Fluorescence Radiative Rate in a Quinoxaline-Based Orange-Red Thermally Activated Delayed Fluorescence Emitter. *ChemComm* **2016,** *52* (73), 11012-11015.

126. Li, Y.; Liang, J.-J.; Li, H.-C.; Cui, L.-S.; Fung, M.-K.; Barlow, S.; Marder, S. R.; Adachi, C.; Jiang, Z.-Q.; Liao, L.-S., The Role of Fluorine-Substitution on the π-Bridge in Constructing Effective Thermally Activated Delayed Fluorescence Molecules. *J. Mater. Chem. C* **2018,** *6* (20), 5536-5541.

127. Albrecht, K.; Yamamoto, K., Dendritic Structure Having a Potential Gradient: New Synthesis and Properties of Carbazole Dendrimers. *J. Am. Chem. Soc.* **2009,** *131* (6), 2244-2251.

128. Jiang, W.; Duan, L.; Qiao, J.; Dong, G.; Zhang, D.; Wang, L.; Qiu, Y., High-Triplet-Energy Tri-carbazole Derivatives as Host Materials for Efficient Solution-Processed Blue Phosphorescent Devices. *J. Mater. Chem.* **2011,** *21* (13), 4918-4926.

129. Dongwook, K., Effect of Topology on the Singlet–Triplet Energy Difference and their Natures: A Density Functional Theory Study of Carbazolyl-Phthalonitrile Derivatives. *Bull. Korean Chem. Soc.* **2017,** *38* (8), 899-903.

130. Solomons, T. W. G.; Fryhle, C. B., *Organic Chemistry*. 6th ed.; John Wiley & Sons: New York, 1996.

131. Atul, C.; Hsiao-Fan, C.; Ken-Tsung, W., Bipolar Host Materials: A Chemical Approach for Highly Efficient Electrophosphorescent Devices. *Adv. Mater.* **2011,** *23* (34), 3876-3895.

132. Zheng, Y.; Batsanov, A. S.; Jankus, V.; Dias, F. B.; Bryce, M. R.; Monkman, A. P., Bipolar Molecules with High Triplet Energies: Synthesis, Photophysical, and Structural Properties. *J. Org. Chem.* **2011,** *76* (20), 8300-8310.

133. Shao, S.; Hu, J.; Wang, X.; Wang, L.; Jing, X.; Wang, F., Blue Thermally Activated Delayed Fluorescence Polymers with Nonconjugated Backbone and Through-Space Charge Transfer Effect. *J. Am. Chem. Soc.* **2017,** *139* (49), 17739-17742.

134. Chunmiao, H.; Yongbiao, Z.; Hui, X.; Jiangshan, C.; Zhaopeng, D.; Dongge, M.; Qiang, L.; Pengfei, Y., A Simple Phosphine–Oxide Host with a Multi-insulating Structure: High Triplet Energy Level for Efficient Blue Electrophosphorescence. *Chem. Eur. J.* **2011,** *17* (21), 5800-5803.

135. Masui, K.; Nakanotani, H.; Adachi, C., Analysis of Exciton Annihilation in High-Efficiency Sky-Blue Organic Light-Emitting Diodes with Thermally Activated Delayed Fluorescence. *Org. Electron.* **2013,** *14* (11), 2721-2726.

136. Mei, L.; Hu, J.; Cao, X.; Wang, F.; Zheng, C.; Tao, Y.; Zhang, X.; Huang, W., The Inductive-Effect of Electron Withdrawing Trifluoromethyl for Thermally Activated

Delayed Fluorescence: Tunable Emission From Tetra- to Penta-Carbazole in Solution Processed Blue OLEDs. *ChemComm* **2015,** *51* (65), 13024-13027.

137. Kim, D.; Coropceanu, V.; Brédas, J.-L., Design of Efficient Ambipolar Host Materials for Organic Blue Electrophosphorescence: Theoretical Characterization of Hosts Based on Carbazole Derivatives. *J. Am. Chem. Soc.* **2011,** *133* (44), 17895-17900.

138. Salman, S.; Kim, D.; Coropceanu, V.; Brédas, J.-L., Theoretical Investigation of Triscarbazole Derivatives As Host Materials for Blue Electrophosphorescence: Effects of Topology. *Chem. Mater.* **2011,** *23* (23), 5223-5230.

139. Kim, D.; Zhu, L.; Brédas, J.-L., Electronic Structure of Carbazole-Based Phosphine Oxides as Ambipolar Host Materials for Deep Blue Electrophosphorescence: A Density Functional Theory Study. *Chem. Mater.* **2012,** *24* (13), 2604-2610.

140. Marc K. Etherington, J. G., Heather F. Higginbotham, Thomas J. Penfold & Andrew P. Monkman, Revealing the Spin–Vibronic Coupling Mechanism of Thermally Activated Delayed Fluorescence. *Nat. Commun.* **2016**.

141. Kim, D., Effect of Topology on the Singlet–Triplet Energy Difference and their Natures: A Density Functional Theory Study of Carbazolyl-Phthalonitrile Derivatives. *Bull. Korean Chem. Soc.* **2017,** *38* (8), 899-903.

142. Geng, Y.; Cui, L.-S.; Kim, J. U.; Nakanotani, H.; Adachi, C., Molecular Design for Blue Thermal Activated Delayed Fluorescence Materials: Substitution Position Effect. *Chem. Lett.* **2017,** *46* (10), 1490-1492.

143. Karon, K.; Lapkowski, M., Carbazole Electrochemistry: A Short Review. *J. Solid State Electrochem.* **2015,** *19* (9), 2601-2610.

144. Noda, H.; Nakanotani, H.; Adachi, C., Excited State Engineering for Efficient Reverse Intersystem Crossing. *Sci. Adv.* **2018,** *4* (6).

145. Zhang, X.; Fuentes-Hernandez, C.; Zhang, Y.; Cooper, M. W.; Barlow, S.; Marder, S. R.; Kippelen, B., High Performance Blue-Emitting Organic Light-Emitting Diodes from Thermally Activated Delayed Fluorescence: A Guest/Host Ratio Study. *J. Appl. Phys.* **2018,** *124* (5), 055501.

146. Lee, D. R.; Choi, J. M.; Lee, C. W.; Lee, J. Y., Ideal Molecular Design of Blue Thermally Activated Delayed Fluorescent Emitter for High Efficiency, Small Singlet–Triplet Energy Splitting, Low Efficiency Roll-Off, and Long Lifetime. *ACS Appl. Mater. Interfaces* **2016,** *8* (35), 23190-23196.

147. Cooper, M. W.; Zhang, X.; Zhang, Y.; Jeon, S. O.; Lee, H.; Kim, S.; Fuentes-Hernandez, C.; Barlow, S.; Kippelen, B.; Marder, S. R., Effect of the Number and Substitution Pattern of Carbazole Donors on the Singlet and Triplet State Energies in a Series of Carbazole-Oxadiazole Derivatives Exhibiting Thermally Activated Delayed Fluorescence. *Chem. Mater.* **2018,** *30* (18), 6389-6399.

148. Kawano, T.; Yoshizumi, T.; Hirano, K.; Satoh, T.; Miura, M., Copper-Mediated Direct Arylation of 1,3,4-Oxadiazoles and 1,2,4-Triazoles with Aryl Iodides. *Org. Lett.* **2009,** *11* (14), 3072-3075.

149. Keznetsov, V. P., Molecular and Crystal Structure of Polyclic Chainlike Compounds - Oxazole and 1,3,4-Oxadiazole Derivatives: I. Symmetric 2,5-Diphenyl-, 2,5-di-2-furyl-, and 2,5-Di-2-thienyl-1-3-4-oxidiazoles. *Crystallogr. Rep.* **1998,** *43* (3), 430-438.

150. Lee, S.; Kim, S.-O.; Shin, H.; Yun, H.-J.; Yang, K.; Kwon, S.-K.; Kim, J.-J.; Kim, Y.-H., Deep-Blue Phosphorescence from Perfluoro Carbonyl-Substituted Iridium Complexes. *J. Am. Chem. Soc.* **2013,** *135* (38), 14321-14328.

151. Wang, Q.; Oswald, I. W. H.; Yang, X.; Zhou, G.; Jia, H.; Qiao, Q.; Chen, Y.; Hoshikawa-Halbert, J.; Gnade, B. E., A Non-Doped Phosphorescent Organic Light-Emitting Device with Above 31% External Quantum Efficiency. *Adv. Mater.* **2014,** *26* (48), 8107-8113.

152. Hsu, C.-W.; Lin, C.-C.; Chung, M.-W.; Chi, Y.; Lee, G.-H.; Chou, P.-T.; Chang, C.-H.; Chen, P.-Y., Systematic Investigation of the Metal-Structure–Photophysics Relationship of Emissive d10-Complexes of Group 11 Elements: The Prospect of Application in Organic Light Emitting Devices. *J. Am. Chem. Soc.* **2011,** *133* (31), 12085-12099.

153. Zhu, Y.-C.; Zhou, L.; Li, H.-Y.; Xu, Q.-L.; Teng, M.-Y.; Zheng, Y.-X.; Zuo, J.-L.; Zhang, H.-J.; You, X.-Z., Highly Efficient Green and Blue-Green Phosphorescent OLEDs Based on Iridium Complexes with the Tetraphenylimidodiphosphinate Ligand. *Adv. Mater.* **2011,** *23* (35), 4041-4046.

154. Yuan, W.; Zhang, M.; Zhang, X.; Cao, X.; Sun, N.; Wan, S.; Tao, Y., The Electron Inductive Effect of CF3 on Penta-Carbazole Containing Blue Emitters: Trade-Off Between Color Purity and Luminescent Efficiency in TADF OLEDs. *Dyes Pigm.* **2018,** *159*, 151-157.

155. Ishimatsu, R.; Matsunami, S.; Shizu, K.; Adachi, C.; Nakano, K.; Imato, T., Solvent Effect on Thermally Activated Delayed Fluorescence by 1,2,3,5-Tetrakis(carbazol-9-yl)-4,6-dicyanobenzene. *J. Phys. Chem. A.* **2013,** *117* (27), 5607-5612.

156. Murawski, C.; Leo, K.; Gather, M. C., Efficiency Roll-Off in Organic Light-Emitting Diodes. *Adv. Mater.* **2013,** *25* (47), 6801-6827.

157. Pouliot, M.-F.; Angers, L.; Hamel, J.-D.; Paquin, J.-F., Synthesis of 1,3,4-Oxadiazoles from 1,2-Diacylhydrazines Using [Et2NSF2]BF4 as a Practical Cyclodehydration Agent. *Org. Biomol. Chem.* **2012,** *10* (5), 988-993.

158. Cooper, M. W.; Zhang, X.; Zhang, Y.; Fuentes-Hernandez, C.; Barlow, S.; Kippelen, B.; Marder, S. R., Control of Singlet Emission Energy in a Diphenyloxadiazole

Containing Fluorophore Leading To Thermally Activated Delayed Fluorescence. *ACS Omega* **2018,** *3* (11), 14918-14923.

159. Li, C.; Duan, C.; Han, C.; Xu, H., Secondary Acceptor Optimization for Full-Exciton Radiation: Toward Sky-Blue Thermally Activated Delayed Fluorescence Diodes with External Quantum Efficiency of ≈30%. *Adv. Mater.* [Online Early Access]. doi.org/10.1002/adma.201804228.